Fracture Toughness of Dental Amalgams

Thesis

FRACTURE TOUGHNESS OF DENTAL AMALGAMS

A THESIS SUBMITTED TO THE

MATERIALS DISCIPLINE OF

THE OPEN UNIVERSITY

FOR THE DEGREE OF

DOCTOR OF PHILOSOPHY

by

D.A.HAYES

(M.Sc.,C.Eng.,M.I.Mech.E.)

September 1992

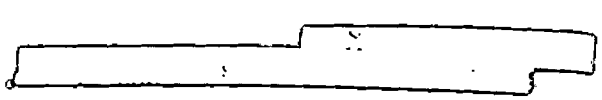

Date of submission: 24.09.92.

Date of award: 16.03.93.

ProQuest LLC.
789 East Eisenhower Parkway
P.O. Box 1346
Ann Arbor, MI 48106 – 1346

D.A.Hayes

The Open University

Ph.D. Thesis

August 1992

THE FRACTURE TOUGHNESS OF DENTAL AMALGAMS

Abstract

This work shows that there is a requirement for a test, in addition to those specified in BS 2938:1985, for predicting the performance of dental amalgams. The SEN type of test to find the fracture toughness (K_{IC}) is capable of distinguishing between amalgams that are reputed to have satisfactory clinical performance, and those which are considered to have poor clinical performance. Factors such as the mode of loading and the age of the specimen influence the calculated value of K_{IC}.

A method of calculating K_{IC} from the Vickers hardness test is reported in this work. Provided the method is conducted with a suitable applied load, to obtain a clearly defined indentation which possesses single cracks at each apex, then K_{IC} values correlate well with those of bulk testing. The indentation method also allows the effects of crack path and constituent phases to be assessed.

ACKNOWLEDGEMENTS

The author wishes to express his gratitude to his supervisors, Dr.A.Greasley and Dr.G.Weidmann for their valued help and support during this research.

Thanks are due to Mr.K.Bate of the support staff at the University of Central England (Birmingham), for his help in the production of this thesis.

This thesis is dedicated to my family who have given me great support, and demonstrated such tolerance, over the period of the research.

Preface

This thesis submitted for the degree of Doctor of Philosophy of the Open University is an account of the research performed in the Materials Science Discipline under the supervision of Dr.A.Greasley and Dr.G.Weidmann between January 1980 and August 1992.

The work reported is original and has been performed without collaboration. This thesis, neither in part nor as a whole, is the same as any thesis submitted in this or any other university.

Where the work of other authors has been included in the text, this has been acknowledged and its source given.

CONTENTS

FIGURES

TABLES

INTRODUCTION

A healthy human tooth, by virtue of its unique composite structure, fulfils its role admirably. However with a decayed tooth, the situation is different. In general when human tissue is damaged, a large degree of self-repair occurs, although this may be assisted by medical intervention. In contrast the human tooth relies exclusively for its restoration on the skills and materials used by the dentist. The demands made by this reliance are best understood in the context of the complex structure of the tooth.

There are three types of permanent teeth in the human mouth: incisors for cutting, canines for tearing and molars for grinding, Figure 1. The geometry of each type is different, but the structure is the same, and comprises a root and a crown.

The root anchors the tooth into the jawbone and is covered by a layer of collagen fibres called the periodontal membrane. This is a complex structure in itself, and responds by varying its stiffness according to the nature of the force being applied to the crown. This ability ensures an effective and uniform transfer of mastication forces through to the bone structure.

The crown is the visible part of the tooth. It is covered with a layer of enamel (approximately 0.6mm thick) which is the hardest tissue in the human body and resists the attrition that inevitably occurs with use and age. In its mature state, enamel is highly mineralised, and comprises by weight 96% inorganic material, in the form of hydroxyapatite crystals, 1% organic material consisting of carbohydrates, lactates, citrates and lipids, and 3% water. It has

a high modulus of elasticity, (approximately 50 GPa (1,2)), and is supported by dentine which forms the bulk of the tooth.

Dentine (Figure 2) is composed of approximately 70% hydroxyapatite in the form of small plates which are bonded together with collagens and approximately 12% water. The modulus of elasticity of dentine has been estimated to be about one third that of enamel (1,2). At the centre of the tooth is the pulp cavity which accomodates the fibrous tissue containing nerves, blood vessels and lymphatics(3).

I.1. Tooth decay

Tooth damage may be caused by accidental impact, excessive mastication forces or can be the result of disease. Considering the latter case only, the most common problem is due to caries which is a process that demineralises the enamel. This occurs because acid is produced when the plaque bacteria, which exist on the enamel surface, are given a sugary substrate arising from an individual's diet. This acid destroys the organic component of the dentine with the result that a cavity is formed once the enamel is breached. The pulp soon becomes infected if this process is allowed to proceed. Examples of two of the most vulnerable sites are shown in Figure 3. Repair is clearly necessary to relieve the pain, but it is also required to restore the anatomical form of the tooth, so as to prevent further decay and to reinstate the structural and aesthetic qualities of the tooth.

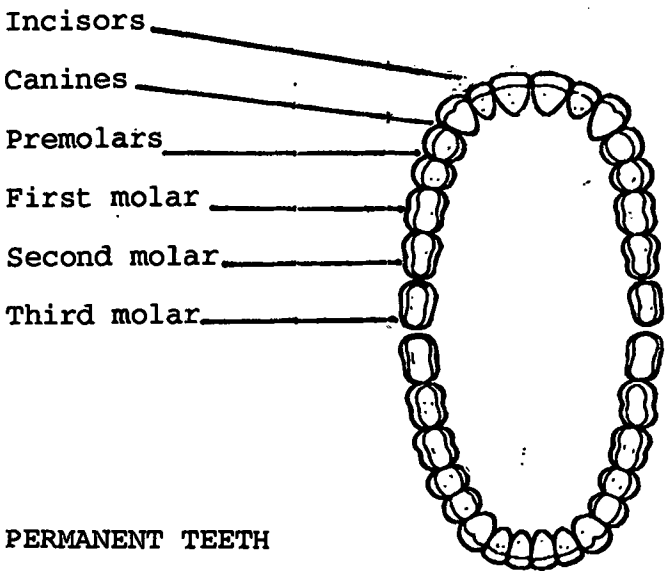

TOOTH TYPES IN THE HUMAN MOUTH

Figure 1

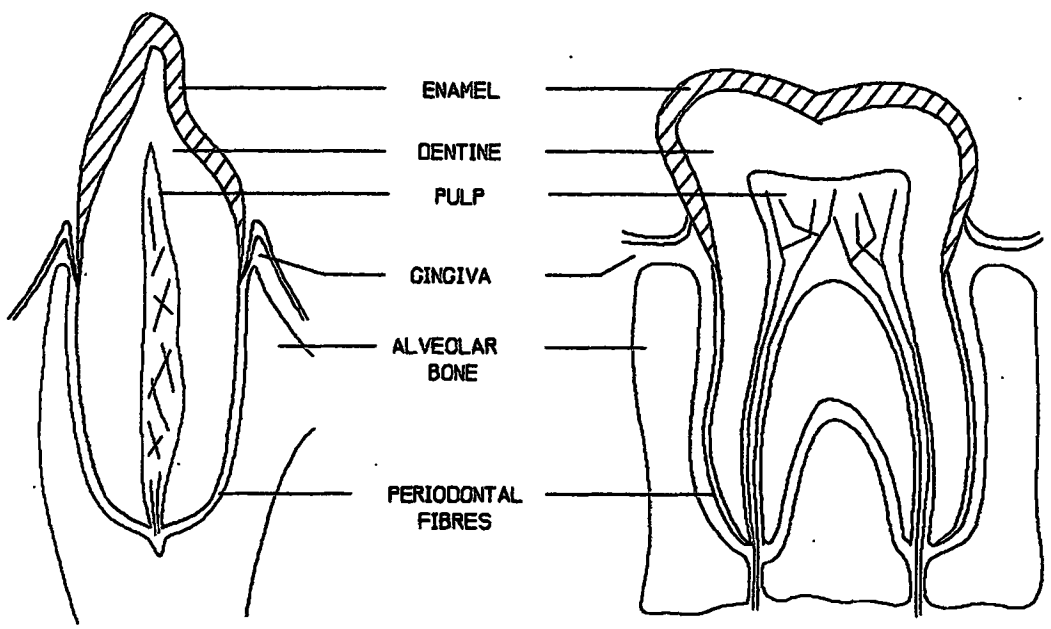

BASIC TOOTH STRUCTURE

Figure 2

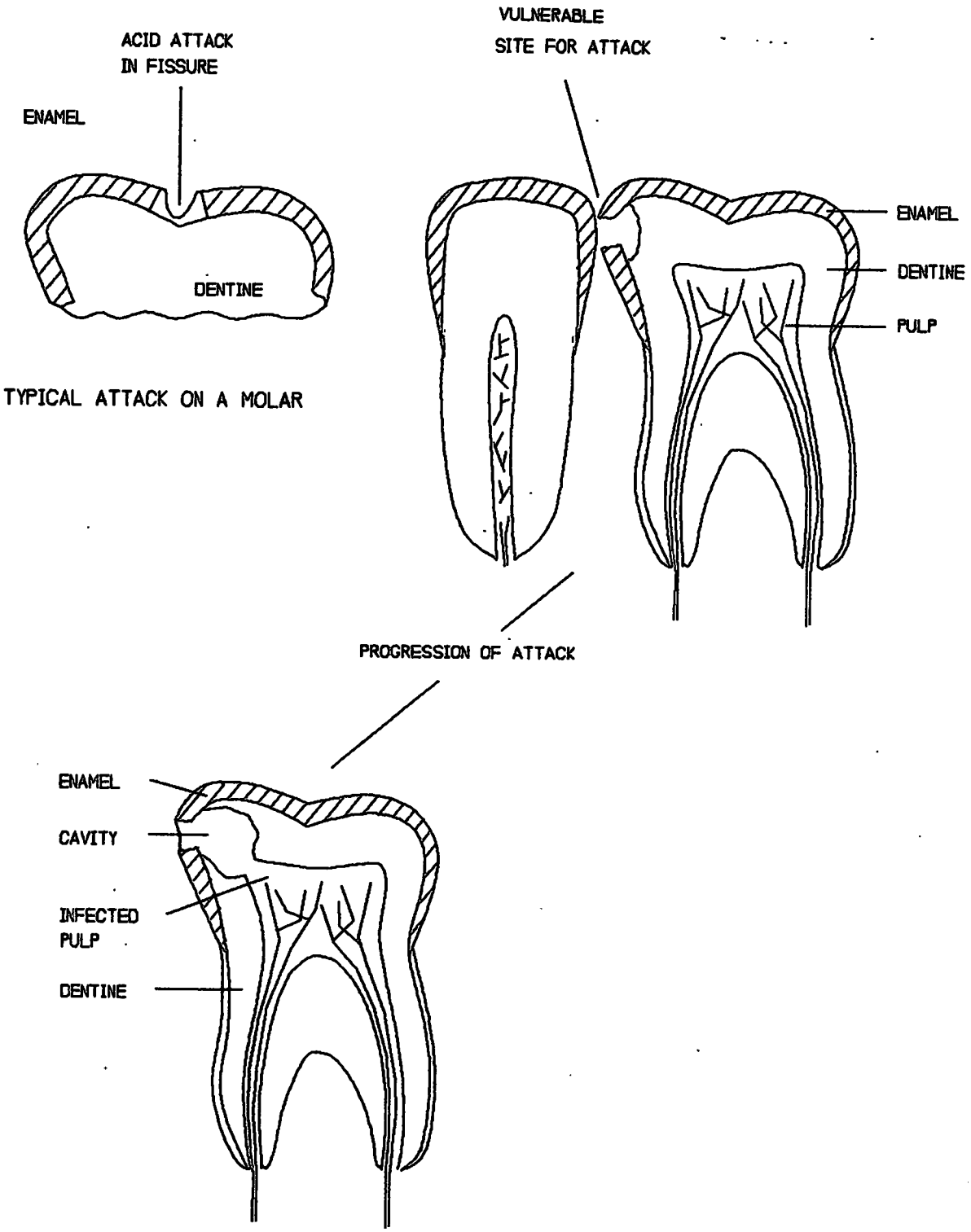

DIAGRAMS OF TWO TYPES OF CARIOUS LESION

Figure 3

I.2. Method of tooth repair

Before considering the materials used for filling a tooth, it is helpful to give a brief description of the method of preparing a tooth for restoration. The process of tooth restoration involves removal by drilling of the decayed tissue, and repair with a suitable filling material. At the turn of the century, G.V.Black(4) laid down the ground rules for restoration by defining five classes of cavity, where each relates to a specific decayed zone on the tooth. Figure 4 shows these classes labelled I to V. Black's classification is only a general means of characterisation, and wide variations in geometry and size may exist within each class. This leads to a different perception by indiviual clinicians of the requirements for cavity preparation. Elderton(5) demonstrated the extent of this problem by asking twenty seven dentists to prepare a minimal cavity in class II, suitable for an amalgam filling. Figures 5(a) to (c) show three interpretations in which the size of cavity that is considered necessary depends very much on the personal view of the clinician. They illustrate the highly subjective nature of assessment which in turn can lead to difficulties in relating in-vitro test data to in- vivo performance.

It can be seen from Figure 5 that the cavity incorporates geometric features which enable the filling material to be retained; thus a certain amount of healthy tissue has to be removed to provide this mechanical locking function.

Other variables involved in the preparation of a tooth for restoration are; choice of surface finish of the cavity walls, restorative material type, and filling technique.

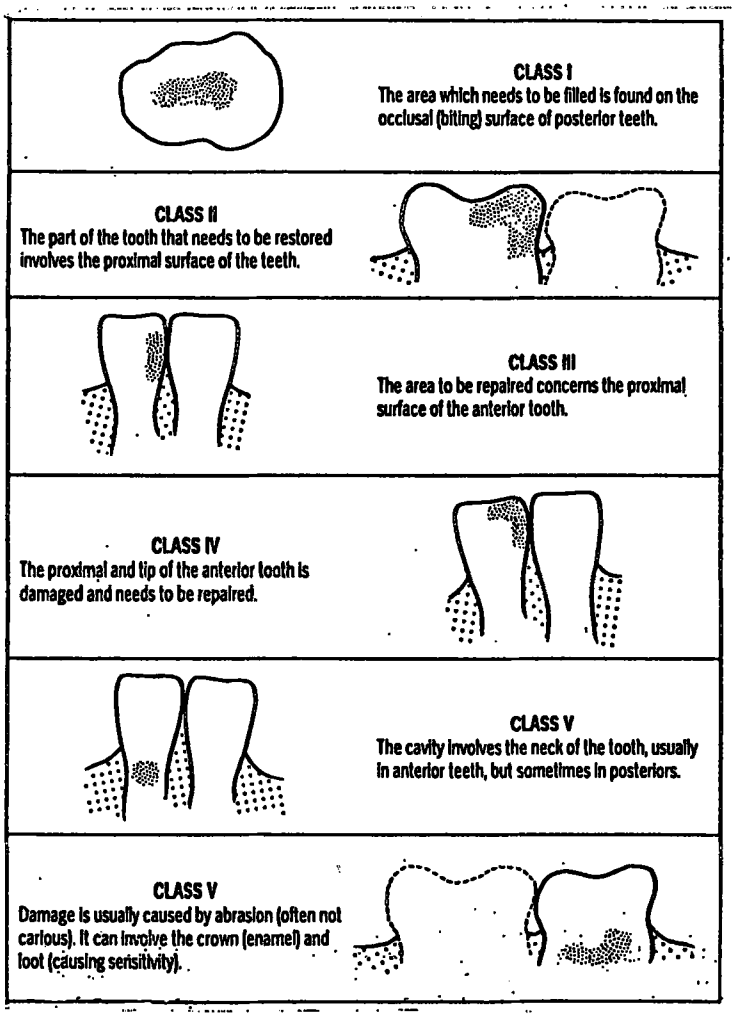

Definition of terms:

Proximal - Site adjacent to neighbouring tooth.
Occlusal - Biting surface.
Anterior - Front teeth.
Posterior - Back teeth.

CONVENTIONAL CAVITY CLASSIFICATION

Figure 4

(b)

(a)

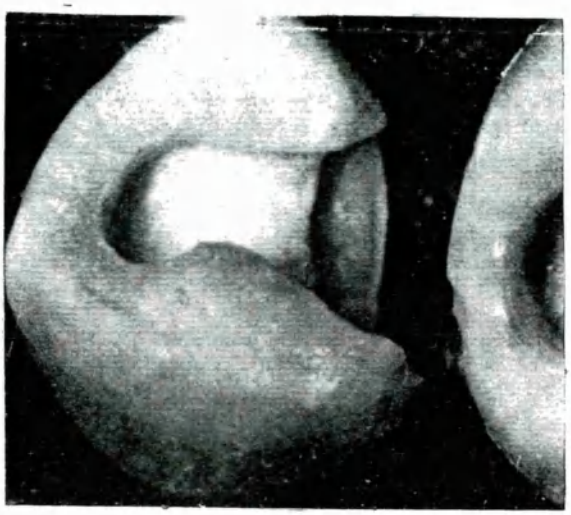

2mm

(c)

The teeth (a),(b) and (c) had the same size of decayed area.

INTERPRETATION BY THREE DIFFERENT DENTISTS OF THE SIZE OF CAVITY NECESSARY TO FILL A TOOTH.

Figure 5

I.3. Filling materials.

The filling materials used to repair teeth that possess the type of fault shown in Figure 3 are either polymer or metal based. The metal types are either gold-based alloys or amalgams based on the silver/tin/mercury system. The research in and development of dental materials are very active areas and have been so over several decades. They are encouraged by the highly competitive commercial market which amounts to many millions of pounds sterling in the UK alone. The share of amalgams has declined in the last twenty years owing to the development of composites and improved dental health. In 1988 Robbins(6), estimated that amalgams accounted for 50% of total expenditure on filling materials. This proportion remains basically unchanged to the present day. Currently on the UK market there are approximately one hundred approved brands of filling materials based on composite resin systems, and about twenty brands of commonly used amalgams.

The advantages of non-metallic materials compared with amalgams include a good initial colour match with the remaining healthy tooth tissue. Originally, silicate cement was used for this purpose but it was found to degrade quickly under oral conditions(7,8,9). Subsequent developments have resulted in various types of composites based on bis-glycidil methacrylate (bis-GMA) polymer (10-12). A distinct advantage with these materials is that an acid pre-etch of the cavity walls results in adhesion between the filling and remaining tissue and minimises further decay (13,14). The absence of mercury and other metallic elements in the formulation is of

obvious importance.

However, in spite of these advantages, amalgams are still used extensively, particularly in molar teeth where the stresses are highest. After a comparatively short time, composites discolour and so their initial advantage in this respect is minimised. Probably of greatest importance is the fact that a properly placed amalgam restoration can be expected to last for approximately twenty years, whereas the life of a composite is between three and five years. One reason for the latter's short life is their lack of abrasion resistance resulting in a rough surface. This subsequently encourages infection or further decay due to increased plaque adhesion.

I.4. The use of amalgams in repair.

The term amalgam is used to describe the plastic (i.e. workable) mass that results when mercury reacts with particular metals. Strachan and Harris(15) found that the propensity of an element to amalgamate could be judged by its solubility in mercury. They characterised the reaction of mercury with a wide range of unstressed metals and demonstrated that those with the highest solubility occur in the B sub-group of the Periodic Table. In fact, those found in dental amalgams occur in groups IB to IVB, namely silver,tin,copper and zinc.

Amalgam for dental restorations was first used in France in about 1826 and was introduced into the USA in 1833 (16). However, it was not until 1895 that a scientific approach was made to the

analysis of the material and it was G.V.Black (17) who was the principal investigator. He recommended that the best metal for dental applications comprised an alloy of 75 at% (73 wt%) silver with 25 at% (27 wt%) tin. The amalgam was formed by mixing the powdered alloy in approximately equal parts by weight with mercury. Black suggested that a further 5 at% copper could be added at the expense of an equivalent amount of silver, although his reasons for this do not appear to have been documented.

Other metal ratios have been developed since Black's work and Bates & Knapton(18) have identified the effects of these components on amalgam characteristics. Silver contributes to amalgam strength and decreases creep. After the alloy has been mixed with mercury, the development of constituent phases in the amalgam continues for at least 24 hours. During this setting period there is an associated dimensional change - the net effect usually producing an overall expansion of the filling. However, the individual contribution of silver when it is present in the alloy in excess of about 68 wt%, is that the setting time is too short and contraction becomes excessive. The tin content should not exceed certain values. When present in excess of about 28 wt%, the strength and hardness are too low and an unacceptably high creep occurs under in-vivo loading.

The product arising from the use of the Ag_3Sn alloy recommended by Black is known as Conventional or Traditional amalgam and was used for several decades without any significant changes to its formulation. Most investigations subsequent to Black's were directed towards obtaining an understanding of the basic metallurgy

of amalgam which will be described later. First, the details of alloy production and the process used to achieve its amalgamation need to be considered.

To make the Traditional alloy, the metals are melted together, usually under an inert atmosphere. A cast ingot is then produced and the rate of cooling is such that usually some coring of the structure occurs. The Ag-Sn equilibrium phase diagram,Figure 6, shows that, although under equilibrium conditions a composition of 27wt% tin and 73wt% silver should form the Ag_3Sn (γ) by a peritectic reaction, the ingot could also contain the β phase. It is therefore homogenised at 400°C for 24h to eliminate most of the Ag-rich β phase (a small amount of β does, however, favourably accelerate the setting time of amalgam). The ingot is then reduced to particulate form by lathe-cutting and then powdered by ball-milling. At this stage, the powder has a high degree of cold work and thus residual stress - a condition which causes such a high amalgamation rate that it would be unusable by the dentist. Therefore, stress relieving is carried out at approximately 60°C for about 4h. This is generally regarded as an ageing procedure which reduces the dislocation density. However, it is quite possible that the phases comprising the powder may change in proportion or composition and this heating stage could accelerate the natural ageing that occurs with storage to give a more 'stable' product. Powder production is concluded by sieving to obtain a particle size of about 40μm and to establish a uniform distribution within a batch.

Some years ago the mixing of the alloy powder with mercury was done manually by use of a mortar and pestle. When the mass had

become plastic, it was further worked between the dentist's thumb and fingers (mulled) to achieve the working state required for its insertion in the tooth cavity. This procedure was unsatisfactory not only because of the health hazard due to the skin contact with mercury, but also the lack of control over the complete process.

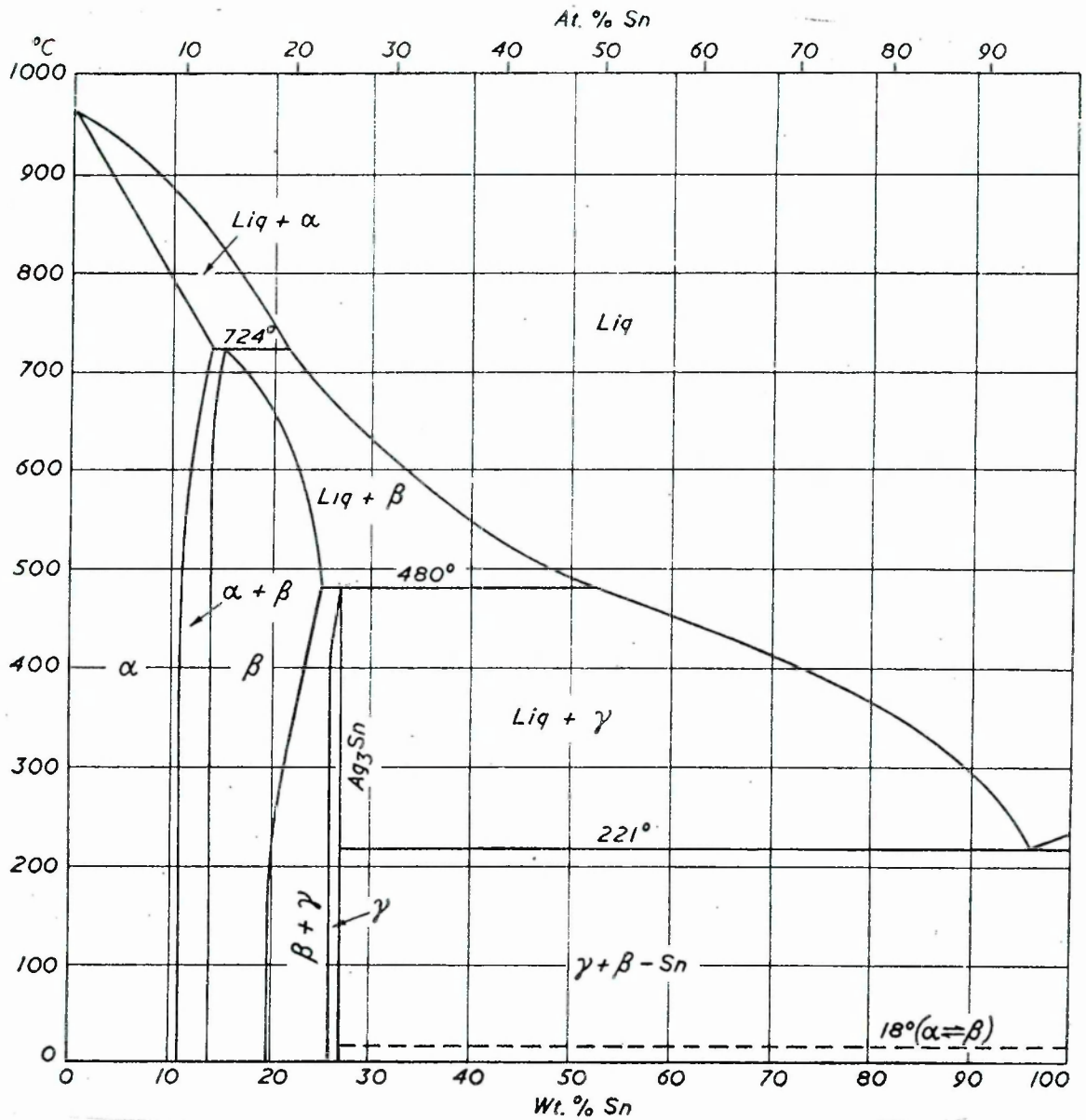

EQUILIBRIUM PHASE DIAGRAM FOR Ag-Sn

Figure 6

The current practice is to have the amalgam components delivered in pre-dispensed plastic capsules. Just before use, a small diaphragm within the capsule is punctured, thus permitting the mercury to contact the alloy powder. A mechanical amalgamator is then used to mix thoroughly the two components within the capsule for a specified time. It has been found that the time, and even the pattern of movement of mixing can have a marked effect on the manipulation properties of the amalgam(19,20). In fact, different manufacturers recommend specific mixing times for their products. After mixing, the resultant plastic mass is packed into the tooth cavity with a force that corresponds to the maximum endurable by the patient. This procedure removes excess mercury and ensures that a well-consolidated filling is obtained. The cavity geometry must be such that it provides mechanical retention to the amalgam without unduly weakening the remaining tooth tissue.

The dentist has approximately ten minutes available to mix the amalgam and subsequently to carve it to recreate the anatomical form of the tooth. Beyond this period, setting has usually proceeded to such an extent that any attempt to work the amalgam causes fracture and crumbling. It is considered that a setting time of one hour should be allowed before the filling is subjected to biting forces, but the setting reaction continues for probably at least twenty four hours(21). The specific nature of this setting reaction will be considered in the next chapter of this thesis.

The restoration should be completed by polishing, which should not be carried out until twenty four hours after amalgamation. If polishing is carried out too soon, mercury is liberated on the

surface of the restoration by the heat generated.

I.5. Clinical failure of amalgams

Restoration faults can be detected in-vivo quite easily but their cause as assessed by the dentist is often unreliable. This situation arises because usually only the secondary effects of the underlying problem can be detected. One example is where caries occurs at a site that is adjacent to an existing filling and this is identified as the sole need for corrective action to be taken. However, the reason for this progression of decay might well be inadequate sealing of the original restoration at its interface with the remaining tooth tissue. Elderton (22) concluded that dentists often have a propensity for identifying a particular type of fault and seek out evidence of this to the exclusion of other contributory factors.

Clearly, there are many factors which may affect the quality of a restoration and the mechanisms concerned with their degradation are not fully understood. This is why clinical assessments of restorations have tended to be very subjective. An added complexity in analysing failure is the nature of the interaction between the filling material and its surrounding tissue (23,24,25).

In the process of surveying previous work to determine common causes of restoration failure, it was noticeable that samples were often taken from a population that had a unique characteristic such as small sample size, specific geographical origins and specific occupation groups (26-29). Comparison between the various data was

made more difficult because there were cases where samples were from the same dental practice, and cases where the age range was particularly narrow. Additionally,it has to be recognised that the type of subject who responds to a monitoring exercise over a long period, probably has a conscientious approach to dental health and diet.

Elderton conducted an extensive survey of published work on clinical failure. By exercising an appropriately cautious approach and adding the benefit of results from his own clinical research (30,31), he identified reasons for inherently low quality amalgam fillings. These were, inadequate cavity preparation, poor manipulation of the amalgam (ie.poor filling technique, moisture contamination), poor carving and incomplete removal of caries from the restoration site. Faults that can arise in use, and which are not necessarily closely linked to poor clinical practice, are corrosion (with its subsequent effect upon structural integrity), fracture of the amalgam, and margin leakage (access of mouth fluids into a gap at the restoration interface causing further decay of the tissue). Some further examples of degradation of a restoration are shown in Figure 7.

Some individuals are particularly prone to tooth fracture, where the crack either partially extends into the structure, or a complete section of tissue may fall away (32). One of the solutions for repairing this type of fault, particularly where a cusp of the molar has to be rebuilt, involves a large amalgam restoration which subsequently has to operate in a highly stressed environment. This type of restoration is particularly vulnerable to fracture of the amalgam filling.

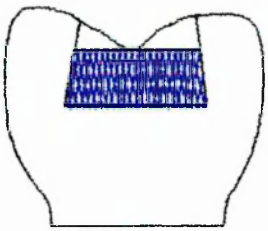

INSUFFICIENT PACKING OF CAVITY LACK OF SUPPORT ON OCCLUSAL SURFACE

(a)

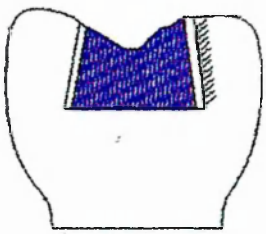

EXCESSIVE CONTRACTION OF AMALGAM (OR SEPARATION OF CAVITY WALLS UNDER MASTICATION FORCES), CAUSES INADEQUATE SEAL AT THE MARGIN.

(b)

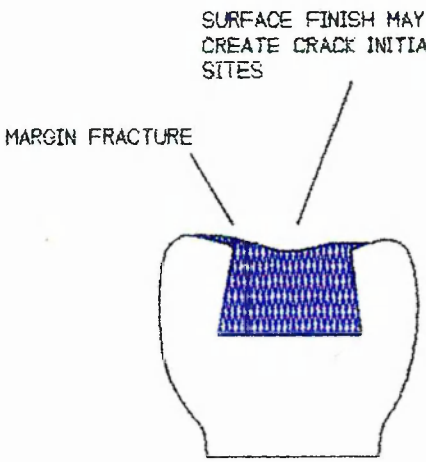

OVERFILLING OF CAVITY AND INADEQUATE CARVING TO FORM

(c)

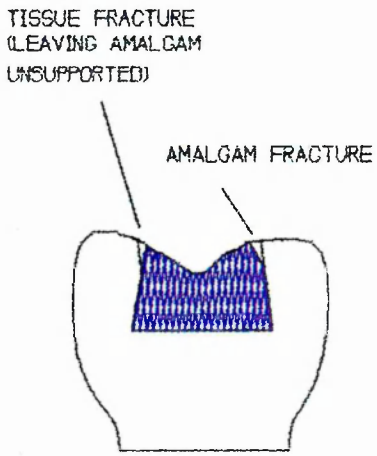

CRACK INITIATION SITES

(d)

VARIOUS TYPES OF FAULT OCCURRING IN RESTORATIONS

Figure 7

I.6. Aims of this work.

The quality of a restoration is influenced by three main factors:

a) the skill of the dentist in preparing the tooth cavity, and in preparing the filling material;

b) the capacity of the filling material to tolerate the highly variable oral environment;

c) undue sensitivity of the filling material to variations in handling techniques.

Amalgam remains a very competetive filling material in the market, and is therefore, the subject of this present work. The current British Standard 2938 (33) for this material only specifies the minimum acceptable values of three characteristic properties, ie. compressive strength at one hour after mixing, creep over a four hour period immediately after mixing, and dimensional changes on hardening over the first twenty four hours. Clearly, this Standard is designed to ensure that the immediate performance of amalgam is clinically acceptable, and it provides quality control for alloy manufacturers.

Cruickshanks-Boyd(34) suggested that the plane strain fracture toughness (K_{IC}) might be a useful means of characterising amalgams and the feasability of this approach is investigated in the present work. The justification for this view is that K_{IC} indicates the tolerance of a material to factors such as surface finish, porosity, composition and environment, and its value would be an accurate reflection of the clinical performance generally.

Hence this work is presented in the following sequence:

a) the metallurgy and laboratory testing of amalgams are discussed in Chapter 1;

b) the method of determining K_{IC} by use of the standard transverse bend test is summarised and the amalgam specimen design is discussed in Chapter 2;

c) the experimental procedure is described in Chapter 3 and the results are presented for four commercial brands of amalgam and two experimental types which represent a range of the different alloy types available;

d) the method used to estimate K_{IC} of the constituent phases of amalgams are reported in Chapter 4. This information is then used to help explain the fracture characteristics of the test amalgams;

e) it will be shown that there are grounds for seeking an alternative method to the transverse bend test, and Chapter 5 describes a novel means of determining K_{IC} by data from the Vickers hardness test procedure;

f) finally, Chapter 6 compares the results of the two test methods and makes recommendations for further development of the fracture toughness approach to performance prediction of dental materials.

CHAPTER 1

THE METALLURGY AND IN-VITRO TESTING OF AMALGAMS

1.1 Introduction

This chapter describes three main areas; firstly, the structural details of the principal amalgams that are manufactured commercially, secondly the in-vitro testing of amalgams, and finally the particular merits of fracture analysis as a means of predicting the in-vivo performance of amalgams.

The nature of the reaction between the alloy powder and mercury is described, using Traditional amalgam to illustrate the main detail. Brief details of two other important types of amalgam are included, namely, those with a high copper content and those with a dispersed-phase structure. Some details are given of the influence that each of the main constituents, silver, tin, copper and zinc has on the properties of amalgam.

1.1.1. Traditional amalgam

Bates (18) suggests that during amalgamation, mercury reacts with the outer layers of the Ag_3Sn (γ) powder to form the body-centred cubic γ_1 phase, and the hexagonal structured γ_2 phase. Detailed information on the crystal structure of the three phases is provided by Fairhurst et al (35,36). The phases resulting from the mercury reaction are often regarded as the matrix in which there is a large number of discrete γ particles. The reaction process is frequently described by: $\gamma + Hg \rightarrow \gamma_1 + \gamma_2 + \gamma$ - the overall

structure comprises approximately 30vol.% γ, (37),60vol.% γ_1(38),and 10vol.% γ_2(39).

The amalgamation process has been variously described as: the wetting of the alloy particles followed by sintering in the presence of liquid mercury (18), and more specifically as; γ_1 forming around the γ particle, generating a reaction zone, followed by the outward diffusion of tin through this zone to further react with the residual mercury to form the γ_2 phase(37,40).

Although there is some difference in opinion regarding the precise equations that define γ_1 and γ_2 formation, it is accepted that the closest whole number stoichiometry gives them as Ag_2Hg_3 and Sn_7Hg respectively. As the alloy particles become coated with crystals of γ_1 and γ_2, the reaction rate decreases. Reaction is further limited because mercury is expelled from the filling under packing pressure(40,41).

It is thought that initially there is some mercury entrapped within the amalgam structure even when mixing is under ideal conditions. This free mercury has been estimated by Wing (42) to be approximately 2vol%, and it enables the reaction to continue for several hours after treatment. In fact, the work of Gayler (43) showed that the 40°C isotherm of the silver/tin/mercury (Ag/Sn/Hg) ternary equilibrium diagram predicts a phase (β_1). In practice this is not detectable until approximately two years after mixing, which suggests that long term structural transformations occur whilst in the mouth. Craig (44) reports that β_1 arises through the interaction between the initially formed γ_1 and residual γ particles and has the composition 45wt%Ag, 8wt%Sn and 47wt%Hg.

Very little work has been reported on the characteristics of the

individual constituent phases, probably because it is very difficult to establish a manufacturing procedure which results in specimens that accurately represent their characteristics in set dental amalgams.

A list summarising the accepted composition of the different phases is given in Table 1.1. Wing (42) and Bates et al (18) have however, independently reported the microhardness values for the constituent phases as: γ 230 - 270 H_V, γ_1 120 H_V and γ_2 which is very soft with a H_V of about 15. Scanning and transmission microscopy analyses of these individual phases have provided useful information on phase morphology, composition and distribution when they exist as components of dental amalgam. Also powder X-ray analysis has enabled the kinetics of amalgamation to be investigated as in the case of Traditional amalgam where it has been determined that both γ_1 and γ_2 develop within ten minutes of mixing.

PHASES PRESENT IN DENTAL AMALGAMS

Identification of phase	Phase composition
γ	Ag_3Sn
γ_1	Ag_2Hg_3
γ_2	Sn_7Hg
ε	Cu_3Sn
η	Cu_6Sn_5
$\alpha+\beta$ (Eutectic) Ratio of $\alpha:\beta$ = 2.5 at mouth temperature.	α is solid solution of copper in tin. β is solid solution of tin in copper.
β_1	45wt%Ag,8wt%Sn,47wt%Hg

	Phases present					
Amalgam type	γ	γ_1	γ_2	ε	η	$\alpha+\beta$
Traditional	■	■	■ (when copper present)	■		
High copper	■	■		■	■	
Dispersalloy	■	■	■ (very low)	■	■	■

Presence of phase is shown by ■ in above table

Table 1.1

1.1.2. High Copper Alloys.

Various alloys have been formulated to provide advantages over Traditional amalgams (45-48) but the elimination of the γ_2 phase is regarded as the most significant improvement that has been made(49-53). An early and reasonably successful attempt to achieve this was to omit tin altogether from the alloy composition by using a mixture of mercury-reacted copper and a silver/mercury amalgam(54). However, the mechanical strength of the resulting amalgam was poor.

Tin has to be present in the alloy to produce the initial γ phase which contributes a significant part of the strength in amalgam. Thus to eliminate γ_2, it is necessary to facilitate the combination of tin with a constituent other than mercury and this is achieved by the addition of a large percentage of copper (up to 28 weight %), to the alloy. The mechanism responsible for the elimination of γ_2 in these so-called high copper, or non-γ_2, amalgams (produced from single melt ternary alloys), is essentially the development of ε and η phases which form preferentially. Figure 1.1 is a photomicrograph of a high copper alloy immediately after casting. The copper-tin and silver-tin regions were detected by X-ray maps and indicate that ε and η could be present before comminution.

Alloys containing high percentage additions of copper show a greater resistance to marginal fracture and lower creep(55) than Traditional types and so also give a superior clinical performance generally.

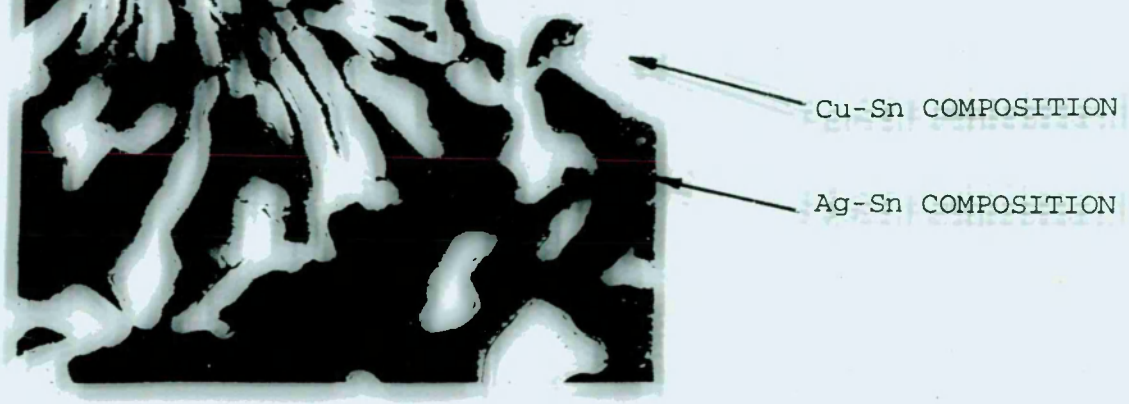
Cu-Sn COMPOSITION
Ag-Sn COMPOSITION

VIEW OF SEGREGATION IN A HIGH COPPER TERNARY ALLOY
BEFORE POWDERING

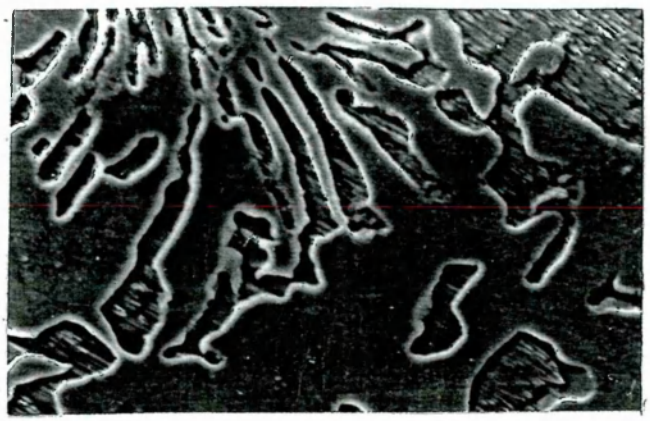

40μm

Cast alloy supplied
by S.S.White Ltd.

Figure 1.1

1.1.3. Dispersed-phase alloys.

Another alloy system where the γ_2 phase is virtually eliminated - approximately 0.5 vol%,according to Darvell (56), resulted in a commercial amalgam known as Dispersalloy(57). The originators of this type, Innes & Youdelis(57), intended to introduce dispersion hardening by the addition of particles of a silver-copper(Ag-Cu) eutectic alloy to the Ag_3Sn ones. However, the large size of the Ag-Cu second phase (~ 20μm) makes this unlikely, and the improved mechanical properties that resulted are more probably due to a second phase hardening mechanism. This improvement in properties, particularly those of creep and fracture resistance, seems to be very dependent upon the the Ag-Cu particle size.

The kinetics of reaction of dispersed phase amalgam involve the

liberation of tin from the γ particles. This liberated tin then combines with copper from the Ag-Cu eutectic to form the η' in set amalgam. About 97 vol.% of the η' phase is located in a 0.5μm reaction zone around the Ag-Cu eutectic (56). The remainder occurs in a further reaction zone around ε particles(58). The suppression of γ_2 is explained in terms of the preferential formation of the tin-rich η' phase. It has been suggested by Boswell(58) that tin diffuses readily at the grain boundaries of ε which produces not only a reaction zone around this phase, but also rod-like η' in the proximity of γ_1.

1.2.0. Alloy Constituents

X-ray data of the crystal structure of the constituent phases are shown in Chapter 4. The compositions of the phases that could exist in dental amalgams are shown in the equilibrium phase diagrams, Figures 1.2 to 1.5 inclusive. The narrow composition ranges over which the phases exist means that they are usually regarded as intermetallic compounds. The exception is the γ_2 phase, which is shown as γ in Figure 1.3. In this case, the tin/mercury ratio of γ_2 has been estimated by powder X-ray analysis techniques. In this section some of the influences that each constituent has on the characteristics of amalgam will now be briefly discussed.

1.2.1 Effect of silver on amalgam

Silver is the major constituent in amalgam alloy powder as dictated by the requirement to obtain the Ag_3Sn (γ) composition.

Although the silver-mercury phase (γ_1) appears in amalgam as approximately equi-axed grains, the high concentration and fast reaction time in relation to the tin-mercury one, results in it adopting the role of a matrix. Thus the remaining two phases ($\gamma+\gamma_2$) in Traditional amalgams are essentially islands within a γ_1 matrix.

The composition of the γ_1 phase is 70wt% mercury and this contributes to the packing characteristics of the amalgam into the tooth cavity. The proportion of silver present in the alloy powder strongly influences the dimensional changes that occur during setting, contraction of the amalgam increasing with an increase in silver. This tendency can be used to offset the expansion that occurs with increasing tin content.

Tests conducted by Young and Wilsdorf(59) on specimens of γ_1 showed that a tensile strength of approximately 13 MPa could be expected, compared with a value of 80 MPa for 24 hour old Traditional amalgams. Clearly, the high volume fraction and low tensile strength of this phase indicate its detrimental influence on the overall strength of the amalgam compared to that of the unreacted γ phase.

1.2.2. Effect of tin on amalgam.

Abbott(60) determined that the production of an alloy of single phase γ corresponds with a 24.6 at% tin content and not the value of 25at% tin that is invariably used for Traditional alloys (this difference is equivalent to 1wt% tin). He suggests that this latter figure results in an alloy occurring in the duplex field $\gamma + \beta$ (see Figure 6 in the Introduction), with the microstructure being in the

form of γ grains with almost pure tin situated at their grain boundaries. The presence of this second phase can have a marked effect on the kinetics of the amalgamation process because mercury preferentially attacks the high energy sites at the grain boundaries of amalgam alloy (61). If these grain boundaries are rich in tin as observed by Abbott, then the amalgamation process will commence with the formation of the predominant tin-mercury phase. This can then flow to the restoration periphery under the action of packing forces as confirmed by Grenoble (62). He found evidence of tin having penetrated the tooth tissue that surrounds fillings (up to a depth of 20μm), the presumed source being the tin-rich restoration margins.

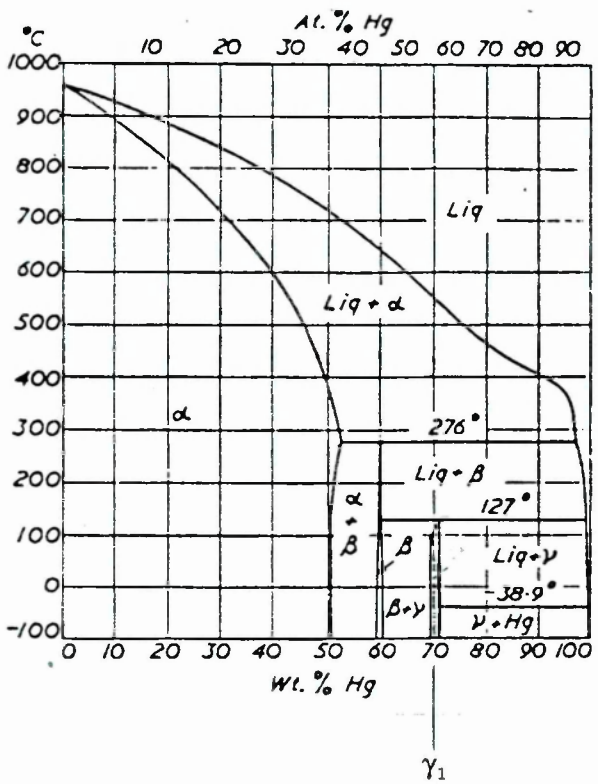

EQUILIBRIUM PHASE DIAGRAM FOR Ag-Hg

Figure 1.2

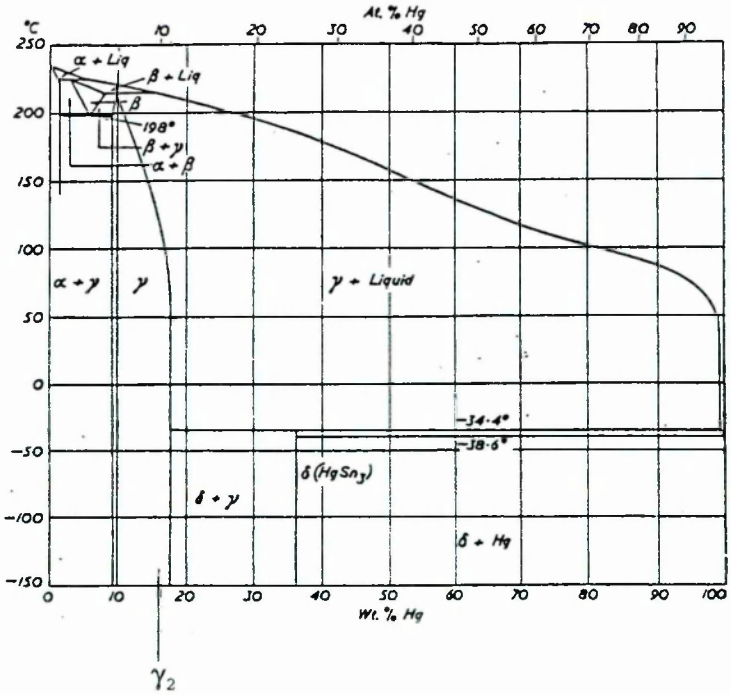

EQUILIBRIUM PHASE DIAGRAM FOR Hg-Sn.

Figure 1.3

1.2.3. Effect of zinc on amalgam.

It is quite common for a small amount of zinc to be included in the ingot melt probably because of its role as a deoxidant in usual foundry practice. No systematic research has been reported on the influence of small additions of copper and zinc on the phase composition of dental amalgam(63).

However, it is known that under ideal conditions the addition of zinc to the alloy is beneficial in providing corrosion resistance to the amalgam. It is anodic in relation to the other alloy constituents and because of this role, it has been suggested that its presence helps to prevent the discolouring effects of the corrosion products, particularly on the γ_2 phase(64). The sacrificial corrosion of zinc in the event of moisture contacting

the amalgam during placement, may give rise to a delayed (or secondary expansion) which can cause extreme pain to the patient(65). This has been overcome in the case of one particular manufacturer by the substitution of indium for the zinc (Brand name 'Indalloy').

1.2.4. Effect of copper on amalgam.

In the Introduction, mention was made of the presence of copper in the alloy and in Traditional powders the amount is in the region of 5 at.%. This copper addition is ignored in predicting the phases in set amalgam but its role is to facilitate the powdering process. It also has a strengthening effect on amalgam, but above 5 at%, it tends to increase expansion to an unacceptable level. The possible reason for the former effect is that copper aids nucleation of the γ phase. This leads to a smaller grain size which subsequently encourages the alloy to break into finer particles during powdering. An advantage of adding copper to the alloy melt is that it may be responsible for providing a precipitation hardening effect in the final amalgam.

Craig(16) reports that when copper is present in excess of the solubility limit of 2.5 wt% (at 37°C), two additional phases, $Cu_3Sn(\varepsilon)$ and $Cu_6Sn_5(\eta')$, may be present in the amalgam.

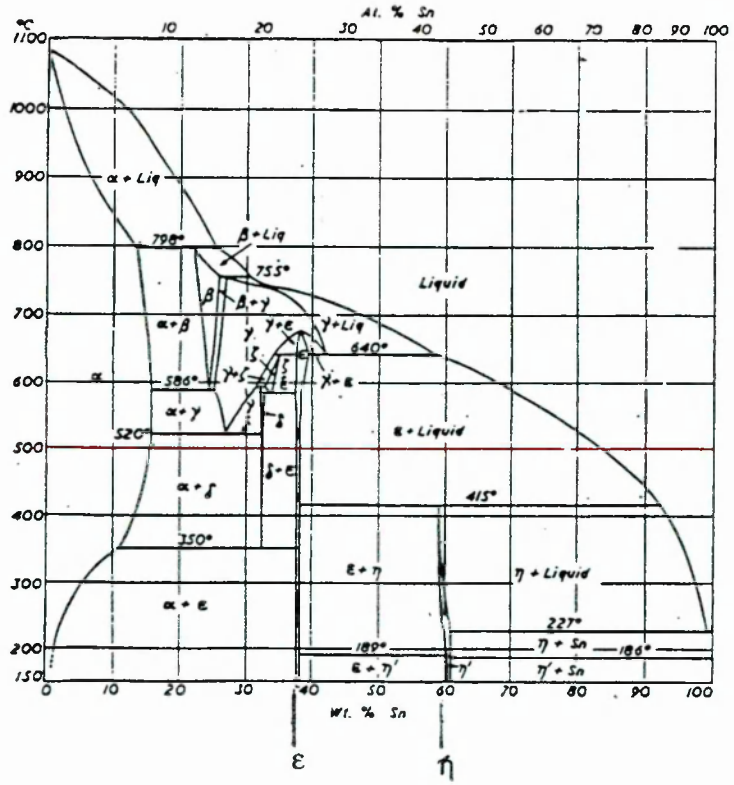

EQUILIBRIUM PHASE DIAGRAM FOR Cu-Sn

Figure 1.4

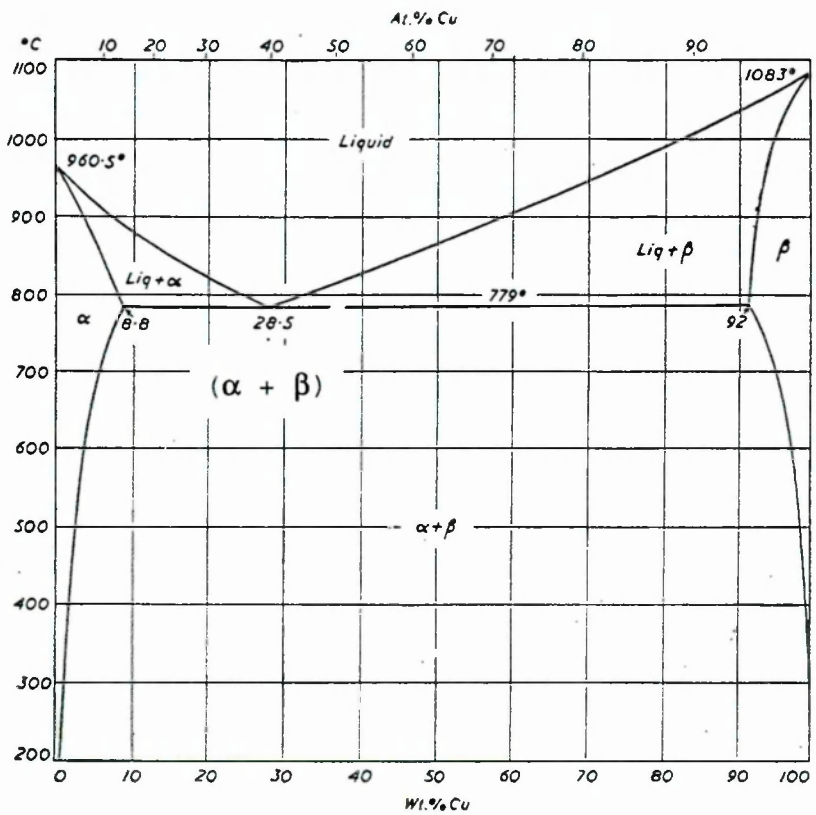

EQUILIBRIUM PHASE DIAGRAM FOR Ag-Cu

Figure 1.5

1.3. Dimensional changes in amalgam.

The dimensional changes that occur in amalgam after packing are important in that they influence the adaptation of the restoration to the cavity wall. A net linear expansion of 0.2% is regarded as clinically acceptable, and is probably of benefit in enhancing retention of the filling material. Beyond this figure it may become the source of extreme pain to the patient. Contraction of the amalgam is generally undesirable because it can cause marginal leakage, loss of retention, and a general reduction in structural integrity of the restored tooth.

Vrijhoef(63) identifies two possible reasons for the occurrence of dimensional change in amalgam. The first he attributes to the elimination, during packing, of the pores that occur in the amalgam and results in a contraction. This consolidation of the amalgam may also be brought about as a result of the creep induced by the action of mastication forces.

The second cause he proposed is due to the mass transport of the constituents. He reports that, depending on the quantity of 'excess' mercury available, phase transformations can occur after restoration is complete which result in a net contraction or expansion, according to the type and condition of the alloy. There exist no appropriate data to be more specific about the extent of the effects of individual phases on dimensional changes.

1.4.0. Alloy:mercury ratio.

It is generally accepted that the ageing procedure is applied

to the alloy powder during manufacture to reduce the high dislocation density at the grain boundaries resulting from the ball-milling operation. However, it is quite possible that the phases comprising the powder may change in proportion or composition and this could equally produce differences in mixing requirements. Another reason for different mixing conditions, and more specifically, different requirements for alloy powder:mercury ratio is attributed to the variations in particle size that exist between commercial brands. A reduction in particle size reduces the length of time that the mixed amalgam remains malleable (i.e. workable). This is because of the accompanying increase in particle surface area/volume ratio, resulting in an increase in reaction rate between the alloy and the mercury. Compensation may be provided by increasing the initial mercury:alloy ratio but this promotes the formation of the weak, and corrosion prone, γ_2 phase especially at the margins of a restoration, an area which in any case is particularly susceptible to failure(42). Clearly, a balance has to be attained between the required reaction rate and its extent, and the workability of the amalgam mass.

The effectiveness of both the homogenisation procedures and the 'ageing' (annealing) process of the comminuted alloy, adopted by manufacturers, accounts for the difference in mixing requirements between commercial brands of Traditional amalgam. The amount of mercury required, and, therefore, γ_2 content can be minimised by the use of rapid-quenched alloys which may be produced in the form of nominally spherical particles by atomization from the melt (61), Figure 1.6. This production method imparts additional benefits, which are; the powdering and possibly the associated ageing

procedures of alloy production are eliminated, maximum strength of the amalgam is attained more quickly, less mercury is needed because of the decreased surface area, and less free mercury. A better restoration surface finish is achievable than with lathe-cut alloys, and lastly, of particular advantage for the filling of children's teeth, is that less packing pressure is required.

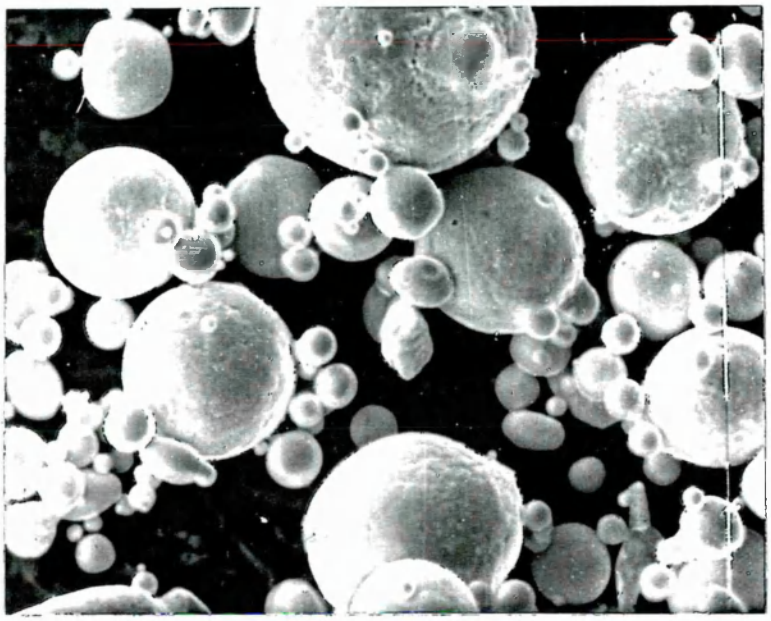

20μm

AMALGAM ALLOY PRODUCED BY ATOMIZING FROM THE MELT

Figure 1.6

Wood et al (66) showed that the grains of Ag_3Sn alloy produced by a controlled atmosphere 'gun'splat quenching procedure were smaller and of greater homogeneity than are achievable by traditional methods. This technique provides a 60% increase in hardness over powdered alloys of the same composition (i.e. surface hardness of γ 380 cf 230 H_v) and the wear resistance of the filling is improved.

Figures 1.7 and 1.8 show some examples of the distribution and morphology of constituent phases in various commercial amalgams of traditional composition. Several independent reports(60,62,67-70) give details of γ_2 occurring in forms other than the approximately equi-axed grain recorded by Wing(42).

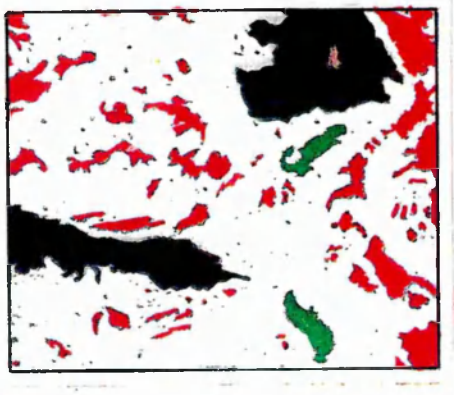

20μm

DIAGRAMMATIC VIEW OF LATHE-CUT TRADITIONAL AMALGAM

Figure 1.7

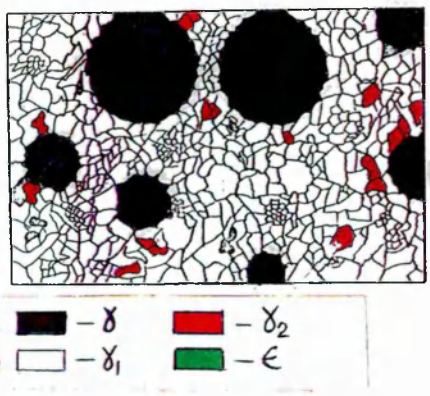

DIAGRAMMATIC VIEW OF SPHERICAL TRADITIONAL AMALGAM

Figure 1.8

One version was essentially a lath-type structure (confirmed in this present research, Figure 1.9). This was evident when the 'excess' mercury that was expelled under packing pressures, was allowed to remain on the amalgam surface at a temperature of 20°C. It was concluded that this structure is not confined to the specimen surface because the ends of the laths could be seen emerging from the plane. When the specimen was placed in an oven at 37°C to simulate body temperature, the lath structure was no longer detectable. This observation is in agreement with Abbott(37) and suggests that the influence of this lath structure on the in-vivo properties of amalgam is difficult to predict. However, this behaviour supports the view that structural changes occur in the early life of an amalgam filling.

Good clinical practice involves the removal of excess mercury

from the filling surface, but this is, of course, not possible at the filling/tooth cavity interface and accounts for the many reports of γ_2 being predominant in this region.

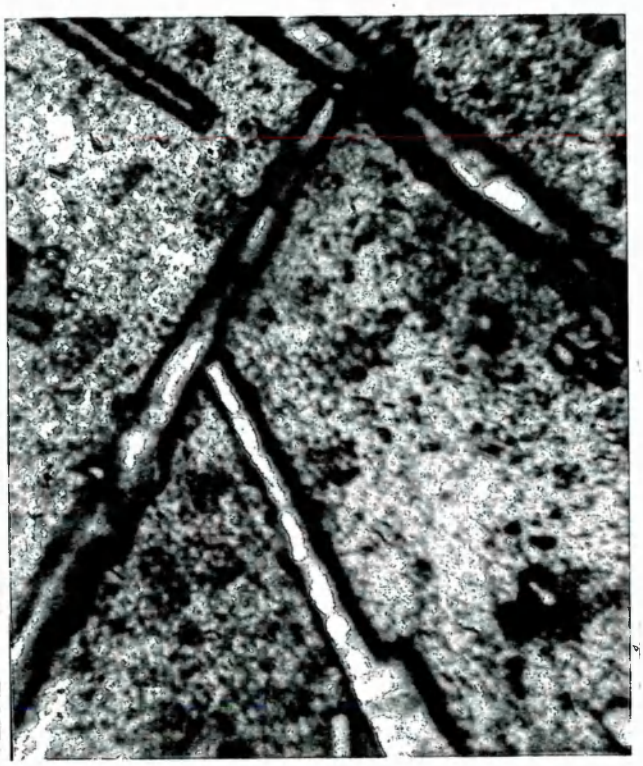

100μm

MICROGRAPH SHOWING LATH STRUCTURE OF γ_2 ON TRADITIONAL AMALGAM SURFACE.

Figure 1.9

Observations of the formation of the laths showed that they are initially very mercury-rich and therefore have sufficient mobility under the action of packing forces to flow into any gap at the tooth/cavity wall interface. It is probable that the γ_2 composition is attained only after further setting time, reaction being most likely with the γ phase.

The mixing and packing techniques used by the dentist strongly influence this proposed sequence of events and thus will have a

significant effect on the mechanical properties of an amalgam. Also, the difficulty in maintaining consistency between specimens is apparent.

Okabe(71) noted that the γ_2 occurred not only as individual laths, or needles, but also in clusters, with a tendency to form an interconnecting three-dimensional network. The SEM of the fracture surface of traditional amalgam, Figure 1.10(a), shows this particular formation of γ_2. Further, there appears to be a natural tendency for pure tin, when reacted with mercury, to form this clustering arrangement, Figure 1.10(b). γ_2 is very vulnerable to corrosion, and this three-dimensional network form means that degradation can penetrate deep into the bulk of the filling. This mechanism is in agreement with that suggested by Jorgensen(72).

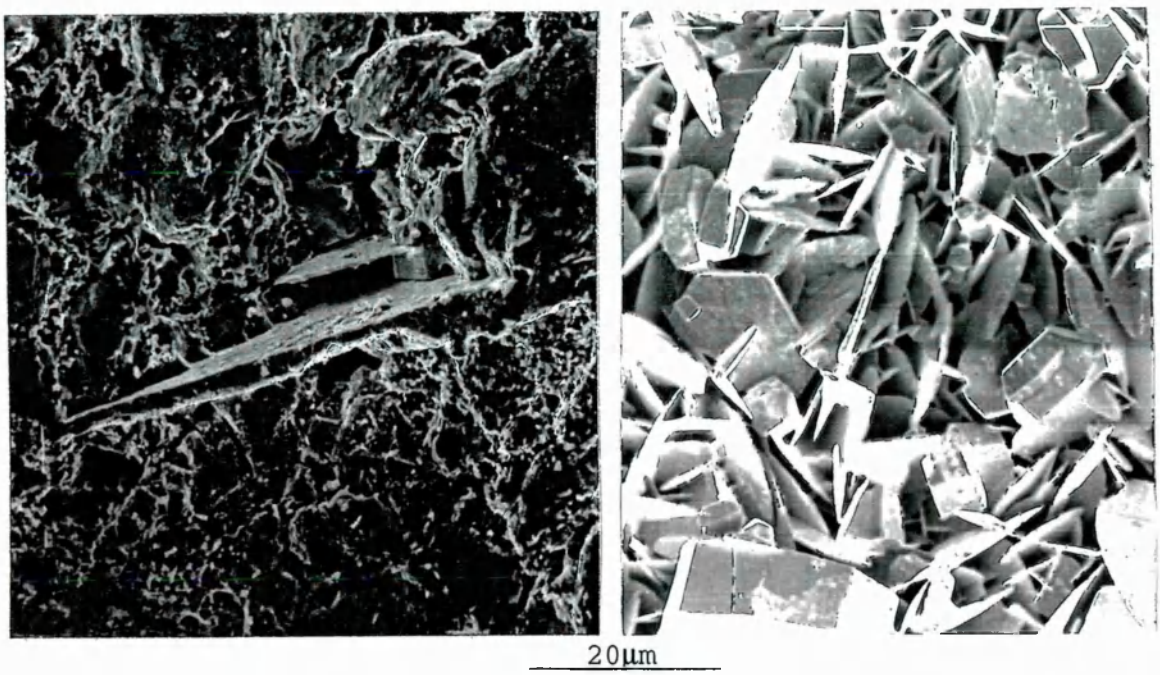

PLATE STRUCTURE OF γ_2 ON AN AMALGAM FRACTURE SURFACE

Figure 1.10(a)

PLATE STRUCTURE OF γ_2 FORMED ON THE SURFACE OF PURE TIN

Figure 1.10(b)

1.5.0. Specimen preparation for optical microscopy.

The morphology of each individual phase of amalgam is clearly of interest in that, as in any structure, it has great significance in the deformation and failure modes likely to occur in service.

Powder X-ray techniques have been used to study single crystals of individual phases(32,67,73) but the microstructure of dental amalgam is difficult to detect by the usual metallographic techniques of polishing and etching (68). This is due to fact that the surface microstructure is affected by the development of an Sn/Hg smear layer on the specimen which masks the surface detail. Also the large difference in hardness between phases makes contouring during polishing evident. The etching reagent and methods recommended by Darvell(67),Makinson & Abbott(73) for γ_2 only,Wing (68) and Allan et al (74), were examined for their effectiveness and the method stated in the last work was found to be the most effective (Table 1.2) and was therefore used in this present work.

Table 1.2

ETCHING PROCEDURE FOR AMALGAMS

Polishing - Progressively finer grades of silicon carbide paper and final polishing is then carried out as follows:
a) 15μm polishing alumina (powder) suspension on a broadcloth.
b) 5μm alumina (No.1) on broadcloth. c) 0.3μm polishing alumina (No.2) on microcloth. The samples are then washed with soap and dried in an air blast. Finally, the specimen is stored in a dessicator for the minimum time possible. **Etching** - Sample is swabbed with solution 4g $K_2Cr_2O_7$, 1g KI, 100ml distilled water for 20 to 40 seconds, followed by a water rinse. This is followed by a subsequent etch as follows: 4g iodine, 96ml ethyl alcohol. Finally, the silver salts that will tend to be deposited out on the specimen surface, are removed with a Hypo swab rinse.

1.6. Characterisation of amalgams

Quality control in the commercial production of amalgam alloy is maintained according to the British Standard 2938:1985 (33) which specifies the values of compressive strength, changes in dimensions during setting and creep. The diametral tensile strength is frequently used for amalgams. This test type is commonly used for brittle materials where the specimen in the form of a disc, is tested in compression across its diameter. Failure occurs in tension on the plane connecting the load application points (Figure 1.11).

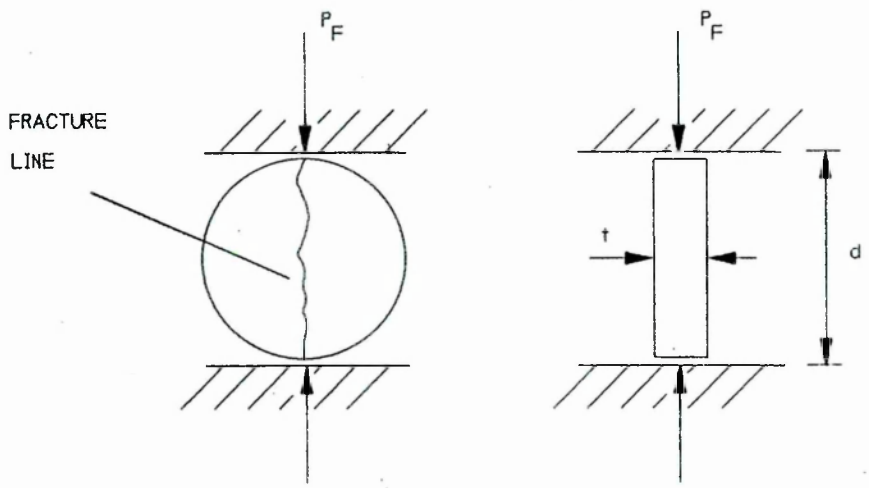

DIAMETRAL TENSILE TEST CONFIGURATION

Figure 1.11

Diametral tensile strength = $P_f/\pi dt$ where,

P_f = fracture force, d = diameter of disc and t = disc thickness.

Examples of results obtained from three brands of commercial amalgams are shown in Table 1.3.

All three of the materials were satisfactory in terms of meeting the minimum standard which ensures that amalgams have a clinically acceptable workability and setting rate. The particular times of testing that have been indicated in the following table are:

a) compressive strength at 60 minutes to ensure that the normal contact force between teeth in the mouth will not prematurely fracture the filling.

b) the dimensional change is based upon the retention of the filling in the tooth cavity.

c) the diametral tensile strength at 15 minutes may be used as an indication of the available working time of the amalgam when the dentist is packing it into the tooth cavity. If the value of this property is excessive, the material is deemed to have a setting rate that is too fast. A lower figure than specified in the table signifies that there is insufficient early strength.

The acceptance of this standard implies that if a test amalgam at least matches the stated property values then it will operate satisfactorily in the mouth.

Table 1.3
PERFORMANCE OF THREE COMMERCIAL AMALGAMS

Material Type (Ranked in order)	Tytin	Revalloy	NTDA	BS 2938:1985 Specification
Compressive strength(60 min)	275.7 MPa	116.2 MPa	110.3 MPa	≥ 50 MPa
Dimensional change (24 hours)	-5μm/cm	+0.04μm/cm	+11μm/cm	-10< >+20μm/cm
Diametral tensile strength(15 min)	6.20 MPa	4.25 MPa	4.15 MPa	≥ 2 MPa
Creep (7 day 37°C)	0.07%	0.82%	0.74%	< 3%

Data supplied by S.S.White Ltd.

Table 1.3 shows that the three test amalgams comply with the required standards specified in BS 2938. Comparison of the materials indicates that differences in clinical performance can be suggested. As predicted (discussion in Section 1.4), the spherical particled Tytin attained higher early strength compared with the other two lathe-cut types. This implies that Tytin has a correspondingly high resistance to early failure. The dimensional change at 24 hours gives an indication of the retention ability of the filling at its interface with the cavity wall.

It is often considered that an increase in compressive or tensile strength results in a corresponding improvement in clinical performance. Also, different amalgams are frequently compared on the basis of their values of ultimate tensile strength (59,75-81) or tensile modulus(82-87). Much of the past research concerned with mechanical property values of amalgam does not give a clear link with the clinical performance. This view is substantiated by the wide range of values that have been quoted for particular amalgams - ie. from 53 to 120 MPa for the ultimate tensile strength (UTS) and 13 to 60 GPa for Young's modulus of high copper amalgams.

The main areas of attention have been on the effects on ultimate tensile strength and Young's modulus of factors such as specimen size and age, test temperature, loading rate, instrumentation, manufacturing and testing techniques(88-90). This approach produces a performance assessment that does not take into account the significant variations that can arise from amalgam preparation techniques and the subsequent effect on mechanical properties(76). The use of techniques such as finite element analysis (1,2,91,92) and of purpose-designed rigs that simulate the dynamic conditions

encountered in the mouth(93,94) have, however, improved the accuracy of prediction of clinical performance.

Laboratory determinations of corrosion and creep characteristics relate more effectively to in-vivo conditions than the UTS and modulus(E) values(95-97).

1.6.1. Creep.

Creep mechanisms for amalgams are significant because their service temperature is usually above their homologous temperature (i.e. above 0.5 x melt temperature (K)). Normal mouth temperature is 310K and the melt temperature of amalgams is approximately 350K. In-vivo creep failure as such has not been identified, but it is widely accepted that it correlates well with marginal fracture (98-100).

Margin fracture has been identified as the most common cause of failure in an amalgam filling and manufacturers interpret the resistance to this in terms of in-vitro creep peformance. One reason for this link is now described.

It has been reported that an amalgam restoration can possess a static stress of approximately 35MPa (94). This condition arises from the elastic deformation of the tooth tissue under the action of packing pressure. The amalgam filling will then experience a uniform compressive stress which will then eventually result in a protrusion from the cavity, Figure 1.12. The overlap at the filling margin is now unsupported and mastication forces will cause fracture at the overhang. Clearly, there is a marked influence of geometry in this degradation process.

The requirement for low creep has to be balanced by the fact that a limited amount of creep is a good thing because the material adapts to the contour of the cavity under the resulting deformation. This subsequently helps to create a seal at the margin between the filling and tooth, thus minimising corrosion and secondary decay(101-105).

Okabe(71) has reported that grain boundary sliding of the γ_1 phase is responsible for the majority of creep deformation in Traditional amalgams. This seems to be a reasonable suggestion because γ_1 is continuous throughout the amalgam structure. Also, body temperature is high for this phase, a liquid phase exists in the Ag-Hg system at 127°C. Even though the γ_2 phase operates at approximately 25% of its melt temperature, its overall contribution to creep is possibly limited by it existing in discrete particles throughout the γ_1 matrix. Creep is also significantly influenced by the surface finish of the unreacted particles(60), and it is minimised if crystals of η' are present in the vicinity of the γ_1 phase. Figure 1.12 shows an SEM view of the needle form of η' as obtained from a melt of copper and tin. According to Okabe (55), the same morphology of η' also occurs in amalgam.

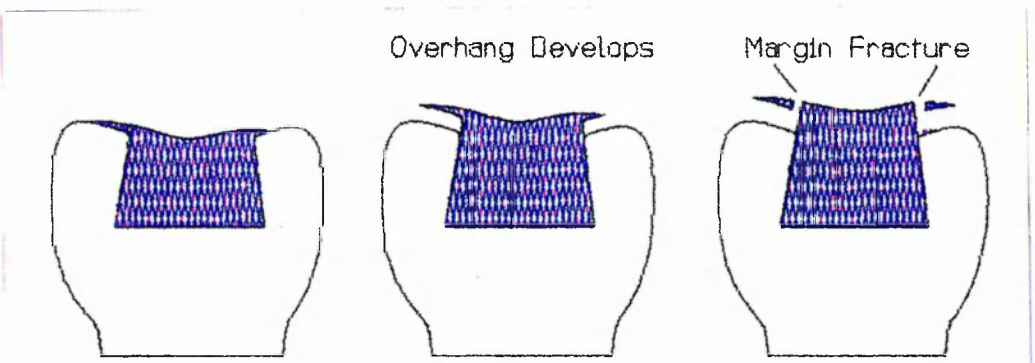

SEQUENCE OF EVENTS
RELATING CREEP TO
MARGINAL FRACTURE

Figure 1.12

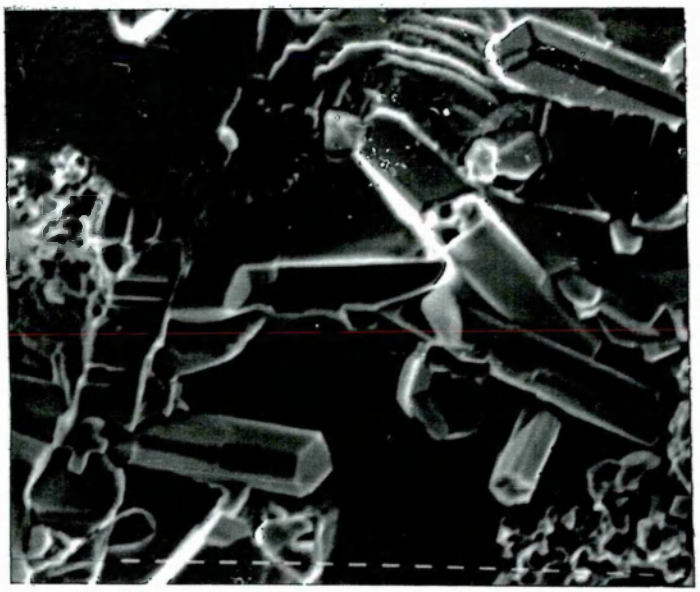

VIEW OF NEEDLE FORM
OF η CRYSTALS.
MANUFACTURED BY
CASTING FROM THE MELT.

25μm

Figure 1.12

1.6.2. Corrosion

The oral environment is a harsh one; saliva contains chlorides, sulphides and oxygen in appreciable concentrations, and forms an effective electrolyte for galvanic action to occur. The pH value of paratoid saliva is 5.7 and that of submandibular saliva is 6.4, Table 1.4. An even more acidic environment is created by the action of the enzymes, that are present in saliva, on food in the mouth. The highly variable conditions that exist in-vivo, in terms of pH and temperature, result in great difficulties in simulating oral conditions for in-vitro tests.

A commonly encountered failure is through the mechanism of crevice corrosion,(106), and an example of the circumstances which can lead to this is now described.

i) A gap can develop between the filling and the cavity wall.

This may be due to contraction of the amalgam that accompanies setting. Alternatively, the gap can develop through deflection of the cavity walls under mastication forces, Figure 1.14(ia). Fracture at the filling margin is also conducive to crevice corrosion, Figure 1.14(ib).

ii) Saliva can then be drawn into the interfacial gap by capillary action,Figure 1.14(ii).

iii) The differential aeration condition between the filling surface and the margin space constitutes a corrosion cell. The anode is in the oxygen-deplete zone (A) and the cathodic area is region (C),Figure 1.14(ii).

An inadequately polished amalgam surface is prone to the formation of plaque and resultant crevice corrosion. Another important in-vivo corrosion mechanism has been described by Vrijhoef(63) which is due to galvanic action. The electrodes of the cell in this case are formed by fillings in proximity and of different composition, i.e. Traditional with high copper. The resulting corrosion current can give rise to a phenomenon known as 'galvanic pain'.

The corrosion rate of an amalgam is influenced by factors such as the amount of dissolved CO_2 (which varies the pH) and the organic substances present which can have a passivating effect, although Guthrow(107) reported that this form of protection is very limited. Johnson(108) suggests that degradation commences when the passive layer is broken down through in-vivo abrasion, for example.

Corrosion occurs on a microstructural scale because of the highly heterogeneous nature of amalgams. The γ_2 phase is anodic relative to γ_1 and the unreacted γ phase is considered to be of

neutral potential under oral conditions. Thus pitting occurs and differential aeration conditions can cause very rapid filling failure, even in the absence of other fillings or margin gaps at the filling/tooth interface. The corrosion products arising in Traditional amalgams involve mainly tin, occurring as stannic and stannous oxide, indicating a marked deterioration of the γ_2 phase. These corrosion products can however have a positive effect when they are precipitated at the interface between the cavity walls and the filling. This is because they act as a margin seal and prevent the penetration of saliva into the area (margin leakage) and minimise the possibility of secondary caries(106,108,109).

Two factors which strongly influence corrosion rate are firstly, the degree of porosity in the filling, and, secondly, the alloy:mercury ratio used in preparation. Thus the clinical variables such as mixing conditions and packing pressure can have a strong influence on the incidence of failure.

High copper amalgams generally have a superior corrosion resistance than Traditional ones although the ability to obtain a better surface finish with the latter group of materials can help offset the effect of the detrimental influence of the γ_2 phase. In this class of amalgams, the phase most prone to corrosion is the η which is to be expected because of its high tin content and correspondingly high electronegativity.

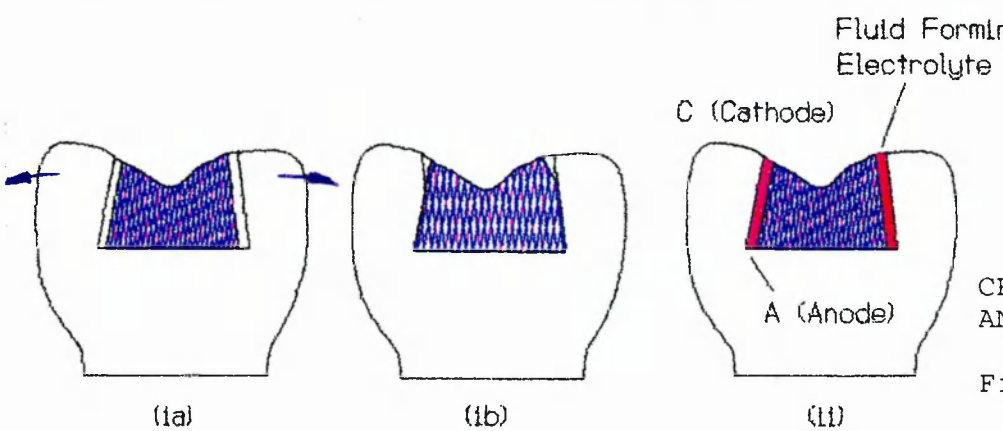

CREVICE CORROSION IN AN AMALGAM FILLING

Figure 1.14

Table 1.4

COMPOSITION AND DETAILS OF HUMAN SALIVA

General note:

Saliva glands are situated at various positions in the mouth and the composition of the secretion depends on the individula gland and the rate of secretion.

The nature of the stimulus has no effect on the electrolyte content, but does affect the enzyme content.

Differences are apparent when samples are from different sides of the mouth, also there are daily fluctuations in pH.

The following shows the composition of a resting saliva, i.e. taken from a healthy adult in the morning before food.

Relative density 1.002	Surface tension (dyne/cm) 15.2-20.6
pH value: Paratoid 5.6	Submandibular 6.4
Water(g/l) 994	Dry substance 6 g/l

Inorganic constituents:

Bicarbonate (mg/l) 2 - 13	Chloride (mg/l) approx.20
Phosphorus:	
Inorganic (mg/l) 250	Organic (mg/l) 55
Fluoride (mg/l) 0.08 - 0.25	Iodide (mg/l) 0.102
Thiocyanate (mg/l) 113	Potassium (mg/l) 20
Sodium (mg/l) 10	Calcium (g/l) 2
Magnesium (mg/l) 0.6	Cobalt (µg/l) 0.1

Nitrogenous constituents

Total nitrogen (g/l) 0.6	Urea (mg/l) 252
Creatinine (mg/l) 5	Ammonia (mg/l) 60
Choline (mg/l) 5	Uric acid (mg/l) 15
Histamine (mg/l) 0.15	Proteins (mg/l) 2.62
Mucins (g/l) 2.7	

Enzymes:

Lysozyme (g/l) upto 0.15	Amylase (mg/l) 1.00

Nitrogen-free substances:

Glucose (mg/l) 26	Citric acid (mg/l) upto 20
Lactic acid (mg/l) 10 - 50	Cholesetral (mg/l) 25 - 500

Vitamins:

Folic acid (µg/l) 2 - 165	Ascorbic acid (mg/l) 2.18

1.7. Discussion.

It can be seen that the approach described so far leads to a design rationale which gives a mainly subjective prediction of in-vivo performance - a conclusion which is in broad agreement with that of Gettelman(110).

The fracture resistance of a material can be described by its fracture toughness, usually determined under plane strain conditions, (K_{IC}) which indicates its tolerance to surface and other flaws. The surface flaws in an amalgam filling can originate from poor surface finish due to inadequate polishing, abrasion in use, pitting corrosion, and sharp features in the filling profile. Further, during the service life of the filling, chewing forces can cause small fragments of tooth or filling to spall, thus leaving a potential fracture initiation site. BS 3928 does not provide a prediction of the performance of amalgams with regard to these factors and therefore this present work considers the use of fracture analysis applied to different amalgams occurring in the categories identified in this chapter. The justification for this approach is that fracture analysis quantifies the tolerance of a material to the service conditions identified above and therefore promises to provide a good indicator of clinical performance.

It could be expected that the difference in powder form and composition as identified earlier in this chapter will produce distinctive differences in the microstructure of the resulting amalgam. The tests reported in this present work focus on material types that occur in three main classes: Traditional alloy, high copper alloy, and finally, dispersed-phase alloy. The commercial

amalgams have the brand names New True Dental Alloy (NTDA) and Revalloy in the first alloy type, Tytin for the second, and Dispersalloy for the third. Further information on the powders is given later, but general views of amalgams made from these alloys, and prepared using the etch procedure given in Table 1.2, are provided below to help identify these major differences (Figures 1.15 to 1.20).

Two further powders were tested, one is a Traditional powder which was manufactured in the laboratory which, unlike NTDA and Revalloy, had no copper addition. This was in an attempt to detect the strengthening effect of small amounts of copper on the resulting amalgam. The other addition to the list of test materials was an experimental high copper alloy in lathe-cut form to enable a comparison to be made with the spherical form of Tytin.

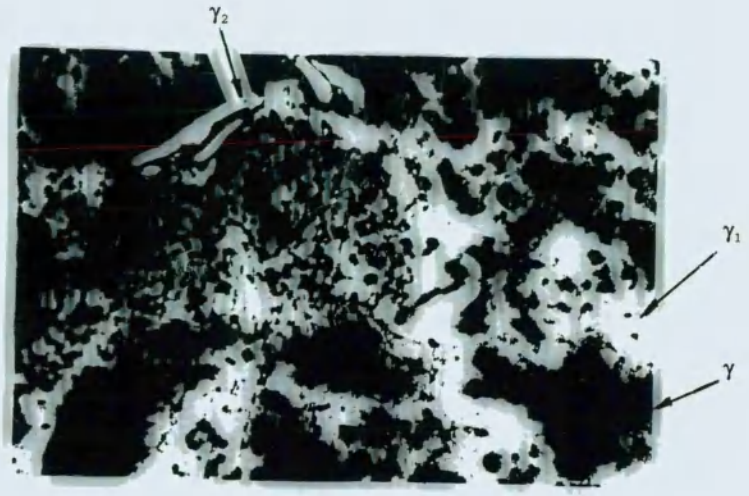
γ2
γ1
γ

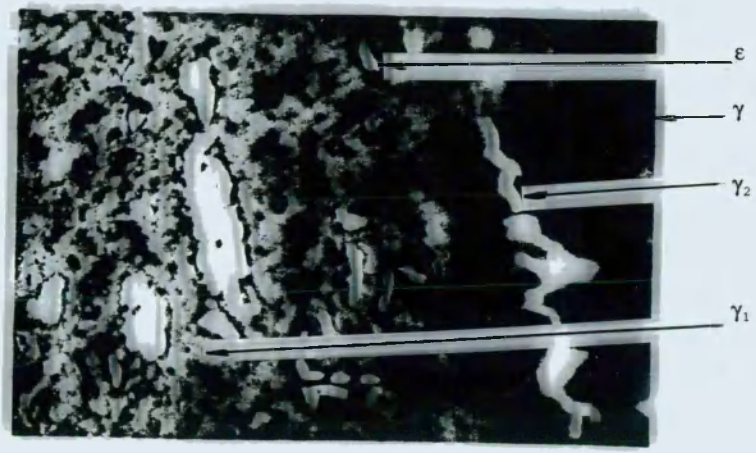
ε
γ
γ2
γ1

Revalloy Lathe-cut -
particle size approximately 30μm

20μm

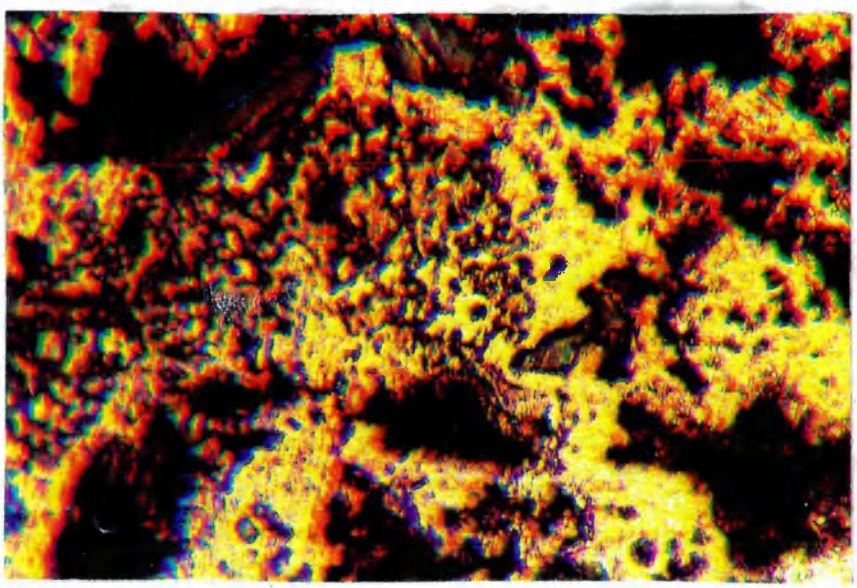

Figure 1.15

NTDA Lathe-cut -
particle size approximately 30 μm

20μm

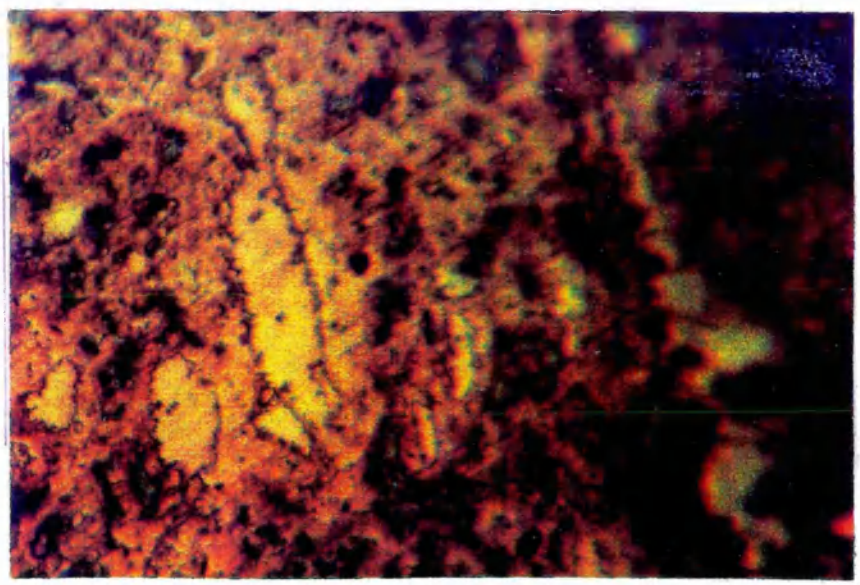

Figure 1.16

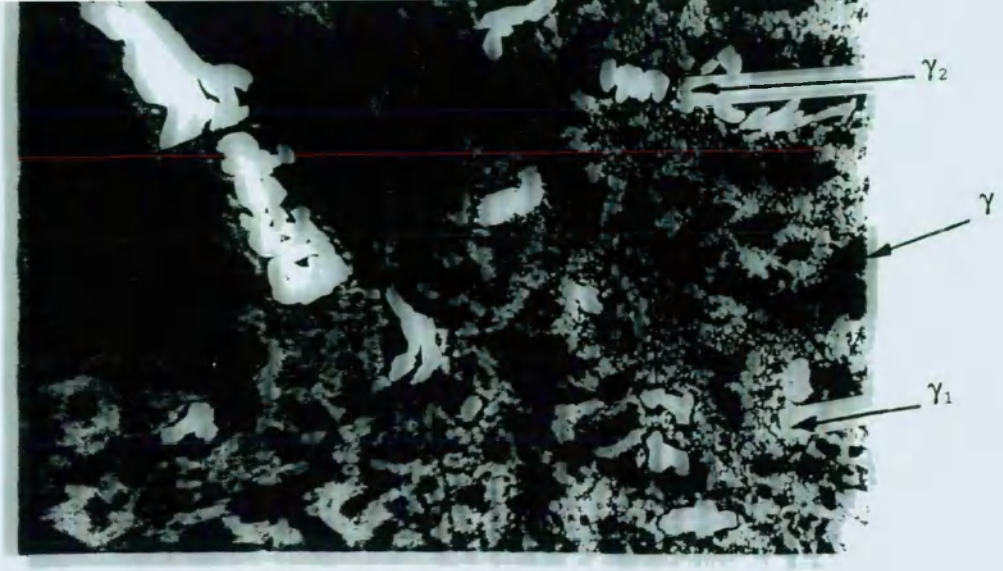
γ_2
γ
γ_1

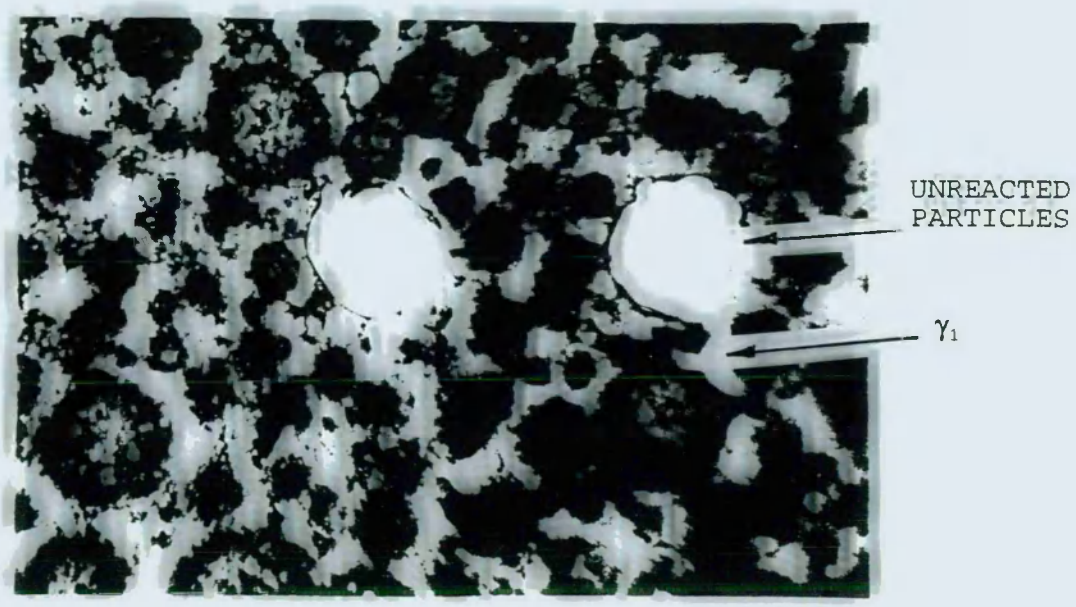
UNREACTED
PARTICLES
γ_1

TRADITIONAL WITH NO COPPER
ADDITION (LABORATORY MANUFACTURE).
Lathe-cut - particle size < 40μm

20μm

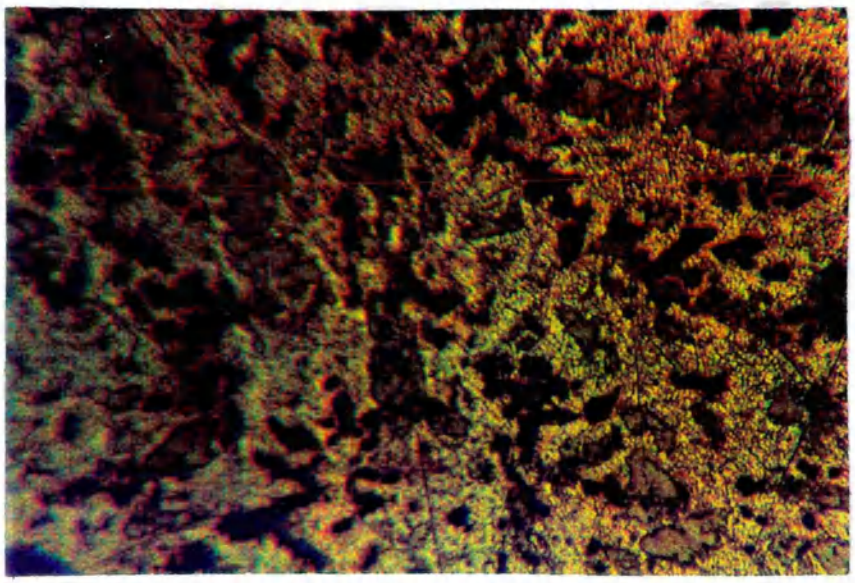

Figure 1.17

HIGH COPPER

Tytin Spherical -
particle size approximately 40μm

20μm

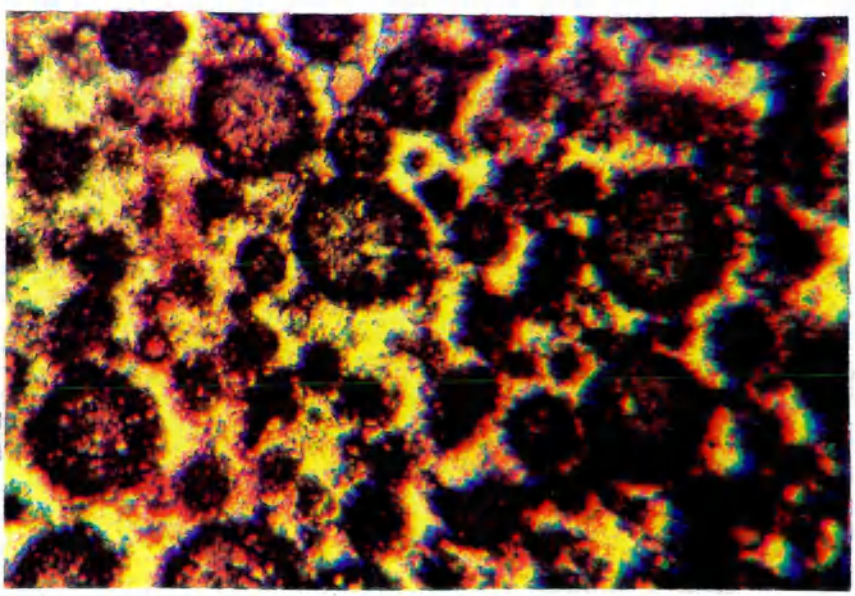

Figure 1.18

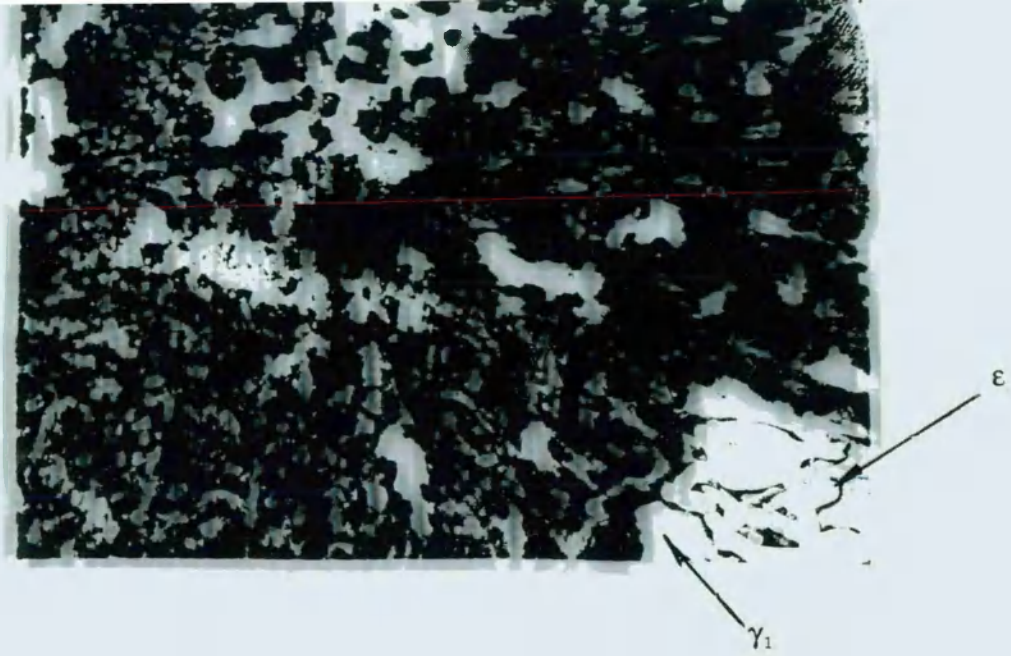
ε
γ1

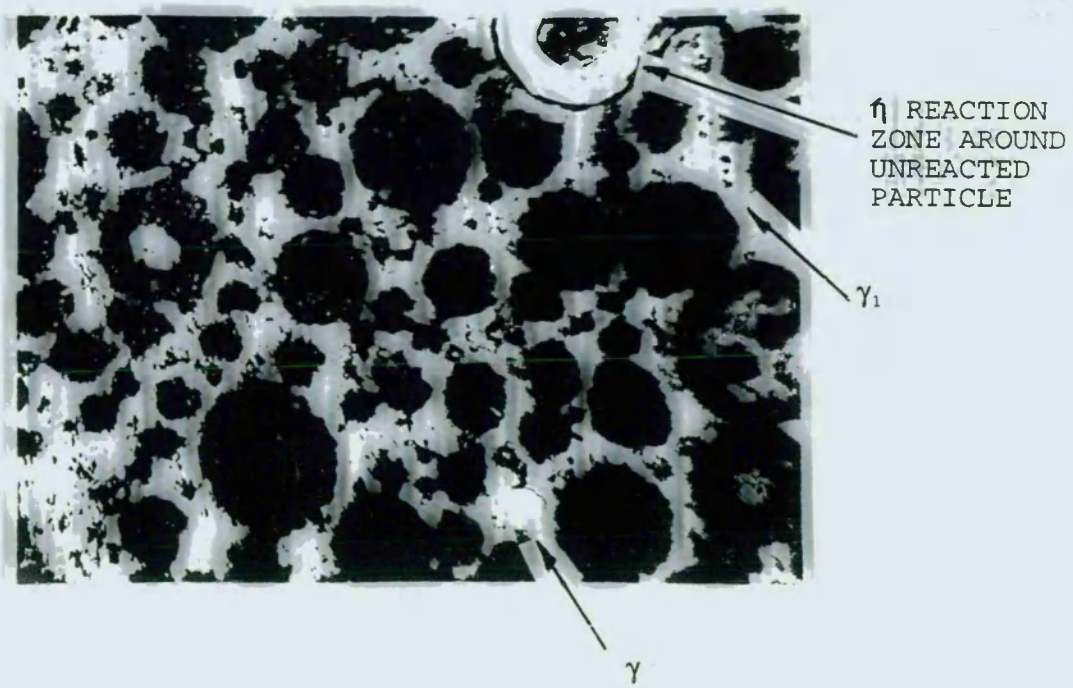
η REACTION ZONE AROUND UNREACTED PARTICLE
γ1
γ

HiCu Lathe cut -
particle size approximately 40μm
experimental alloy

20μm

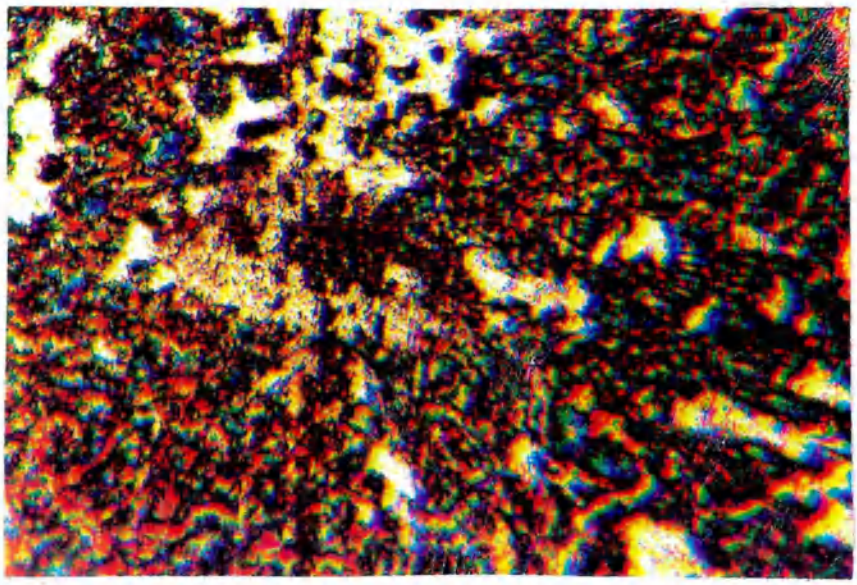

Figure 1.19

DISPERSED PHASE

Dispersalloy
Lathe cut Ag_3Sn + spherical CuAg

20μm

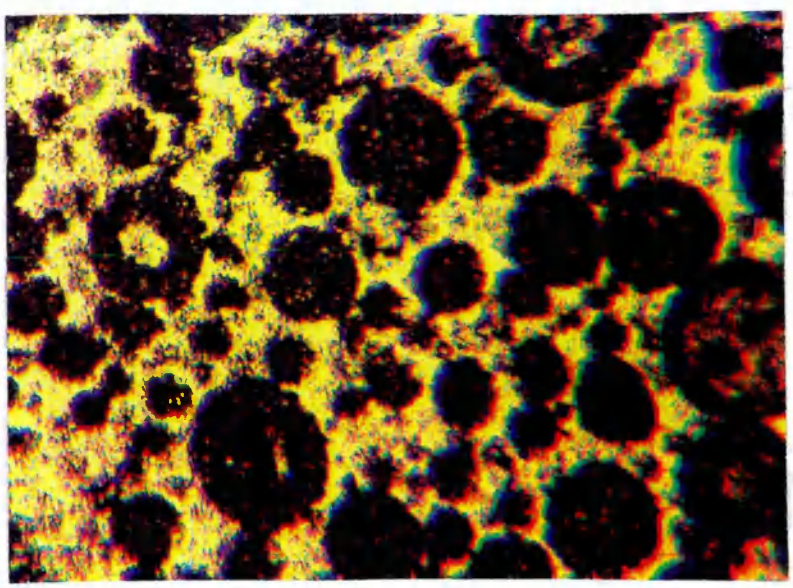

Figure 1.20

The main features to be seen in these views of the amalgams are:

a) the small powder size of Revalloy (average of 30 μm), results in a large proportion of the area being occupied by mercury-reacted phases (γ_1 and γ_2);

b) the spherical shape of the particles of Tytin and Dispersalloy is retained after amalgamation, and reaction is confined to the surface as is generally assumed. The significant proportion of unreacted phase will have an obvious effect on the fracture characteristics of the amalgam;

c) boundaries of γ_1 grains can be seen clearly and show that this phase occurs with quite a small grain size. However, the concentration of this phase is high, which supports the suggestion by previous work that it may be regarded as a matrix for the other, more isolated phases such as γ, and where appropriate, ε and η.

The several phases comprising amalgams have a wide range of hardness which results in difficulties in minimising surface relief and the effects of distortion when polishing. The polishing action in specimen preparation generates sufficient heat to liberate mercury. This mechanism has the potential to promote re-amalgamtion of some of the phases present. The more marked features distinguishable on the photomicrographs of each test amalgam are now identified.

The etching procedure used in this work shows the γ phase as black regions, γ_1 appears as a continuous 'matrix' in which individual grains cannot usually be distinguished and is yellow in colour. Finally, the γ_2 is revealed as pale green areas which are isolated within the matrix.

Revalloy The three main phases present in this amalgam (γ, γ_1 and γ_2) are readily distinguished, Figure 1.15. The γ apparently occurs over a wide size range in the reacted state (3μm to 20μm). This feature has been described by Wing(68) as a manifestation of different extents of reaction according to variation in particle composition. It is equally likely that the apparently small γ areas are the visible parts of larger particles which exist beneath the polished surface. Young et al(80) have established a dependance of tensile strength of Traditional amalgam on γ particle distribution and size.

The texture that is visible at the centre of the photomicrograph view is probably due to artefacts developed during specimen preparation resulting from the mercury liberation referred to above.

It is not possible to identify a copper rich phase even though 2.8wt% exists in the original alloy composition.

NTDA The γ_2 phase in this amalgam type is of the approximately columnar form described earlier in this Chapter, Figure 1.16. This phase occurs as discrete areas in a γ_1 matrix - a similar form to that occurring in Revalloy.

The 3 to 5μm dark green areas are the Cu_3Sn (ε) phase arising from the 2.4wt% copper present in the original alloy melt.

Copper Free Traditional (Figure 1.17) γ occurs in a size range from 6 to 15μm. The remaining part of each unreacted particle is of irregular profile due to the intrusions generated as part of the amalgamation process by the mercury attack at preferential sites on the powder surface. It is possible that these sites play an important role in the influence of the unreacted particle on crack

arrest.

In spite of extensive trials in specimen production, it was not possible to detect either porosity or the individual grains of the γ_1 phase. Silver and mercury react at a greater rate than tin with mercury and this possibly accounts for the isolation of the γ_2 from γ_1. The γ_2 grain dimensions are typically 25 x 7μm, although smaller ones (10 x 5μm) can be clearly seen. The mean free path between γ grains is approximately 20μm which is in agreement with the conclusion of Young et al(80).

The overall view of all microstructures tends to be somewhat blurred. This may be due to a smear layer that originates from the Hg-reacted phases during the polishing procedure.

Tytin This has a spherical particle shape and a much larger copper content than the previous three amalgams (approximately 13wt%). No γ_2 can be detected in the micrograph, Figure 1.18, and it is probable that all the tin is combined with the copper at the alloy manufacture stage to form ε and η. The unreacted particle in the final amalgam is approximately 25μm diameter, although it is apparent that some particles have reacted to a greater extent than others, as shown by a size range from 5μm to 25μm. This is most likely to be determined by the specific composition of an individual particle and its original size.

HiCu It was not possible to obtain a very clear view of this amalgam. The very high copper content (30wt%) produces a particularly high hardness difference between the unreacted particle and the mercury-containing ones.

SEM analysis of the original HiCu alloy showed that the phases present were mainly of ε composition and γ. Tests showed that ε

does not react readily with mercury. The liberation of silver by dissolution in mercury during amalgamation, forms an essentially γ_1 matrix phase which shows as a yellow colour on the photomicrograph, Figure 1.19. Because no γ_2 is visible, it is considered that the tin is retained as ε or forms η during amalgamation.

Dispersalloy The absence of γ_2 as claimed by the manufacturer is confirmed from the view of its microstructure, Figure 1.20. It is convenient to consider the two main components of this alloy seperately, i.e. the lathe-cut Ag_3Sn particles and the spherical Ag-Cu eutectic.

Upon mixing with mercury, the tin from the lathe-cut particles is liberated and subsequently combines with the copper at the surface of the Ag-Cu ones to form a reaction zone. The composition of this zone is η and the feature is readily identifiable on the largest of the particles (those in the region of 20μm diameter), Figure 1.20. It is suggested that the silver of the lathe-cut particles reacts with mercury to form the γ_1 matrix in which the Ag-Cu spherical particles are dispersed.

The width of the η reaction zone is approximately 4μm as scaled from the photomicrograph, which is in agreement with the dimension quoted by Boswell (58). Boswell suggests that the presence of this zone enhances the interfacial bonding between the unreacted particle and the matrix with the potential to improve the mechanical properties of the amalgam.

CHAPTER 2

FRACTURE TOUGHNESS

No material is entirely free of defects and even on a microscopic scale these defects act as stress raisers which can initiate the growth of cracks(111). Fracture mechanics enables a quantitative relationship to be established between the applied stress necessary to cause failure with the size of any defect or geometric feature that can be regarded as a precrack(112).

The first successful criterion of fracture to be employed, resulted from the analysis by Griffith, which was based on the premise that a system will move to a state which lowers its free energy(113). The relationship $\delta U/\delta A \geq \delta S/\delta A$ describes the minimum criterion for a pre-existing crack to propagate. Griffith states that a crack will move if the reduction in elastic strain energy of a body due to an incremental increase in crack length, is greater than the energy required to form the resulting new cracked surfaces.

U = elastic strain energy, S = surface energy,
A = crack surface area.

By considering the specific case of a through-cracked body in an infinitely large plane elastic plate of constant thickness (t) (Figure 2.1) and using the usual relationships between the elastic constants for metals(114), the following can be developed(115):

$$\sigma_F(a)^{1/2} \geq \{2E\gamma/\pi(1-\upsilon^2)\}^{1/2} \text{ for plane strain} \qquad (2.1a)$$

$$\sigma_F(a)^{1/2} \geq \{2E\gamma/\pi\}^{1/2} \qquad \text{for plane stress} \qquad (2.1b)$$

where, σ_F = applied fracture stress.
a = length of the crack or flaw situated at the edge of the specimen from which the crack propagates.
a = half total length of a centre-cracked body.
E = Young's modulus

γ = surface energy of the crack faces.

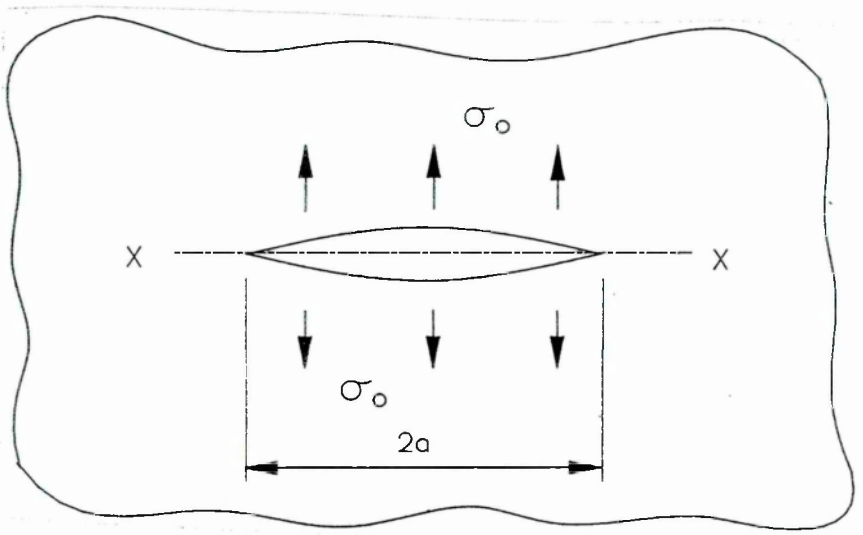

CRACK MODEL AND ASSUMED STRESS SYSTEM (After Bueckner, 115)

Figure 2.1

Further development of Griffith's criterion, results in a term described as the strain energy release rate, $\delta U/\delta a$, which is given the symbol 'G' (116). This attains a critical value (G_c) at the instant at which crack advance occurs and can be regarded as a material constant relating the stress required to cause fracture to propagate from a pre-existing flaw of length 'a'.

$G_c = \sigma_F^2 \pi a(1 - \upsilon^2)/E$ for plane strain (2.2a)

$G_c = \sigma_F^2 \pi a/E$ for plane stress (2.2b)

The connection between γ and G can be shown by considering the maximum of the total energy changes involved in loading a cracked body, i.e. $\sigma^2\pi a/E = 2\gamma$ and substituting in equation 2.2.

There is an implicit assumption in equation 2.1 that the material under consideration is brittle but a more general use of the theory to account for the energy absorbed in plastic flow at the crack tip has been considered by Irwin(116). A crack can be propagated by a combination of three opening modes (Figure 2.2) but the most commonly found failures are due to cracks propagating in predominantly mode I and the theories discussed in the following work will therefore be based upon mode I only.

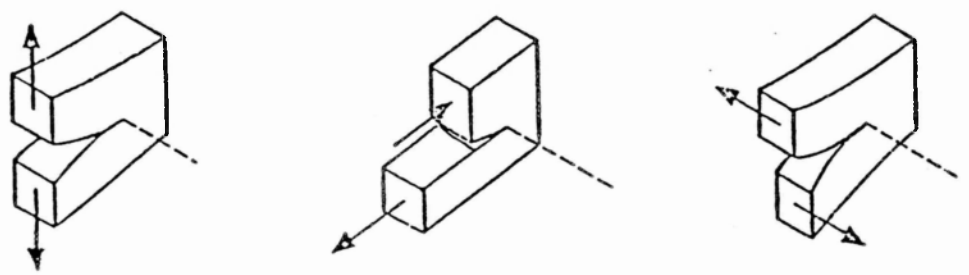

THREE CRACK OPENING MODES

Figure 2.2

2.1. Stress Intensity Factor

Griffith's energy approach does not account for the actual stress distribution near the crack tip and consequently is somewhat inflexible. An alternative model, Figure 2.3, enables a relationship to be developed that describes the stresses at a distance 'r' from the crack tip (where r << a),(117-119).
The stress field at the crack tip is described by:

$$\begin{vmatrix} \sigma_{xx} \\ \sigma_{yy} \\ \tau_{xy} \end{vmatrix} = \frac{K_I \cos\phi/2}{\sqrt{2\pi r}} \begin{vmatrix} 1 - \sin\phi/2\sin3\phi/2 \\ 1 - \sin\phi/2\sin3\phi/2 \\ \sin\phi/2\cos3\phi/2 \end{vmatrix} + \text{converging series in } 'r'$$

K_I in the above formula is given by $K_I = \sigma_{APPLIED}\ (\pi a)^{0.5}$, and is regarded as a crack tip characterising parameter, termed the stress intensity factor.

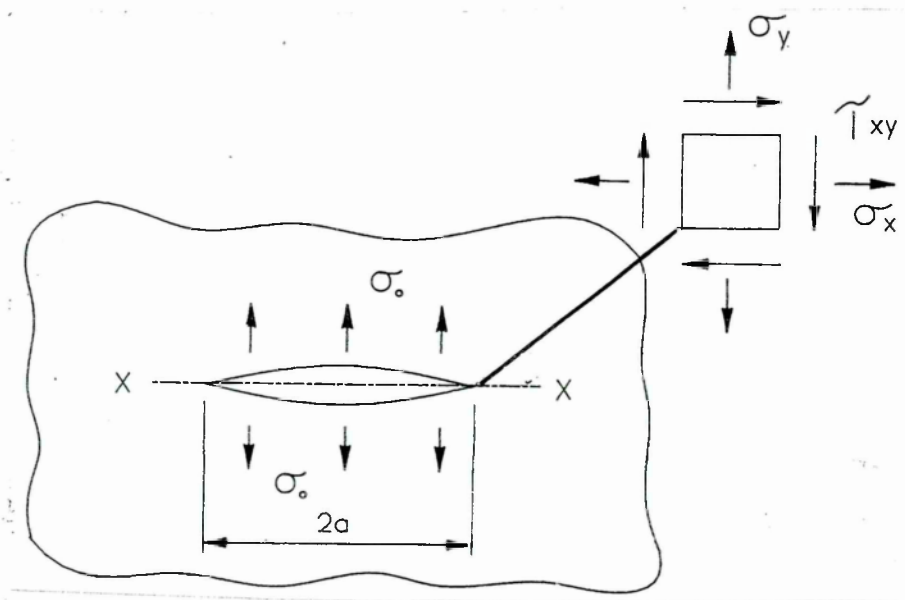

CENTRE-CRACK BASED ON IRWIN'S MODEL

Figure 2.3

The value of K_I for a particular material is dependent upon specimen thickness under plane stress conditions, Figure 2.4. This figure indicates that K_I can be relied upon as a material constant only if the zone, or extent, of yielding is small,(112,120-122), compared with the dimensions of the test piece in the plane of the crack (a and W- a). Also, if plane strain conditions prevail, and fracture propagates from the crack tip, then K_I can be used to characterise the test material - it is then termed the material's fracture toughness(K_{IC}). Amalgams exhibit brittle behaviour as manifested by the absence of any shear lip on the fracture surfaces (Figure 2.5) and the linearity to fracture of the uniaxial tensile characteristics. It is therefore assumed that crack propagation occurs under plane strain conditions in the tests described in the remainder of this present work.

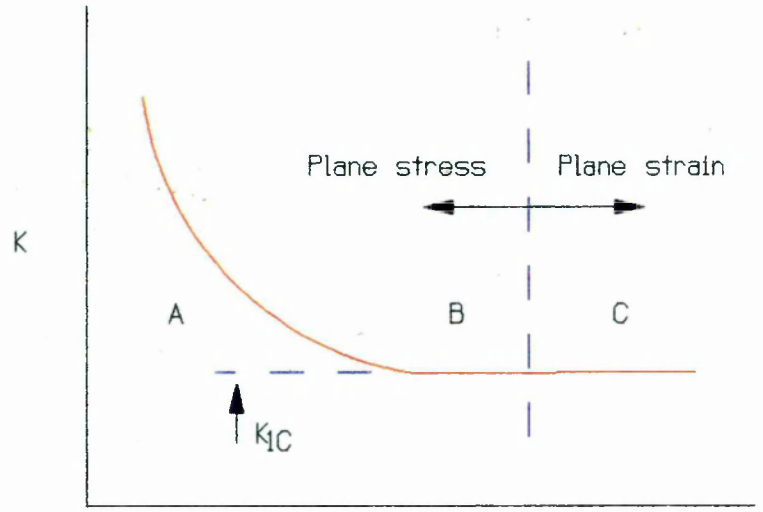

RELATIONSHIP BETWEEN K_c AND SPECIMEN WIDTH 'B'.

Figure 2.4

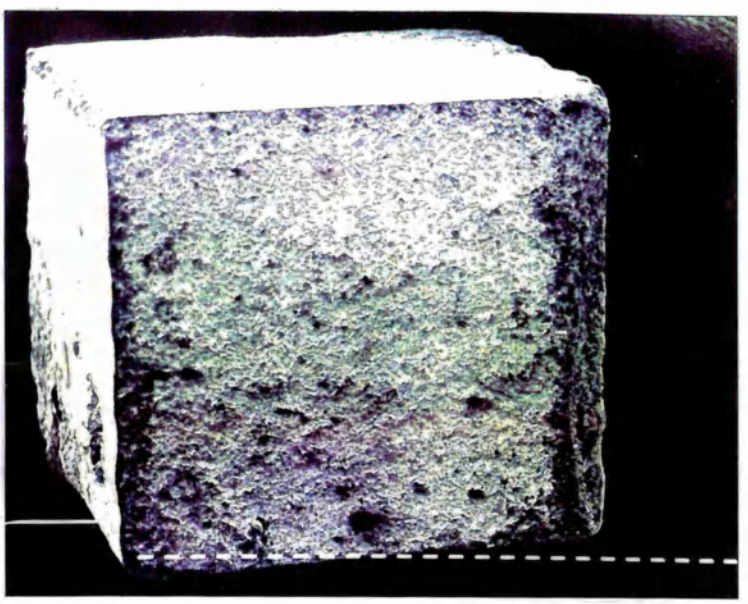

VIEW OF FRACTURED AMALGAM BEAM SHOWING NO EVIDENCE OF SHEAR LIP

Figure 2.5

It can be shown that there exists an equivalence between G_{IC} and K_{IC} showing the consistency between the Griffith's energy balance approach and Irwin's analysis based on the consideration of the stress field in the vicinity of the crack tip (119,123). The advantage of using the K_{IC} approach is that it eliminates the need to evaluate the energy terms required in the Griffith theory.

This present work seeks to confirm that K_{IC} is a material constant when applied to amalgams and can provide a guide to overall performance and that different commercial brands can be compared on the basis of their fracture toughness value.

The conditions assumed thus far are:

a) the cracked body is linear elastic;

b) the crack is situated in an infinite plane body, ie. in practical terms, the plate dimensions are >> a;

c) the crack tip is sharp.

Before the experimental work is described (Chapter 3), it remains to consider the influence of specimen design on the fracture results.

2.2. Effect of specimen geometry on fracture toughness

The relationship, $K = \sigma(\pi a)^{0.5}$ may give a good approximation when applied to large structures possessing small defects. However, the working characteristics of amalgams are such that specimens must be as small as possible. In fact, ideally they should be of a size comparable to that occurring as a filling. Therefore, for the laboratory test pieces of amalgam used in this present work, it is

necessary to take account of the finite boundaries of the small specimen.

There are two specimen configurations that could be used for amalgams, either the single-edge notched type (SEN) which is tested in transverse bending, or the compact tensile specimen (CTS). Details of the latter specimen type are available in BS 5447(120) but presents formidable manufacturing problems for amalgams. It was decided on this basis that this present work should use SEN specimens.

The stress distribution that exists for a specimen of infinite dimensions will be modified by the proximity of the boundaries, the presence of other cracks, orientation of the crack under consideration, and finally, the shape of the crack. In order to characterise a material by K_{IC}, due account must be made of specimen geometry because this has a strong influence on the stress field in the vicinity of the crack tip. These factors are taken into consideration by a technique known as boundary collocation (124-128).

The result of this procedure is a modification to the basic form of equation $K = \sigma(\pi a)^{0.5}$ by introducing a multiplicand 'Y', called the geometry, or finite plate correction, factor. It is expressed as a polynomial in terms of the ratio a/W. For an edge-notched specimen loaded in transverse, three-point bending, the form of equation for K becomes:

$$K_{IC} = (3P_QL/BW^{3/2})(1.93(a/w)^{1/2} - 3.07(a/W)^{3/2} + 14.53(a/W)^{5/2} - 25.11(a/W)^{7/2} + 25.8(a/W)^{9/2}) \quad (2.3)$$

where, P_Q = load at fracture (if the force-deflection characteristic

is linear to the point of catastrophic failure), and all other symbols represent the specimen dimensions as shown in Figure 2.6.

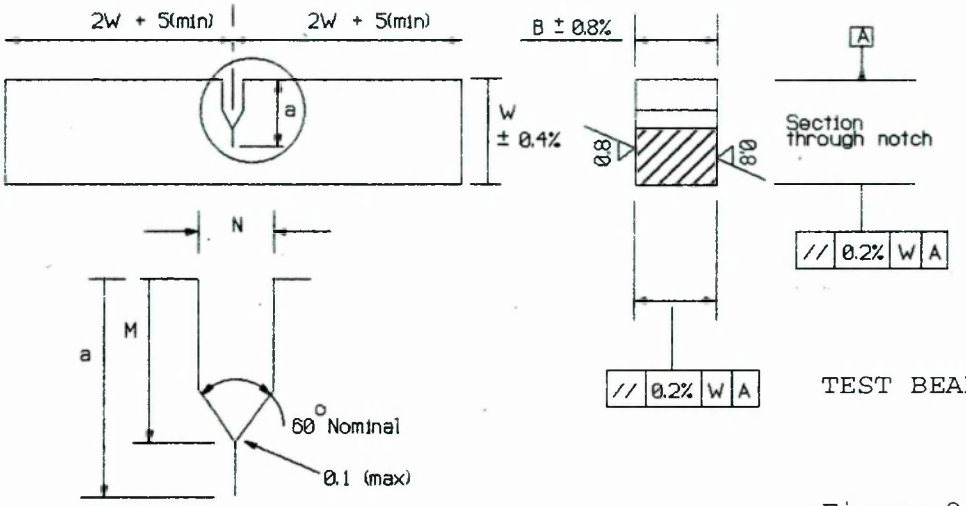

TEST BEAM DESIGN

Figure 2.6

The polynomial is the best fitting form of Y to express K when a/W lies in the range 0.2 to 0.6 (129), and describes the influence of finite specimen boundaries on the stress distribution.

Differences in yield zone shape occur according to specimen size (130) due to the influence of biaxial stresses. A brief explanation is that the stress that is co-linear with the crack (σ_{xx}) assumes different values according to specimen size. The yield zone then spreads under correspondingly different bi-axial stress states. However, the extent of this effect is less in single-edge notched(SEN) specimens than it is in compact tensile specimens(CTS), Figure 2.7. An additional reason for adopting this specimen geometry is because it presents little difficulty in specimen manufacture, thus helping to minimise variability between specimens.

There is some experimental evidence(130,131) which shows that the measured value of K_{IC} may be dependent upon the ratio of a/W used

in the test specimen design, however there are no reports specific to amalgams.

DEVELOPMENT OF BIAXIAL STRESS IN TEST PIECES

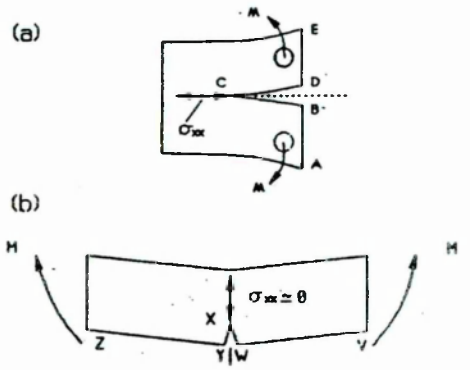

a) In CTS test pieces, the arms ABC, EDC deform like cantilever beams and produce a tensile stress (σ_{xx}) ahead of the crack tip.
b) In SEN test pieces 'arms' such as ZYX,XWV have a high second moment of area to such bending, and σ_{xx} is approximately equal to zero.

FIGURE 2.7

2.3 Fracture analysis applied to amalgams

This is a brief review of the previous reported work that has been concerned with the fracture of amalgams. Over the last decade there has been considerable interest in using fracture toughness as an indicator of in-vivo performance but, in the main, research has concentrated on polymer-based composites (132-135). This particular emphasis is a reflection of the increased commercial interest in composites in recent years. As previously discussed, it is difficult to analyse precisely the reasons for failure of a filling but estimations obtained from analysis of a large sample of cases (28,29,32), was that amalgam fracture accounts for approximately 20% of restoration failures.

Few accounts have been found of K_{IC} determination on amalgam specimens and they do not contain sufficient data to enable any

reliable conclusions to be made, other than that the value is in the range 1 to 2 $MN/m^{3/2}$. These reports either lacked information on the test conditions, or they were concerned with sample sizes of up to four specimens.

Cruickshanks-Boyd(34) provides some useful data but his work was mainly concerned with high copper amalgams, and fracture testing comprised only a minor part of his complete research aims. The values from Cruickshanks-Boyd(34) are shown in Table 2.1. Although his results were not conclusive as regards the strain rate sensitivity of amalgams, they do indicate a possible trend in agreement with the work discussed in Chapter 1 (86,89). This uncertainty arises because insufficient data are available to analyse Cruickshanks-Boyd's work on a statistical basis. The values of K_{IC} for Sybraloy and Tytin are not significantly different and it will be shown that they compare closely with those found in this present work.

There is a clear need, as indicated by Cruickshanks-Boyd, to determine the fracture toughness values for various commercial brands of amalgam under well defined test conditions to determine whether or not they can be used for comparison purposes. Indeed, it must first be confirmed that it is realistic to assign a single value of K_{IC} to any one amalgam type.

Table 2.1

K_{IC} VALUES REPORTED BY Cruickshanks-Boyd(158)

Material	K_{IC}(0.05mm/min) ($MN/m^{3/2}$)	K_{IC}(0.5mm/min) ($MN/m^{3/2}$)
Aristaloy (high copper single melt)	1.98(±0.03)	1.74(±0.06)
Sybraloy (High copper spherical)	1.26(±0.03)	1.09(±0.11)
Ease (Traditional lathe-cut mixed with Ag/Cu spherical)	1.35(±0.13)	No value quoted.
Tytin (high copper spherical)	1.44(±0.08)	No value quoted.

(Figures shown in parenthesis indicate the range of values in test).

Various aspects of fracture, other than K_{IC}, have been reported which are now summarised.

Young and Wilsdorf(80) and Sutfin(136), for example, concluded that fracture occurs through the mercury reacted phases (γ_1 and γ_2). However, it was noted that after the alloy powder had been subjected to an acid wash procedure, fracture also propagated through the γ unreacted phase. This feature may be explained in terms of the change in surface topography that would result from this acid treatment. Manufacturers often employ this acid wash on the basis that it removes any oxide layer on the powder surface and subsequently enhances the interfacial contact with the mercury-reacted phases. However, it is also possible that some preferential etching of the powder might occur, thus forming a mechanical key between the mercury-reacted phases (regarded as the matrix), and the unreacted remains of the powder particle, thereby

significantly changing the interfacial characteristics of the composite towards an advancing crack.

Evidence of the degree of influence that alloy powder production methods have on the long term performance is provided by Sutfin who noted from SEM studies, that in the case of lathe-cut alloys, the machining marks were still evident on the powder surface even when it existed as a component phase of amalgam. Not unexpectedly,these marks were considered to be a source of weakness within the structure. They noted by SEM that when the crack occurred through an unreacted particle, its path was seen to coincide with these marks. This was not evident in this present work, however the notch effect of the machining marks would lower the K_{IC} compared with a smooth particle surface.

It is reasonable to suggest that amalgam made with spherical particle alloy powders would show a fracture path that is mainly confined to the mercury reacted phases. This is because of the absence of the surface irregularities arising from the production technique. The additional energy absorbed in diverting the crack in this manner could be expected to raise the fracture toughness of spherical powder amalgams compared with lathe-cut types.

Younis(137) has reported that specimen age has a marked effect on the force required to initiate fracture. By comparing two day specimens with ones that had been stored for four months, he noted that this force could double in value - the actual figure depending on the amalgam type. Thus, it could be expected that K_{IC} also would increase according to the specimen age.

Figure 2.8 shows a photoelastic model beam under three- and four- point bending demonstrating the different stress distributions

according to the load conditions. The values of the coefficients of a/W in the polynomial describing the compliance factor, allow for the stress conditions applicable to each case. The literature search did not reveal existing comparisons of results under different loading modes (ie. 3- and 4-point loading). In theory, use of the appropriate relationship for 'Y' should yield the same K_{IC} result from a test on a specific material type. The accuracy of this assumption will be particularly relevant to highly brittle materials that exhibit little, if any, signs of yield. However, it is likely that the four point case will give less scatter of results within a batch because the bending moment on the beam is constant over the notch area, and fracture conditions should be more representative of the material characteristics ie. not so sensitive to slight assymetry in loading.

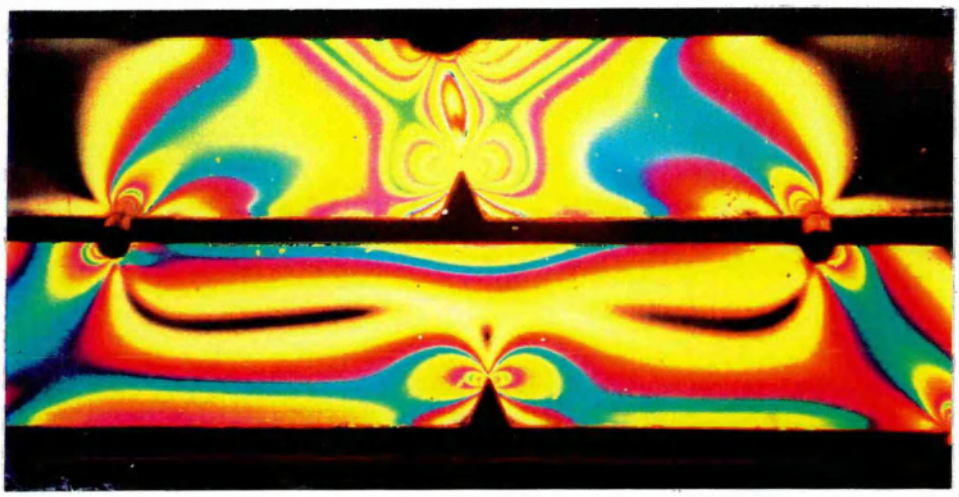

PHOTOELASTIC MODEL OF STRESS DISTRIBUTION
IN 3- AND 4-POINT LOADING

Figure 2.8

Koblitz(138) used a cylindrical specimen design with a chevron notch shape, Figure 2.9. His values of K_{IC} were very much lower than those quoted by Cruickshanks-Boyd (in the region of 0.8 $MN/m^{3/2}$ for both Sybraloy which is similar to Tytin,and Aristaloy). It was noted that Koblitz did not report the crosshead speed used for his work, and the radically different specimen geometry may account for the differences.

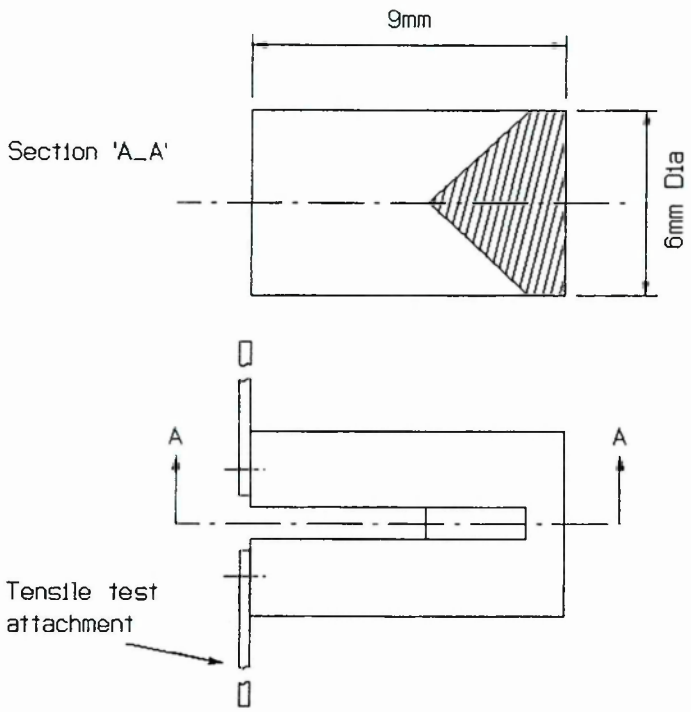

CHEVRON NOTCH SPECIMEN (After Koblitz,138)

Figure 2.9

2.4. Summary

In reviewing literature for this chapter, it became obvious that much experimental test experience lies behind the accepted rules for validity of K_{IC} (120) as, for example, in BS 5447 and the work of Morozov (139). In the present work K_{IC} is to be determined for a range of dental amalgams to see if it can be used to characterise these material types and to distinguish between commercial brands on the same basis. A direct interpretation of the in-vitro test results to in-vivo circumstances will not be considered.

The aims of this section of the experimental work were to provide the information that has been identified as lacking in current knowledge, and they are summarised below:

i) To assess the effect of test-piece configuration on K_{IC} for dental amalgams as follows:
   a) a/W value - Traditional amalgam was chosen as the subject of this test;
   b) 3- and 4-point loading.

ii) To investigate how specimen age influences K_{IC} and to consider the optimum ageing time if such tests are used to assess commercial amalgams.

iii) To apply statistical analysis to determine if K_{IC} can be used to characterise different types of dental amalgams.

iv) To discuss the microstructural features that lead to differences in the value of K_{IC}.

CHAPTER 3

FRACTURE TOUGHNESS TESTING OF DENTAL AMALGAMS

A range of amalgam types was tested comprising four commercial brands which occur in the three categories described previously. In addition, there are two further alloy powder types, namely: a Traditional composition with no copper addition, and an experimental high copper alloy.

Each alloy type produces a quite distinctive structure and it was anticipated that each amalgam microstructure could have been qualitatively related to its K_{IC} value.

Brief details of each alloy type are now given in order to emphasise the difference between them (Figures 3.1-3.6). The method of specimen manufacture is then described, followed by a summary of the K_{IC} results.

3.1. Choice of test materials.

3.1.1. Traditional alloy.

Revalloy - This is a commercial lathe-cut alloy of approximately 25μm particle size (Figure 3.1). It is basically of Ag_3Sn composition, but has a small quantity of copper and zinc added to the melt (Table 3.1).

NTDA - This commercial alloy is very close to the composition of Revalloy and the principal difference is its significantly greater particle size (Figure 3.2). It is expected that this characteristic will result in a larger unreacted γ particles existing in the amalgam microstructure with an associated effect on fracture toughness.

Traditional powder - This lathe-cut alloy of 40μm size was produced in the laboratory (Figure 3.3). The alloy was manufactured to a precise silver:tin ratio, a factor that has been discussed earlier (see Section 1.2.2). No copper or zinc was added to the melt.

3.1.2. High copper alloy

Tytin - This commercial brand is a ternary alloy (Table 3.1) of spherical particle form (Figure 3.4). It contains 13 wt% copper, with a corresponding reduction in silver. The tin content is comparable to the Traditional types and as a result, there are three mercury-free phases in the set amalgam, namely, Ag_3Sn, Cu_3Sn and Cu_6Sn_5.

HiCu - This alloy was an experimental one being investigated by S.S.White Ltd. It has a very high copper content (Table 3.1). Two versions were used as follows:

HiCu(1) Silver and tin were melted together initially, and then the copper added subsequently.

HiCu(2) Copper and tin were melted together initially, and then the

silver added subsequently.

In both cases, the powder was produced by lathe-cutting and it was noted that it had a poor surface finish compared with the Traditional types (Figure 3.5). It is not clear what effect this feature will have on the strength of the amalgam.

3.1.3. Dispersed-phase alloy

Dispersalloy - This commercial alloy comprises a spherical copper-eutectic powder which is added to a lathe-cut Ag_3Sn powder (Figure 3.6). Table 3.1 shows that the overall composition has a significantly lower tin content than other test powders.

Table 3.1

COMPOSITION OF COMMERCIAL AMALGAMS

Material	Chemical Composition(wt%)			
	Ag	Sn	Cu	Zn
Revalloy	70.5	25.8	2.80	1.10
NTDA	70.9	25.8	2.40	1.00
Ag_3Sn	74.0	26.0	00.00	0.00
Tytin	59.4	27.8	13.00	0.00
HiCu #	41.2	27.8	30.00	1.00
Dispersalloy	69.7	17.7	11.90	0.00

Composition detail supplied by S.S.White Ltd.

REVALLOY POWDER

Figure 3.1

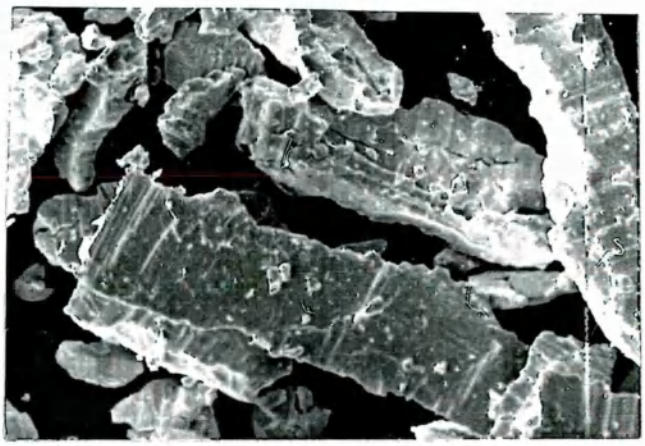

80μm

NTDA POWDER

Figure 3.2

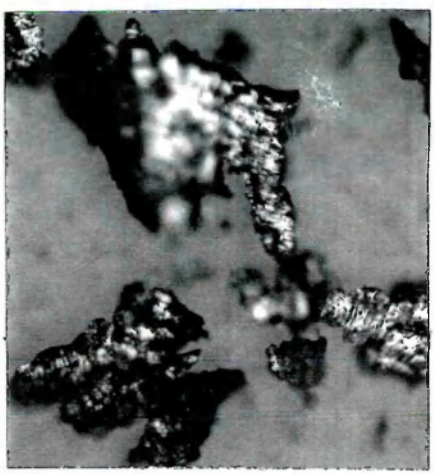

TRADITIONAL POWDER

Figure 3.3

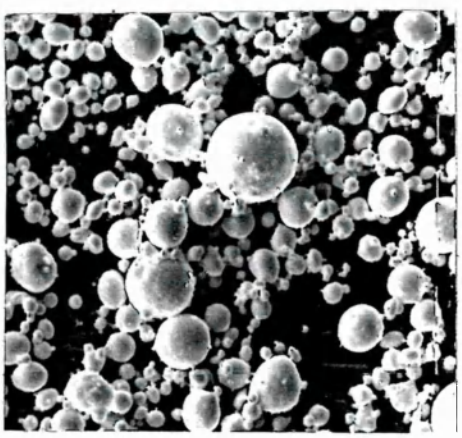

80μm

TYTIN POWDER

Figure 3.4

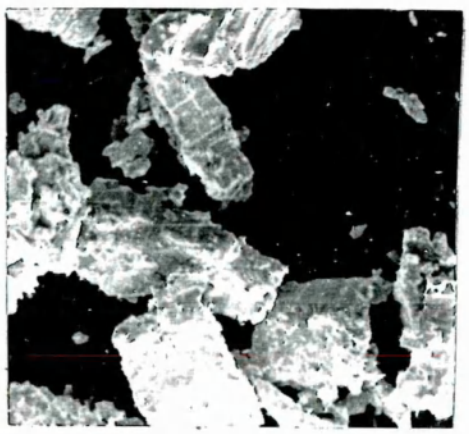

HiCu POWDER

Figure 3.5

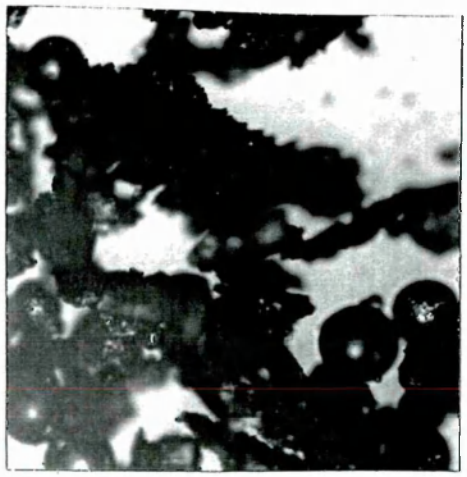

80μm

DISPERSALLOY POWDER

Figure 3.6

3.2. Specimen preparation.

The alloy powder with the appropriate quantity of mercury was dispensed into a capsule to enable the amalgamation to be carried out in the usual way. The table below shows the mixing conditions specified by the different manufacturers. It will be noted that in some cases, a pestle is required for mixing. This is a small, standard size cylinder of steel which is placed in the mixing capsule and its role is to enhance the interaction between the alloy powder and mercury.

Material	Alloy/Hg Ratio	Mixing Time
Revalloy	1:1.20	25s (Pestle)
NTDA	1:1.40	20s (No pestle)
Ag_3Sn	1:1.00	25s (Pestle)
Tytin	1:0.77	25s (No pestle)
HiCu	1:1.20	25s (Pestle optional)
Dispersalloy	1:1.00	25s (Pestle)

The mass of the specimen was 6 grammes and it was necessary to mix the alloy and mercury in two batches just prior to packing it into the mould (Figure 3.7). A static load was then applied to the specimen so that setting occurred under a pressure of 14 MPa. With this amount of amalgam the specimen was produced in a very short time, which helped to minimise void formation by ensuring that reaction is capable of occurring at the batch interfaces. Twenty four hours later, the specimen was removed from the mould and was then available for fracture testing.

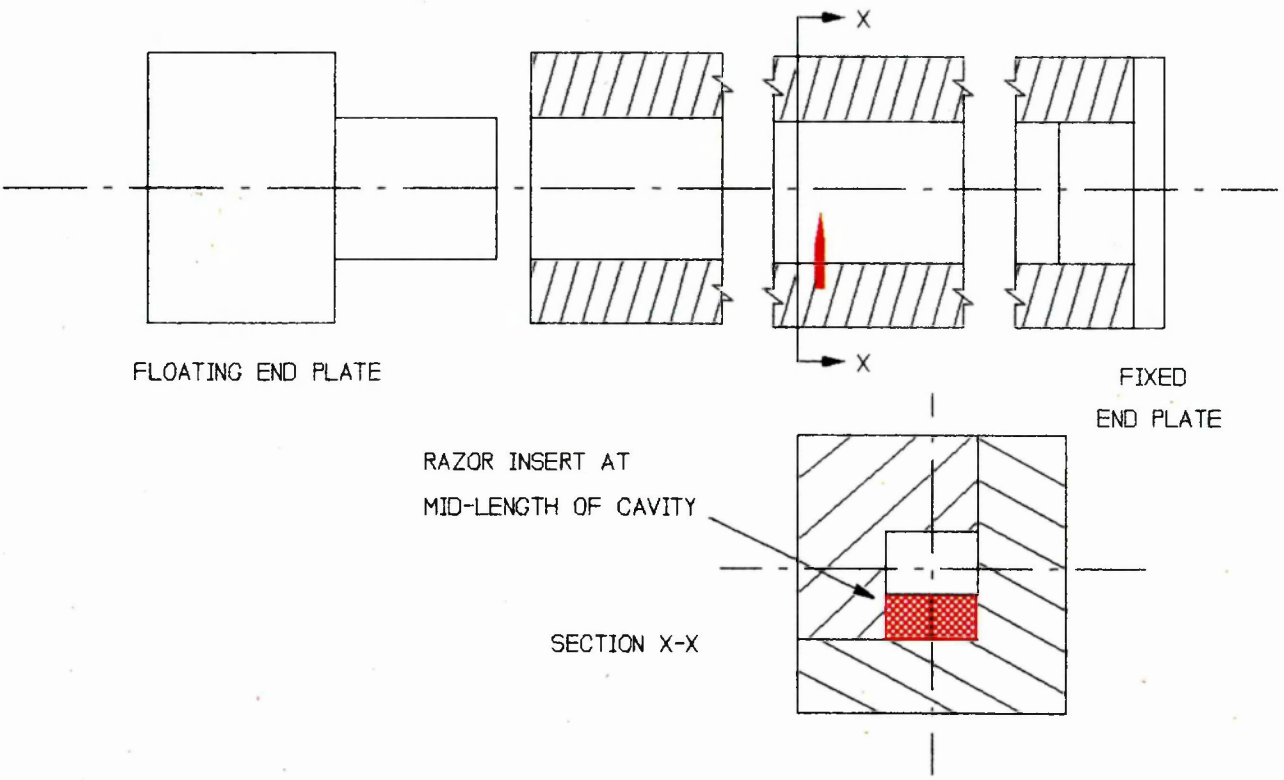

SPECIMEN MOULD DESIGN

Figure 3.7

The specimen mould incorporated a razor blade insert so that the required notch was automatically formed during the packing operation. In conventional testing, the next procedure is to fatigue a crack from the notch root to sharpen this region. This procedure is difficult with amalgams and introduces an unacceptably high specimen scrap rate. Cruickshanks-Boyd(34) tested amalgams with and without a fatigue crack and found that there was no significant difference in K_{IC} between the two conditions. It was decided to omit the fatigue stage and use the specimens with a moulded-in notch only for this present work.

The specimen dimensions (Figure 3.8) and its proportions, were in accordance with the recommendations of BS 5447.

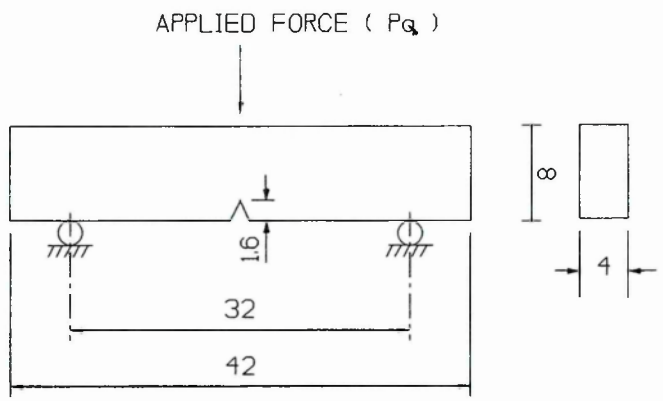

THREE - POINT SEN BEND SPECIMEN

ALL DIMENSIONS
IN MILLIMETERS

SPECIMEN GEOMETRY FOR THREE-POINT LOADING

Figure 3.8

This standard is in agreement with the specimen design used by Lloyd(134) and it results in a good combination of ease of handling, efficient use of material and meets the conditions that result in minimum error between the actual stress incurred and the theoretical stress (derived from $M/I = \sigma/y$), which is used in developing equation 2.3 (140,141).

The maximum size of the amalgam specimens was limited by two factors:

i) The high cost of amalgam which acted as a restriction on supply.

ii) Voids can develop during the packing of amalgam into the test specimen mould which have a subsequent deleterious effect on K_{IC} value. For large specimens, these voids are more likely to be trapped within the structure and clearly the smallest specimen size possible must be used.

The load cell range and output amplification were selected according to the recommendations of Tattersall and Tappin(142). The risk of specimen breakage when it was extracted from the mould gave rise to a preference for the smallest possible value of a/W for which the compliance factor 'Y' is valid, ie. a/W = 0.2 instead of the usual value of 0.5 recommended in BS 5447.

The value of K_{IC} for each specimen was to be calculated from the dimensions of the specimen, its fracture force and the loading configuration. From these data, the following were to be investigated:

a) the statistical significance of K_{IC} for each amalgam type and whether or not there is a statistically significant difference between the mean K_{IC} values of:

(i) three- and four-point bend test results;

(ii) 24 hour and 3 year aged specimens tested under three-point loading;

b) the mean value and standard deviation of K_{IC} for each amalgam type;

c) the ranking of the various amalgam types according to mean K_{IC} value.

A comparison was also made with the amalgams ranked according to other properties.

3.3. Test procedure for K_{IC} determination of amalgams

A compression cage (Figure 3.9) was fitted to a screw-driven tensile testing machine for the 3 point bend testing. The cross-head speed was set at 10mm/minute which imposed a rate of stress intensity factor increase of approximately 61 $N/mm^{3/2}$ per second which was within the range recommended in BS 5447 (para.9.3.1). This crosshead speed was regarded to be sufficiently high to operate in the region where the amalgam, according to Sutfin(136), is not sensitive to strain rate. Sutfin found that the fracture stress of amalgams (albeit on un-notched beams) reduces significantly up to about 6.35 mm/minute crosshead speed.

The test procedure was to set the specimen centrally on the rollers of the cage and then to load the beam to fracture.

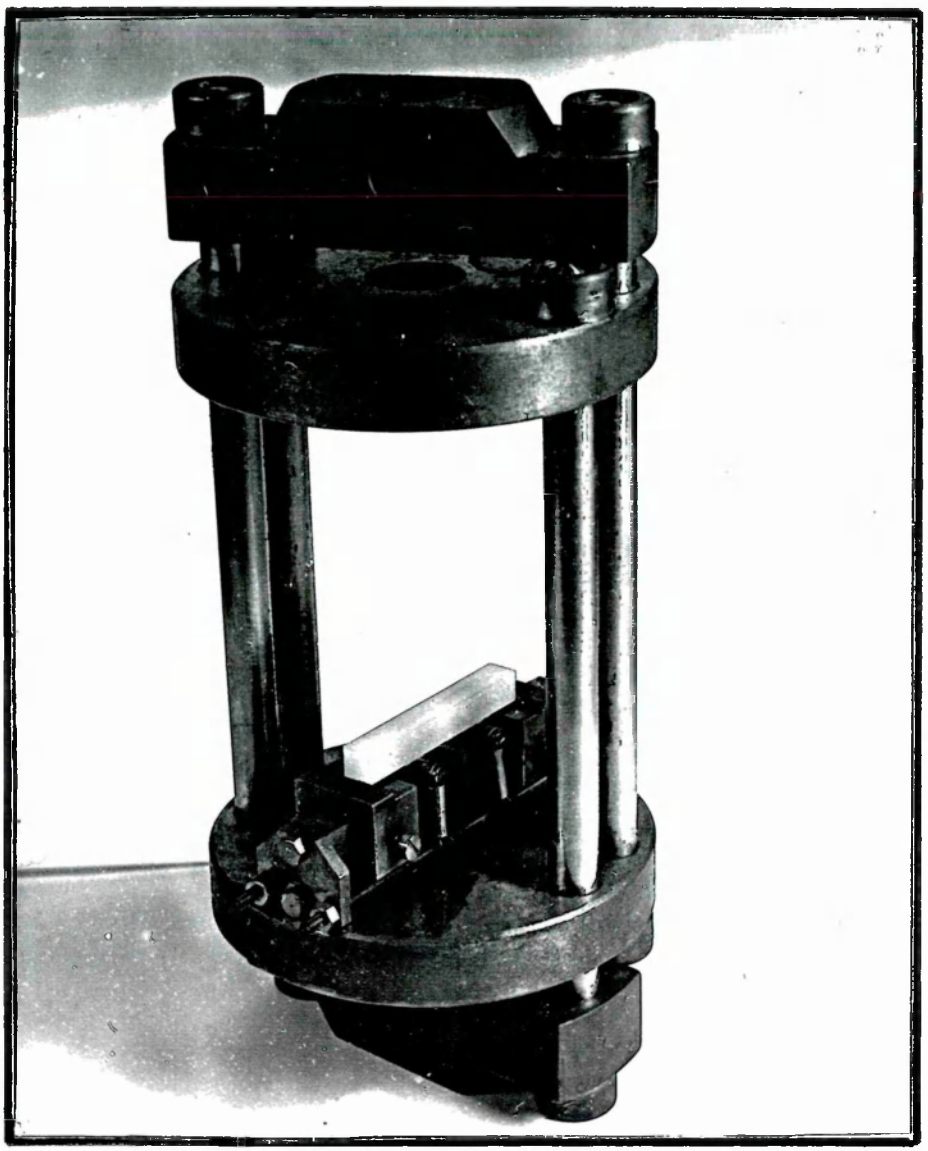

COMRESSION CAGE

Figure 3.9

3.4 Results.

The force-deflection relationship was automatically recorded on an X-Y plotter to check for linearity, and to record P_Q for substitution in equation 2.3. The linearity of the results complied with the requirements specified in BS 5447.

For each specimen tested, the fracture surface was inspected for evidence of a shear lip, the presence of which would have indicated plane stress conditions and invalidated the test. Another check on the fracture surface was for signs of porosity because it clearly has an influence on the fracture toughness value and in excess, would have indicated the need for improved specimen production techniques. The porosity of the specimens was estimated to be approximately 4% on an area basis and from the literature survey, it is clear that this is a fairly representative figure and regarded as acceptable.

HiCu had particularly marked void formation originating from the packing action of the amalgam into the mould, Figure 3.10. Clinical trials conducted by the manufacturers, S.S.White Ltd.,subsequent to this present research showed that this amalgam type had a particularly poor performance.

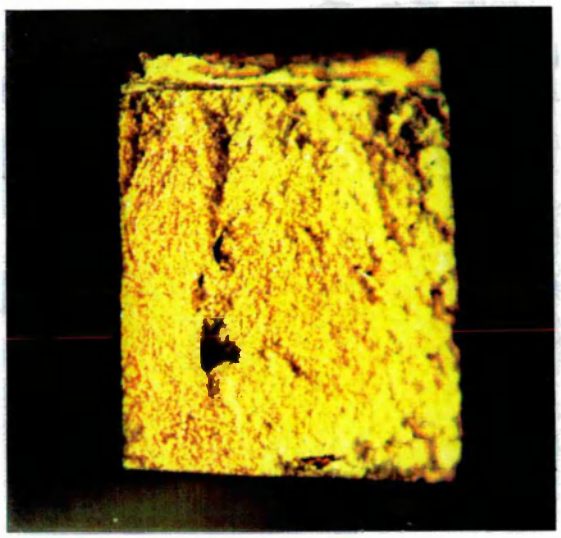

POROSITY OCCURRING IN THE HiCu AMALGAM

Figure 3.10

3.4.1. Effect of a/W ratio on K_{IC}

The test now described was to see if a dependence of K_{IC} on a/W could be detected for dental amalgams. The crack length 'a' must be larger than the plastic zone size at the crack tip if the stress and strain fields are to be described adequately by the single-valued crack tip intensity factor K. Also, if the ligament size (W-a) is not sufficiently large, the plastic zone size for a given K value becomes significantly affected by the close presence of a free surface (the back face of the specimen)(143). Conversely, the reason for specifying a minimum a/W ratio is to ensure that the fracture stress is attained before yield occurs. The various

criteria stated in BS 5447 have been derived by extensive testing on high strength aluminium alloys and low alloy steels. Thus, they do not give an appropriate guide to the specimen design of brittle materials such as amalgams. It is likely that the demands made on a/W and (W-a) on these materials can be considerably less rigorous. The brittleness of amalgam, as judged by the linearity to fracture of the stress-strain relationship in uniaxial tension, and the absence of a shear lip on the fracture surface, leads to a prediction that K_{IC} is insensitive to the value of a/W. The following test was to confirm this assumption.

Six specimens of amalgam, made from the Traditional alloy, were manufactured with a/W = 0.5 and the test beam was loaded under 3 point conditions until fracture occurred. The K_{IC} value was calculated for each specimen, using equation (2.3) and the test was then repeated for an a/W value of 0.2. Table 3.2 shows that there is no significant difference between the two sets of results at a 5% significance level using Student's 't' test and Snedecor's 'F' test. The 'F' distribution is used to test the hypothesis that two variances from different samples are equal - a requirement when examining the difference of sample means using the Student's 't' test(144). Therefore the validity of the 't' test has to be verified first by ensuring that the ratio of sample variances is acceptable according to a particular level of significance (the value chosen for this present work being 5%). The criterion for 'F' was set by reference to the statistical tables by Murdoch & Barnes(145). If the 'F' criterion is not met, then the sample means cannot be compared on the basis of the 't' test. A slightly higher

mean K_{IC} was obtained for the lower a/W value as expected on the basis of the investigation reported by Knott(146).

Table 3.2

EFFECT OF a/W VALUE ON K_{IC} VALUE FOR Ag_3Sn (TRADITIONAL) AMALGAM

Specimen No.	a/W = 0.5		a/W = 0.2	
	Fracture force (N)	K_{IC} ($MN/m^{3/2}$)	Fracture force (N)	K_{IC} ($MN/m^{3/2}$)
1	17.76	0.81	61.3	0.84
2	18.35	0.84	62.9	0.86
3	18.35	0.84	59.6	0.82
4	17.69	0.81	64.4	0.88
5	18.35	0.84	59.1	0.81
6	18.22	0.83	67.3	0.92
	Mean K_{IC} = 0.83 $MN/m^{3/2}$ Standard deviation = 0.096		Mean K_{IC} = 0.86 $MN/m^{3/2}$ Standard deviation 0.108	

Statistical analysis on the results of the a/W tests showed that for amalgams, the value of K_{IC} is not affected by the ratio used. There was a slightly lower standard deviation with the higher ratio (a/W = 0.5), but the difference was considered to be insignificant (0.096 cf 0.108).

3.4.2. Effect of loading configuration.

All six material types were tested under both three- and four-point loading, according to the procedure just described. Batches of six specimens in each group were used.

The compression cage could be readily adapted to cater for

three- or four-point loading. The specimen design and polynomial for 'Y' for the 4 point loading test are shown in Figure 3.11.

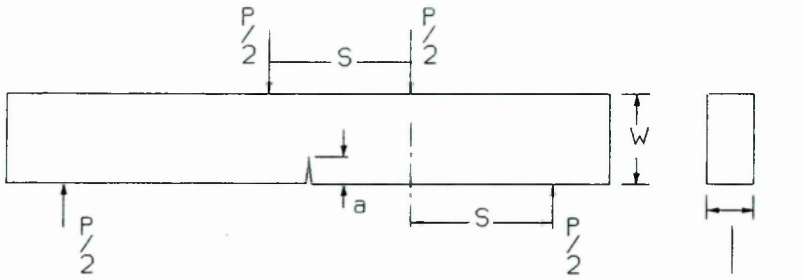

W = 8mm
B = 4mm
S = 12mm
a = 1.6mm

$$Y = 1.93(a/w)^{1/2} - 3.07(a/w)^{3/2} + 14.53(a/w)^{5/2} - 25.11(a/w)^{7/2} + 25.80(a/w)^{9/2}$$

SPECIMEN DESIGN (4-point load)

Figure 3.11

Table 3.3

BATCH MEANS AND STANDARD DEVIATIONS FOR K_{1C} TESTS

	3-Point Test		4-Point Test	
Material	24h Mean ($MN/m^{3/2}$)	sd	24h Mean ($MN/m^{3/2}$)	sd
REVALLOY	1.68	0.146	1.80	0.075
NTDA	1.64	0.083	1.63	0.062
TRADITIONAL	0.86	0.041	0.78	0.037
TYTIN	1.16	0.085	1.26	0.156
HiCu(1)	0.63	0.044	0.69	0.044
HiCu(2)	0.83	0.178	0.63	0.150
DISPERSALLOY	1.76	0.058	1.84	0.017

The probability that the K_{IC} value is ± one standard deviation from the mean value is high (approx. 0.6 for a Normal distribution). Considering the Revalloy results as an example, for the 3-point tests there is a high probability that K_{IC} can be in the range 1.68 to 1.83 $MN/m^{3/2}$ (i.e. up to the mean + one standard deviation). This range encompasses the mean value of the 4-point test, indicating that there is no significant difference between the loading configurations. The same result is reached by considering the 't' value of the samples. The above table shows that this conclusion is reached for the complete range of amalgams and there is no statistical difference between the mean value of K_{IC} for three point loading and four point loading.

3.4.3. Effect of specimen age.

A batch size of six specimens at age 24 hours, were tested in the manner just described and the procedure repeated for specimens that had been stored at 20°C for three years. The aim was to establish if the long term phase changes that are assumed to occur in set amalgam, manifest themselves as an increase in fracture toughness.

The slight increase in mean K_{IC} value with age (Table 3.4) is not as significant as the greatly reduced scatter within the batch - as indicated by the reduction in standard deviation.

Table 3.4

BATCH MEANS AND STANDARD DEVIATIONS FOR K_{IC} TESTS

3-Point Test

Material	24h Mean ($MN/m^{3/2}$)	sd	3year Mean ($MN/m^{3/2}$)	sd
REVALLOY	1.68	0.146	1.92	0.053
NTDA	1.64	0.083	1.70	0.026
TRADITIONAL	0.86	0.041	0.82	0.024
TYTIN	1.16	0.085	1.23	0.090
HiCu(1)	0.63	0.044	0.68	0.045
HiCu(2)	0.83	0.178	*	*
DISPERSALLOY	1.76	0.058	1.84	0.043

* No specimens available at the three-year stage.

3.5. Analysis and discussion.

The mean values of K_{IC} for the range of amalgams were ranked as shown in Table 3.5. The specimens at age twenty-four hours are the combined results from 3-point and four-point loading. The results for the specimen age of three years are also shown in an attempt to reflect the longer term clinical performance. An insufficient number of specimens was available at three years to provide results under four-point loading.

Table 3.5

RANKING OF DENTAL AMALGAMS BASED UPON K_{IC}

Specimen Age - 24 hours

Combined 3- and 4-point loading

Ranking	Material	K_{IC} MN/$m^{3/2}$
1)	DISPERSALLOY	1.80
2)	REVALLOY	1.74
3)	NTDA	1.64
4)	TYTIN	1.21
5)	TRADITIONAL	0.82
6)	HiCu(2)	0.71
7)	HiCu(1)	0.66

Specimen Age - 3 years
3-Point loading

Ranking	Material	K_{IC} MN/$m^{3/2}$
1)	REVALLOY	1.92
2)	DISPERSALLOY	1.84
3)	NTDA	1.70
4)	TYTIN	1.23
5)	TRADITIONAL	0.82
6)	HiCu	0.68

The following comments are based on the statistical analysis followed by a discussion incorporating metallurgical features of fracture.

Effect of a/W ratio on K_{Ic}

Just one material type was tested, namely the Traditional amalgam, and the mean fracture toughness was found to be independent of the ratio initial crack length to depth of the specimen (a/W between values of 0.2 to 0.5). However, the standard deviation of 0.096 for the larger a/W value, compared with a value of 0.108 for a/W = 0.2, shows a slightly superior repeatability of values at the higher figure. This trend can be explained by the proximity of the free surface of the specimen to the notch tip and the consequent effect on the stress field. Specimens with the low a/W value would then yield results which are more affected by surface finish variations.

Effect of age of specimen

A general comment on statistical theory is relevant first. The use of the Student 't' distribution for a sample size of six specimens shows that the probability that the mean K_{IC} value will vary ± one standard deviation, is approximately 0.4. Bearing this in mind, although the mean K_{IC} increased with time, this cannot be regarded as significant for the HiCU(1),HiCu(2) and Traditional amalgams. However for the group of amalgams that is regarded as clinically superior, ie. Revalloy,NTDA,Tytin and Dispersalloy, the increase in mean K_{IC} is significant.

Comparison of the standard deviations at 24 hours with those of age 3 years, indicates that K_{IC} at 3 years is a more effective discriminator in differentiating between commercial brands. The smaller standard deviation for each batch is most likely to be due to continuing setting, or phase development, over this long period.

This possibility was suggested in the introduction section of this present work.

A small variation in K_{IC} results within a particular batch of material (low value of standard deviation), is a manifestation of good workability which in turn produces a consistent standard of specimen. Traditional amalgam has good mixing characteristics, reflected in its extremely low standard deviation, but it also had a low K_{IC} value which predicts a poor clinical performance.

The mean value of K_{IC} of Revalloy increased by the equivalent of one and a half standard deviations for which there is statistically, a one in ten probability of this occurring by chance. It is therefore difficult to state, at these levels of confidence, whether or not K_{IC} increases with age. It is probably most realistic to conclude that the trend is generally an increase with storage time demonstrating that amalgam does not deteriorate with age. However, of greater significance is the reduction in standard deviation, showing that the accepted 24-hour specimen age makes the test insensitive in terms of discriminating between amalgam types.

Effect of loading type.

A decrease in the spread of values for K_{IC} within batches was noted by changing from the three- to the four-point loading configuration. This was predicted from consideration of the constant bending moment that exists over the notch area. Clearly, for this reason alone, the four-point situation is to be preferred for testing. Statistically, there is no significant difference between 3- and 4-point loading in determining the mean K_{IC}.

Comparison between powder types.

For this purpose, the three year, three point bend results will be compared. Revalloy and Dispersalloy have quite different composition and particle characteristics, but were statistically of the same mean K_{IC} values. They ranked as the highest in the range and have a good reputation from the clinical viewpoint.

The low values of K_{IC} for Traditional and HiCu amalgams correspond with a poor performance assessment concluded by the manufacturer, S.S.White. Experience gained in specimen manufacture revealed that HiCu had a very fast setting time. This powder had a very jagged profile (Figure 3.5) which is reputed to account for rapid setting rate.

It is now concluded that the K_{IC} figures enable the six amalgam types to be divided into two broad categories only: those with a reputation for a good clinical performance, i.e. Revalloy, Tytin, Dispersalloy and NTDA; and those with poor in-vivo performance, namely Traditional and HiCU. The former group had a K_{IC} in the range between 1.2 and 2 $MN/m^{3/2}$ and the latter group had values that were well below $1MN/m^{3/2}$.

The ranking order on the basis of compressive and diametral strength according to BS 2938 (Table 3.6) does not correspond with that based on K_{IC}, which further suggests that fracture toughness tests of the type described would be a useful addition to identify the long term potential of clinically acceptable amalgams.

Table 3.6

RANKING OF TEST AMALGAMS ON THE BASIS OF BS 2938

Material	Compressive strength(MPa)	Flow (3 to 24 h)	Dimensional change (24h)	Diametral tensile strength(MPa)	Creep (7 days)
Tytin	275.7	0.15%	- 5.0μm/cm	6.20	0.07
Dispersalloy	183.4	0.12%	- 3.0μm/cm	5.92	0.04
Revalloy	116.2	0.98%	+ 0.04μm/cm	4.25	0.82
NTDA	113.0	1.12%	+11.0μm/cm	4.15	0.74
HiCu	55.0	0.50%	- 3.0μm/cm	3.25	1.50
Traditional	46.0	2.00%	+ 7.0μm/cm	2.50	2.40

Data supplied by S.S.White Ltd.

The fracture toughness values of the constituent phases of amalgam are clearly of interest in establishing their influence on the macro fracture toughness. Chapter 4 shows details of K_{IC} tests conducted on specimens of composition corresponding to the phases. These data are then used to discuss the metallurgical factors which influence the fracture characteristics of the test amalgams.

CHAPTER 4

K_{Ic} OF THE CONSTITUENT PHASES OF AMALGAMS

4.1. Introduction

An estimate of K_{Ic} for the constituent phases enables the crack path occurring in the bulk amalgam specimens to be described. No published work could be found that reports this approach. The only detailed account of the analysis of constituent phases is that of Johnson and Wilsdorf(69) and they limited their study to the tensile strength of mercury-containing γ_1 and γ_2. Their production method involved mixing the appropriate mass of silver powder (for γ_1) and tin powder (for γ_2) with the corresponding amount of mercury. They also used an alternative hot casting technique. A major problem with the first method was that the outside of the metal powder particle reacted with mercury, but the core was identified as either unreacted, or insufficiently reacted to give the required composition throughout. Thus, they had essentially a composite structure of an unreacted particle in a matrix of the mercury-reacted phase. The objection to their second production method is primarily one of safety. In view of these disadvantages, a method of manufacture was devised which is based on the priciple of electrodeposition.

This chapter contains a brief account of the method used to manufacture transverse bend specimens of the constituent phases of amalgams. Details are provided of the techniques applied to verify

the composition of the individual constituent phases, and the results of the SEN tests have been recorded. Finally, the fracture of the test amalgams is discussed with reference to the constituent phases.

4.2. Manufacture of phase specimens.

The specimens were divided into three categories:

a) The Ag_3Sn (γ) and the high copper ternary alloy from which the HiCu powder was produced. Two billets of alloy were supplied by the manufacturer (S.S.White Ltd) from which the fracture specimens were machined. Thus, the structure was regarded as nominally the same as used commercially and should give a reasonable estimate of K_{IC} of the unreacted phases in the amalgams;

b) The copper-tin ε and η phases and the copper-silver $\alpha+\beta$ eutectic were cast in the laboratory;

c) The mercury-reacted phases, γ_1 and γ_2 manufactured by electrodeposition.

4.2.1. Manufacture of γ and HiCu alloy specimens.

The billets of material were approximately 70mm in diameter and the fracture specimens were machined by obtaining a slice of the required thickness for the specimens. From this slice, the final dimensions of the specimen were machined, with the length being in a radial direction as shown in Figure 4.1.

The HiCu specimens were produced in different melt orders, as described previously in Chapter 3, ie HiCu(1) and HiCu(2).

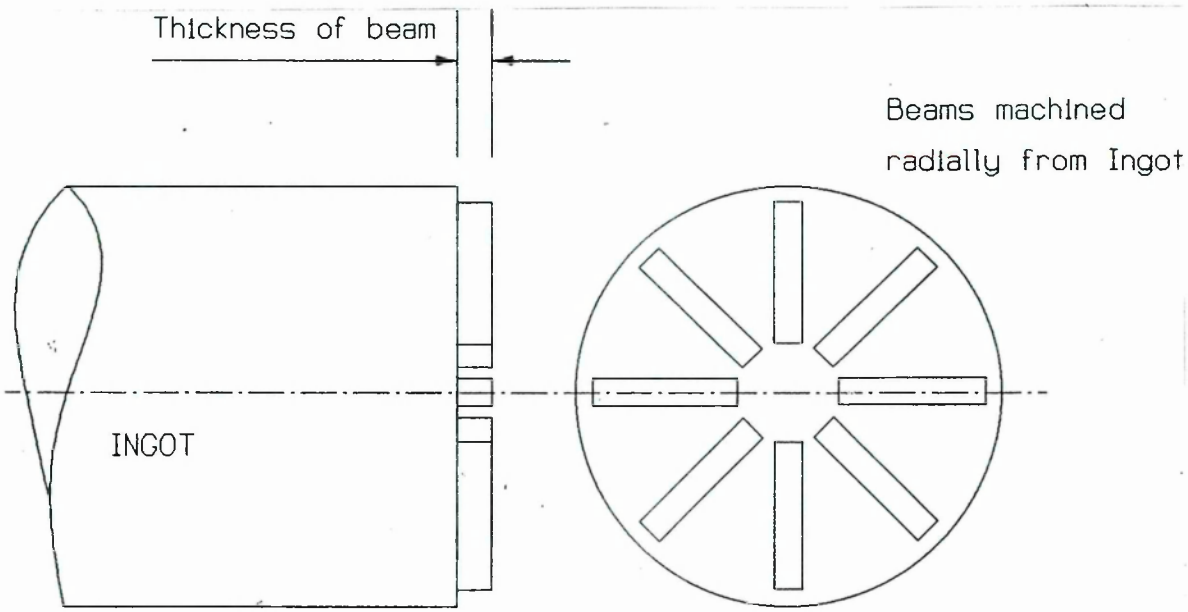

SPECIMEN MANUFACTURE FROM EXISTING BILLET

Figure 4.1.

4.2.2. Manufacture of the ε, ή and (α+β) phases.

The compositions and relevant temperatures for phases in this section were obtained from equilibrium phase diagrams given in Chapter 1, Figures 1.4 and 1.5. The specimens were cast under a reducing atmosphere of Argon into a multi-cavity mould, Figure 4.2. The mould was pre- heated to 250°C to minimise the coring of the structure. The melt temperature for ε was 750°C, the ή phase was 660°C, and (α+β) was 800°C. It can be seen that the mould was designed to enable the melt to flow along the longitudinal axis of the beam cavity. Thus, the impurities and high degree of porosity,

that inevitably concentrate at the free surface, could be removed upon cooling by machining the ends from the castings.

The ε and ή phases were homogenised in an argon atmosphere for 100 hours at 500°C and 200°C respectively. The specimens were furnace cooled at approximately 2 degrees C/minute and then all surfaces were ground to remove scale, polished, and inspected for surface flaws. Those specimens with surface imperfections were rejected.

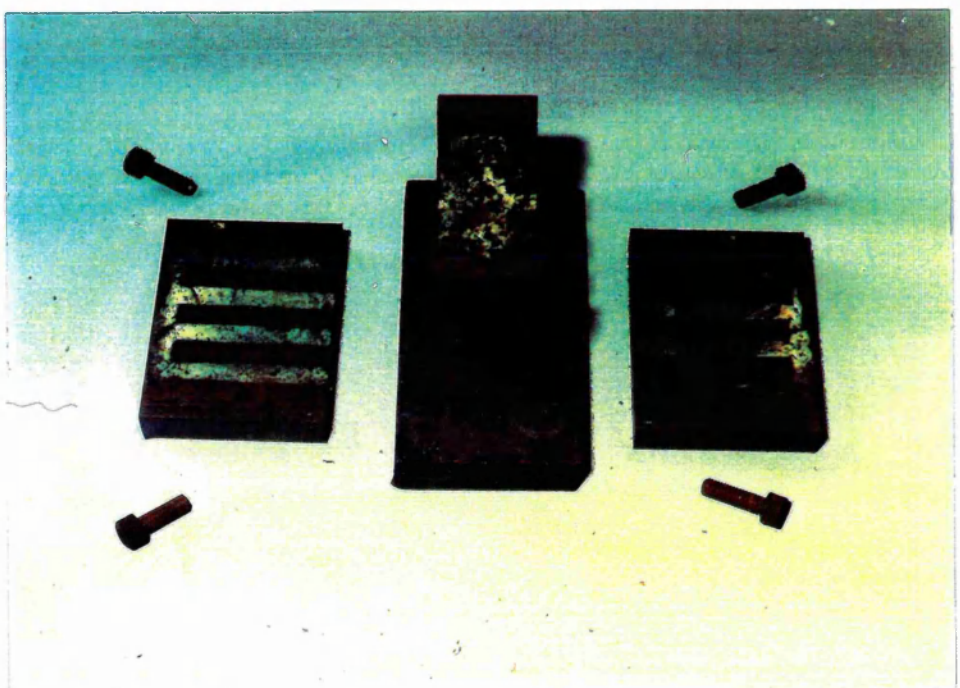

MOULD DESIGN FOR ε, ή AND (α+β) SPECIMENS

Figure 4.2.

4.2.3. Manufacture of the mercury-reacted phases.

The equipment, Figures 4.3 and 4.4 comprised a constant current, pulsed power supply and three other main elements:

a) a cathode which is the mass of mercury required ultimately to form a specimen of pre-determined overall mass;

b) an anode in the form of a rod (dimensions 6mm diameter and 80mm length) of the remaining constituent of the phase (ie. silver or tin);

c) the electrolyte, which is a saturated solution of the salt of the anode metal.

The mass transferred from the anode to the cathode (and thus reacted with the mercury) is related to time by Faraday's law of electrolysis:

$$\text{Deposited mass}(m) = \frac{I \times t \times \text{Atomic weight of anode material}}{96\,500 \times \text{Ionic charge of anode material}} \qquad (4.1)$$

The pulse plated supply was necessary to prevent the situation referred to as polarisation of the electrodes, occurring. This basically is when the negative electrode for example, progressively becomes more positive due to the ion cloud that develops with time. The reverse is true of the other electrode and plating efficiency falls rapidly with time. Pulsing the supply prevents this situation developing. To ensure that equation 4.1 can be applied in its simple form, a constant current supply was also necessary. This power source was designed by, and loaned from, The Open University.

Two further features were incorporated into the design in order to optimise the accuracy of manufacture. A sump (Figures 4.3 and 4.4) was sited below the anode to collect any material leaving it by any mechanism other than electrolysis. Also, the plating rig was vibrated at 20Hz at low amplitude to enhance the reaction of the metal ion from the anode, with the mercury cathode. This latter feature was particularly necessary when the final mass was being approached.

A series of tests was carried out specifically to check the accuracy of the manufacturing method. The cathode mass was recorded at selected plating time intervals, and the values compared with the theoretical mass derived from equation 4.1. The maximum error between the theoretical and experimental cathode mass may be seen on the graph, Figure 4.5, to be approximately 2%. This was a typical level of accuracy obtainable throughout the tests.

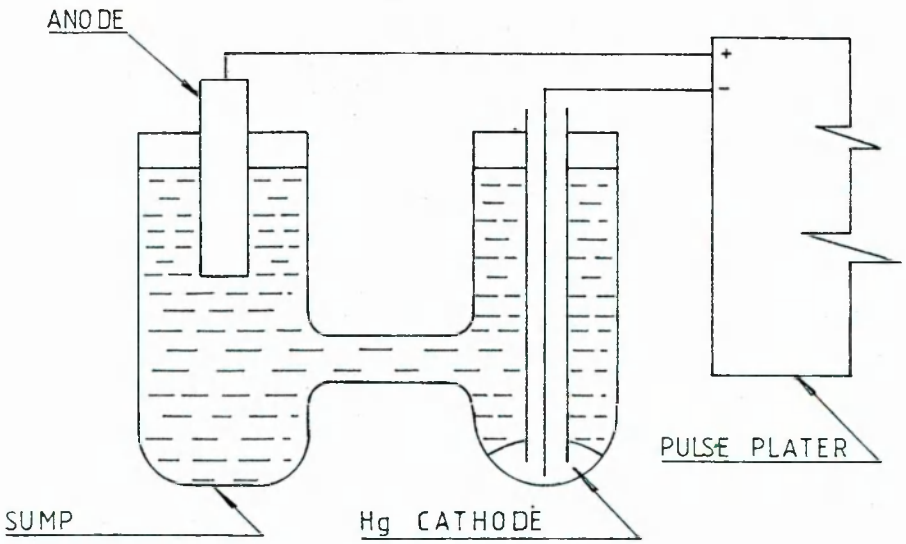

DIAGRAMMATIC VIEW OF ELECTROPLATING RIG

Figure 4.3.

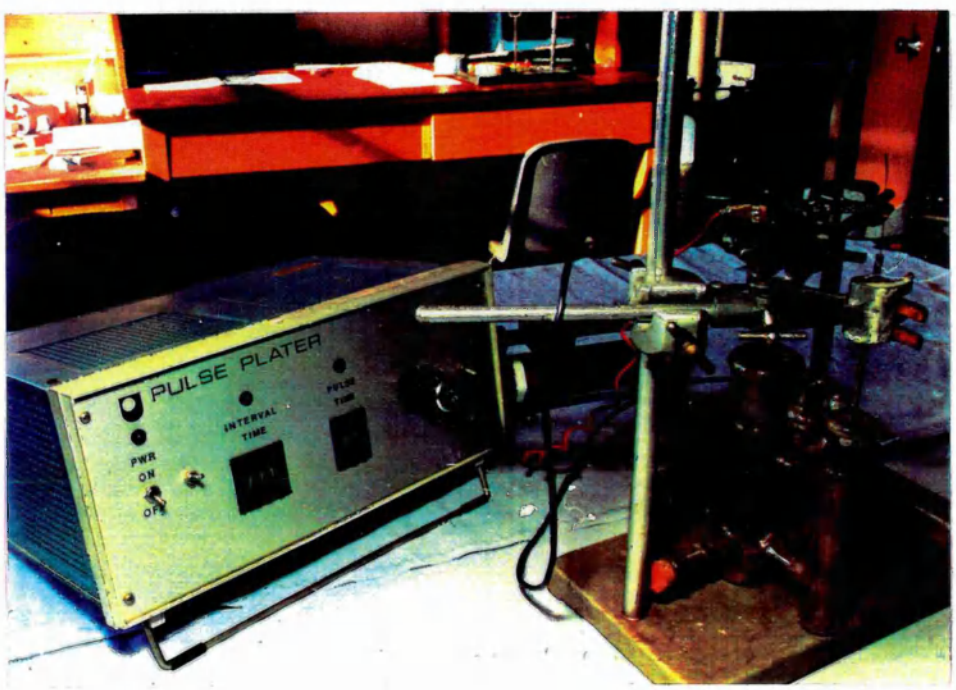

GENERAL VIEW OF ELECTROPLATING RIG

Figure 4.4.

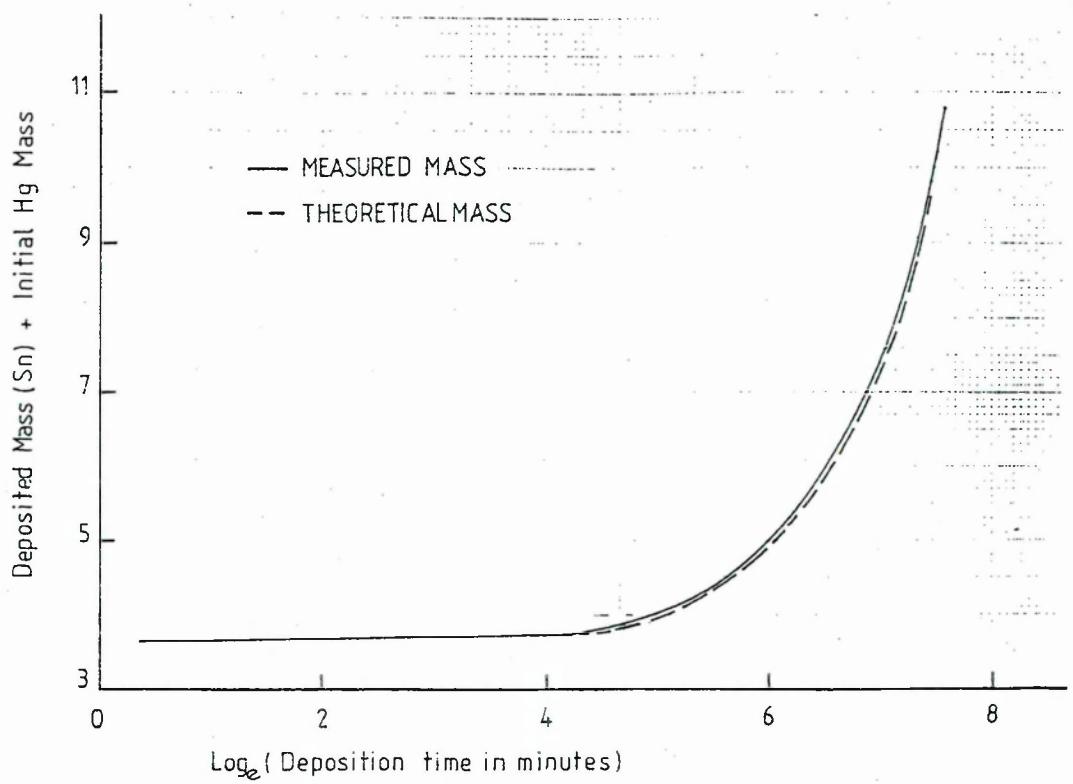

COMPARISON BETWEEN THEORETICAL AND MEASURED MASS FOR γ_2 PRODUCTION BY ELECTRODEPOSITION

Figure 4.5.

At the completion of the calculated plating period, the cathode comprised a solid mass of the appropriate phase composition. The final stage was to compact this mass into the same mould as used for the amalgams, Figure 3.7 (Chapter 3). It was noted that under a compaction pressure of 14 MPa, no mercury could be detected by the squeezing action. This stage had to be conducted with great care in order to obtain consistent specimens. The main reason was the possibility of incurring porosity due to air entrainment during the packing of the mercury-reacted material into the mould. It was possible to generate an interface between the increments of material as shown in Figure 4.6 which could have a significant effect on fracture toughness.

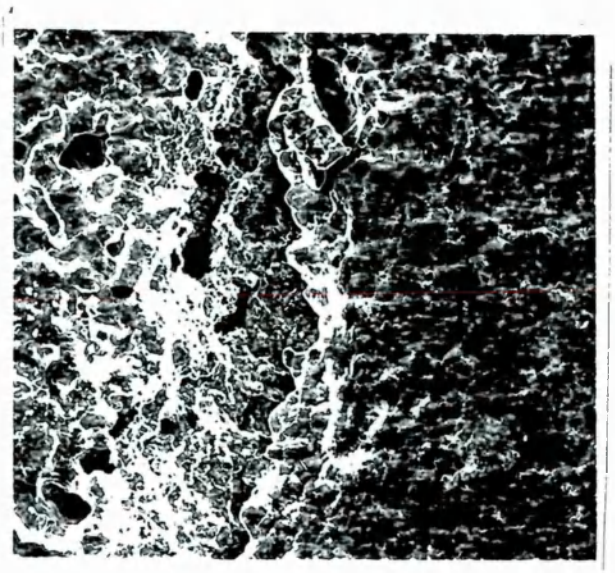

30μm

SEM VIEW SHOWING THE INTERFACE BETWEEN BATCHES
DUE TO PACKING PROCEDURE

Figure 4.6

An illustration of the quantities involved in this method of production of a γ_1 specimen are:

mass of the specimen = 10g

supply current constant at 2 amps

required deposition time 1340 seconds.

4.3. Assessment of phase composition.

The identity and composition of the specimens were assessed by differential scanning calorimetry (DSC), powder X-ray diffraction, and scanning electron microscopy (SEM). It is acknowledged that the

results of the work described in this chapter produces only approximate figures for K_{IC} for the constituent phases. However this information is useful in deciding on the role of a particular phase when it exists as a component of dental amalgams.

The procedures adopted for phase verification are described below. DSC was used to compare the transition temperatures of the specimens with those obtained from the relevant equilibrium phase diagram. The structure of the phases were assessed by x-ray powder diffraction. Finally, qualitative assessment was carried out on the Cu-Sn phases by the use of EDAX.

4.3.1. DSC analysis

The type of calorimeters used were the Perkins-Elmer Mk.2 and the DuPont Model 1090. The use of aluminium sample pans in the DSC equipment imposed an upper temperature limit of 700K, which meant that the higher temperature transitions could not be verified. Differences between the transition temperatures obtained by experiment, and those taken from the equilibrium phase diagrams were expected due to the use of a heating cycle, as opposed to cooling. The former was used to avoid the possible effects on the specimen structure due to the volatility of mercury. A heating rate of 10deg.C/minute was employed for this test.

The results confirmed, by comparing the expected transitions with those recorded by DSC, that the electrodeposited specimens corresponded closely with those expected under equilibrium conditions.

The expected transitions for γ_1 (from Figure 1.2) are:

$$(\text{liquid} + \alpha) \xrightarrow[276^{\circ}C]{} (\text{liquid} + \beta) \quad \text{and} \quad (\text{liquid} + \beta) \xrightarrow[127^{\circ}C]{} \gamma_1$$

Measured transitions by DSC:

Specimen number.		
1	220°C	115°C
2	267°C	117°C
3	278°C	120°C

The expected transitions for γ_2 (from Figure 1.3)

$$\text{liquid} \xrightarrow[220^{\circ}C]{} (\gamma + \text{liquid}) \quad \text{and} \quad (\gamma + \text{liquid}) \xrightarrow[100^{\circ}C]{} \gamma_2$$

Measured transitions by DSC:

Specimen number.		
1	214°C	106°C
2	222°C	107°C

Due to the temperature range limitations of the DSC system, the ε and ή phases were checked instead using cooling curves. An insulated refractory containing the melt of copper and tin was monitored by a thermocouple attached to a Y-time plotter. The characteristic curves were thus obtained (Figures 4.7 and 4.8).
In the case of the ε phase, two transitions were detected from the experimental cooling curve, namely:
732°C for the liquid → (γ + liquid) and 671°C for the (γ + ε) → ε.
The expected transitions from Figure 1.4 are 730°C and 670°C respectively.
For the ή phase, the measured value of the liquid → (ε + liquid) transition was 640°C and the (η + liquid) → ή was 227°C.
The expected transitions from Figure 1.4 were 630°C and 250°C repectively.

The temperature for the (α + β) silver-copper eutectic phase is 779°C and was again verified by a cooling curve for the specimen.

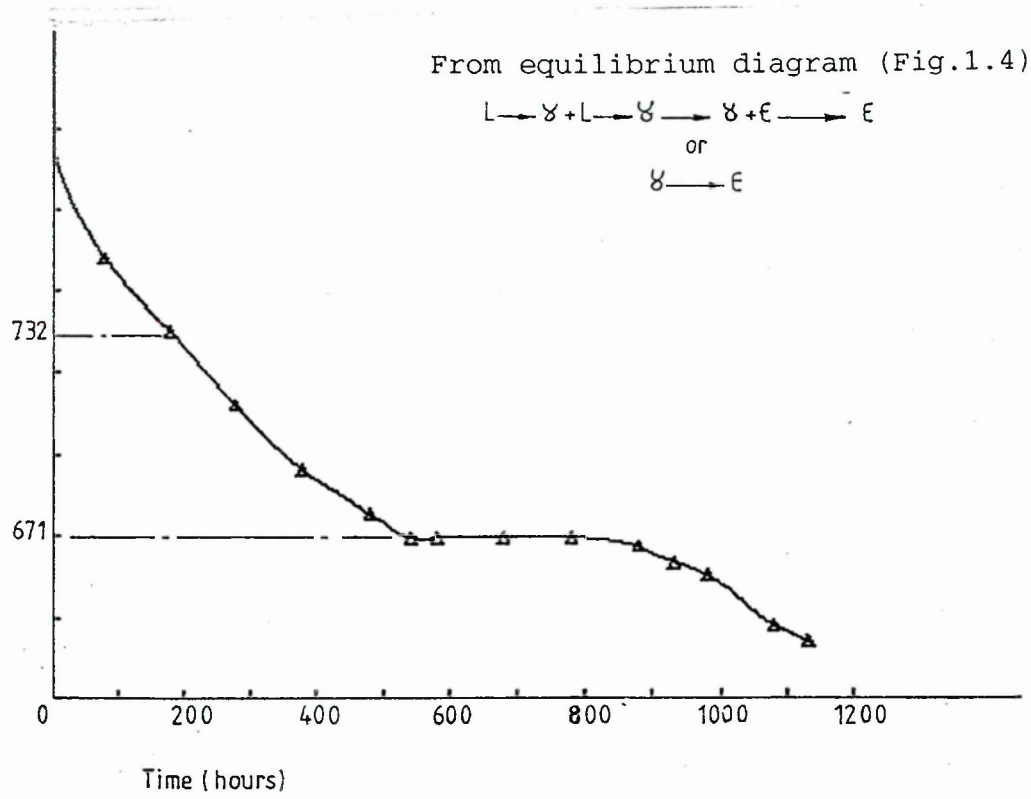

EXPERIMENTAL COOLING CURVE FOR THE ε PHASE

Figure 4.7.

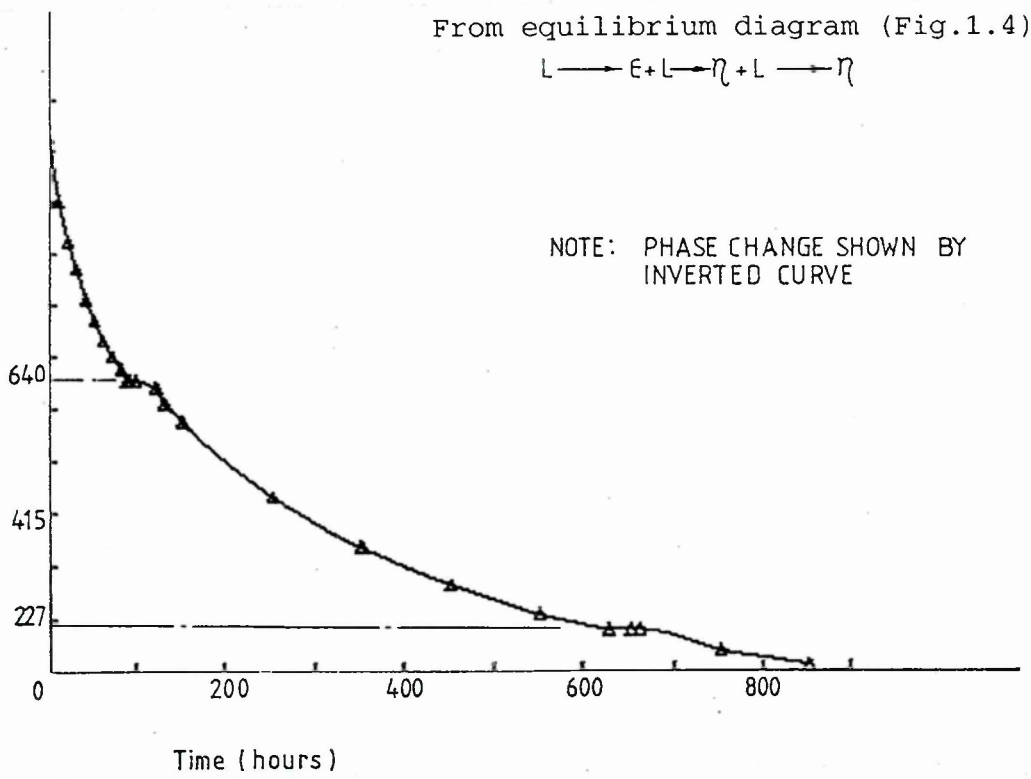

EXPERIMENTAL COOLING CURVE FOR THE ηPHASE
Figure 4.8.

4.3.2. X-ray analysis.

The four phases, γ_1, γ_2, ε and η' were tested by the powder diffraction method by staff at Birmingham University. A Phillips powder camera system was used with a CuKα source. The scan rate was 0.75degrees/minute starting at 7.5° with 1° and 0.2mm slits.

The reference values of lattice parameters expected of the phases were obtained from the Fulmer Research Institute (Figure 4.9), the work of Pearson(147) and Butts(148) and Fairhurst (35,36). The most effective means of confirming crystal structure from x-ray diffraction analysis is to use dedicated computer data systems. However, this facility was not available and therefore the following procedure was adopted.

The interpretation of the x-ray test data obtained on the γ_1 phase is now presented to illustrate the analysis method. The scan results were in the form of a chart showing the diffraction peaks with their corresponding angle (2θ). 'θ' is the Bragg angle, i.e. the glancing angle of incidence of the x-ray on a crystal plane. This angle is related to the interplanar distance 'd' by the Bragg Law, $2d \sin\theta = n\lambda$ where n is an integer and λ is the x-ray source wavelength. The portion of the scan chart possessing the data necessary to derive the unit cell dimension (a) for γ_1 is shown in Figure 4.10.

The Bragg angle (θ) is related to the lattice parameter for γ_1 by $\sin^2\theta = (\lambda/2)^2\left(\frac{h^2+k^2+l^2}{a^2}\right)$ (see Taylor,149)

h,k, and l are the Laue indices for the reflection from a specific

plane and are given in Figure 4.9 for different peak intensity ratios. For clarity, the index card for γ_1 has been enlarged, Figure 4.11 and it shows the maximum peak intensity obtained from the scan (i.e. I/I_0) as 100. Other peaks are identified by their intensity ratio quoted as a percentage of the maximum and Figure 4.11 shows the Laue indices of these in turn. Taylor(149) describes in detail the relationship between Laue and Miller indices.

Knowledge of the chart speed and scan rate enable the θ values to be found for any chosen peak. Figure 4.10 shows that the maximum peak occurs at $2\theta = 37.88^{\circ}$, and Figure 4.11 shows that h=3,k=3,l=0. For the phase being considered, the maximum peak intensity also occurs for Laue indices of h=4,k=1,l=1. Either of these sets can be used to calculate 'a' because the numerical value of $(h^2+k^2+l^2)$ is the same regardless. Taylor(149) gives a value for λ for CuKα of 1.537395 Å, thus, $\sin^2 37.88^{\circ}/2 = (1.537395/2)^2\left(\frac{3^2+3^2+0^2}{a^2}\right)$

Solving this equation gives a value for 'a' of 10.048 Å. The value for 'a' given on the index card, Figure 4.11 is 10.04 Å which is clearly very close to the experimental result and considered to confirm the structure of the specimen as γ_1. Fairhurst and Cohen(35,36) quote a value from their literature survey of 10.0506 Å whilst their own test result was '*....approximately 10 Å*'.

For a cubic structure, it is necessary to consider just one peak to determine the lattice parameter. Structures that possess more than one cell dimension require consideration of the appropriate number of peaks to form a set of simultaneous equations. Thus, the γ_2 hexagonal structure has two cell dimensions, 'a' and 'c' which

were found by considering hkl and θ values corresponding to two peaks on the test chart and substituting in the appropriate formula.

The experimental test results for the four phases that were tested in the manner just described, are summarised below.

γ_1 phase (Cubic structure) $\sin^2\theta = (\lambda/2)^2\left(\frac{h^2+k^2+l^2}{a^2}\right)$

Peak intensity I/I_o used to derive 'a'

I/I_o 100 $2\theta = 37.88^\circ$ hkl = 330,411

Experimental value: a = 10.048±0.002 Å

Reference value: a = 10.040 Å(Fig. 4.11), 10.0506 Å and 10 Å(35)

γ_2 phase (Hexagonal structure) $\sin^2\theta = (\lambda/2)^2\left\{4/3\left(\frac{h^2+k^2+l^2}{a^2}\right)+(l/c)^2\right\}$

Peak intensities I/I_o used to derive 'a and c'

I/I_o 100 $2\theta = 32.26^\circ$ hkl = 100 and I/I_o 65 $2\theta = 44.58^\circ$ hkl = 101

Experimental value: a = 3.160±0.002 Å, c = 2.980±0.002 Å

Reference value: a = 3.204±0.002 Å, c = 2.984±0.002 Å(36)

No reference card was available for this phase, therefore the Laue indices were taken from the work of Fairhurst and Ryge(36).

ε phase (Orthorhombic) $\sin^2\theta = (\lambda/2)^2\{(h/a)^2+(k/b)^2+(l/c)^2\}$

Peak intensities I/I_o used to derive 'a,b and c'

I/I_o 70 $2\theta = 39.0^\circ$ hkl = 120,200; I/I_o 100 $2\theta = 41.8^\circ$ hkl = 002

I/I_o 100 $2\theta = 44.4^\circ$ hkl = 121

Experimental value: a = 5.567 Å, b = 35.312 Å, c = 4.317 Å

Reference value: a = 5.621 Å, b = 33.250 Å c = 4.328 Å (148)

ή phase (Hexagonal structure) $Sin^2\theta = (\lambda/2)^2 \left\{ 4/3\left(\frac{h^2+k^2+l^2}{a^2}\right)+(l/c)^2 \right\}$

Peak intensities I/I_o used to derive 'a and c'

I/I_o 100 $2\theta = 33.4^o$ hkl = 202 and I/I_o 50 $2\theta = 36.0^o$ hkl = 002

Experimental value: a = 4.180 Å, c_o = 5.317 Å

Reference value: a = 4.200 Å, c_o = 5.09 Å (148).

The above table shows that the experimentally determined unit cell dimensions for the specimens compare favourably with previously published figures. Differences between experimental and reference values would arise if the actual crystal structure does not correspond precisely with that assumed. An example of this situation is in the case of the ή phase, where Butt(148) has identified the structure as *approximately* hexagonal.

4.3.3. SEM analysis (EDAX).

SEM was used determine if any contaminants were present in the final castings of the Cu-Sn phases. The work was carried out by personnel at British Telecom, Birmingham and it was possible to obtain qualitative information regarding relative amounts of copper and tin in the ε and ή phases only. Figures 4.12 and 4.13 show the relative magnitudes of the tin and copper peaks obtained by SEM analysis and the absence of contaminants.

4.4. Fracture toughness of the individual phases of amalgam.

The procedure previously described in Chapter 3 was used to test

the specimens of the constituent phases. The specimen dimensions are designated B,W,L and a in accordance with the standard procedure, Figure 2.6 and the results are shown in Table 4.1.

6-0565

d	2.36	1.36	1.23	2.90	
I/I1	100	80	80	20	SILVER AMALGAM

Rad. CuK λ 1.542 Filter
Dia. 6.406cms Cut off 3.29 Å Coll.
I/I1 Visual d corr. abs.? No
Ref. Dr. S. Rama Swamy, Prof. of Physics Univ. of Mysore, Trichur, India

Sys. Cubic (Body centered) S.G.
a_o 9.998 b_o c_o A C
α β γ Z
Ref. Ibid.

ε α n∞β ε γ Sign
2V D mp Color Silvery-white
Ref.

d Å	I/I1	hkl	d Å	I/I1	hkl
2.935	20	222	1.200	40	653
2.679	40	321	1.190	40	822,660
2.358	100	411	1.167	60	750,743
2.243	40	420	1.149	40	662
2.145	40	332	1.136	10	752
1.972	60	510,431	1.123	10	840
1.936	60	521	1.109	20	910,833
1.672	60	600,442	1.082	20	
1.584	5	620	1.070	5	664
1.549	40	541	1.058	20	
1.513	60	622	1.035	40	
1.480	60	631	1.022	5	844
1.449	60	444	1.005	60	
1.419	60	710,550	0.994	60	
1.392	10	640	.984	40	
1.364	80	721, 633,552	.976	40	
1.341	40	642	.967	40	
1.275	60	732	.957	60	
1.234	80	811	.941	60	

Ag AMALGAM

4-0800 MINOR CORRECTION

d 4-0798	2.28	2.39	1.76	2.59	γ-Ag_3Sn
I/I1 4-0800	100	80	80	60	GAMMA SILVER TIN

Rad. FeKα λ 1.93"3 Filter None
Dia. ? Cut off Coll.
I/I1 Visual d corr. abs.? Yes
Ref. Nial, Almin and Westgren, Z. phys. Chemie 14, 81-90 (1931)

Sys. Orthorhombic S.G.
a_o 2.995 b_o 5.159 c_o 4.781 A 0.581 C 0.927
α β γ Z 3.97 (4)
Ref. Nial, Almin and Westgren, Z. phys. Chemie 14, 81-90 (1931)

ε α n∞β ε γ Sign
2V D mp Color
Ref.

Phragmen focussing camera used.
25 atomic o/o Sn

d Å	I/I1	hkl	d Å	I/I1	hkl
2.59	60	110, 020	1.14	50b	042
2.39	80	002	1.09	90b	114, 024
2.28	100	111, 021	1.01	90b	223
1.76	60	112, 022	1.00	90b	043
1.50	80	200, 130			
1.36	60	113, 023			
1.30	50b	220			
1.29	40	040			
1.27	70b	202			
1.27	90b	132			
1.25	90b	221			
1.25	70b	041			
1.20	70b	004			
1.14	70b	222			

1845

Ag-Sn (γ)

1-1240 MINOR CORRECTION

3480 d 1-1242	2.08	2.16	1.24	2.38	ε-Cu_3Sn
I/I1 1-1240	100	40	40	20	EPSILON COPPER TIN

Rad. CuK λ Filter No
Dia. Cut off Coll.
I/I1 d corr. abs.?
Ref. Jones and Evans, Phil. Mag 1, 1302 (1927)

Sys. Orthorhombic S.G. V_H^{17} - Cmcm?
a_o 5.621 b_o 33.25 c_o 4.329 A C
α β γ Z 16
Ref. Carlson and Haegg, Z. Krist. 83 308-17 (1932)

ε α n∞β ε γ Sign
2V D mp Color
Ref.

Epsilon phase. Superstructure of hexagonal close-packed lattice.

d Å	I/I1	hkl	d Å	I/I1	hkl
2.38	20				
2.16	40				
2.08	100				
1.60	27				
1.38	30				
1.24	40				
1.19	5				
1.16	30				
1.15	17				
1.08	7				
1.04	7				
0.98	8				
.92	20				
.90	7				
.88	20				
.85	24				
.83	12				

581

Cu-Sn (ε)

Figure 4.9.

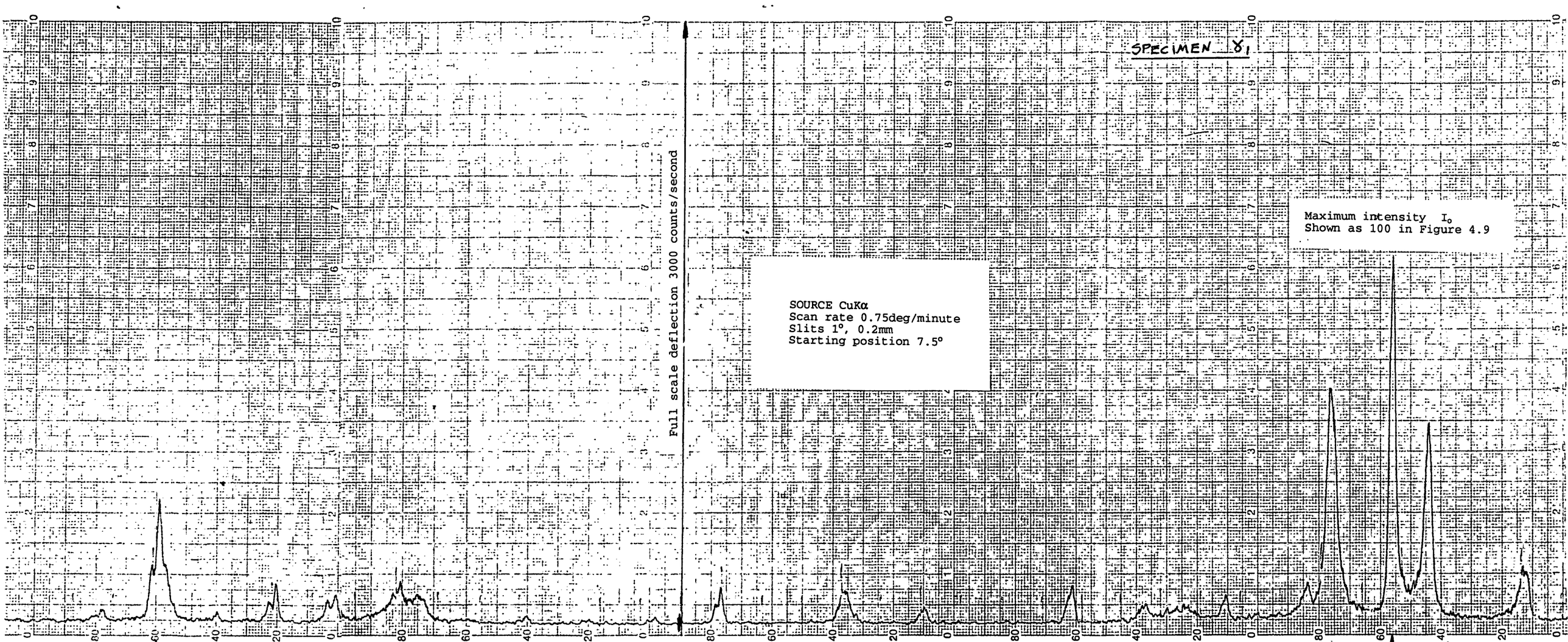

SAMPLE OF γ_1 X-RAY DATA SHOWING PEAKS AND CORRESPONDING ANGLES

Figure 4.10

11-67

d	2.36	1.37	1.24	4.08	γ-Ag_2Hg_3
I/I$_1$	100	70	60	10	GAMMA MERCURY SILVER — MOSCHELLANDSBERGITE

Rad. CuKα λ 1.5418 Filter Ni Dia. 57.3mm
Cut off I/I$_1$ VISUAL ESTIMATE
Ref. R.M. THOMPSON, UNIV. BRITISH COLUMBIA, VANCOUVER, CANADA

Sys. Cubic S.G. Im3m (229)
a_o 10.04 b_o c_o A C
α β γ Z 10 Dx 13.41
Ref. IBID.

ε α nω β ε γ Sign
2V D13.5–13.7mp Color SILVER WHITE
Ref. D_7

SAMPLE FROM MOSCHELL, GERMANY.

d Å	I/I$_1$	hkl	d Å	I/I$_1$	hkl
4.08	10	211	1.275	50	651,732
3.53	10	220	1.236	60	811,741
2.88	30	222	1.217	5	
2.67	40	321	1.199	20	
2.36	100	330,411	1.185	20	
2.24	30	420	1.168	30	
2.13	30	332	1.152	20	
2.05	10	422	1.137	5	
1.965	40	510,431	1.122	5	
1.828	20	521	1.110	10	
1.667	40	600,442	1.096	5	
1.629	10	611,532	1.083	20	
1.583	10	620	1.059	10	
1.547	20	541	1.036	30	
1.512	10	622	1.014	30	
1.478	30	631	1.002	20	
1.447	40	444	0.985	20	
1.419	40	710,543	.976	10	
1.365	70	721,552	.968	10	
1.341	20	642	PLUS 1	LINE	TO 0.784

X-RAY INDEX REFERENCE CARD FOR THE γ_1 PHASE

Figure 4.11

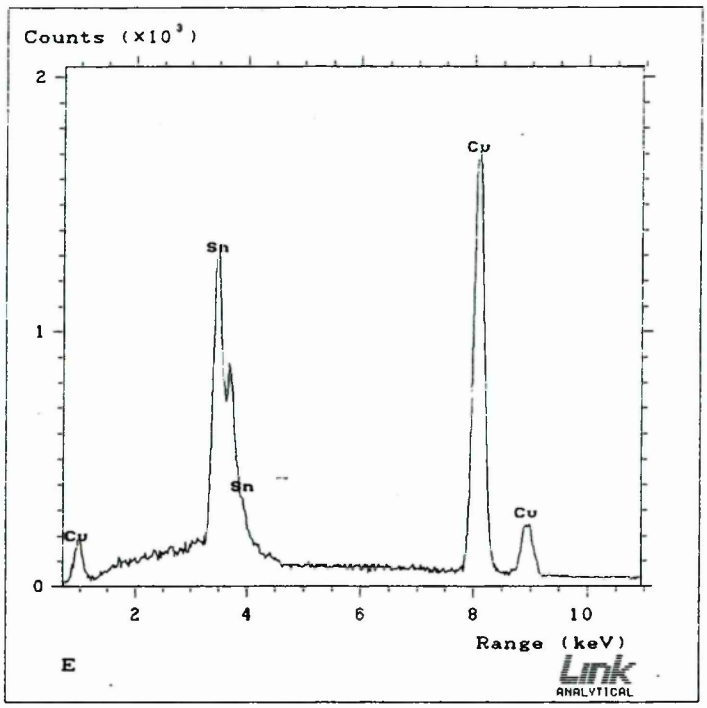

X-RAY SPECTRA OF THE ε PHASE

Figure 4.12

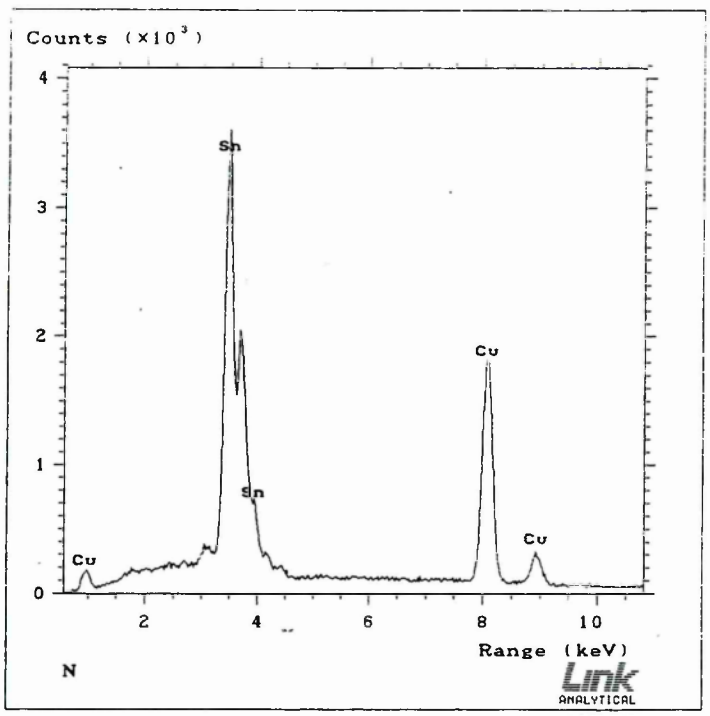

X-RAY SPECTRA OF THE ή PHASE

Figure 4.13

Table 4.1

K_{IC} OF THE CONSTITUENT PHASES 4-POINT BEND

Alloy	B	W	L	a	K_{IC} ($MN/m^{3/2}$)
HiCu(1)	5.406	6.78	28	0.68	14.55
HiCu(2)	4.904	6.72	28	0.63	16.06
γ	5.560	7.25	28	0.57	12.37
$(\alpha+\beta)$	5.620	6.91	28	3.45	12.14

γ_1

Specimen	1	2	3	4	5	6
K_{IC} ($MN/m^{3/2}$)	0.65	0.53	0.58	0.60	0.66	0.57

γ_2

Specimen	1	2	3	4	5	6	7	8	9	10	11	12
K_{IC} ($MN/m^{3/2}$)	0.4	0.35	0.49	0.40	0.33	0.46	0.39	0.40	0.38	0.38	0.41	0.42

ε

Specimen	1	2	3	4	5	6	7
K_{IC} ($MN/m^{3/2}$)	0.75	0.72	0.78	0.51	0.69	0.54	0.66

η

Specimen	.1	2	3	4	5	6	7	8	9	10	11	12
K_{IC} ($MN/m^{3/2}$)	3.66	3.13	4.29	2.66	2.73	3.17	3.17	3.65	2.88	3.68	3.39	3.86

MEAN K_{IC} OF CONSTITUENT PHASES

Material: Alloy	(γ)	γ_1	γ_2	ε	η	(α+β)
K_{IC} MN/$m^{3/2}$	14.14	0.6	0.44	0.66	3.44	12.14
	(1.86)	(0.05)	(0.04)	(0.1)	(0.49)	(1.4)

4.5. Amalgam fracture and microstructure.

There are two main factors that impede a rigorous analysis of the fracture surface of the specimens;

a) the difficulty in distinguishing between the two mercury-reacted phases γ_1 and γ_2 by optical microscopy, and,

b) The possibility of damage by the mercury vapour from the specimen, to SEM systems. This meant that there was a reluctance on the part of operators to allow SEM systems to be fully utilised for these materials.

The etching procedure as recommended by Allan et al(74) and described in Table 2.4 was applied to one specimen from each test batch for the 3 point bend test. The etched section included an edge of the fracture face and revealed the unreacted particles satisfactorily. However, as will be seen in Figures 4.14 to 4.19, distinction between the mercury-based phases was poor.

The presence of the highest fracture toughness phase (γ), in the crack path does not mean that the crack is necessarily diverted into the phase with the lower values. Clearly, whether this happens, or not, depends upon the orientation of the crack when it encounters the particle. There are many instances where the crack was seen to propagate through the particle, but naturally the K_{IC} value for the material as a whole increases due to the extra

expenditure of energy in so doing. The complex range of possibilities for fracture dynamics, means that for this form of specimen, a rigorous analysis is not possible.

It is clear that K_{IC} values of the phases are only approximate because of the difficulty of producing a representative structure. The main problem with production of these constituent phases was the probable heterogeneity and porosity of the macro specimens. However, they do provide a guide to the reasons for the differences occurring between material types. Each material type will now be briefly discussed.

Revalloy - The small powder size(approximately 30μm) results in a correspondingly lower than expected fraction of the unreacted γ phase in the amalgam (Figure 1.15). On an area basis, the fraction of γ of Revalloy is about 20% whereas it is usual to observe in the region of 50% for Traditional amalgams. The crack path is confined to the mercury reacted phase with some deviation enforced by the γ phase (Figure 4.14). However it became clear that the overall K_{IC} value cannot be estimated from a restricted consideration of the fracture toughness of the γ_1 and γ_2 phases. It should be emphasised that the preferred crack path on the free surface of the specimen may have different influences than in the bulk, ie. there is probably less 'constraint' to crack propagation on the specimen surface.

There is evidence (Figure 4.14) that small (40 to 50μm) cracks branch from the main fracture surface into mercury-reacted phases - a feature that will tend to raise the fracture toughness because of the energy expended.

NTDA. The powder size of this alloy type is approximately ten times that of Revalloy (300 cf 30μm). This results in an increase in the γ phase area in the subsequent amalgam compared with the previous amalgam type (≈ 40%), Figure 1.16. There is also evidence of more discrete areas of the low fracture toughness γ_2 phase and this could account for a lower K_{IC} value than for Revalloy (Table 3.5). However, this reasoning is complicated by the effect of the very high fracture toughness of the more prolific, and larger, γ phase. Further, although not clear on Figure the fracture path appears to prefer to circumvent the weak γ_2 phase showing that it is not possible to have predicted the fracture path solely from the fracture toughness of the individual phases.

The coarse γ phase in NTDA could be responsible for very marked crack branching evident in Figure 4.15.

Ag_3Sn. This amalgam possessed an abundance of γ_2 reasonably easily differentiated from the γ_1 phase (Figure 1.17). It also has a large volume fraction of the unreacted γ phase which could originate from the powder manufacturing techniques used in the laboratory. However, the characteristics which were used to account for the lower fracture toughness of NTDA, are even more pronounced in this alloy (Figure 4.16). Thus, the K_{IC} of this amalgam would be expected to be the lowest of the three in the Traditional category. This is indeed the case (Table 3.5). No distinction could be made on the photomicrograph between the γ_1 and γ_2 phases (Figure 4.16).

Tytin. The spherical powder shape is retained in the amalgam structure, Figure 1.18, which results in a fracture path confined to the mercury reacted phases. The deflection of the fracture path

around the spherical particles will account for a final fracture toughness that is higher than either the γ_1 or γ_2 phase. This amalgam did not feature the small crack branches that were clear in Revalloy amalgam. It will be noted in Chapter 3 that the alloy from which Tytin is manufactured has a K_{IC} that is approximately 30% higher than specimens of Ag_3Sn. This characteristic, together with the regular spherical surface will tend to raise the overall fracture toughness of the amalgam from which it is manufactured, due mainly to the energy expended in crack deflection and particle 'pull-out' (Figure 4.17).

HiCu. X-ray maps of this alloy showed that the large amount of copper combined with tin formed a large fraction of Cu_3Sn in addition to the γ phase. In fact it was not possible to detect the γ phase in discrete zones as it was with the other amalgams. The matrix appeared from x-ray maps to be essentially silver reacted with the mercury. Thus, the amalgam could be approximated to the ε phase in a 'matrix' of γ_1. The fracture toughness of both these phases is 0.66 and 0.60 $MN/m^{3/2}$ respectively. Although the energy absorbing mechanisms of crack branching and deviation must still exist, Table 3.5 indicates that the overall fracture toughness as 0.68 $MN/m^{3/2}$ is comparable to the figures for the individual constituent phases. The unreacted particle is very irregular which may well prevent the crack from deflecting to the same extent as Tytin when it encounters this phase. The ε (Cu_3Sn) phase was seen to be unique as a constituent in that it showed no signs of reaction with mercury. This seemed true under both static and dynamic conditions and over an eighteen month period. It is probable,

therefore, that the ε phase has no tendency to react with the matrix and contributes very little to the overall fracture toughness of HiCu. Figure 4.18 shows the fracture path around the unreacted particles.

Dispersalloy. Figure 4.19 shows that the Ag-Cu spherical particles have ή' reaction zones surrounding them, in accordance with the view of Boswell(58). The fracture path does not cut through the nucleus of these particles, which have a high fracture toughness, but through the ή zone. The K_{IC} of ή is comparatively high at approximately 3.5 $MN/m^{3/2}$ and thus must make a considerable contribution to an increased K_{IC}. The fracture path also cuts the γ_1 and γ_2 phases arising from the Ag_3Sn component of this alloy type. Thus, a K_{IC} value for the amalgam can be expected to be within the limits defined by the low value of γ_1 and γ_2, and the high value of ή and the Ag-Cu particles. This can be seen to be the case (Table 3.5).

4.6. Summary of bulk fracture tests

In specimen design it is preferable to incorporate the longest notch possible, thus maximising the a/W ratio. The extent of this aim is limited by the damage that can occur in extracting the amalgam from the specimen mould.

The four-point loading case produces less scatter in the batch results and is therefore to be recommended. However, the mean K_{IC} values of three-point loading tests are consistent with the view that either loading case is satisfactory.

The specimen age does produce a small increase in K_{IC} which is most likely to be a manifestation of long term setting mechanisms. When the specimens were made, the alloys were rotated to eliminate bias occurring due to the developing proficiency in mixing and packing techniques.

K_{IC} can be used with confidence to distinguish between amalgams that are reputed to be clinically good or poor, but it is considered to be unwise to make distinctions between alloy types within the two broad categories.

The two highest fracture toughness values were obtained with the small-particle Traditional alloy, namely Revalloy and, the silver-copper eutectic Dispersalloy also containing a Traditional phase as a component of its formulation. It is considered that the small particles of the former amalgam give rise to good working characteristics with minimum porosity which accounts for the high value of K_{IC}. The cohesion between the unreacted particles and the mercury-reacted phases through the high fracture toughness ή phase accounts for the good performance of the latter type. Dispersalloy is known to require very specific mixing conditions involving high energy amalgamators. This requirement of some amalgams was noted in the introduction, and has been verified by this research. The other amalgams were more tolerant of variation in mixing conditions, which probably favours Revalloy for the best performance in terms of achieving a good quality filling.

The transverse bend method of testing, as described in this chapter has four distinct disadvantages:

a) it provides little information regarding the influence of the

constituent phases on fracture toughness value;

b) it is extremely difficult to produce identical amalgam specimens and this variability could be a source of an unacceptable amount of scatter in experimental data;

c) the scope for acquiring sufficient data for accurate analysis is limited by the amount of amalgam required to produce the beam type specimen;

d) specimens could could not be made from amalgams in extracted or broken teeth that have 'failed' in-vivo.

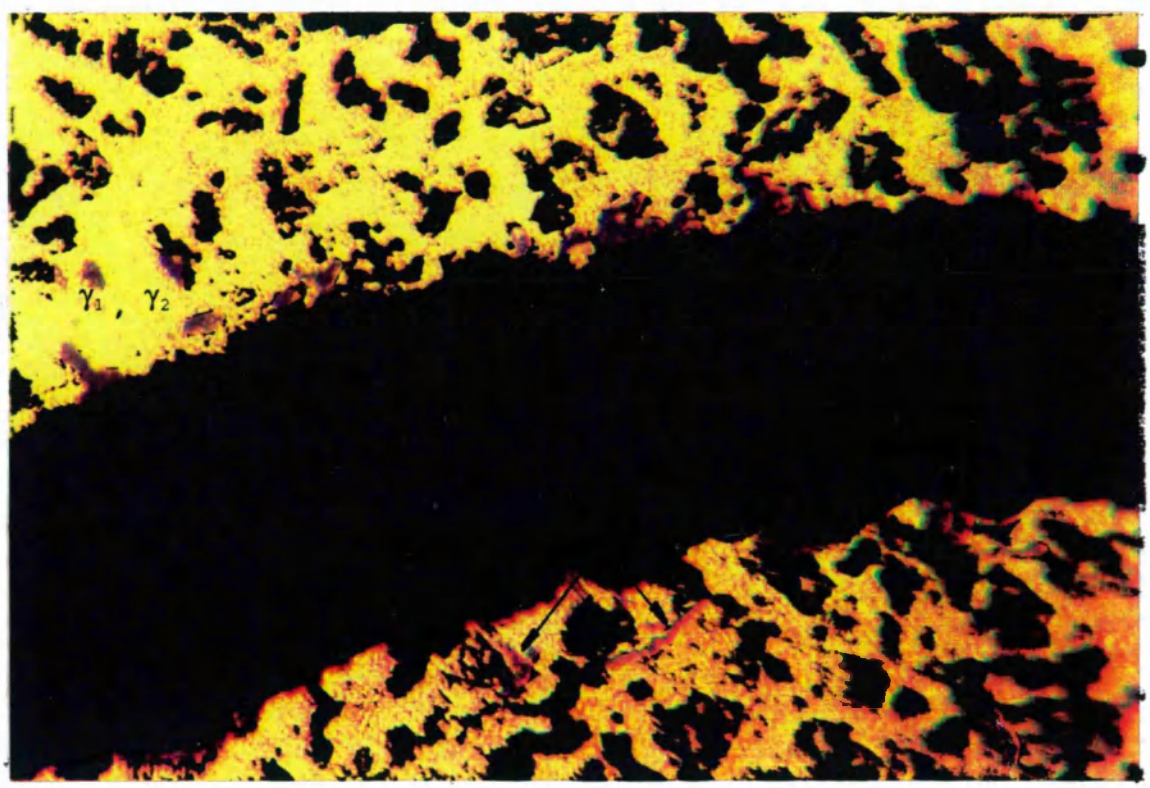

FRACTURE EDGE OF REVALLOY 50μm

Figure 4.14

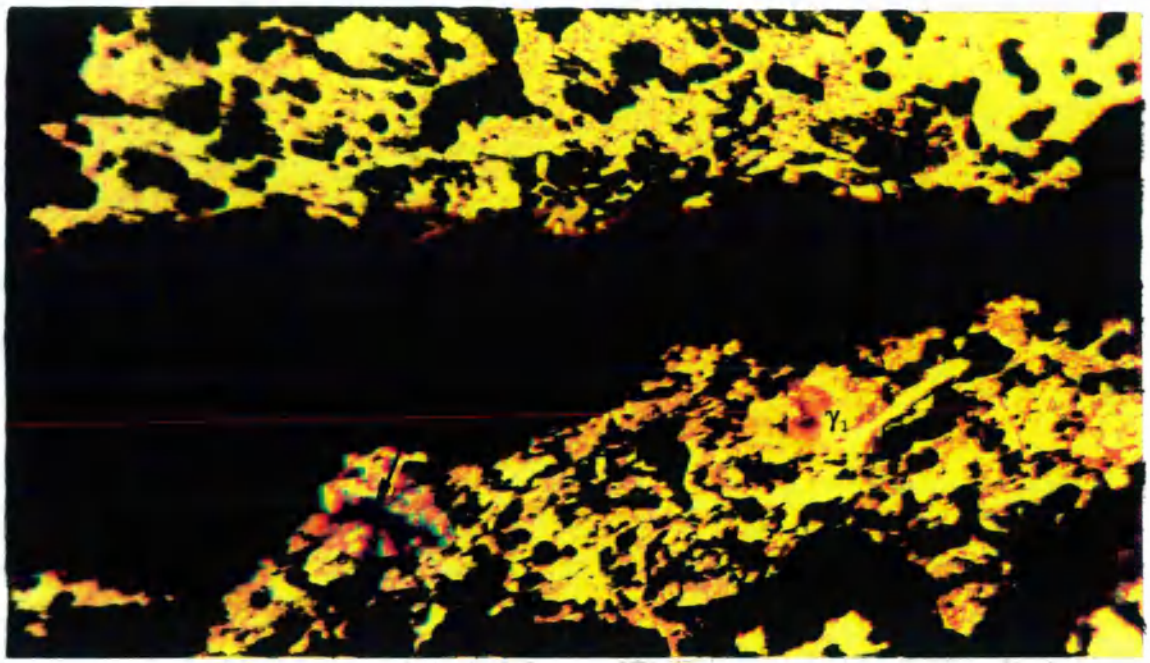

FRACTURE EDGE OF NTDA 50μm

Figure 4.15

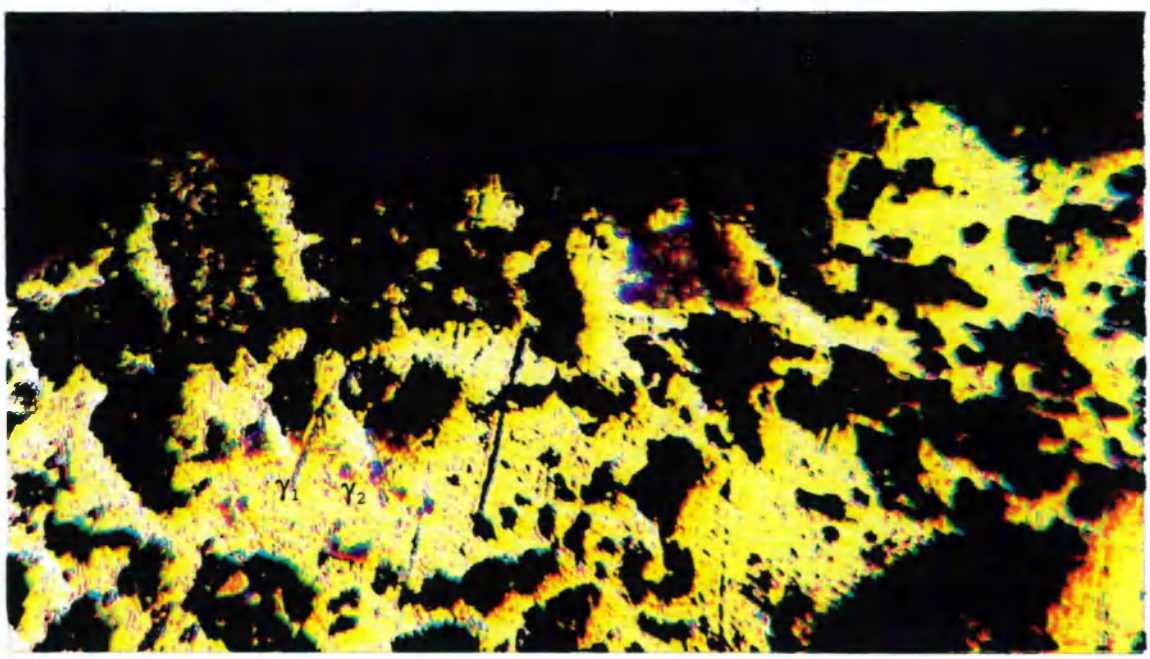

FRACTURE EDGE OF TRADITIONAL 50μm

Figure 4.16

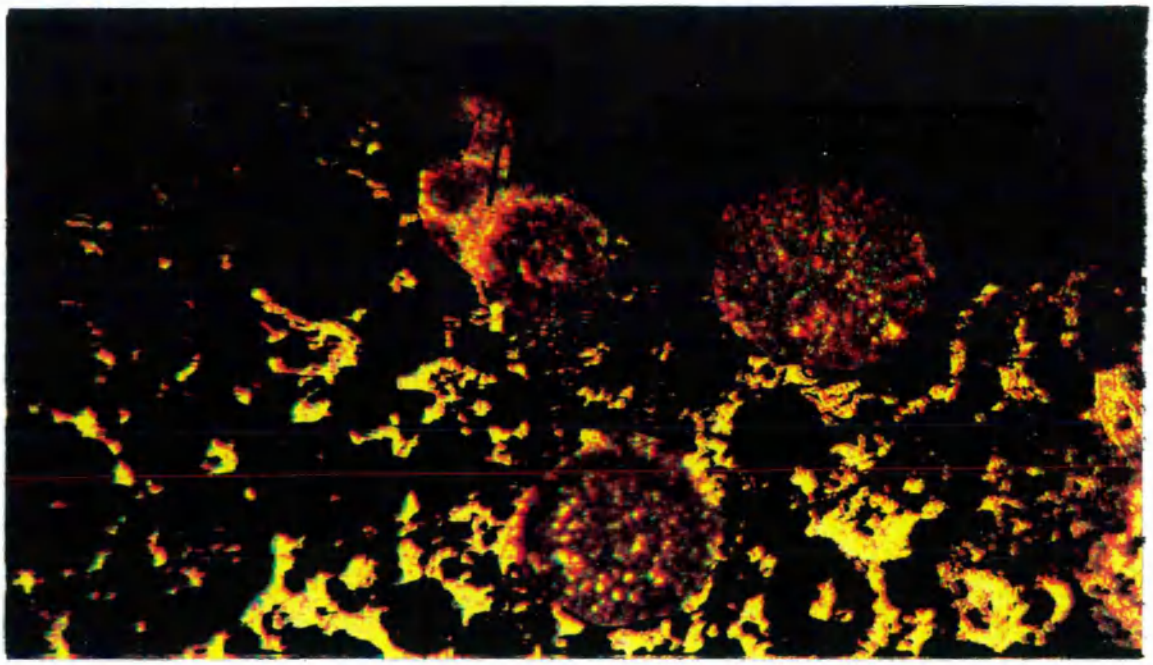

FRACTURE EDGE OF TYTIN

Figure 4.17 50μm

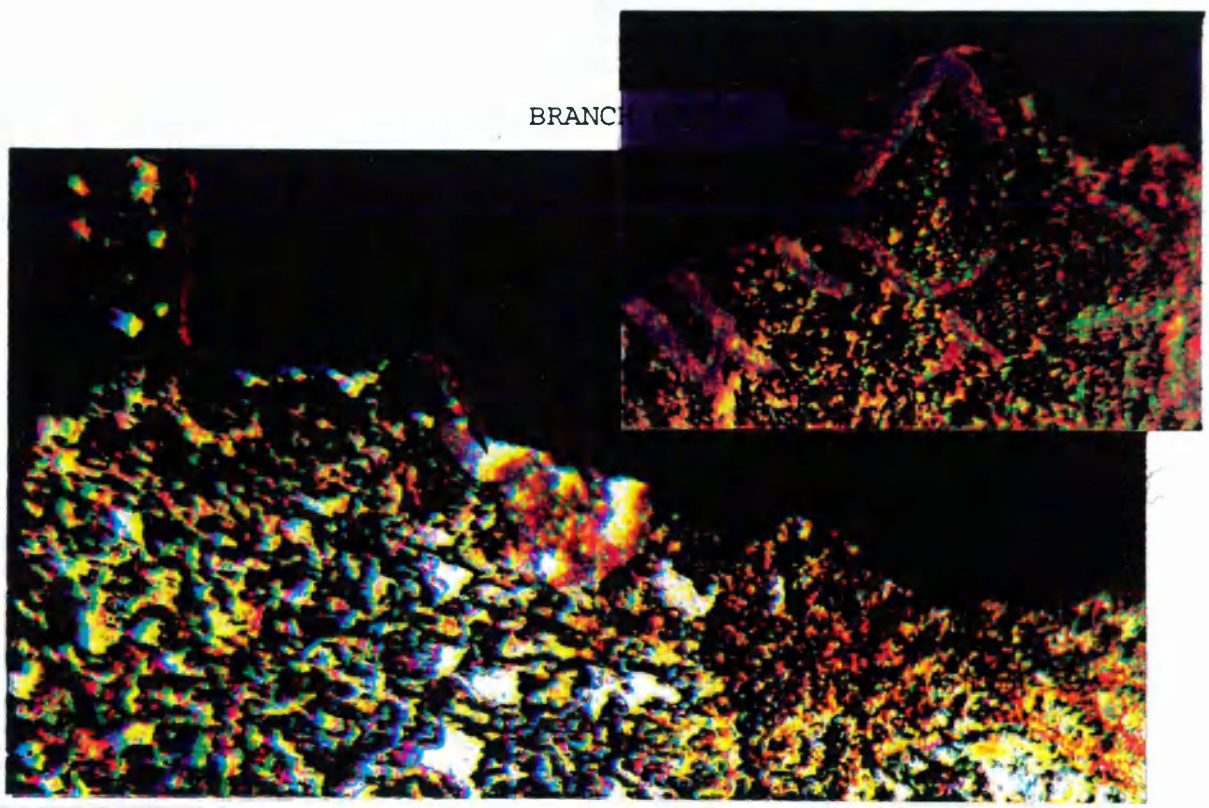

FRACTURE EDGE OF HiCu

Figure 4.18 50μm

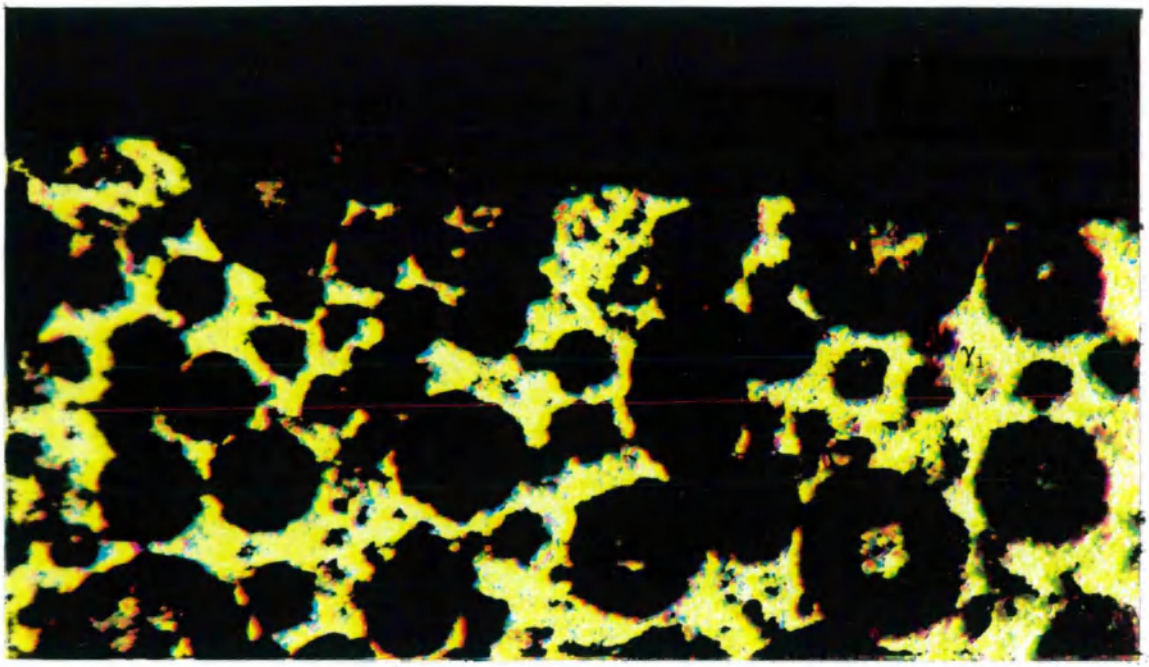

FRACTURE EDGE OF DISPERSALLOY 50μm

Figure 4.19

Fracture testing by indentation, as originally described by Evans and Wilshaw(150) and Evans and Charles (151), if shown to be valid for amalgams, overcomes the criticisms stated above. The next chapter of this present work describes this method of fracture toughness determination for amalgams.

CHAPTER 5

INDENTATION METHOD OF FRACTURE TOUGHNESS DETERMINATION.

Fracture testing by indentation, was originally described by Evans and Wilshaw(150) and subsequently developed by Evans and Charles (151). A brief outline of their approach is presented in the first part of this chapter.

The procedure is based upon the Vickers hardness test and the fact that a measurable radial crack develops at the corners of the diamond impression for certain materials, Figure 5.1.

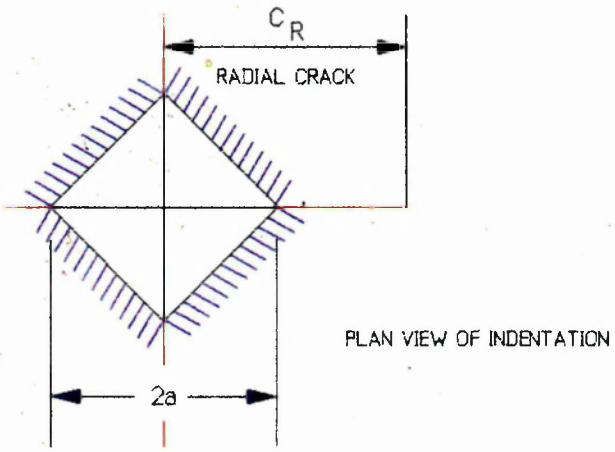

DIAGRAMATIC VIEW OF IMPRESSION AFTER VICKERS HARDNESS TEST ON A 'HIGHLY ELASTIC' MATERIAL

Figure 5.1

The relationship between the results of the hardness test, the crack length, and fracture toughness (K_{IC}) is shown by equation 5.1. The class of materials for which this equation is considered valid will be described later in this chapter and it will be shown that

amalgams can be included.

The relationship developed by Evans and Wilshaw is:

$$K_C = ([H_V \sqrt{a}]/[\phi.10^3)](C_R/a)^{-3/2}(H_V/\phi E)^{0.4} \qquad (5.1)$$

where,
ϕ = constraint factor which depends upon the yield stress,E and hardness of the test material. The method of evaluating this factor is described later.
H_V = Vickers hardness value (MPa)
a = half of the apex to apex dimension of the indentation (μm), (see Figure 5.1.)
E = Young's modulus (MPa).
C_R = radial crack length (μm)
K_C = fracture toughness. Evans was not specific about the fracture mode i.e. he did not refer to the plane strain fracture toughness but left open the possibility of a mixed mode crack propagation.

Theoretical analysis (150) predicts a purely tensile stress field at the periphery of the indentation, which suggests K_{IC} may be assumed.

The particular merits of the indentation method compared with the transverse bend tests are:

a) The microstructure local to the apex of the indentation has a strong influence on the propagation path of the crack and this provides the possibility of detecting the effect of the constituent phases on overall fracture toughness;

b) A typical test area is approximately 600μm by 600μm, therefore many tests can be conducted on one specimen of a size comparable to that used for transverse bend testing. This is important, not only because the effects of inter-specimen variability are minimised, but also cost;

c) A test technique would be available that has very simple instrumentation and data interpretation procedures;

d) It is possible to measure a true 'materials' property that is not influenced by porosity and other specimen manufacturing problems;

e) if valid, the amount of material needed is so small that the test could be done on amalgams that have been extracted.

5.1. Estimation of fracture toughness from Vickers hardness data.

A full explanation of the development of equation 5.1. is lengthy and the following sections are intended only to emphasise the main assumptions made in its derivation.

5.1.1. Material response to the Vickers indentor.

The proposed model for the response of the test material to indentation by a pyramid indentor is shown in Figure 5.2.

The distinction between the inelastic (hydrostatic) core, and the plastic region is described by Lawn and Wilshaw(152). The inelastic deformation may occur by shear-induced flow (either plastic or viscous), or pressure induced densification produced by phase changes or compaction of an 'open' structure. Clearly, it is not possible to speculate which of these mechanisms dominate for any given material. Each deformation mode is characterised by its own complex stress-strain response. This region immediately below the indentor is regarded as an outwardly expanding core which exerts a uniform hydrostatic pressure on its surroundings.

Adjacent to this 'core' is a plastic region within which flow occurs according to some yield criterion. A further complication in analysis is that the small inelastic zone is surrounded by the confining elastic material. The major simplifying assumption is that the the deformation field possesses spherical symmetry.

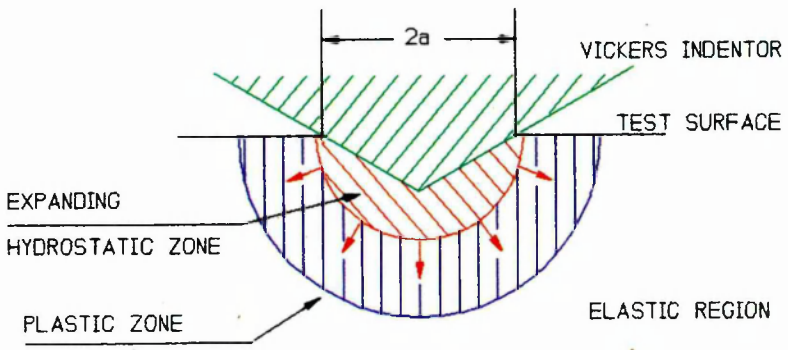

MODEL OF MATERIAL RESPONSE TO A VICKER'S HARDNESS TEST
(After Lawn and Wilshaw, 152)

Figure 5.2

5.1.2. Crack events during the loading and unloading cycle.

Evans and Wilshaw recorded by acoustic and visual methods, both surface and sub-surface cracking events of seven materials which had markedly different properties.

Crack development is in three stages. Figure 5.3 shows these

under the action of a spherical indentor, but the sequence is the same for the Vickers geometry. The difference in material response between these two indentor types is that under the latter one, the crack extension under the unloading stage (stage 3 below) is much greater than occurs under the former one(151).

The three stages of crack development are:

1. The first event observed upon loading was the appearance of shallow, radial surface cracks;
2. As the load value increased during the cycle, an additional circular crack formed with its plane parallel to the axis of loading, ie. vertical, and immediately beneath the indentor. Evans and Wilshaw termed this 'the median crack' and it originates from the development of the Hertzian cracks which initiate while the material is still wholly elastic, i.e. at the start of the loading cycle. Simultaneously, subsurface lateral cracks propagated between the radial cracks;
3. At the instant of unloading, all three crack types extended dramatically.

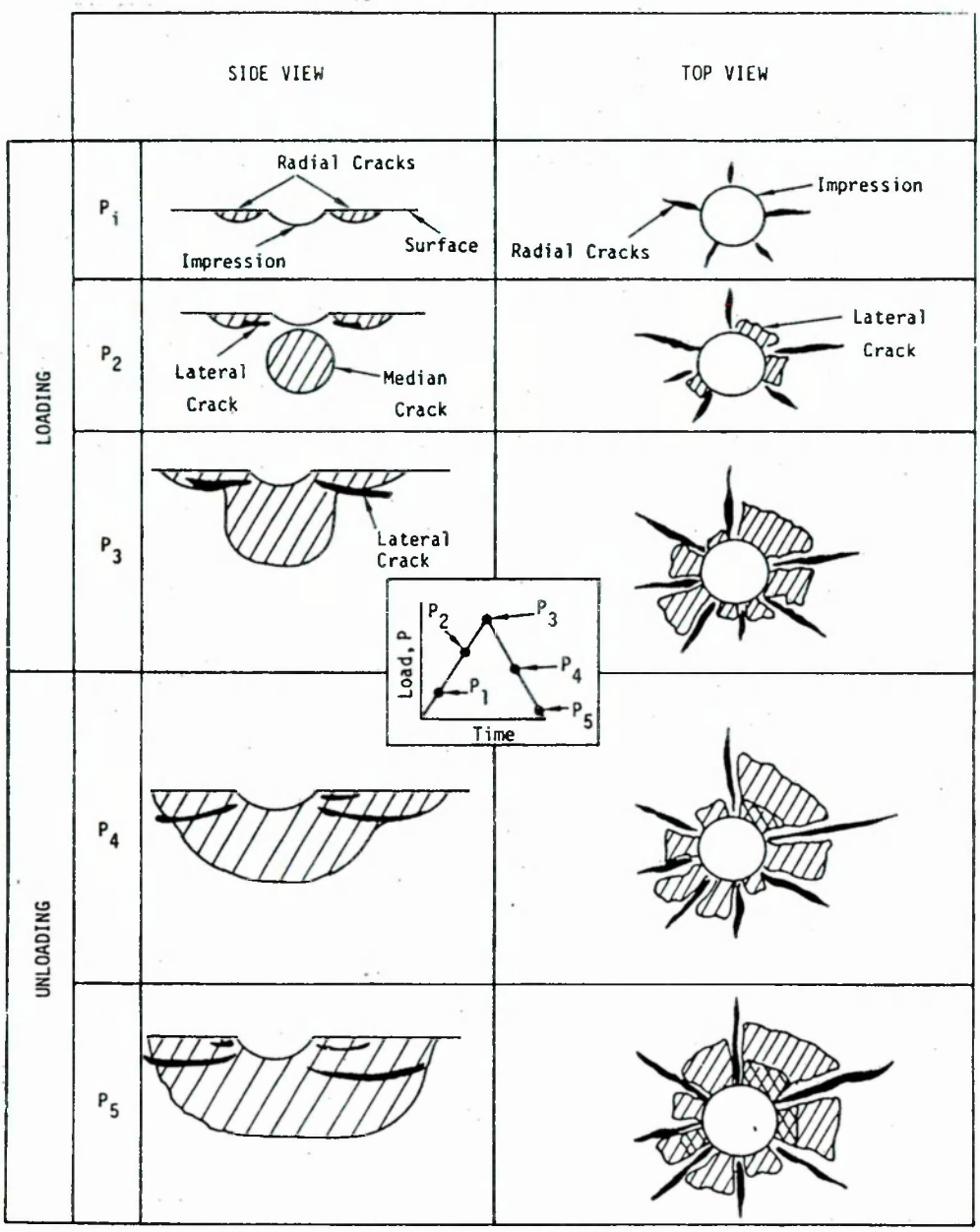

A SCHEMATIC SHOWING THE SEQUENCE OF CRACK FORMATION AND GROWTH EVENTS DURING LOADING AND UNLOADING (After Evans and Wilshaw,150)

Figure 5.3

5.1.3. The dimensional analysis approach in deriving equation 5.1.

Dimensional analysis involves a selection of factors that have an influence on a process which is too complex for theoretical analysis, and in the case of fracture toughness, the factors include yield stress and modulus. By equating the dimensions of the subject with those of the selected factors, the relationships involved in the analysis can be more specifically defined. However, after this stage, the function power indices are still unknown and these must be found by laboratory tests on the material.

The above approach was made by Evans and Charles(151) to overcome the analytical complexity involved in the elastic/plastic deformation involved in the hardness test(152-154). It obviously relies for its accuracy on a full and correct choice of the influencing factors, and a general correspondence between the test materials used to establish the function terms and other materials to which the empirical relationship is to be applied.

Evans developed a relationship between K_{IC} and the parameters involved in the Vickers hardness test, by combining both theory and test results. The tests that were conducted by Evans enabled the functions involved in the dimensional analysis to be determined and various single crystal and polycrystalline specimens were used.

The standard generalised form of equation for describing the critical stress intensity factor for the situation that approximates to the indentation geometry is:

$$K\sqrt{a} = f_1(C/a) \int_{-c/a}^{+c/a} f_2[(C/a),(r/a)]\ \sigma\ d(r/a) \qquad (5.2)$$

where, C and a are defined in Figure 5.1

r = distance from a chosen origin of the point at which the stress (σ) is being considered.

$f_1(C/a)$ and $f_2[(C/a),(r/a)]$ are dimensionless functions of (C/a) and [(C/a) & (r/a)] respectively.

The equation 5.2 was selected from a large number of case studies that were carried out at Lehigh University, USA and recorded in a compendium of stress intensity factors(155).

The next stage in the analysis is to consider σ. Mindlin's analysis(156), when applied directly, enables the stress distribution to be determined for the case of an elastic, semi-infinite solid resulting from deformation by a rigid spherical indentor. The situation is complicated by the existence of two zones other than the elastic region (Figure 5.2). The hydrostatic core and the plastic zone result in modifications to the basic Mindlin theory(156) being necessary and a full description is provided by Lawn and Wilshaw(152). From these considerations, Lawn and Wilshaw developed a rationale so that σ in equation 5.2, can be replaced by the expression:

$$\sigma = \sigma_Y[f_3(R_Y/a),\ f_4(r/a),\ f_5(\upsilon),\ f_6(\mu)] \qquad (5.3)$$

where,

R_Y is the radius of the yielded region, Figure 5.2.

υ = Poisson's ratio of the test material.

μ = coefficient of friction between the test material and the indentor face.

σ_Y = uniaxial yield stress.

When equation 5.3 is substituted into equation 5.2 to replace σ, and integration is carried out, the following form is obtained:

$$K_{IC}/\sigma_Y \sqrt{a} = F_1(C/a)F_2(\upsilon,\mu,R_y/a) \qquad (5.4)$$

F_1 and F_2 are the integral forms of the functions occurring in equations 5.2 and 5.3.

It is necessary to develop equation 5.4 into a form comprising terms that are obtainable from the hardness test. This is achieved in part, by noting that the expanding spherical hydrostatic core (Figure 5.2) can be described by the expanding spherical cavity theory, Hill(157). This theory was later adapted by Marsh(158) to apply to the hemi-spherical cavity of the indentation geometry.

From this approach the uniaxial yield stress can be expressed in terms of the Vickers hardness value (H_V) and a constraint factor (ϕ), thus $H_V/\sigma_Y. = \phi$

Further details of the method of evaluating ϕ are given in the following section, however, equation 5.4 may now be expressed as:

$$K_{IC}\phi/H_V \sqrt{a} = F_1(C/a)F_2(\upsilon,\mu,R_y/a) \qquad (5.5)$$

At this stage certain simplifying assumptions have to be made:

a) the coefficient of friction (μ) is approximately independent of the test material for a particular geometry of indentor(150);

b) Poisson's ratio is in the range 0.22 and 0.3 - which encompasses the value for amalgams.

Reference to the analysis of the expansion of a spherical cavity (Hill,157), shows that the term (R_Y/a) is a function of E/σ_Y. Also, because $H_V/\sigma_Y = \phi$, R_Y/a can be expressed as, $F_2(H_V/E\phi)$ and consequently the equation 5.5 can be modified to:

$$K_{IC}\phi/H_V \sqrt{a} = F_1(C/a)F_2(H_V/E\phi) \qquad (5.6)$$

Up to this stage the analysis has been quite general although there are some constraints on the type of material, notably that they must comply with the expansion of a spherical cavity theory in their response to indentation.

The functions F_1 and F_2 were determined by Evans and Charles(151) from tests on a range of single crystal and polycrystalline specimens. The gradient of the plot of $K_{IC}\phi/H_V \sqrt{a}$ against C/a for the various test materials (Figure 5.4a) enabled F_1 to be evaluated. This approximated to $(C/a)^{-3/2}$. There was, however, a significant degree of data scatter according to the test material being considered. Further experimentation showed that when the function F_2 was applied in the power form $(H_V/E\phi)^{0.4}$, this corrected the data (Figure 5.4b).

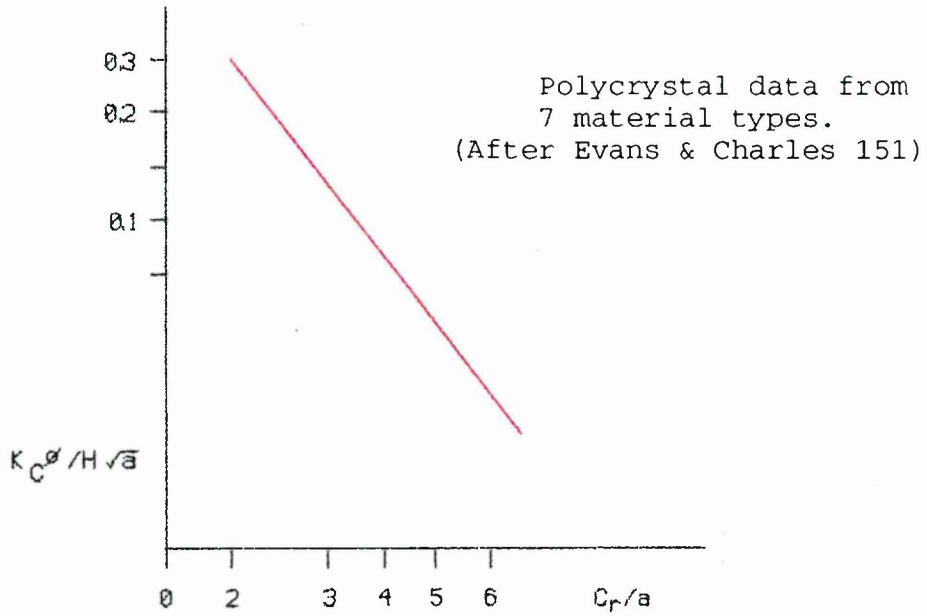

Figure 5.4(a)

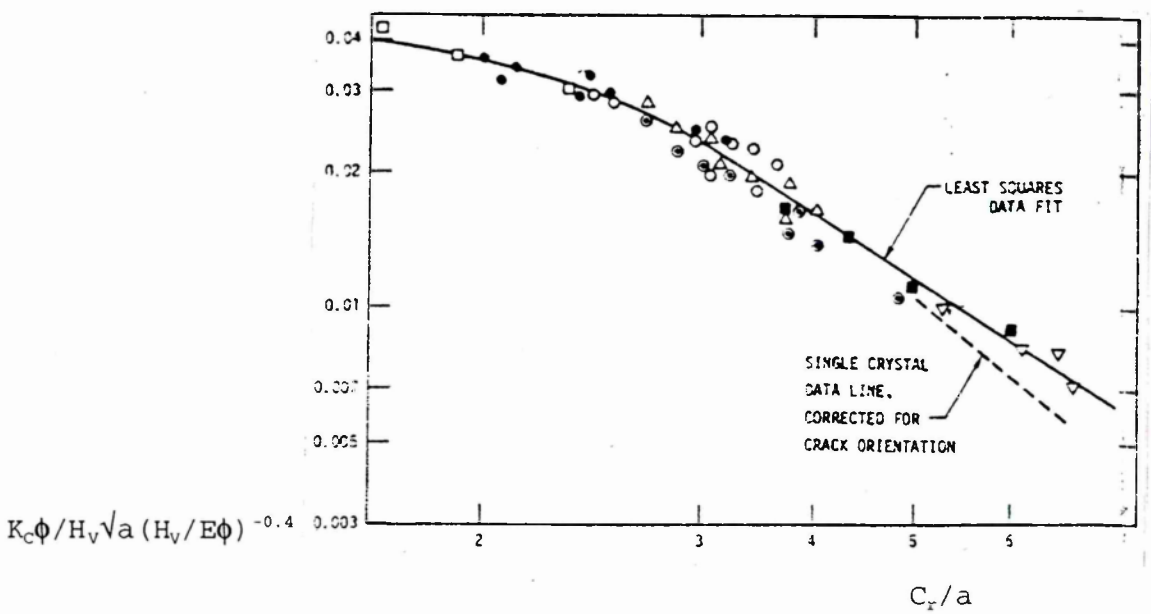

RADIAL CRACK EXTENSION DATA FROM FIGURE 4.4(a) CORRECTED FOR DEPENDENCES ON $E\phi/H_V$ AND CRACK MISORIENTATION.

Figure 5.4(b)

These graphs show that linearity is established when the ratio of C/a is greater than 2. Because K_{IC} used in the construction of these graphs were the 'bulk' values determined by the double-torsion method(159), it is probable that the non-linearity at low C/a values arises from the sensitivity to the microstructure at the apex of the indentation.

Finally, with these functions established, the equation 5.1 is presented in a form that enables K_{IC} for the material to be determined providing C_R, H_V, a, E and ϕ are known.

5.1.4. Method of determining ϕ

Marsh describes two classes of materials,

a) those which conform to the Tabor relationship $H_V/\sigma_Y \approx 3$ (160), and
b) those which are pertinent to this present work, ie. are regarded as 'highly elastic' where fracture stress and yield stress are very close in value. This latter group does not comply with the Tabor relationship, but can be described by the analogy of an expanding spherical cavity (157).

Reference to the works of Hill and Marsh provides full details on the development of a relationship connecting Vickers hardness (H_V) and the yield stress (σ_Y). The final result of their analyses for materials relevant to (b) above, is:

$$H_V/\sigma_Y = 0.6\log_e(E/\sigma_Y) + 0.28 + 0.6\log_e(3/[4 + \upsilon]) = \phi. \qquad (5.7)$$

The experimental method is simplified by the graphical solution of this equation as shown by Marsh (Figures 5.5 and 5.6). Thus, if Young's Modulus (E) and the value of H_v are known for a particular material, these graphs enable ϕ to be evaluated. An example of this graphical solution for ϕ is shown later, Figure 5.23.

5.1.5. Control test.

A comparison between the two methods described for evaluating K_{IC} was made using soda glass as a control material. This material was chosen because it is isotropic and amorphous. Both characteristics are considered to be conducive to obtaining straight, radial cracks which originate from the apex of the indentation. It was also reasoned that there should be minimal variations in length between cracks at different apexes. These conditions simplify the interpretation of the parameters involved in equation 5.1.

The transverse bend result of a glass specimen, of the same dimensions as the amalgam ones reported in Chapter 3, was 0.8 $MN/m^{3/2}$. This value is in general agreement with reported values of 0.7 $MN/m^{3/2}$(161) and 0.8 $MN/m^{3/2}$ (152). The notch in the glass was formed by an ultrasonic machining process. The hardness test method used under different loads produced the results shown in Table 5.1. The value of E used in equation 4.1 was assumed to be 70 GPa - this figure was quoted by Marsh(158). The value of ϕ equal to 1.5 was found by using the graphical method shown by Figure 5.23, and is in agreement with Marsh.

Table 5.1

K_{IC} UNDER VARIOUS LOADS

Load(kg)	'a' μm	H_V	C_R μm	K_{IC} ($MN/m^{3/2}$)
1.0	31	498	113	0.77
2.5	45	505	189	0.81
5.0	65	540	320	0.85

Examples of K_{IC} obtained from various cracks on the same specimen under 1 kg are shown below:

Load 1 kg, H_V = 498(constant), E = 70 GPa, ϕ = 1.5

Trial	C_R(μm)	K_{IC}($MN/m^{-3/2}$)
1	113	0.77
2	110	0.80
3	115	0.75
4	110	0.80
5	110	0.80
6	108	0.82
7	110	0.80
8	114	0.76
9	110	0.80
10	111	0.79
Mean K_{IC} = 0.79 $MN/m^{3/2}$	Standard deviation = 0.022	

The results of using this method on glass were excellent; the readings of crack length were identical from whichever apex was being considered, within the accuracy of the reading system.

It is clear from the above table that the K_{IC} values from the two methods are very similar and provide a basis for the hardness test to be applied to amalgams and compared with SEN values. The cracks were straight and radial, as anticipated, and this enabled unambiguous measurements of C_R to be made. Photographic evidence of the results could not be obtained because of the transparency of the test material - the specialist photographic equipment necessary was not available.

The composite nature of amalgams presents particular interpretation difficulties, but this control test indicates that the technique is particularly useful for basic design of composite materials generally, i.e. various combinations of ceramics, polymers or metals where the properties of the components are accurately known..

5.1.6. Assessment of amalgams for validity of equation 5.1.

Marsh found that the mode of deformation under the Vickers indentor enables a distinction to be made between the two classes of materials described in section 5.1.4. and this is achieved by sectioning the diamond impression and viewing its edge. The materials for which the flat rigid die analogy of Tabor is accurate, show a build-up in the region of the indentation periphery, whereas those conforming to the spherical expansion cavity theory show a 'sinking- in' as expected from the radial flow that would occur under the 'expanding core' model shown in Figure 5.2. Finite element analysis has shown this transition from one deformation mode to the other (153)(Figures 5.7a and 5.7b).

The dental amalgams tested in this present research fell into the latter category.

The view of the cross section of the indentation in a specimen of amalgam shows that the 'sinking-in deformation is evident (Figure 5.8) and the clear evidence of cracking shows that amalgams are promising candidates for this procedure.

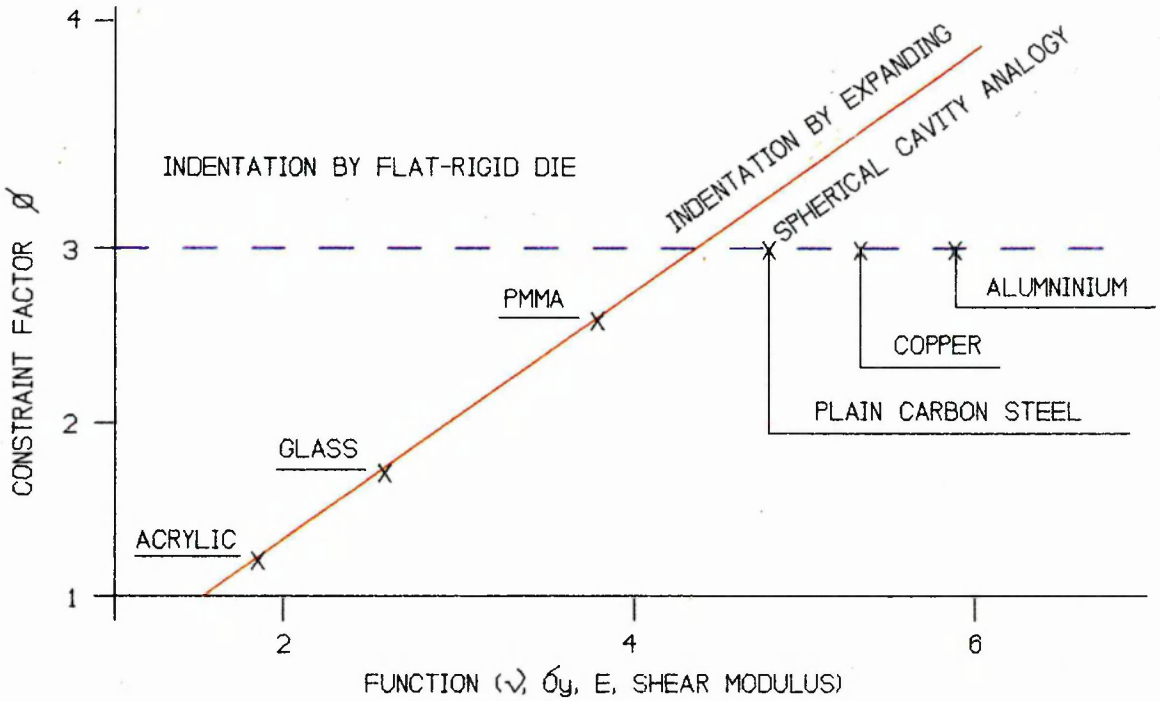

THE VALUES OF ϕ FOR VARIOUS MATERIALS (Ref.Marsh,158)

Figure 5.5

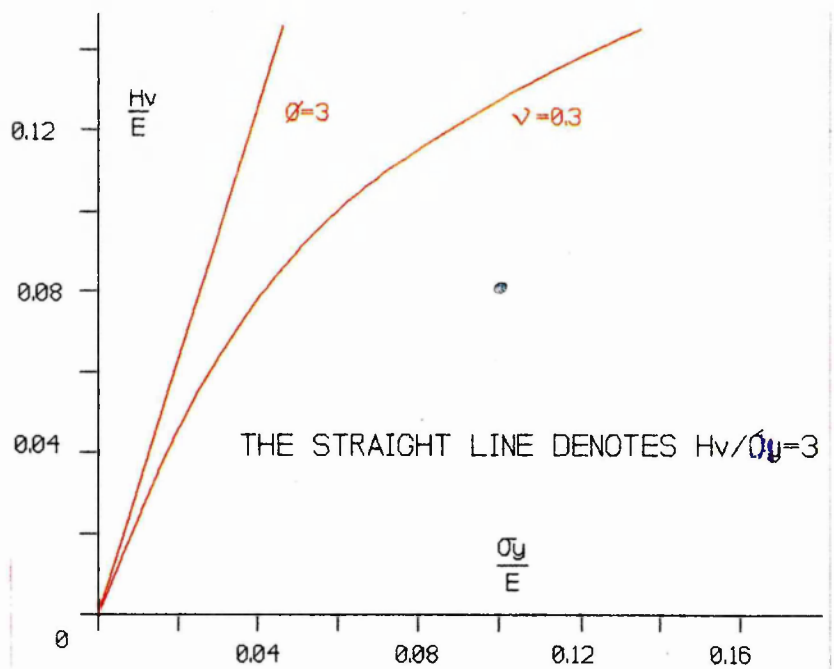

CONVERSION GRAPH SHOWING H_v/E AND σ_Y/E

Figure 5.6

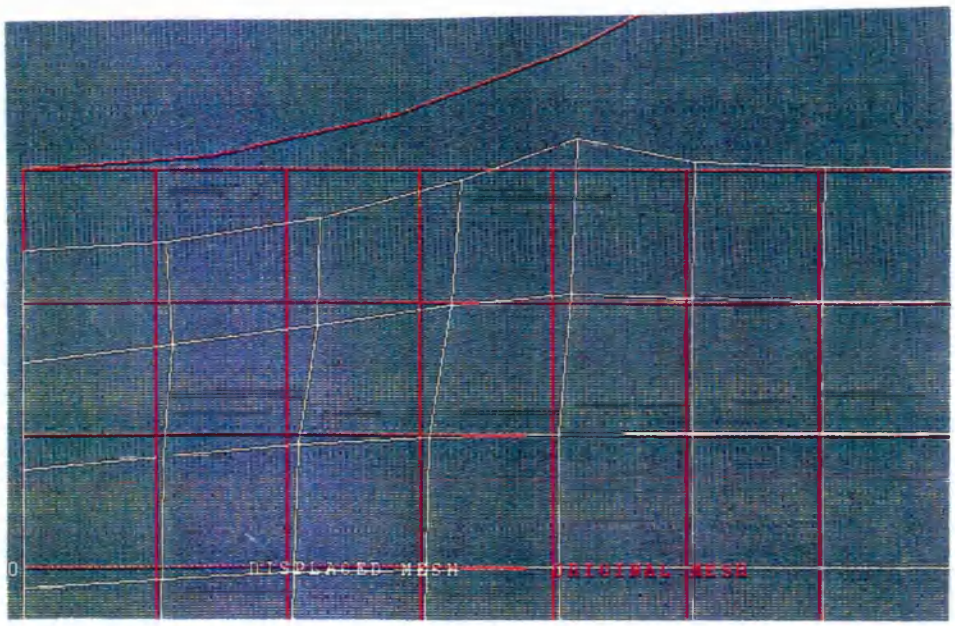

(a) Built-up edge of a material complying with $H_V/\sigma_Y \sim 3$
Model material 0.1%C steel.

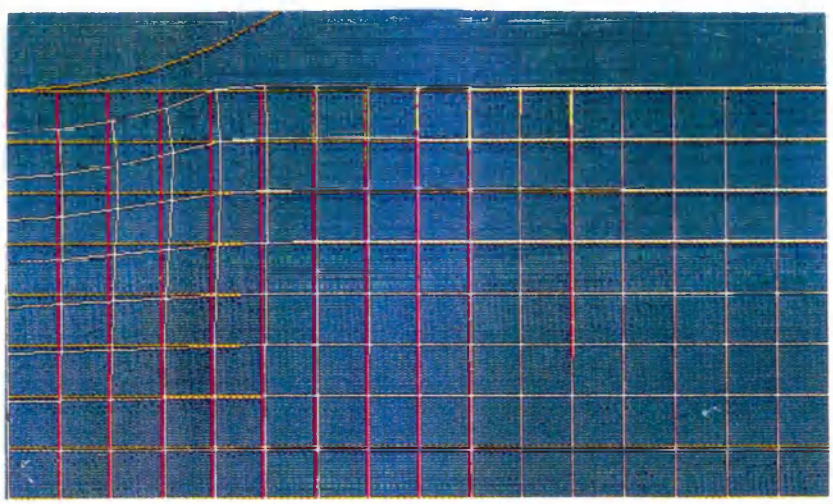

(b) Edge appearance of a material complying with observations of Marsh. Model material 0.54%C steel.

FINITE ELEMENT MODELS OF MODE OF SURFACE DEFORMATION SHOWING TRANSITION FROM 'BUILT-UP' TO 'SUNKEN- EDGE' CONDITIONS.
(After Hartill,153)

Figure 5.7

CROSS-SECTION OF INDENTATION
(SIDE VIEW)

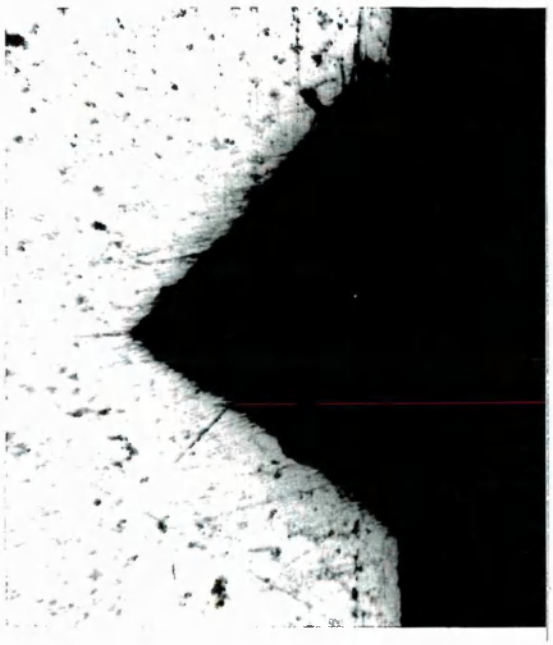

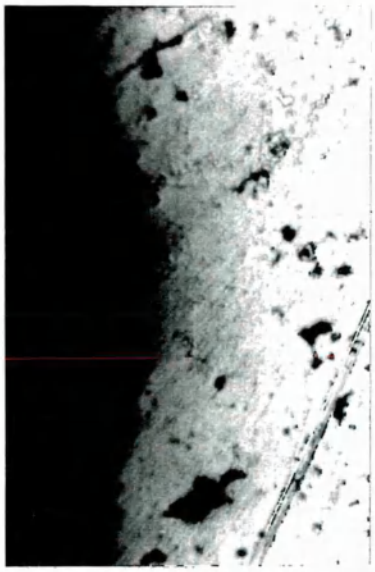

PLAN VIEW OF INDENTATION

150 μm

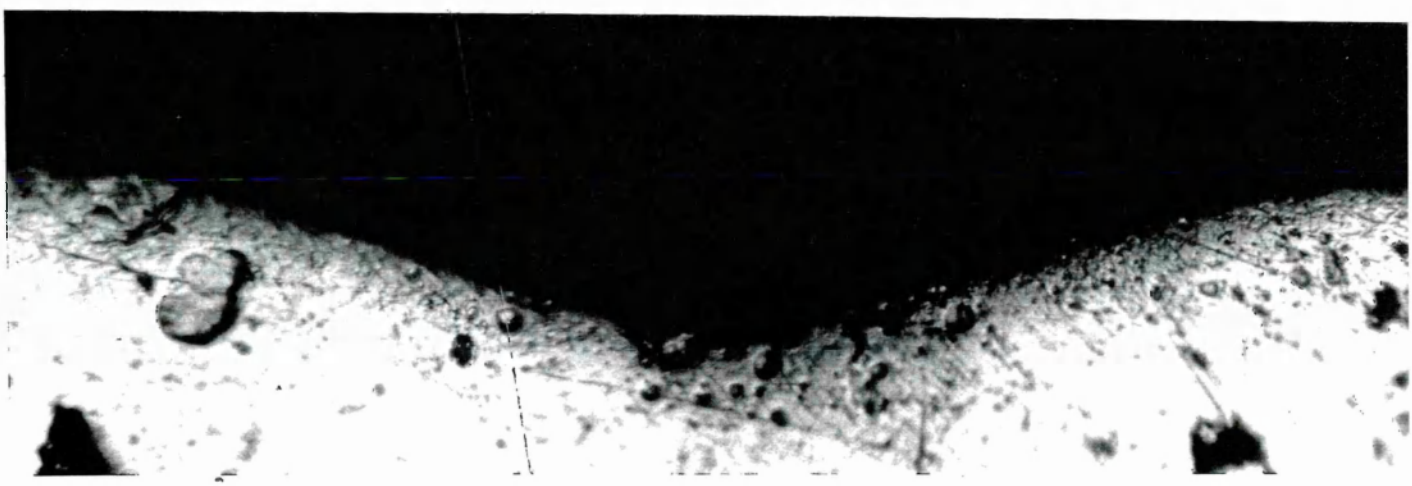

75 μm

SUNKEN EDGE OCCURING IN AMALGAMS.

ENLARGED VIEW OF SECTIONED INDENTATION - OVERLEAF

SUNKEN EDGE OCCURRING IN AMALGAMS.

Figure 5.8

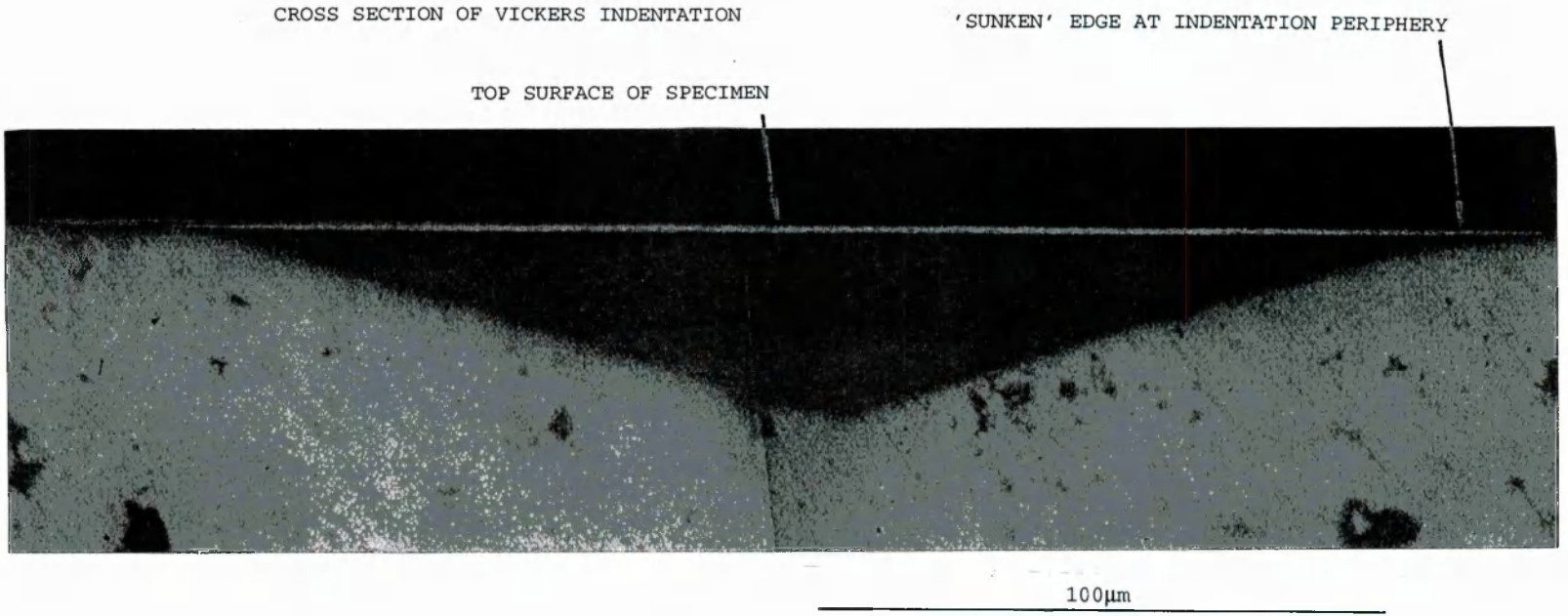
CROSS SECTION OF VICKERS INDENTATION
'SUNKEN' EDGE AT INDENTATION PERIPHERY
TOP SURFACE OF SPECIMEN
100µm

Figure 5.8

5.1.7. Discussion.

Hassan (162) assumed that the work of Evans applies equally to amalgams and used a simplified version of equation 5.1 to estimate K_{IC}. His values were significantly lower than the ones found by transverse bend tests (approximately $0.8MN/m^{3/2}$), mainly because he assumes that the value of ϕ was constant at 3. It will be shown that this is incorrect and a value of $\phi = 1.5$ would be more appropriate which would bring Hassan's results of K_{IC} more in agreement with the transverse bend test values quoted in Chapter 3. The work of Hassan lacks detail of the test used and therefore it was considered necessary to make a close study of the effect of test parameters on the fracture toughness of amalgams.

Evans et al (150,151) assumed a spherical indentor in their initial theoretical approach to K_{IC} determination. Analysis was thus simplified because elastic contact could be maintained up to the instant of fracture. They subsequently made empirical adjustments to their analysis to allow for the Vicker's geometry. Haggag et al (163,164) did not follow this but retained the spherical geometry for their test procedure. The resulting relationship between K_{IC} and the test parameters is limited to cases where plastic flow during indentation is evident. Although the experimental results do not clearly explain the means of assessing this, it is assumed that it is manifested by the 'pile-up' of material around the periphery of the indentation, i.e. the expansion of a spherical cavity model does not apply. For brittle materials such as amalgams and a variety of intermetallics, published work has concentrated on the Vickers test for small specimen testing, or when appropriate, the SEN method is

common (165,166).

Currently, manufacturers of ceramic-tipped cutting tools use the Vicker's micro test and quote the length of the cracks originating from the indentation as a general material grading system. Recent developments by Ochi et al (167) have produced a quantitative approach to the evaluation of silicon carbide ceramics. However some aspects of the interpretation of results need to gain universal acceptance before industry can confidently apply the technique for product quality control.

One particular feature of concern is the manner in which the cracks are considered. Each crack from a specific indentation can be used to derive K_{IC}. Alternatively, an average of two or more cracks measured from specified positions on an indentation may be used to obtain a 'bulk' value of K_{IC}. The variation in crack length occurs due to structural or stress anisotropy. The chosen approach clearly depends on the purpose of the test - K_{IC} from a single crack gives information about the influence of microstructure in the locality of the indentation apex. This describes the work of Duncan-Hewitt et al (168), where analysis was conducted on individual pharmaceutical crystals.

The procedure of averaging crack lengths was used by Ashizuka (169) to compare the fracture toughness of a range of amorphous glasses. Byakova (170) also used the averaging method on a wide range of materials, including many types tested by Evans et al.

A basic assumption in the development of equation 5.1 is that the side view of the radial crack is 'half-penny' shaped, Figure 5.3. Laugier (171) described a modification which does not impose this constraint with regard to crack profile. He states that the

crack configuration is more likely to be of the Palmqvist type, Figure 5.9, particularly if there is a ductile phase present as in the case of cermets.

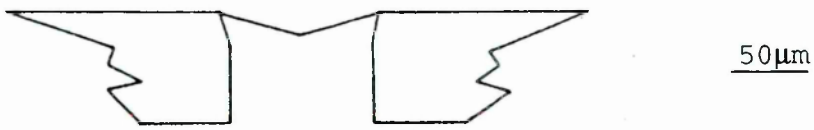

PALMQVIST-TYPE CRACK FROM VICKER'S INDENTATION.

Figure 5.9

The Laugier equation, $K_{IC} = 0.15(1/a)^{-1/2} (E/H_V)^{2/3} P/C_R^{3/2}$ produces very similar values for the test material used by Evans et al. The symbols a, E, H_V and C_R have the same meaning as defined for equation 5.1. P = the applied load in the Vicker's test.

Although Laugier's equation promises a wider choice of materials suitable for indentation testing, there are some doubts about the assumptions made in deriving the constant 0.15. Use of Evans' equation 5.1 is preferred for this present work because, it is thought that Laugier has assumed that the ratio H_V/σ_Y is constant at a value of 3. The possibility of errors arising from this assumption is noted at the beginning of this section.

This present work compares the response of amalgams to the indentation process with that of the specimens used by Evans. It will be shown that there are sufficiently close comparisons of crack initiation and propagation to justify using the technique on the range of amalgams described in Chapter 3.

5.2. Test procedure

K_{IC} was estimated using equation 5.1 for the same amalgams that were tested for transverse bend values. Finally, the results will be discussed in terms of the fracture toughness values obtained, and the factors that may affect the results.

Part of the test procedure was to determine E for each amalgam type to enable ϕ to be evaluated for every indentation.

5.2.1. Crack initiation and profile.

It was considered that if amalgams exhibit identical, or similar, crack initiation and growth stages as the materials used by Evans, then the application of equation 5.1 in unmodified form could be regarded as justified.

Monitoring of the crack sequence and geometry in the original investigation by Evans was aided by the fact that his specimens were transparent and he had elaborate acoustic-emission instrumentation at his disposal. Neither of these facilities was available in this present research, therefore it was decided to check for only two features:

a) to determine the stage in the loading cycle when a crack initiated and then to confirm that the major part of its growth occurred in the unloading step;
b) to investigate the geometry of the radial crack.

5.2.1.1. Crack initiation stage.

The procedure now described was to determine the point of crack initiation.

A Rockwell hardness testing machine was adapted to accomodate a Vickers indentor. The Rockwell machine provides the facility to apply a constant load for an indefinite time period which is required for this approach.

A reservoir containing dye penetrant (Figure 5.10) was used as a carrier for a test piece of HiCu amalgam. This particular amalgam was used because crack growth was more easily discernable than with other types. There was sufficient dye to totally submerge the specimen.

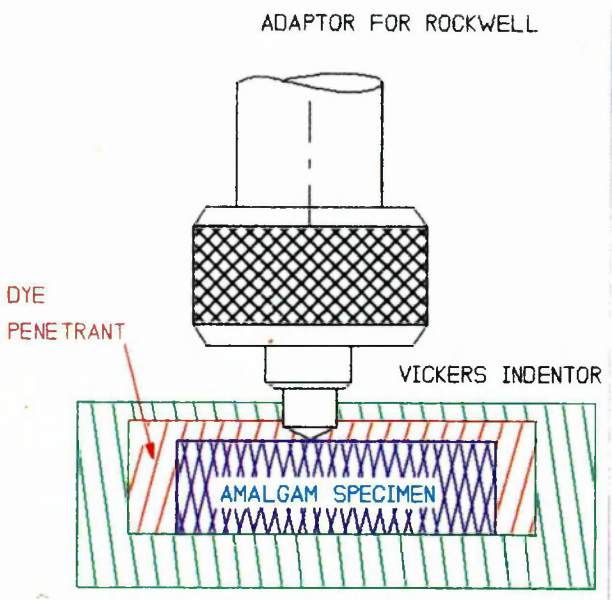

TEST SET UP FOR DETECTION OF CRACK INITIATION

Figure 5.10

A load of 5kg was then applied to the specimen surface through the adapted indentor, which simulated the Vickers test. Any crack forming under the loaded condition would have an immediate ingress of penetrant. The next stage was to drain the dye from the

reservoir in the shortest time possible, and to thoroughly clean the specimen surface with the proprietary solution. The standard developer spray was then applied to the test surface to reveal the crack length under load.

The load was then released and any further crack growth is masked by the developer. The crack length that existed under load, at this stage was shown by the dye contrast (Figure 5.11). The developer was then cleaned off the specimen surface and a further application of dye was sprayed onto the area to clarify any further growth during unloading. The total extent of the final crack is shown in Figure 5.11.

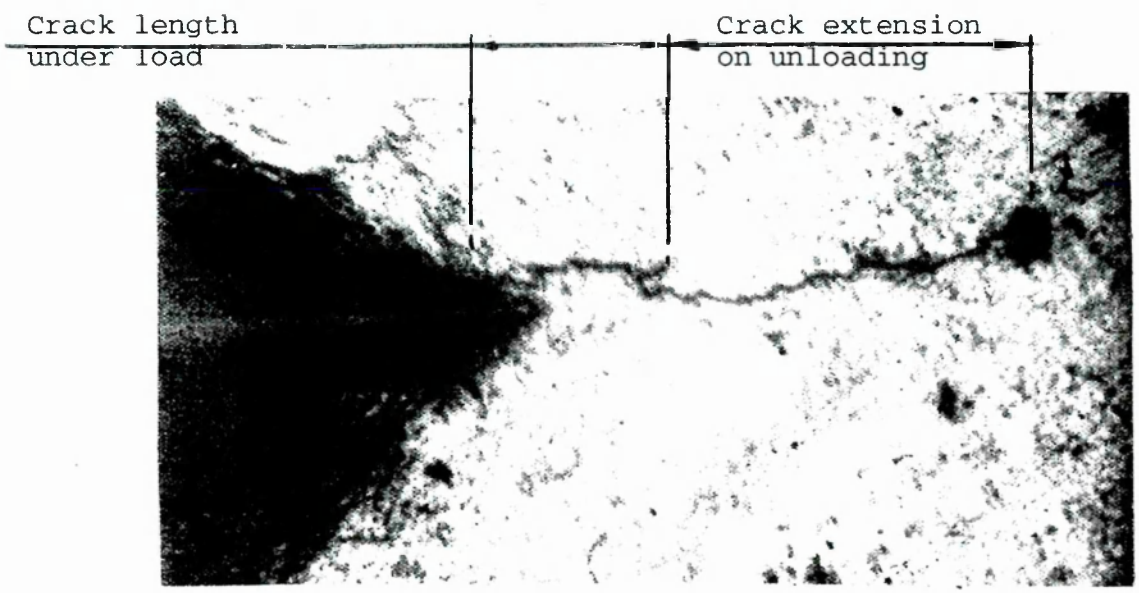

VIEW OF HiCu AMALGAM AFTER CRACK INITIATION TEST

Figure 5.11

The observed sequence was in general agreement with that proposed by Evans in section 5.1.2. The conclusion was that the small crack observed at the loaded stage was of a dimension

comparable to the grain size of the unreacted γ phase. This suggests that initiation can be very sensitive to conditions local to the impression apex. It is also probable that the growth stage is initiated at the instant of unloading.

It is appreciated that this is a very approximate approach but it certainly confirms that amalgams behave in a similar manner to the materials tested by Evans. It should be noted that the time that the specimen was under load had to be kept to a minimum because of possible time-dependency of crack growth. This effect would have minimised the difference in crack length between the loaded and unloaded conditions.

5.2.1.2. Crack profile.

Several unsuccessful approaches were made to obtaining an estimate of the crack profile. Because of the unavailability of resources, a basic appraisal only could be made. However, the penny-shaped radial crack profile proposed by Evans was confirmed.

A plan view of the indentation of Dispersalloy showed quite clearly the extent of the horizontal projection of the crack at its origin. This is shown diagramatically for clarity in Figure 5.12, with the measured dimensions. Using the information that the inclusive angle of the indentor is 136°, the depth at the crack origin was calculated as 7μm.

By focusing on the root of the crack during SEM analysis, it was possible to estimate that its depth was zero at its termination point. Thus an approximate profile may be deduced.

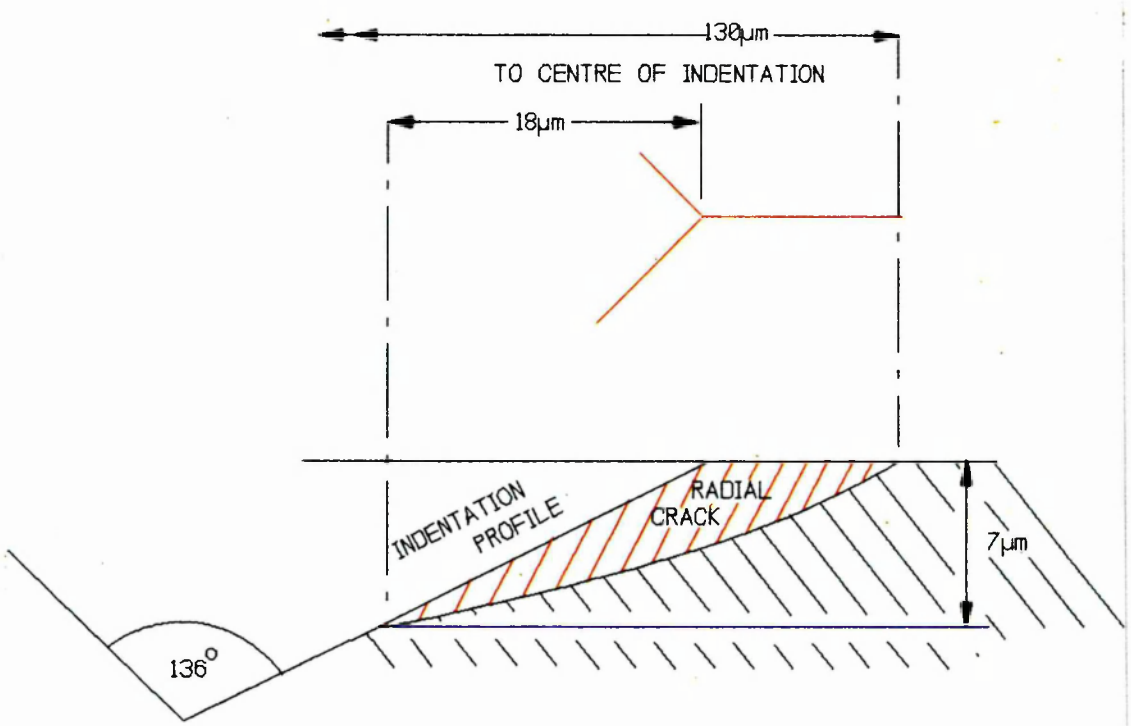

ESTIMATED CRACK PROFILE FOR DISPERSALLOY

Figure 5.12

5.2.1.3. Conclusion.

There are reasonably clear indications that there are no anomalies between the crack sequence of amalgams compared with those of the materials observed by Evans. Therefore, it is felt that for an initial study such as this, equation 5.1. may be justifiably used without adjustment to the empirical functions F_1 and F_2.

5.2.2. Effect of load on each amalgam type.

The Vickers hardness value was obtained for the range of test amalgams under loads ranging from 2.5kg to 10kg. For each test load

case, the definition of the diamond impression was checked.

Figures 5.13 to 5.17, show the results of this investigation on HiCu. The optimum load is defined as one which gives a clear diamond indentation with well-defined, single radial cracks. Although in most cases, 5kg was found to produce the best results, there was an exception which will be discussed later.

Some comments will now be made on the details of the indentation profile.

The phases coincident with an indentation edge can produce evidence of fragmentation, probably due to the growth of lateral cracks as described by Evans. Figure 5.14 shows an unsatisfactory situation arising from excess load where the edges of the diamond have collapsed. Figure 5.15 shows a satisfactory loading condition. A second check was made to ascertain if well-formed cracks were present at the corners of the impression. On low loads (ie. 2.5kg), no cracks were present in many test impressions, and at high loads (ie.10kg), multi-cracks developed (Figure 5.18).

BS 427(172) indicates that the hardness figure obtained from a Vickers test may show a dependence on the test load that is applied, for low values. The above tests showed that 5kg was in the load independent regime as described in this Standard and was thus used as the minimum throughout the test programme. This is generally in agreement with the value found by Hassan et al(162).
However, on two materials a higher load could be used without losing the quality of impression definition.

It is possible to have a situation where two or more cracks unite from several sources (Figure 5.19). Readings from this type of situation were ignored for consistency of results.

IMPRESSION UNDER 2.5kg
Figure 5.13

IMPRESSION UNDER 3.5kg
Figure 5.14

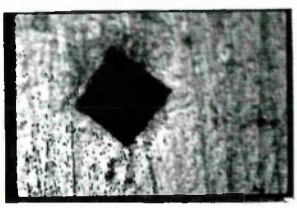

100μm

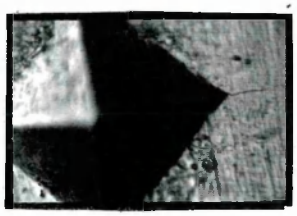

100μm

IMPRESSION UNDER 5kg (Crack develops at 5kg)
Figure 5.15

IMPRESSION UNDER 6.0kg
Figure 5.16

100μm

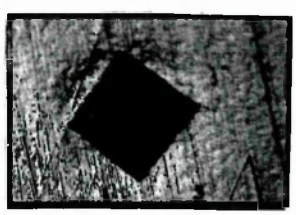

IMPRESSION UNDER 10.0kg
Figure 5.17

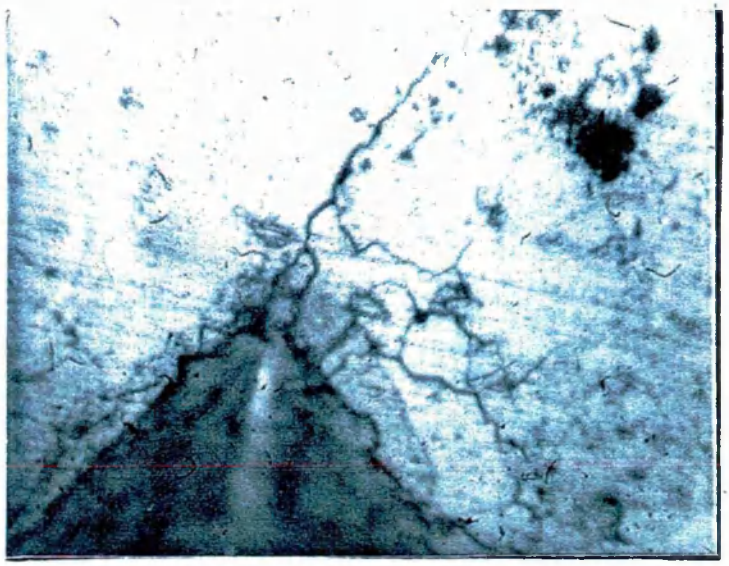

TYPE OF CRACKING UNDER 'EXCESSIVE' LOAD(HiCu)

Figure 5.18

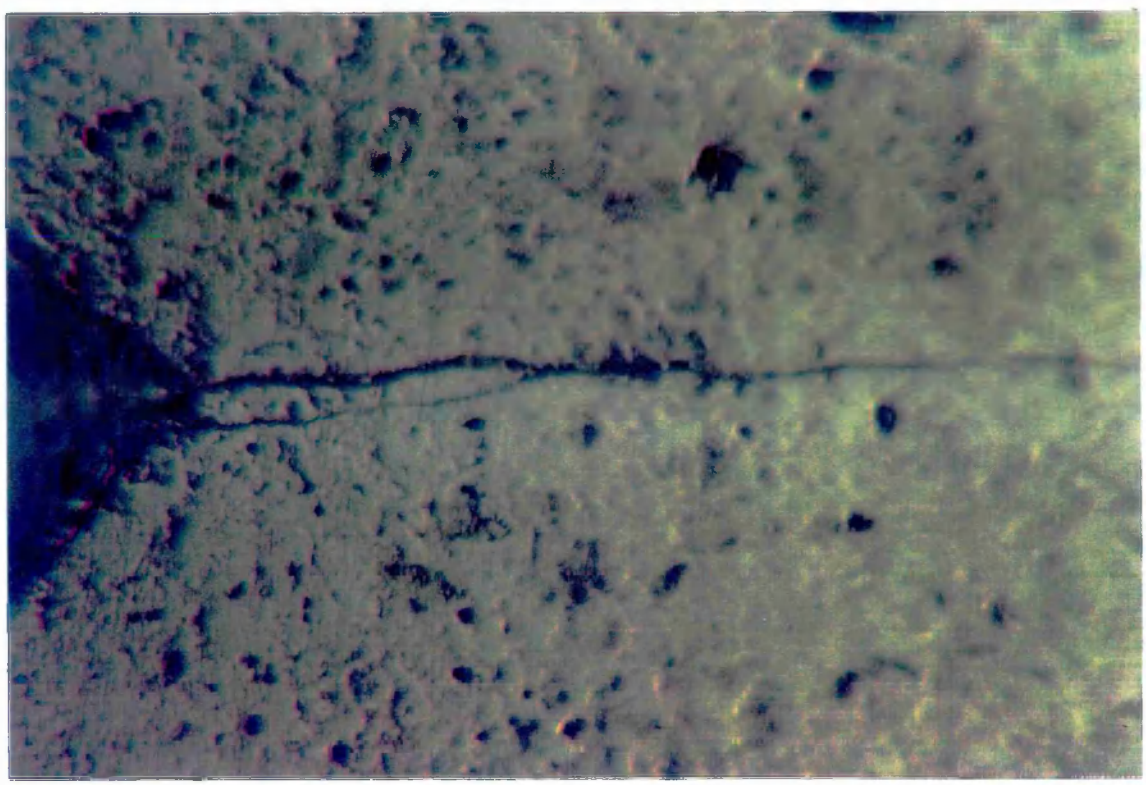

EXAMPLE OF CRACKS FROM MORE THAN ONE ORIGIN(HiCu)

FIGURE 5.19

5.2.3. Calculation of ϕ for each amalgam type.

Use of Figure 5.6, enables ϕ to be established which, itself is dependent on the local hardness value. Therefore, it is incorrect to assume a constant ϕ value for a particular specimen material, but it must be derived for each test impression, as shown in the following test results.

Initially, the value of E was determined for each amalgam type, this information was then used in conjunction with the individual hardness values to calculate ϕ.

5.2.3.1. Determination of elastic modulus(E) for dental amalgams

This part of the test programme was established primarily to find the value of E for each amalgam type which is then used to determine ϕ by the method described by Marsh (158).

The specimen was of 2mm gauge diameter, age 24 hours and its overall design complied with BS 18 (173) for uniaxial tensile testing. The tensile testing machine was designed specifically to accomodate very small specimens and was controlled by a microcomputer to provide the force - extension data in graphical form direct to a printer, Figure 5.20. The grip attachments were such that alignment of the specimens could be assured and only tensile failure occurred. The cross-head speed was set at 10mm/minute, which was judged to be fast enough to eliminate specimen creep effects. The tensile modulus value of each amalgam type, averaged over three trials, was derived from the respective force - extension plots (Table 5.2).

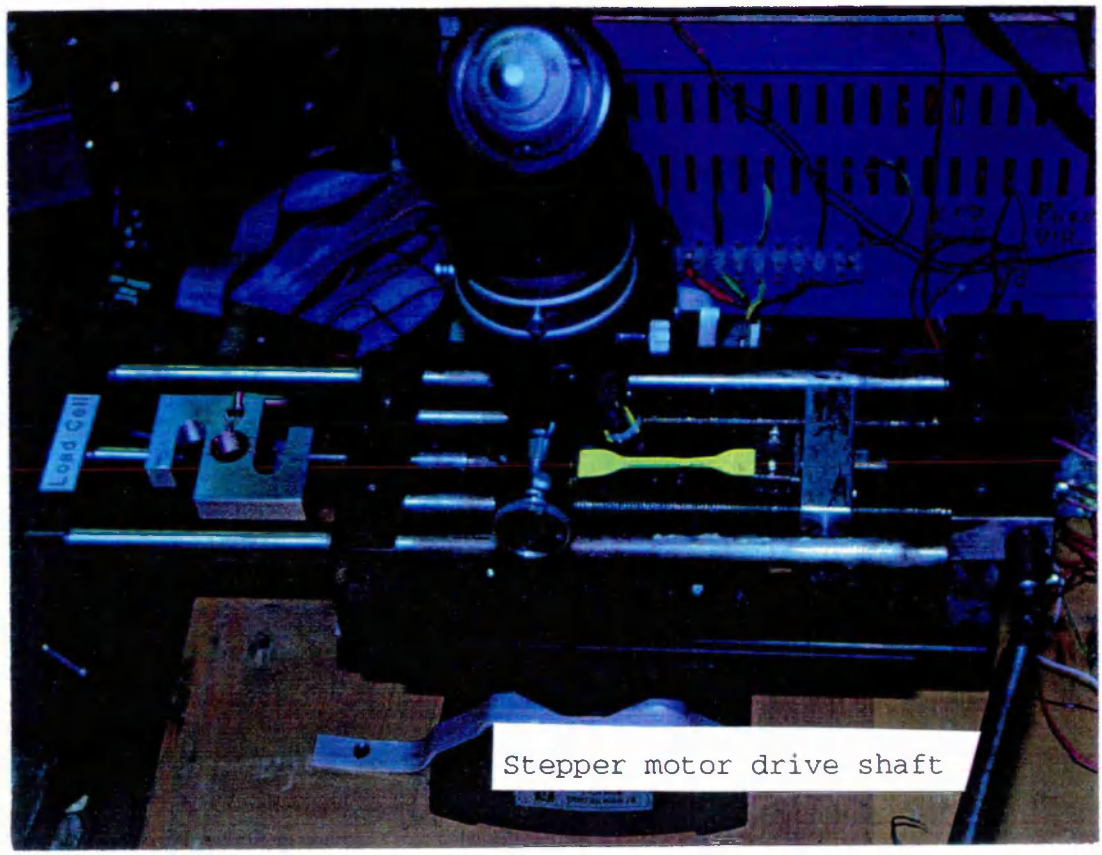

TENSILE TESTING MACHINE

Figure 5.20

The force-extension data plot for Tytin is shown in Figure 5.21 as a typical example. The gauge diameter of all the amalgam specimens was 2mm, giving an area of 3.142mm^2, and the gauge length was 10mm. The Modulus (E) = stress/strain (in the elastic portion of the stress-strain characteristic).

Therefore, E = (force/gauge area)/(extension/gauge length). This can be arranged to the form,

E = (force/extension) x (gauge length/gauge area), i.e.

E = slope of force-extension graph x 10/3.142 The slope was found to be 118/(21 x 10^{-3}) N/mm, i.e. 5 619. Thus, for this particular specimen, the estimate for E is 5 619 x 10/3.142 MPa = 17.88 GPa.

It can be seen from Figure 5.20, that the cross-head of the

machine was controlled by a stepper motor driving through a gearbox reduction of 300:1. The small specimen size meant that it was not possible to attach an extensometer. The tensile testing machine was designed to use the driving pulses to the stepper motor to establish the deflection axis plot on the monitor. This was readily achieved through a knowledge of the step angle of the drive motor, the gearbox ratio and the driving thread pitch.

Clearly if the deflection of the cross-head is significant at the maximum applied force, then corresponding errors would be incorporated into the resulting *E* value. The machine was of a stiff construction to minimise this error source but two checks were carried out to estimate the magnitude of its effect. The first check was to calculate the magnitude of the crosshead deflection at maximum applied force. The second check was to use a control material of known *E* to compare the results of the technique.

The maximum force required to produce failure in the specimen range was 120N. From the fixture dimensions the maximum calculated deflection of the crosshead at its mid-span was 0.1μm. The overall extension of the amalgam specimen was approximately 20μm (using Tytin as an example). This represents an approximate error due to machine stiffness of 0.5%. This figure suggests that the method of determining specimen strain is acceptable.

It was decided to verify this conclusion by manufacturing a plain carbon steel (080M20) specimen as a test control. The value of *E* for this material is known to be 198 GPa and by selecting a cross-sectional area to ensure that the yield force is equal to the maximum experienced by the amalgam specimens, then the test method should produce a closely comparable *E* value if no intrinsic errors

exist. A gauge diameter of 1mm (area 0.78mm^2) was used for this control test, with a gauge length of 5mm to conform to BS18 (173). Thus, the slope of the force-extension graph for this example of the control material, Figure 5.22, is now $100/(3 \times 10^{-3})$ i.e. 33 000. Therefore E = 33 000 x 5/0.78 MPa = 211 GPa. It will be noted from Figure 5.21 that the average of three tests produced an estimate of 201 Gpa for steel. The main factor governing accuracy was in determining the value of slope of the force-extension graph.

It is considered that the results of the tests on the control material demonstrate that the method of determining E for amalgams is acceptable.

Table 5.2

VALUES OF E FOR TEST AMALGAMS

Material	E GN/m^2
REVALLOY	12.4
NTDA	13.0
TRADITIONAL	10.0
TYTIN	18.0
HiCu	12.0
DISPERSALLOY	16.8

Values of E are the average of three tests.

5.2.3.2. Calculation of ϕ values.

Table 5.3 shows the average values of hardness used to evaluate a representative value of ϕ for each amalgam. It is emphasised that in the following 'Results' section, ϕ was calculated for each test indentation. To illustrate the procedure, an example for Revalloy

will now be shown.

The most common value of H_V for Revalloy is 148, ie. a value of 1480 MPa. Thus H_V/E = (1480/12 400) = 0.12 and this is marked off on the graph of Figure 5.6 to obtain a corresponding value of σ_Y/E of 0.08, therefore, H_V/σ_Y = 0.12/0.080 = 1.50 (= ϕ). This construction is shown on Figure 5.23

Table 5.3

TYPICAL VALUES OF H_V AND ϕ FOR AMALGAMS.

Material	H_V (kg/mm^2)	H_V/E	σ_y/E	$(H_V/\sigma_y)\phi$
REVALLOY	148	0.120	0.080	1.50
NTDA	122	0.092	0.055	1.67
TRADITIONAL	81	0.080	0.042	1.90
TYTIN	210	0.110	0.075	1.47
HiCu	101	0.080	0.042	1.90
DISPERSALLOY	216	0.126	0.082	1.54

Note: Value of ϕ for any particular amalgam varied according to test site. The values in this table are the most frequently occurring ones.

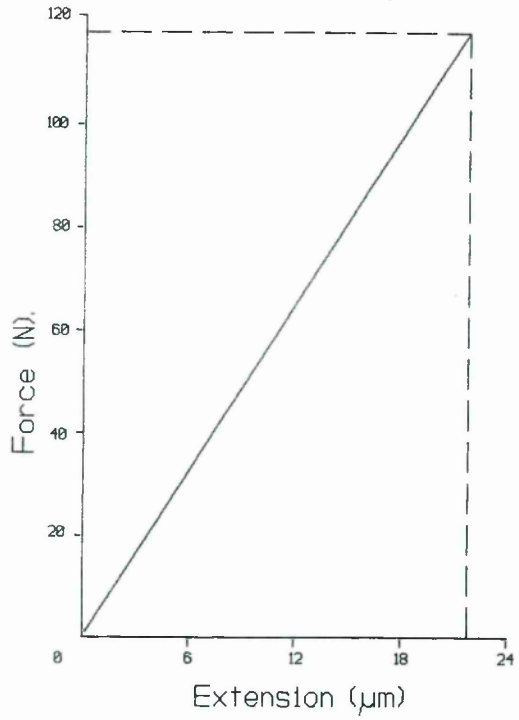

FORCE-EXTENSION OUTPUT FOR TYTIN
Figure 5.21

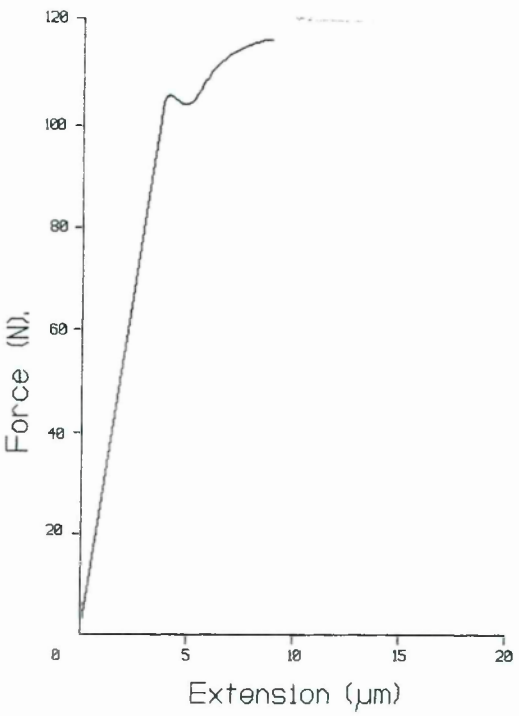

FORCE-EXTENSION OUTPUT FOR PLAIN CARBON STEEL CONTROL MATERIAL

Figure 5.22

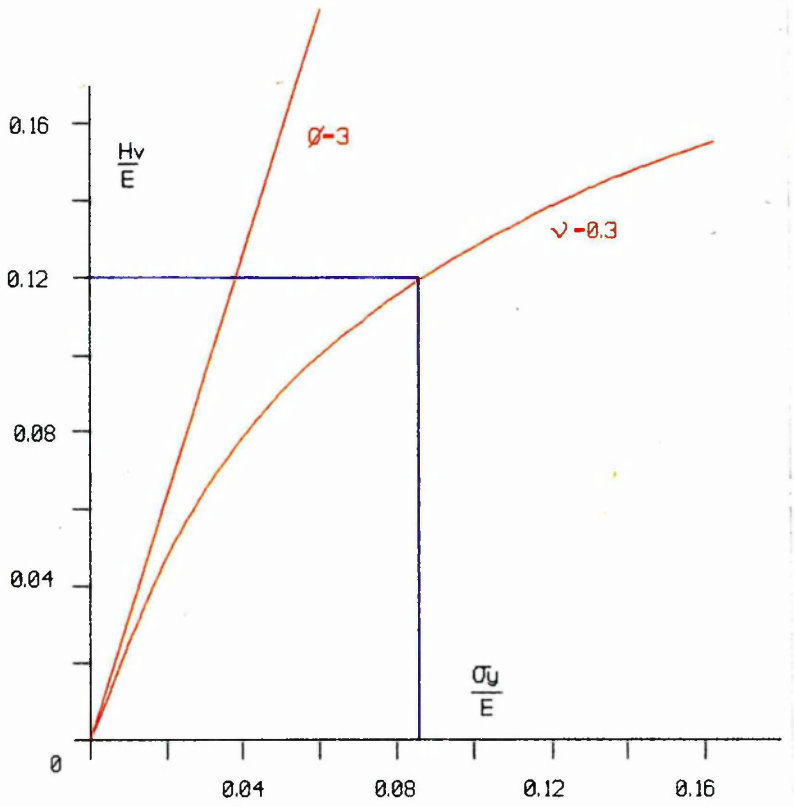

GRAPHICAL SOLUTION TO FIND ϕ

Figure 5.23

5.2.4. K_{IC} test method.

The beam halves from the transverse bend tests were retained and mounted in an acrylic cold setting compound which evolved very low exotherm during its setting reaction. This was to avoid the liberation of mercury that arises from the heat of resin reaction that could precipitate structural changes in the amalgam. The mounted specimen was then polished progressively to a last stage condition with 1µm diamond paste.

The test was performed to obtain the value of H_V and the corresponding dimension 'a' for each amalgam. The impression was then placed under a metallurgical microscope at 400 magnification. However, in order to retain a wide field of view at high magnification, the microscope eye-piece was replaced with a video

camera so that the diamond impression could be viewed on a 60cm screen monitor. An overall magnification of 1140 was thus obtained which was considered appropriate for the measurement of the crack length 'C_R' that emanated from the corners of the diamond.

Crack lengths were measured by obtaining a screen copy of all specimens with a Mitsubishi video copier. Ones that deviated from the radial by more that 10° were ignored for this present research. Examples of the output are shown in Figures 5.24 and 5.25. From these data, K_{IC} was calculated using equation 5.1. Using the video output, a copy of a graticule was obtained which was subsequently transferred to overhead transparency. The transparency was overlaid on the view of the crack and the C_R measurement noted.

160µm

EXAMPLE OF VIDEO OUTPUT (HiCu)
Figure 5.24

160µm

EXAMPLE OF VIDEO OUTPUT (TYTIN)
Figure 5.25

It was noted that often there was a marked difference in fracture toughness according to which apex of the diamond impression was under consideration. Clearly this feature arises because crack propagation (and therefore, C_R) is strongly influenced by the microstructural features which exist in its locality.

Approximately 50 samples were taken on each amalgam type and individual values are shown in Figures 5.26 to 5.31. The value of K_{IC} obtained from the transverse bend tests and the estimated K_{IC} value for the constituent phases are shown on each graph for comparison purposes.

5.2.5. K_{IC} results for each amalgam type.

Shown (in brackets) in the following figures are values of the mean K_{IC}, followed by the standard deviation.

5.2.5.1. Revalloy

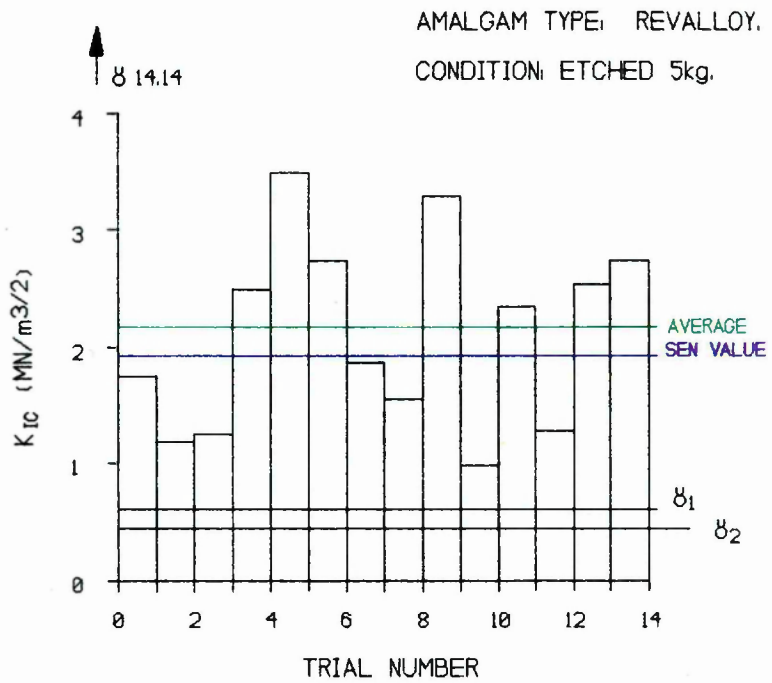

(a) K_{IC} VALUES FOR REVALLOY OBTAINED BY INDENTATION (2.92,0.45)

Figure 5.22

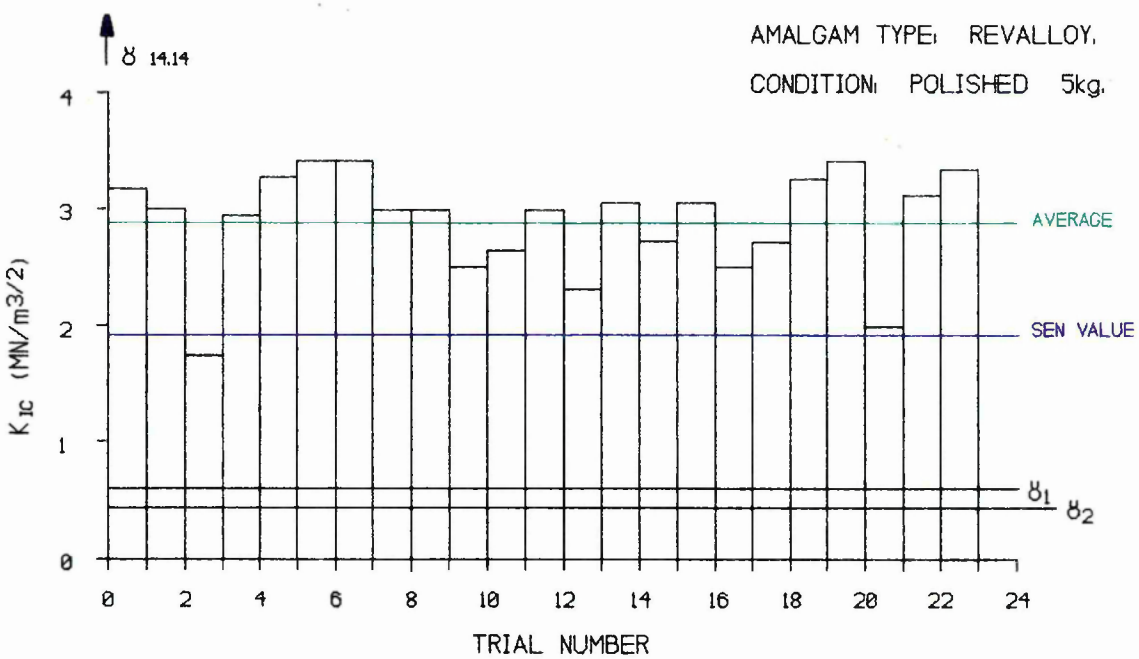

(b) K_{IC} VALUES FOR REVALLOY OBTAINED BY INDENTATION (2.2,0.82)

Figure 5.22

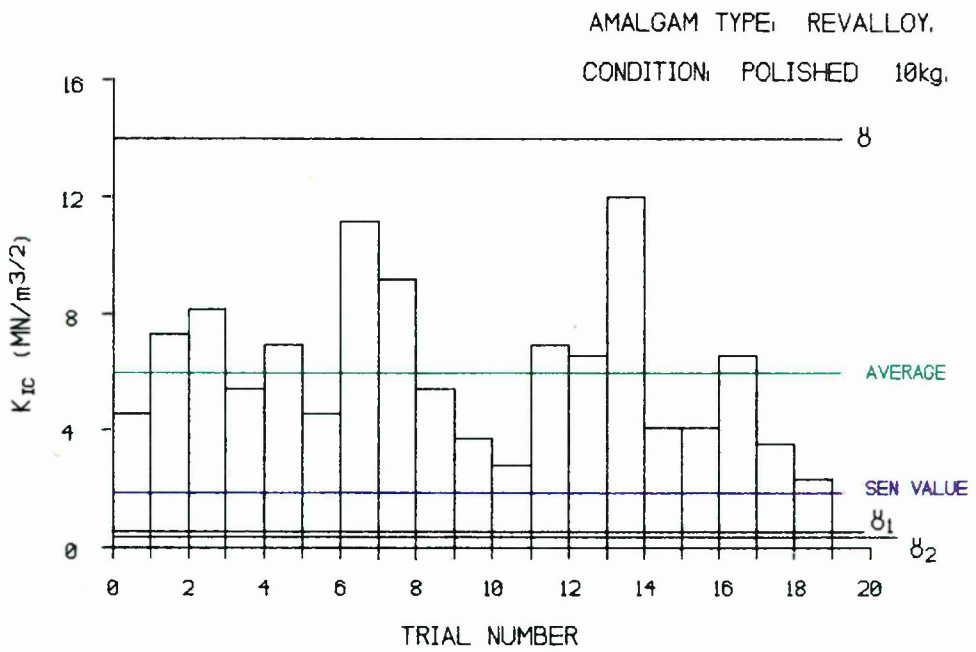

(c) K_{IC} VALUES FOR REVALLOY OBTAINED BY INDENTATION (5.9,2.6)

Figure 5.22

5.2.5.2. NTDA.

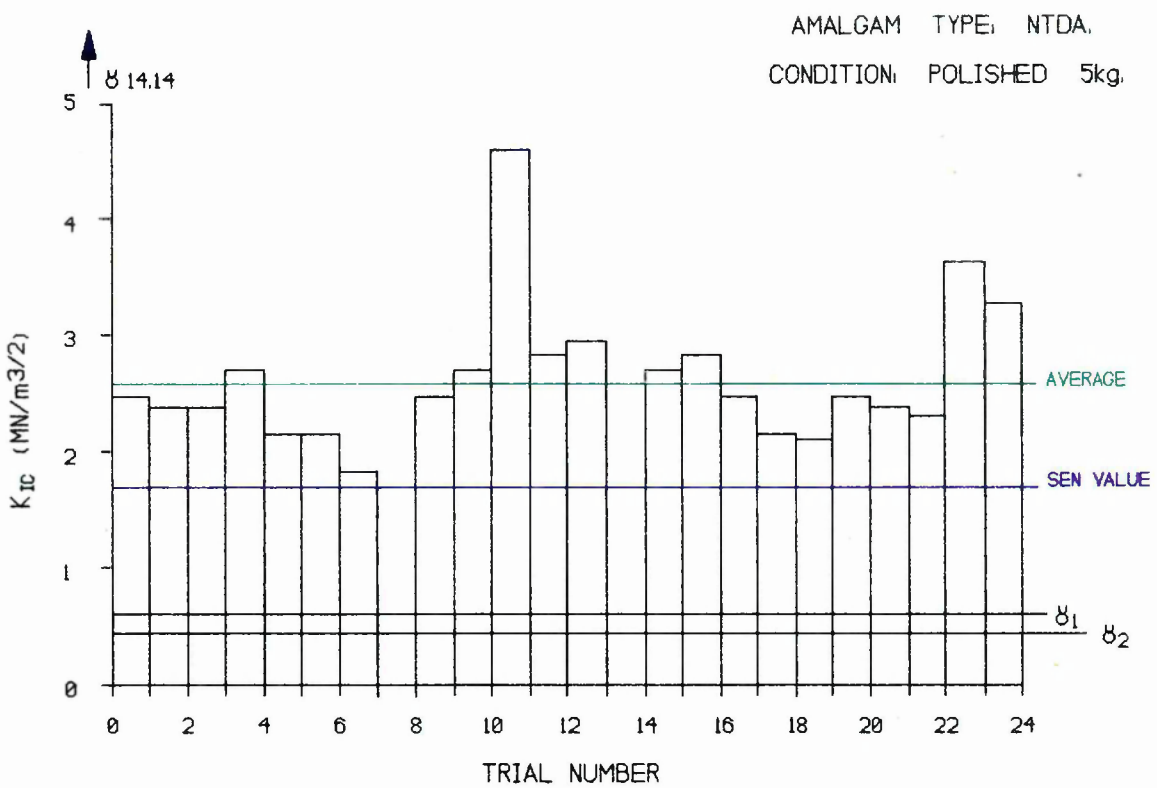

(a) K_{IC} VALUES FOR NTDA OBTAINED BY INDENTATION (2.6,0.61)

Figure 5.23

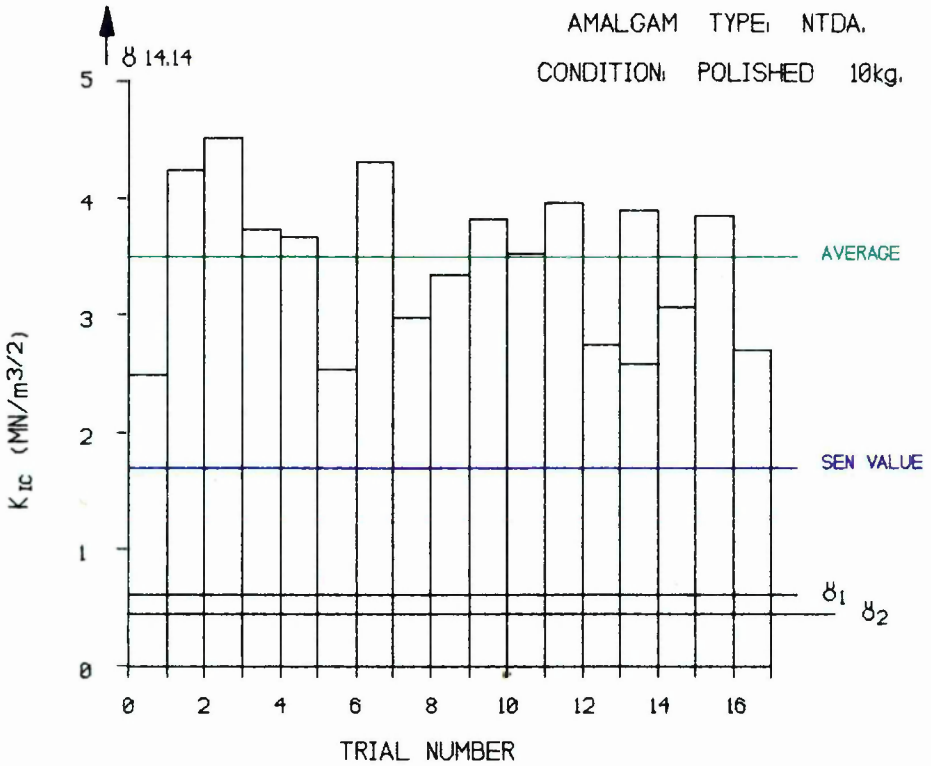

(b) K_{IC} VALUES FOR NTDA OBTAINED BY INDENTATION (3.52,0.65)

Figure 5.23

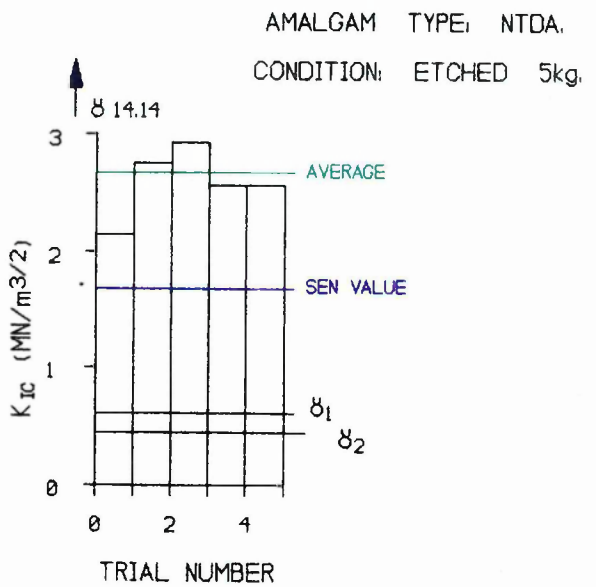

(c) K_{IC} VALUES FOR NTDA OBTAINED BY INDENTATION (2.7,0.3)

Figure 5.23

5.2.5.3. Traditional.

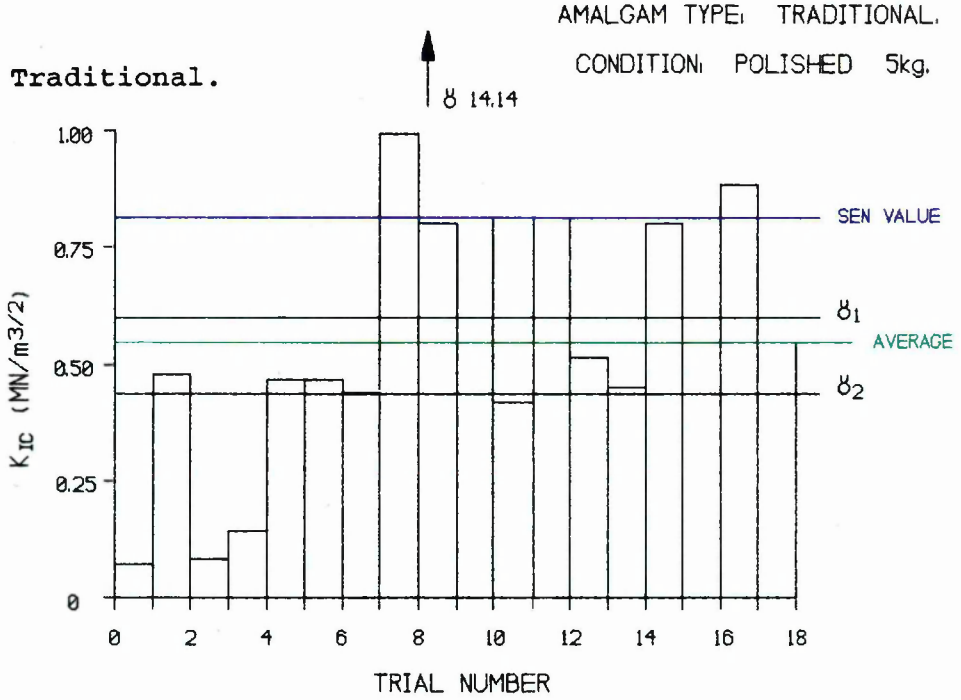

K_{IC} VALUES FOR TRADITIONAL OBTAINED BY INDENTATION (0.55,0.27)

Figure 5.24

5.2.5.4. Tytin.

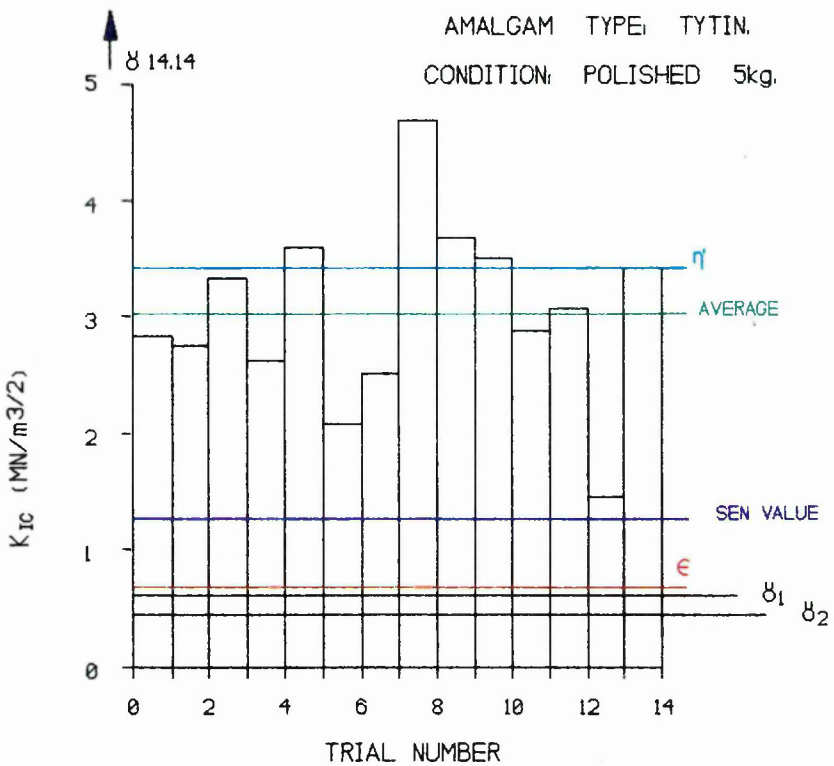

(a) K_{IC} VALUES FOR TYTIN OBTAINED BY INDENTATION (3.05,0.79)

Figure 5.25

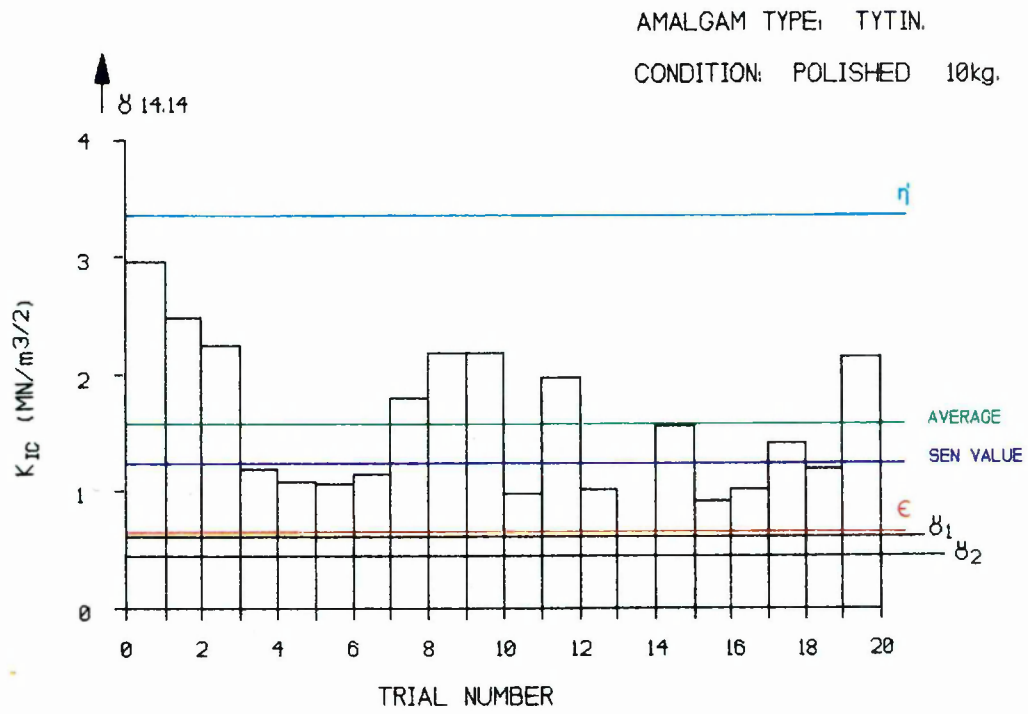

(b) K_{IC} VALUES FOR TYTIN OBTAINED BY INDENTATION (1.6,0.64)

Figure 5.25

5.2.5.5. HiCu.

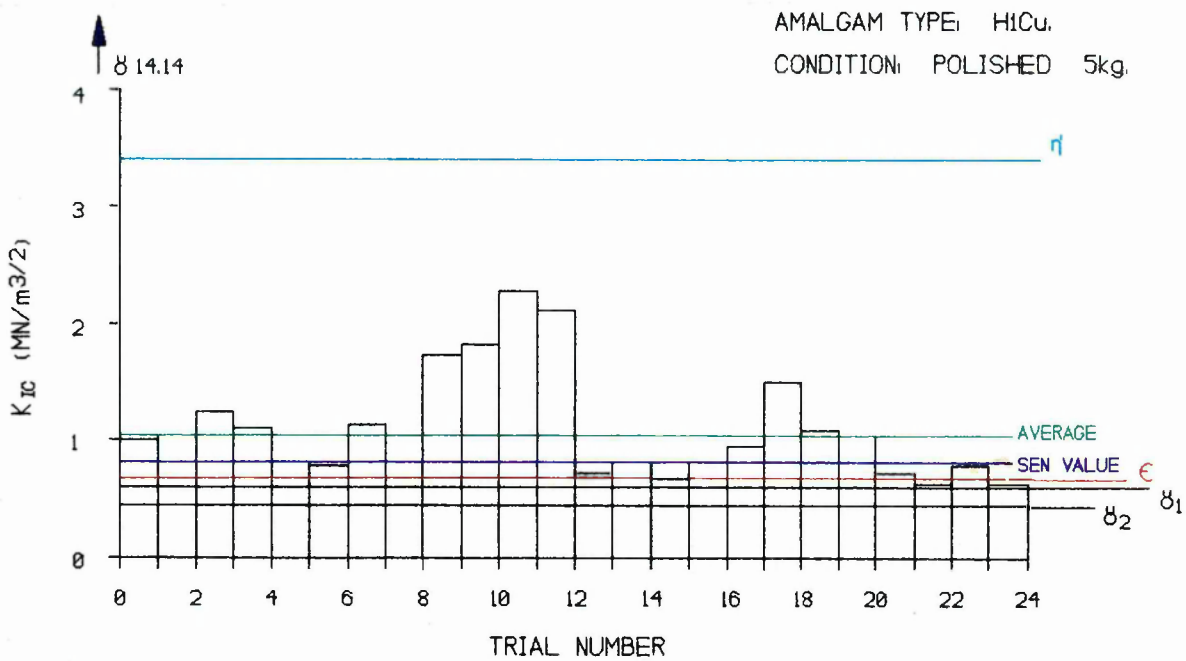

K_{IC} VALUES FOR HiCu OBTAINED BY INDENTATION (1.05,0.47)

Figure 5.26

5.2.5.6. Dispersalloy.

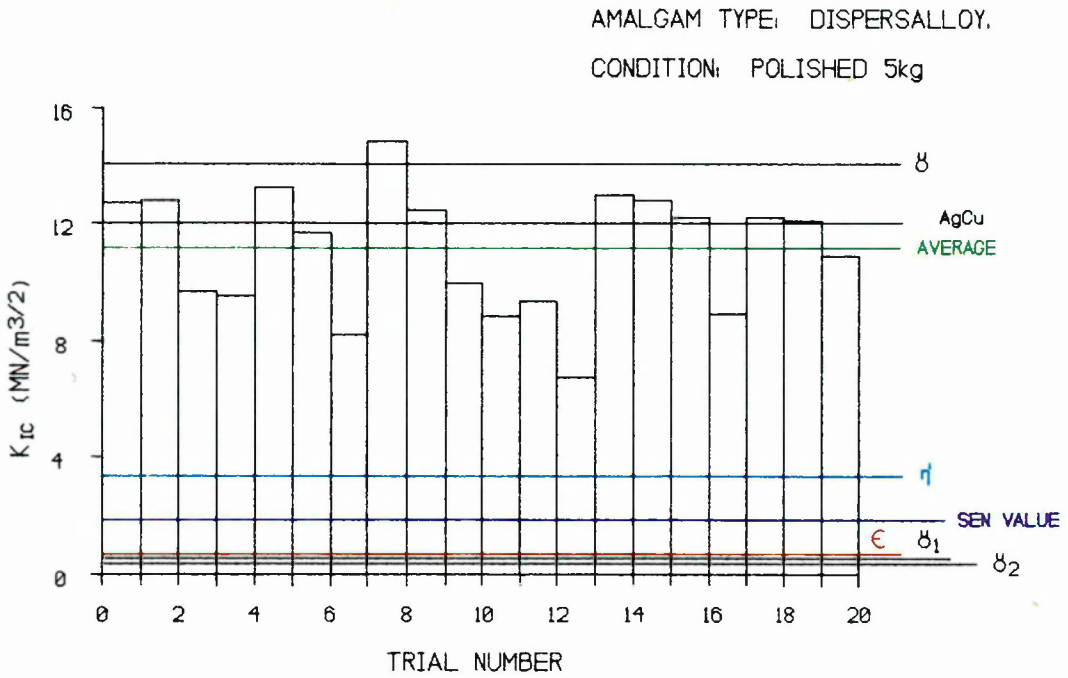

(a) K_{IC} VALUES FOR DISPERSALLOY OBTAINED BY INDENTATION(11.25,2.1)

Figure 5.27

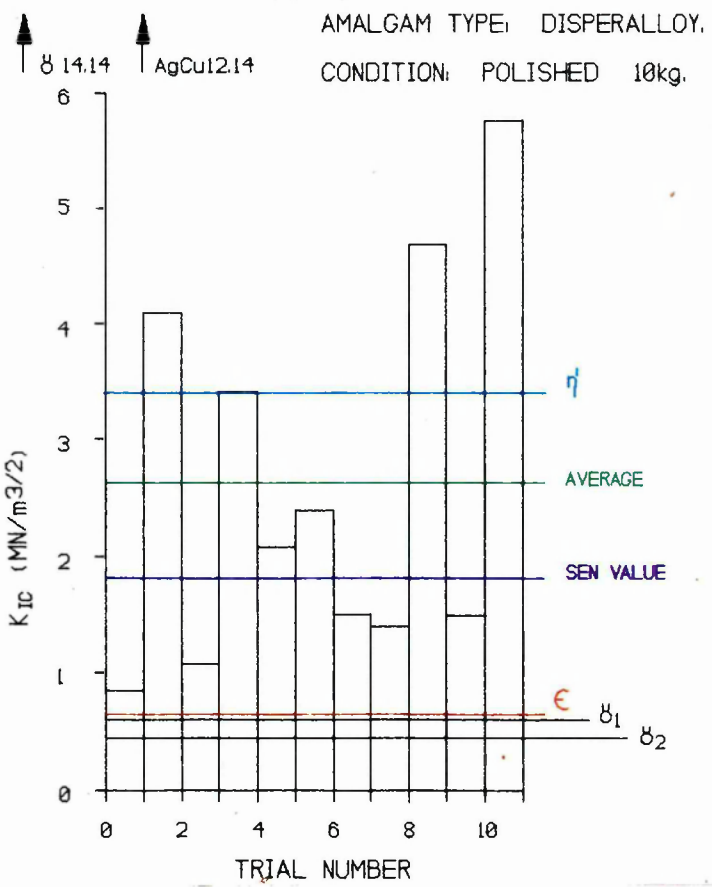

(b) K_{IC} VALUES FOR DISPERSALLOY OBTAINED BY INDENTATION(2.65,1.68)

Figure 5.27

5.2.6. Variability between results.

The individual values of K_{IC} taken from each crack on a carefully selected indentation are shown in Table 5.4.

Table 5.4

K_{IC} FOR INDIVIDUAL CRACKS (Specimen age - 24 hours)

Material	$(C_r)_1$	K_{IC}	$(C_r)_2$	K_{IC}	$(C_r)_3$	K_{IC}	$(C_r)_4$	K_{IC}
REVALLOY	165	2.6	230	1.6	150	3.0	247	1.4
NTDA	189	1.3	90	4.0	172	1.5	177	1.5
TRADITIONAL	260	0.8	255	0.8	264	0.7	257	0.8
TYTIN	332	0.9	215	1.7	259	1.3	182	2.2
HiCu	276	0.7	284	0.7	209	1.0	239	0.9
DISPERSALLOY	147	3.1	222	1.7	198	2.0	221	1.7

Units of K_{IC} - $MN/m^{3/2}$ C_r in μm

When these individual values are averaged, the K_{IC} value was very close to the transverse bend test value, Table 5.5.

Table 5.5

COMPARISON OF DATA BETWEEN INDENTATIONS WITH SEN VALUES.

Material	Half diagonal dimension 'a' μm	Crack Length 'C' μm (average)	K_{IC} ($MN/m^{3/2}$) (average)	K_{IC} (SEN) ($MN/m^{3/2}$)
REVALLOY	125	198	1.97	1.74
NTDA	138	157	1.74	1.64
TRADITIONAL	169	259	0.77	0.82
TYTIN	105	247	1.40	1.21
HiCu	152	252	0.81	0.69
DISPERSALLOY	103	197	2.00	1.80

The value of *E* used in equation 5.1 for the amalgams is the bulk property. In contrast, the technique involves parameters which are

highly dependent on local microstructural detail. Thus, there is an inherent approximation in evaluating K_{IC}.

5.2.7. Effect of microstructure on crack propagation.

The plates, Figure 5.32 and 5.33 show the influence of the unreacted particles on crack path. The spherical particles of unreacted Tytin show particularly well that fracture is essentially through the mercury-based phases (the light areas of the view). However, there is also evidence that some trans-crystalline fracture occurs in the unreacted particle. This unreacted particle provides a crack arrest mechanism.

The offset of the apparent origin of the crack that was seen on some of the samples was due to the coincidental presence of an unreacted particle at the point of crack initiation. This initiation stage occurs at some stage on the downward movement of the indentor. Microscopic examination suggests that this unreacted particle deflects the direction of the crack from the radial position. In the case of the HiCu amalgam, there is evidence from X-ray maps (Figure 5.34) that the crack is confined to the mercury-reacted phases. The copper-tin phases of ε and η are probably present and the tendency of the former phase to be unreactive with mercury would encourage the crack path to follow its contours. The comparatively high K_{1c} of the latter phase (η), would also tend to minimise the occurrence of the crack through this phase. Clearly, the combination of interface characteristics, and the fracture toughness of the particular phase encountered by the crack, determines the overall (or macro) K_{1c} value.

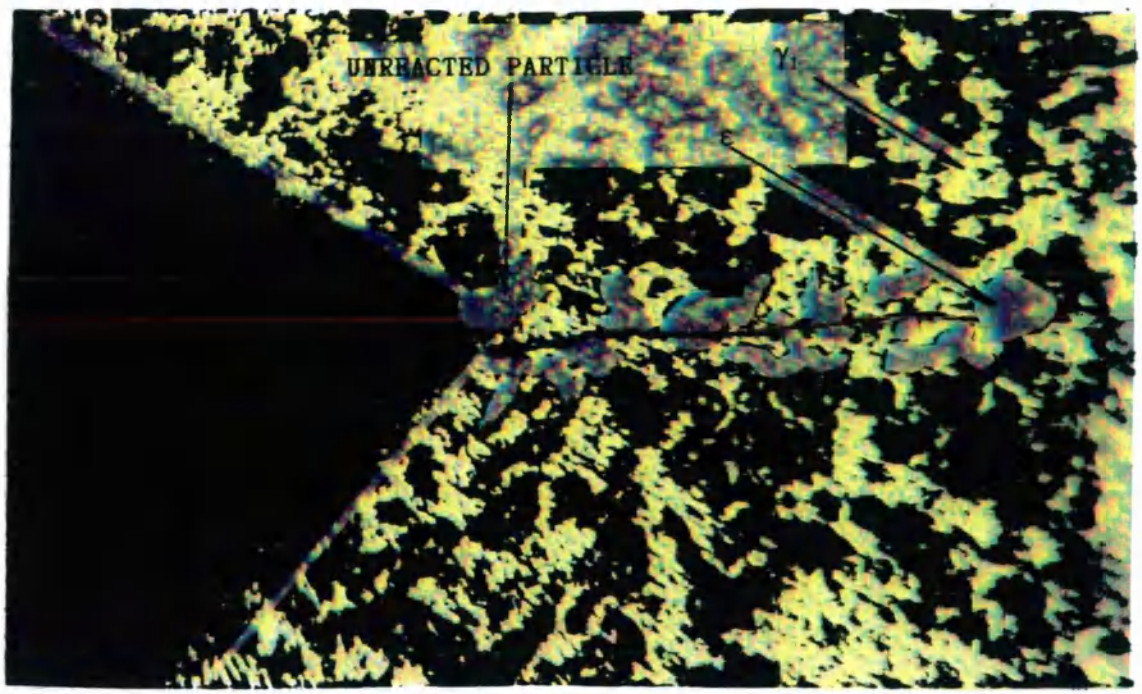

INFLUENCE OF UNREACTED PARTICLE ON CRACK PATH (HiCu) 20μm

Figure 5.32

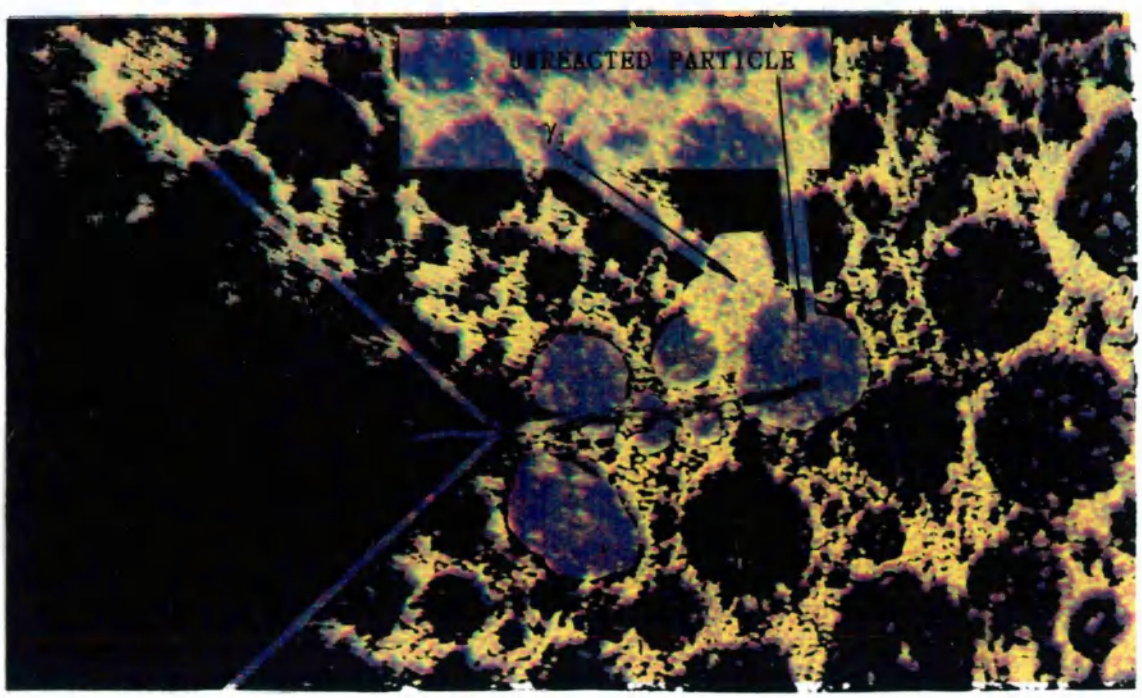

INFLUENCE OF UNREACTED PARTICLE ON CRACK PATH (TYTIN) 20μm

Figure 5.33

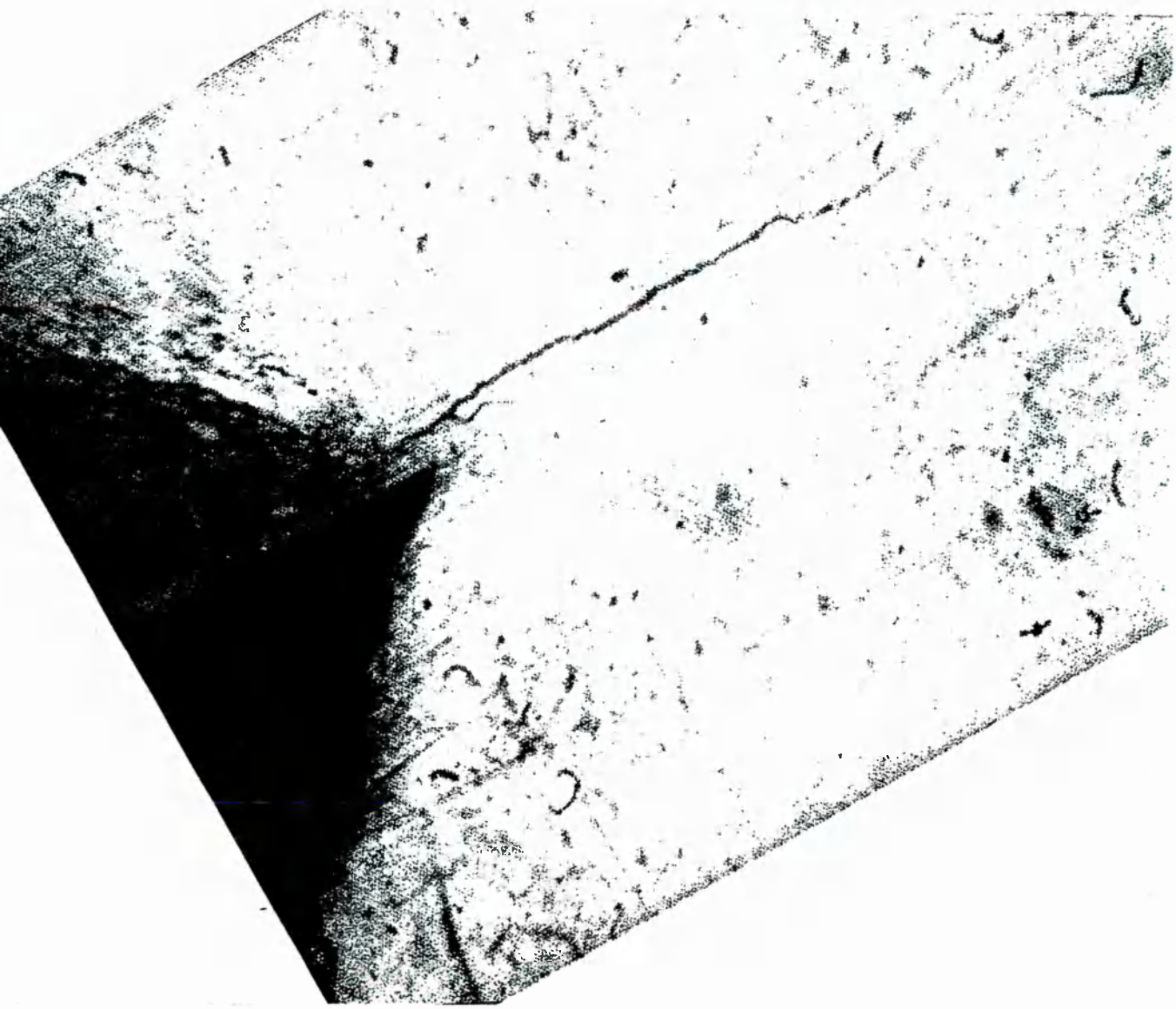

(i)

HiCu FOR ANALYSIS (X-RAY MAPS - Figure 5.34(a))

Figure 5.34

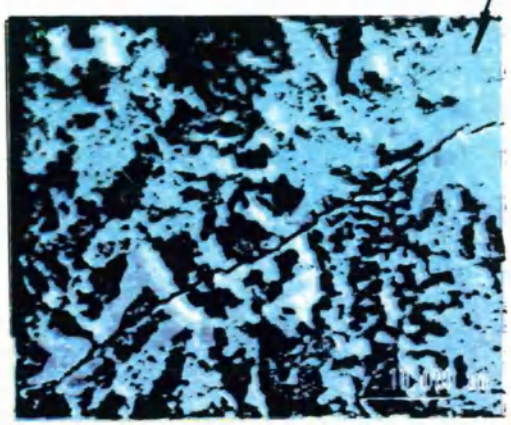

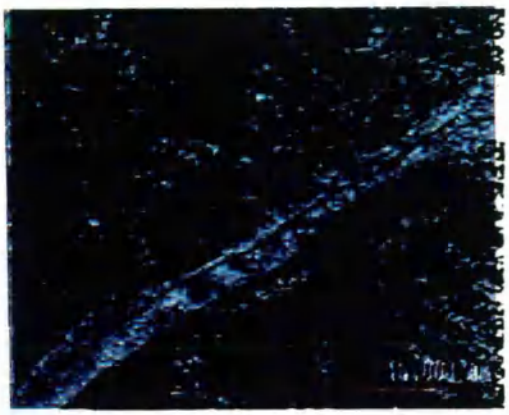

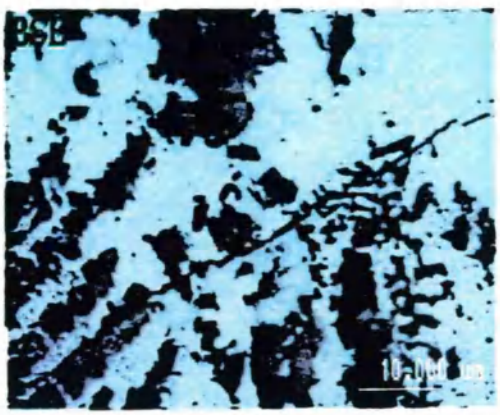

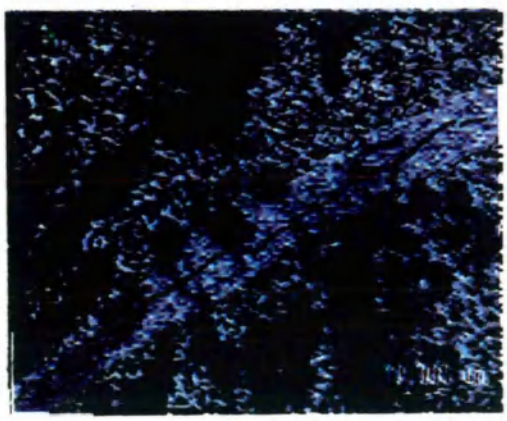

X-RAY MAPS HiCu SHOWING CRACK PATH

Figure 5.34(a)

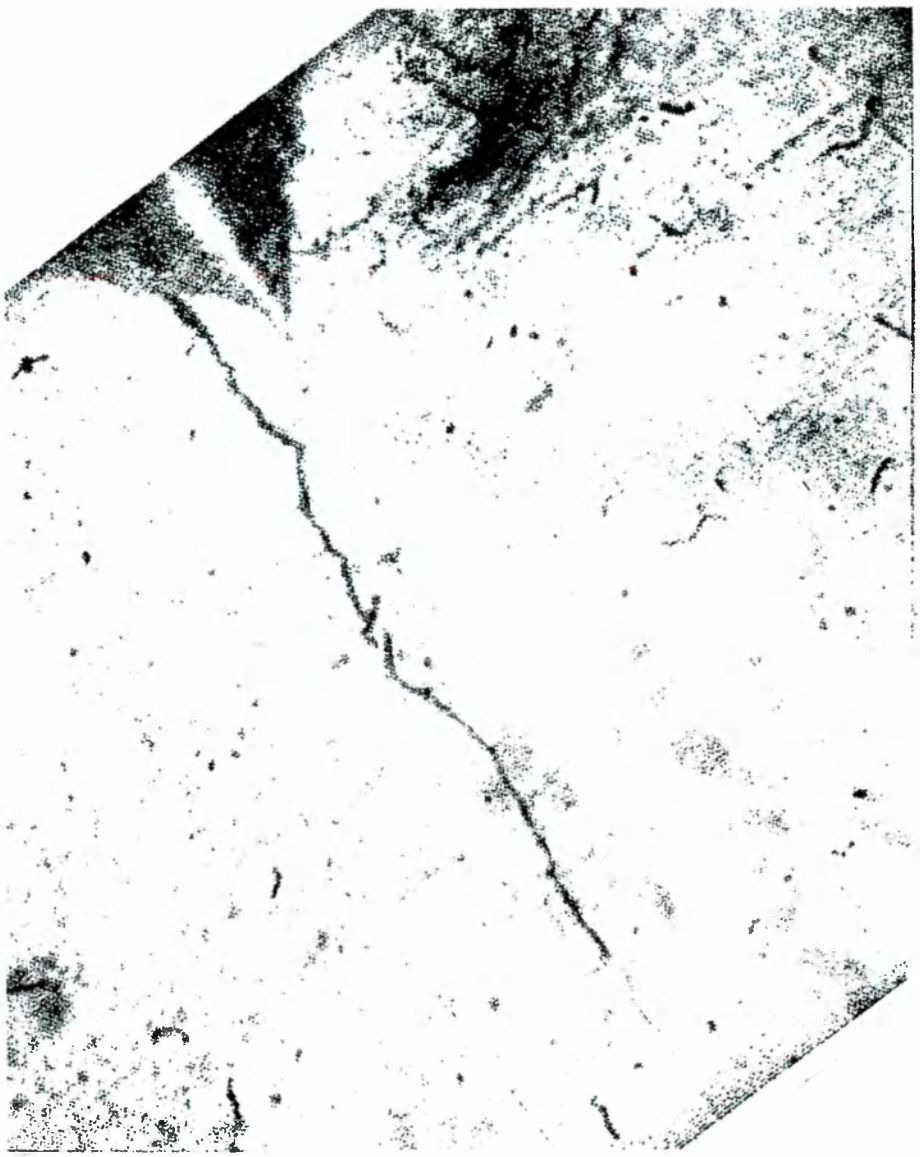

(ii)

HiCu FOR ANALYSIS (X-RAY MAPS - Figure 5.34(b))
SAME INDENTATION AS PREVIOUS FIGURE,

DIFFERENT APEX ORIGIN OF CRACK

Figure 5.34

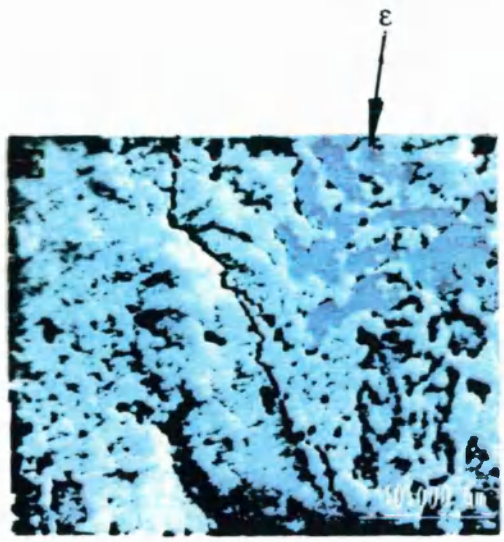


Sn

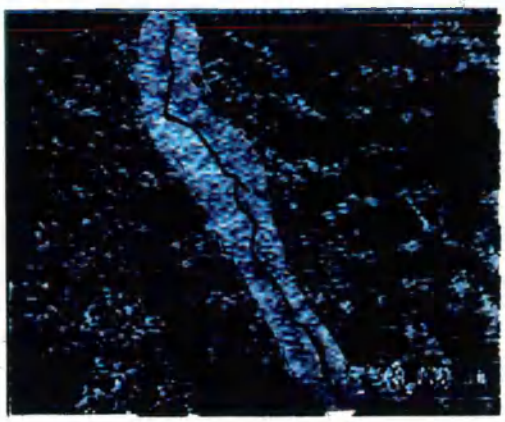
Ag

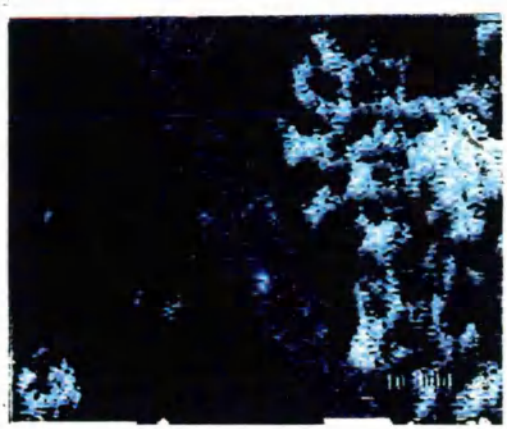
Cu

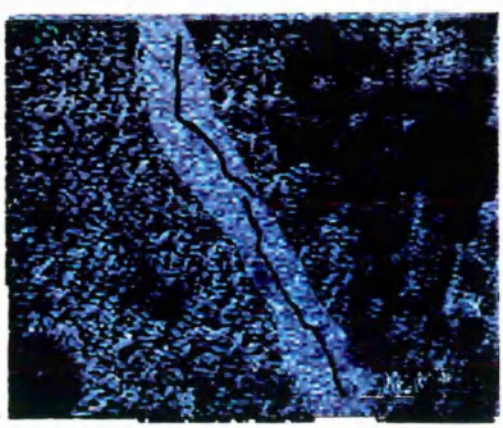
Hg

X-RAY MAPS HiCu SHOWING CRACK PATH

Figure 5.34(b)

5.2.8. Test factors influencing K_{Ic} values.

The validation of the functions proposed by Evans was made by determining K_{Ic} by the double torsion method(159). Whereas for this present work comparison was made on the basis of the SEN transverse bend test. Clearly the accuracy of the present results depends upon these two methods producing the same values. The value of ϕ depends upon the accuracy of the elastic modulus used. In the literature review, the point was made that *E* for amalgams has been quoted within quite a wide range. The values obtained in this present research agreed well with reported values of Young and Wilsdorf and others(59,76,79,84). However, as an example of the errors that might occur and their effect on the K_{Ic} value, the following represents a pessimistic assessment of the error that could occur: If H_v was in error by 0.5%, 'a' by 0.5%, which could be achieved for a clear and well defined indentation, ϕ by 10%, *E* by 10%, and C by 10%, then the overall effect on the accuracy of K_{Ic} would be ± 6%.

A reason for some uncertainty was when the indentation was not symmetrical (Figure 5.35). In this case the value of 'a' for the right hand apex is different from the remaining three, which is not a problem for substitution in equation 5.1. However, the hardness value H_v is derived from an average of the two diagonals, and the equation 5.1 is based upon a symmetrical indentation. Thus, under the circumstances shown in Figure 5.35 significant errors in the computed value of K_{Ic} may arise.

It was frequently difficult to assess the precise point at which the crack terminated, particularly when it occurred in the grain boundary of an unreacted particle. The crack length also had to be

defined as the shortest distance between the origin and the termination point. This definition of crack length is discussed in the following section. There were occasions when the crack path deviated quite considerably, and the method used would have resulted in an over-estimate of K_{IC}. This deviation sometimes occurred due to polishing marks on the specimen surface, and sometimes to the presence of a structural feature such as an unreacted particle.

5.3.0. Discussion and summary.

Specimens of the the individual constituent phases of amalgam namely, γ, γ_1, γ_2, ε, η and Ag-Cu eutectic, which were manufactured as given in Chapter 4, were tested by the hardness method for K_{IC}. Six indentations were placed on each sample, producing 24 crack lengths per sample for analysis. A very distinctive feature of these tests was that the crack lengths were very consistent in length. Any variation that occurred was more in terms of the deviation of the direction from the radial. It is assumed that this is due to the influence of the grain boundaries. SEN values of K_{IC} for the constituent phases are included in Table 5.6 for comparison.

Table 5.6

Phase	Ave.'a' μm	Ave.C_R μ	Ave.H_v kg/mm^2	Ave.K_{IC} MN/m$^{3/2}$	K_{IC}(SEN) MN/m$^{3/2}$
γ	93	91	268	13.30	14.14
γ_1	138	181	115	0.57	0.60
γ_2	125	176	16	0.48	0.44
ε	55	86	310	0.73	0.66
η	197	247	107	5.13	3.44
Ag-Cu	73	79	242	11.95	12.14

Units of K_{IC} - MN/m$^{3/2}$ C_r in μm

It was expected that the SEN values of K_{IC} for the constituent phase specimens would be lower than those found by hardness testing. The reason for this assumption is that the manufacturing techniques used for specimen production were thought to be insufficiently developed to produce high integrity, mainly in terms of porosity, However, Table 5.6 shows that the hardness method resulted in a lower average, except for the η and γ_2 phases. It is not possible to explain this without an extensive test programme. The largest difference between the values from the two methods is 6%, which for experimental purposes means that they can be regarded as producing nominally the same results for K_{IC}.

Surface finish influences the toughness determined by the hardness test quite dramatically, for example a scratch mark can deflect the crack from the radial direction.

Each amalgam type will now be considered with reference to the approximate K_{IC} of the constituent phases where appropriate.

Revalloy It is useful to consider, not only the average values of K_{IC}, but also the range and the estimated values of the constituent phases.

Under the 10kg load, branched cracks appear, leading to some ambiguity as to how to define C_R for use in equation 5.1. However, by selecting only single, well-formed crack configurations it was found that the lowest K_{IC} value under the 10kg condition was $2.43 MN/m^{3/2}$, and the highest value obtained on the specimen was $12.09 MN/m^{3/2}$. Caution has to be exercised in interpreting the individual values of K_{IC} of the amalgams in terms of those of the individual phases. However, it is reasonable to assume that a general influence may be detected from the data. For example,

Figure 5.26(c) shows individual values that are close to that of the γ phase and there were examples on the etched specimens where the highest values of K_{IC} were obtained when the γ phase could be seen at the apex of the indentation with the crack propagating through it.

The small powder size gives rise to a correspondingly small unreacted γ phase within the amalgam, and in the majority of cases there were signs that this phase tends to deflect the crack path within the mercury-reacted phases. There were few instances where the γ phase in Revalloy was seen to act as a crack arrest mechanism.

Attempts were made to view the crack path through the various phases by etching the specimen surface. This was not very successful because the process tended to mask the crack details, particularly at the termination of the crack. The range of K_{IC} values obtained by crack measurement on an etched surface, under 5kg loading, was 1.0MN/$m^{3/2}$ to 3.32MN/$m^{3/2}$ -, compared with 1.76MN/$m^{3/2}$ to 3.45MN/$m^{3/2}$ for a polished surface under the same load. The higher maximum of the latter case indicates that the etching process tends to truncate the crack at its tip. The likelihood of the existence of this effect is supported by the estimate that the maximum crack depth is only approximately 7μm and the thickness of material removed from the specimen surface during etching can easily reduce this by half, resulting in an under-estimate of C_R.

The SEN value of 1.92 MN/$m^{3/2}$ is encompassed by the minimum and maximum limits obtained under the 5kg loading condition. Further, the minimum value of K_{IC} is significantly greater than that of either of the two mercury-reacted phases, demonstrating the toughening effect of the γ phase.

NTDA Similar comments apply to this amalgam type as for the previous case. It is possible that the larger unreacted γ phase of this amalgam can account for the higher K_{IC} than for Revalloy. The capacity of this phase to divert the crack is greater because of the larger grain size and this is an energy-absorbing mechanism tending to increase the fracture toughness. The larger γ powder size altered the amalgam mixing and packing mixing characteristics. It was more difficult to obtain a low-porosity, coherent mass with this amalgam and as a consequence of this, it would be expected that its fracture toughness would be lower than for the small particle Revalloy. This was the case for the SEN values reported in Chapter 3. However, one advantage of the indentation method is that the K_{IC} value becomes less dependent upon porosity and therefore gives a better assessment of the material type.

Under 10kg, the fracture toughness values ranged from 2.55 $MN/m^{3/2}$ to 4.55$MN/m^{3/2}$. Under 5kg, 1.71$MN/m^{3/2}$ to 4.62$MN/m^{3/2}$, these values encompass the SEN value of 1.84$MN/m^{3/2}$.

Traditional This amalgam contained quite a high proportion of voids which may account for some very low K_{IC} figures within the range - the lowest value was 0.07$MN/m^{3/2}$. This possibility would obviously depend on the void coinciding with the apex of the indentation. However, most of the values were in the range 0.48$MN/m^{3/2}$ to 1.00$MN/m^{3/2}$, comparing very favourably with the SEN figure of 0.82$MN/m^{3/2}$. The minimum value exactly corresponds to that for γ_2, and is also quite close to the γ_1 phase (0.57$MN/m^{3/2}$). It is suggested that K_{IC} of Traditional amalgam is dominated by the mercury-reacted phases with, unlike the previous two types, little toughening effect of the γ phase.

Tytin The better results for this amalgam,in terms of crack linearity and clear definition of indentation, were obtained with the higher load of 10kg and not the 5kg condition.

Under 5kg, values of K_{IC} range from 1.45 to 4.72MN/$m^{3/2}$ compared to an SEN value of 1.23MN/$m^{3/2}$. It was noticeable that under this load, there were many of examples were a crack did not propagate at all, or the crack was very short. The percentage error in crack measurement is higher under these circumstances than with a long crack length. Figure 5.35 shows the situation where an unreacted particle coincides with the apex of the indentation and it can also be seen in Figure 5.36 that the crack arrests at an unreacted particle. Under 10kg the crack has a greater tendency to be deflected around the unreacted particle and thus to continue to propagate within the mercury-reacted phases - this results in a lower calculated value of K_{IC}. The suggested deflection of the crack by the existence of an unreacted particle at the apex of the indentation is further shown by Figures 5.37 and 5.38. It can be seen that the offset of the crack origin can vary from one indentation to another.

The 10kg results gave a K_{IC} range from 0.96MN/$m^{3/2}$ to 2.98MN/$m^{3/2}$. The comparatively low K_{IC} value of Tytin is surprising considering the existence of the the high fracture toughness phase ή (approximately 4MN/$m^{3/2}$), in addition to the γ phase. This emphasises the difficulty in relating in simple terms, the fracture toughness of the constituent phases with that of the bulk K_{IC}.

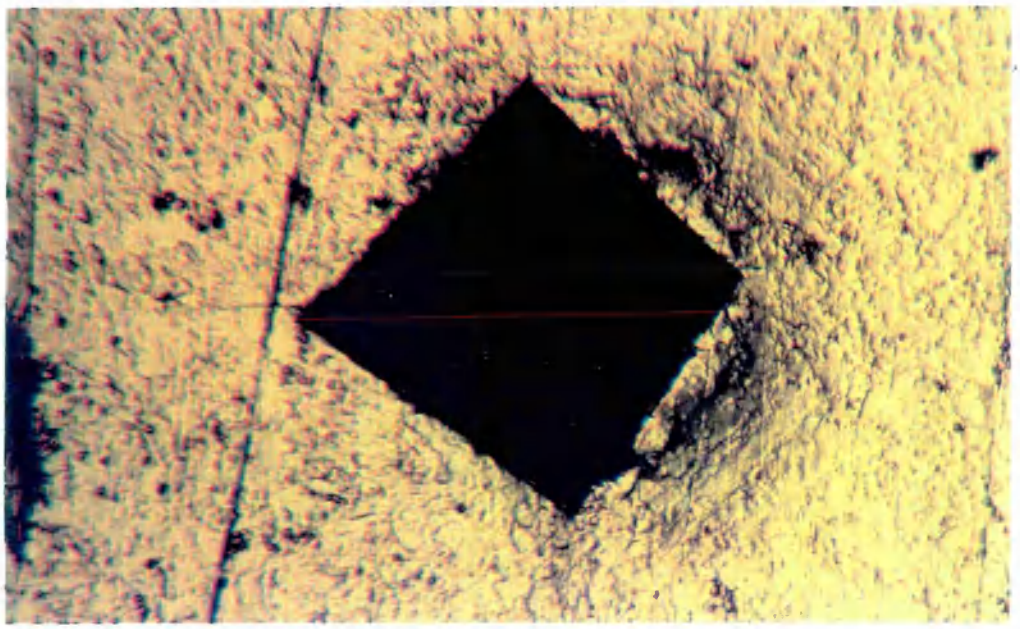

VIEW SHOWING THE ASSYMETRY OF AN INDENTATION IN HiCu

Figure 5.35

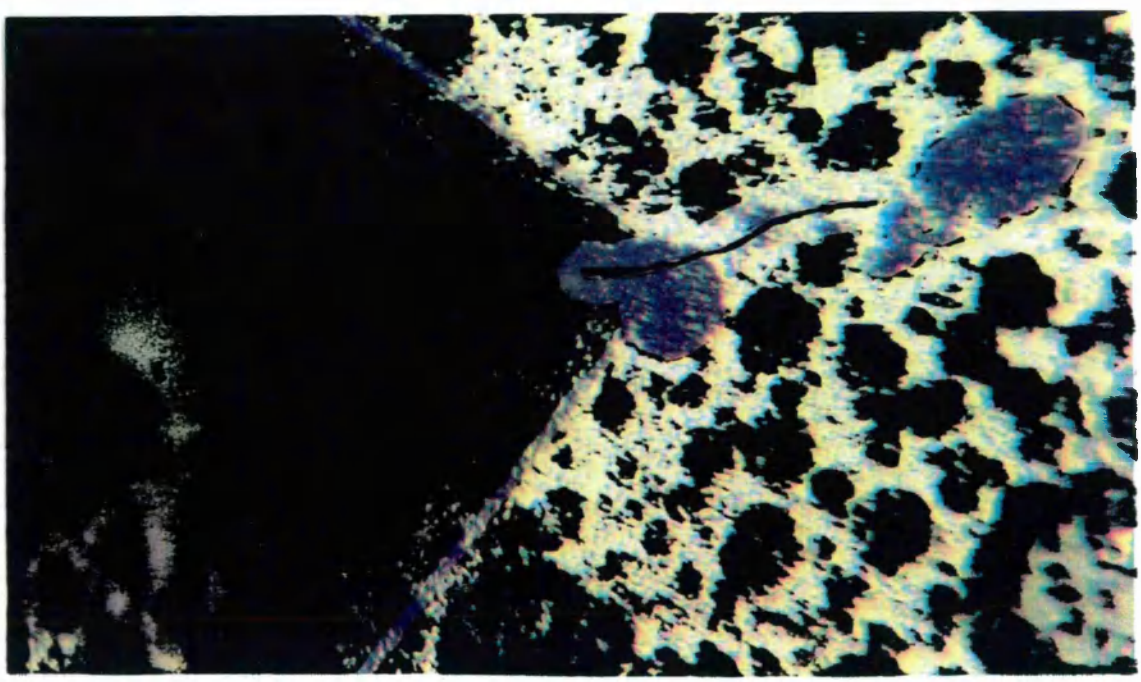

MICROSTRUCURE OF TYTIN SHOWING PARTICLE AT THE APEX 20μm

Figure 5.36

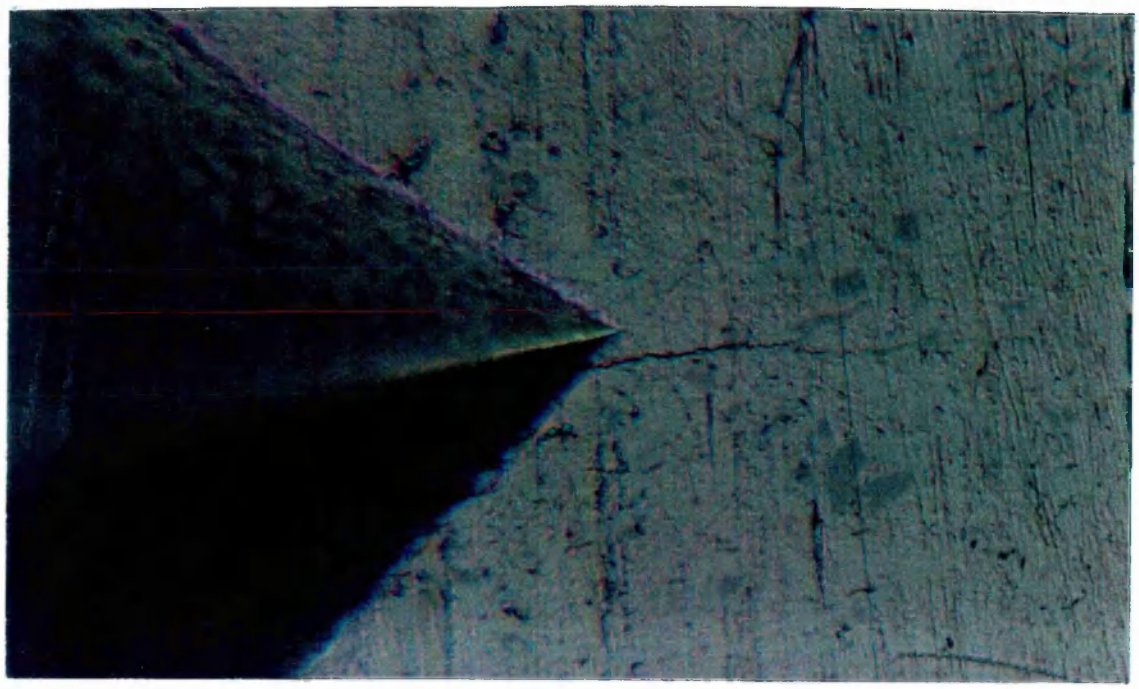

TYTIN SHOWING OFFSET OF CRACK ORIGIN 20μm

Figure 5.37

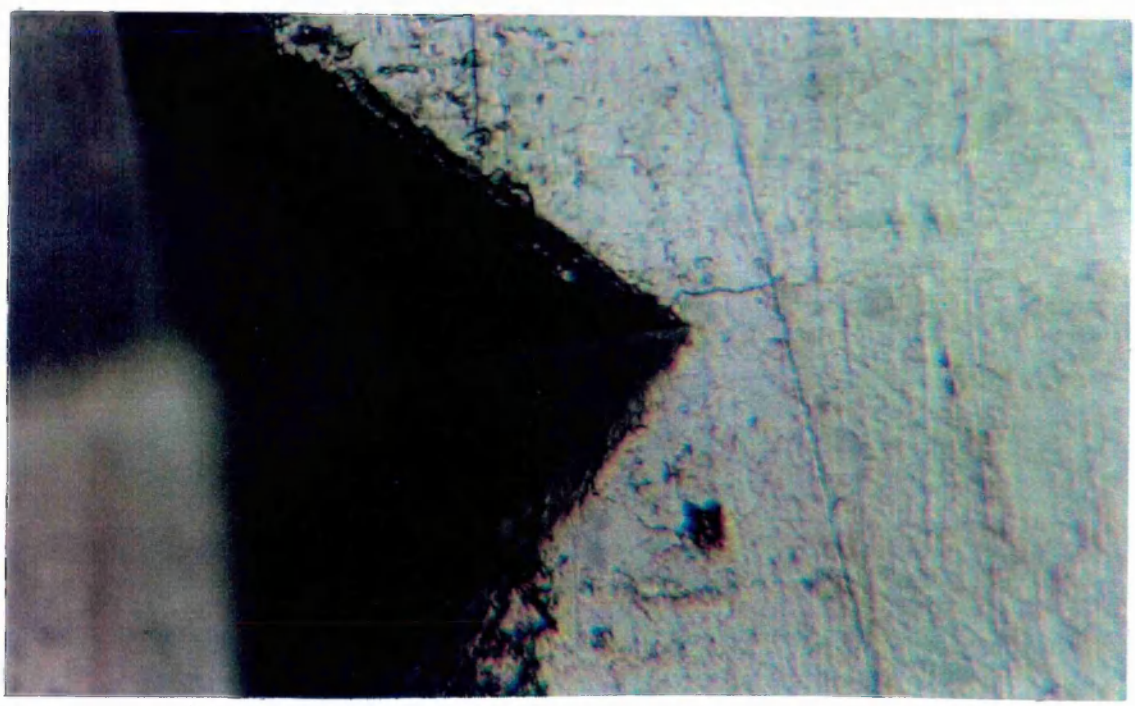

TYTIN SHOWING OFFSET FROM OTHER SIDE OF THE SAME APEX AS IN PREVIOUS FIGURE, BUT FROM A SECOND INDENTATION. 20μm

Figure 5.38

HiCu The range of K_{IC} values for this material was 0.63 to 2.31MN/$m^{3/2}$ compared with an SEN value of 0.7MN/$m^{3/2}$. Two distinctive features of the crack formation in this case were, the offset of the crack origin which is estimated to be approximately 20μm (ie. comparable to the unreacted particle size), Figures 5.39(a) and (b). The second feature was the very straight crack path which, it is suggested is an indication of both inter- and trans-crystalline fracture. The unreacted phase in HiCu is mainly the ε phase (K_{IC} value 0.73MN/$m^{3/2}$), originating from the high copper and tin content of the alloy powder.

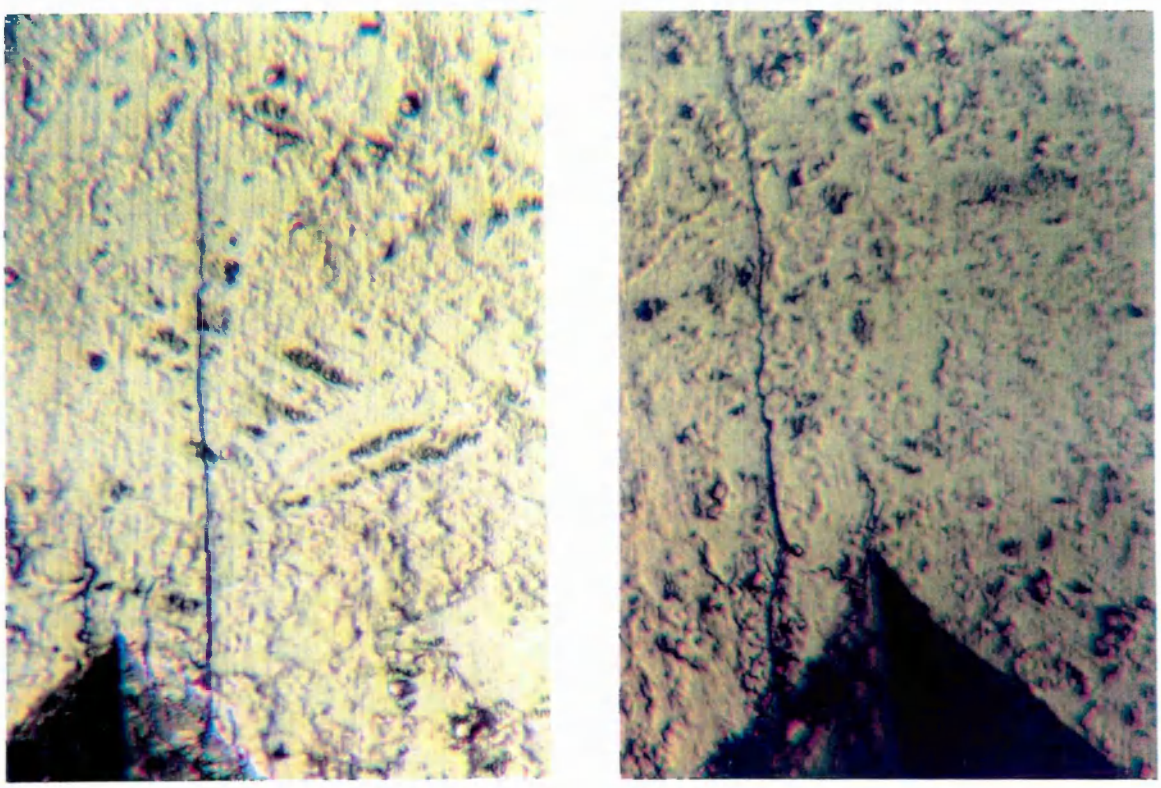

VIEWS SHOWING THE OFFSET OF THE CRACK ORIGIN AND THE STRAIGHT CRACK IN HiCu AMALGAM - THE CRACKS ARE FROM DIFFERENT INDENTATIONS
Figure 5.39

Dispersalloy This amalgam is another case where the 10kg load was considered to be the most suitable because the K_{IC} range of 0.87 to 5.97MN/$m^{3/2}$ encompassed the SEN value of 1.84MN/$m^{3/2}$. A second reason for this opinion is that the cracks were well formed and straight under this load. Under the lower load of 5kg, the K_{IC} range was 6.8 to 14.9MN/$m^{3/2}$. This maximum of the range coincides with the K_{IC} of the unreacted phases of γ and the Ag-Cu eutectic phases. The lower value in the range is approximately the same as the η phase, which as has been suggested, plays an important role in determining the properties of Dispersalloy. This indicates that the lower loads produce values which are more sensitive to local microstructure, whereas the higher loads approach a value representing overall fracture toughness with less trials being necessary.

A final comment on these results is that there is no direct correlation between the hardness figure of a material and its K_{IC} value. A not unexpected result as this complies with the general case of any brittle material, probably best illustrated by glass with a hardness of 510 H_V and a fracture toughness of about 0.8MN/$m^{3/2}$. Comparison between Tables 5.2 and 5.4 shows a similar case exists for amalgams.

CHAPTER 6

6.1. Conclusions.

Amalgam manufacture and placement procedures affect restoration quality. K_{IC} quantifies the resistance to fracture from pre-existing flaws, which can originate at any stage in the restoration production process, and therefore can be used as a gauge of the overall performance.

The critical flaw size of a material is obtained from the relationship previously discussed, $K_{IC} = \sigma_f \sqrt{(\pi\ a_c)}$, where σ_f = fracture stress, and a_c is the critical flaw size. Thus the fracture toughness figure is related to the critical flaw size which in turn is a measure of the required surface finish of a filling. The applied stress on molar teeth can be 17 MPa(174), the specific value depends on the individual. When this information is applied to the above equation, it gives a critical flaw size for Revalloy and Dispersalloy of 0.4mm The polishing operation must achieve an adequate freedom from flaws of this depth, but this stage is frequently omitted by dentists, and the 'carving to form' process may well leave critical flaw sizes that lead to fracture under biting forces.

The use of the single-edge notch(SEN) specimen in transverse bending is a common method of finding K_{IC}.

Amalgam specimens are necessarily small, partly because of the high material cost, and partly because of the limitations imposed by

the mixing and packing techniques. The maximum quantity of alloy powder and mercury that can be mechanically mixed at one time is about 5g, and the practical maximum specimen mass is 10g. In spite of the small size, the highly brittle nature of amalgams means that yielding at the crack tip does not present any analytical problems, and linear elastic fracture mechanics can be applied directly. However, the small specimen size does require that the appropriate compliance, or geometric correction factor (Y) has to be applied. The specimen a/W ratio does not affect the calculated value of K_{IC} value because of the brittleness of the amalgam. An a/W ratio of 0.2 is recommended for convenience of production.

Transverse bend tests in both 3- and 4-point loading showed that statistically, there is no difference in the resulting sample mean K_{IC} values. However, a preference for 4-point loading is indicated by its very low standard deviation.

There is a significant increase in fracture toughness when K_{IC} values are compared at 24 hours and 3 years. This is probably a manifestation of the long term phase changes that are reputed to occur. The results of the three year 3-point bend test enables a distinction to be made between analgams that have a good clinical reputation and those that are considered unsatisfactory. K_{IC} above 1 $MN/m^{3/2}$ represents the boundary between the two categories. The ranking of K_{IC} of material types is essentially the same for three year as for 24 hour specimens when the results of three- and four-point SEN specimens are combined. The exceptions are Revalloy and Dispersalloy, which change place in the ranking order. This suggests that Dispersalloy has higher early toughness than Revalloy

and will give a better performance in the initial life of the filling.

To enable a test programme to be conducted within commercially practical time limits, the 24 hour specimen age is the most convenient.

It is concluded that amalgams can be judged by their fracture toughness and there are indications that the SEN K_{IC} value encompasses mixing and packing capability.

In common with all manufactured composites, it is clear that the techniques used for specimen production create features that could influence K_{IC}. The most important variable in an amalgam is the volume percentage and distribution of its porosity. An alternative test method is necessary to ensure that the calculated K_{IC} is a material property.

The hardness method of establishing K_{IC} provides a solution to the problem and has the added advantage that the value from a single crack, originating from the apex of the indentation, provides information about the local microstructure. The prediction of in-vivo performance with in-vitro test results is more reliable if the variables involved in mixing and packing techniques are similar. This can be achieved by ensuring that the amalgam specimen is comparable in size to that of a filling. Clearly, the hardness method fulfils this criterion.

The validity of equation 5.1, relating K_{IC} to Vickers hardness, indentation dimension, the uniaxial tensile modulus and the constraint factor ϕ, had to be examined in the course of this work. Soda glass was selected as a control material as a part of this

research. The reason for this choice was that reliable values of both K_{IC} and E are readily available in published work. Confirmation of the ϕ value for glass was obtained from the range of values given by Marsh. Soda glass is an amorphous, isotropic material and thus provides highly repeatable values of hardness which are confirmed by published figures.

The uniformity of the structure was demonstrated by the very small standard deviation of K_{IC} for the control material. In contrast, the standard deviation of amalgams ranges from 100 to 1000 times (depending on type) greater than glass. This high standard deviation shows that the range of individual values of K_{IC} within a batch, are not attributable to experimental inaccuracy alone. The conclusion is that the reason for the wide range of individual values is the variation in microstructure between test sites.

A relationship can be detected between the individual values of K_{IC} obtained by indentation testing and the fracture toughness of the individual constituent phases. For example, the maximum value for Dispersalloy was 14.9 $MN/M^{3/2}$, which corresponds with the two constituent phases with maximum fracture toughness (γ and Ag-Cu). This supports the view that the fracture toughness of the constituents local to the indentation apex is reflected in the K_{IC} result obtained from equation 5.1. However, due to the difficulty of manufacturing the constituent phase specimens, some reservation has to be exercised when considering specific conclusions.

It is estimated that fifty trials are necessary to obtain an average hardness K_{IC} value that compares favourably with that of the transverse bend tests. However, the hardness test method is

particularly useful for detecting the influence of the morphology and composition of the constituent phases on crack propagation.

The test features that produce variations in K_{IC} according to measurement site are:

a) The type of constituent phase that exists in the vicinity of the indentation. There are examples presented in Chapter 5 where the K_{IC} was markedly influenced by the presence of the high fracture toughness residual γ phase, and in the case of Dispersalloy, the (α + β) phase. The crack was seen either to arrest or undergo significant deflection around these phases.

b) The value of K_{IC} is increased when a phase that does not have mercury as a constituent coincides with the apex of the indentation. It is assumed that the reason for this is the extra energy expended by diverting the crack around the particle.

c) The phase, or phases that are directly under the indentation will strongly influence H_V and 'a', used in equation 5.1 and therefore K_{IC}.

d) The way in which the crack length is defined, i.e. a straight line from the origin to the termination point, results in some ambiguity in applying C_R to the equation for K_{IC}. Cracks that deviated significantly from the radial and linear were not used for this present research. Unfortunately the possibility of the SEM being damaged by mercury in the amalgam, made it impossible to conduct microscopic analysis which would have provided useful data on crack kinetics.

The effect of error in evaluating K_{IC} can be minimised by selecting the highest allowable load for the hardness test. The

applied load must be within a defined range, so that a single crack from the indentation apex can be obtained. If the load is below a particular minimum value, a measureable crack is not evident. Conversely, if the maximum value is exceeded, then considerable peripheral damage occurs to the indentation which induces multi-cracks or crazing. The working range of load for amalgams depends on the specific material type, i.e. 10 kg is ideal for Tytin but well above the maximum for HiCu. In the majority of cases, 5 kg was a suitable test value.

The purpose of the test determines the load selection. The highest possible value of load maximises the crack length and K_{IC} is less sensitive to the microstructure at the origin and also gives optimal accuracy of C_R. Crack initiation features, such as surface imperfections and phase detail at the test site, dominate when the applied load is just above the minimum of the working range.

It is clearly important to set the sampling scheme so that the number of tests is appropriate to the aim of the investigation.

The hardness test method is particularly useful for detecting the influence of the morphology and composition of the constituent phases on crack propagation.

6.1.1 Summary.

The results presented in Chapter 3 show that the mean SEN K_{IC} enables different amalgams to be ranked in an order that corresponds with their clinical reputation. This conclusion is based on the view of a very limited number of dentists, because little published

work exists on the in-vivo performance of commercial brands of amalgams.

The hardness method gives results that are strongly influenced by the load used, in addition to the phase configuration at the indentation apex. Qualitative improvements to amalgams can be predicted from the morphology of the indentation cracks, without the need for large specimens and difficult microscopy on the fracture edge.

Use of results obtained from single cracks from the hardness method enables the effects of microstructure to be investigated. Comparison of data from Chapters 3 and 6 shows that by averaging the hardness results, the SEN value is approached as the number of hardness trials is increased thus approaching a bulk property.

6.2. Recommendation for further work.

Amalgams can be classified as composite materials because the mercury-containing phases form a matrix, and the residual (e.g. the γ unreacted) phase may be regarded as a particulate filler. The hardness method of determining K_{IC} described in this present work could be applied to characterise a wide range of composites, particularly ceramic-based materials.

The perception of a good material, as applied by dentists and patients is based on workability, cost, the absence of secondary decay, appearance, absence of pain subsequent to filling, and the longevity of the restoration. A quality index system will have to be devised in order to be able to relate the K_{IC} of an amalgam to its

clinical performance. However, it is impractical to conduct clinical trials of the whole range of commercial amalgams in order to identify accurately the causes of failure in fillings.

It is recommended that the hardness testing method should be used to relate the microstructural features of failed fillings to both the fracture toughness and the clinical performance.

Equation 5.1. produces results of K_{IC} that relate to the amalgam type and compare favourably with SEN values. More basic research is required into the validity of the two empirically found functions, $(C/a)^{-3/2}$ and $(H_v/E\phi)^{0.4}$. This could be achieved by following the same experimental procedures of the originators of the test method (150-152).

A knowledge of the fracture toughness of the constituent phases can lead to a rationale for new alloy development, by relating these data to the fracture toughness of the amalgam. This aim demands improved techniques for manufacturing specimens of the phases. The main problem with the specimens which were used for this present research was caused by production methods. Homogeneity could not guaranteed for the copper-tin and silver-tin cast specimens. The degree of porosity and its distribution within the packed material was unknown for the mercury-reacted phases. The polycrystalline structure of the consitituent phase specimens is acceptable because there is no difference when they are components of amalgam. More insight into the effect of individual phases can be obtained using single crystal specimens of each constituent. It may well be that the Vickers micro test can be developed to achieve this, or alternatively, appropriate sizes of single crystal could be grown by

the already well-established techniques.

It is also necessary to address the problem of how to define the crack length from the indentation, because of variation in direction and geometry. In this present research the method adopted to definine the crack length (C_R) as a straight line joining the origin to the termination point, would result in an overestimation of K_{IC}.

It is recommended that the hardness test method should be extended to the use of polymer-based types of dental filling. These have been the subject of a considerable amount of research in recent years for three main reasons. Firstly, they have the potential to adhere to natural tooth tissue: when adherence is achieved there is an associated reduction in tissue failure in service. Secondly, there is no time limit for light-cured composites on their use in construction of the filling, as there is with amalgam. Lastly, the appearance of the filling is easily matched to that of the tooth, which is impossible with amalgams.

REFERENCES

1. Peters,M., Poort,H.W. - Biomechanical stress analysis of the amalgam tooth interface. J.Dent.Res. v.62 No.3 Mar.1983 pp.358-362.

2. Wright,K. & Yettram,A. - Finite element stress analysis of a class I amalgam restoration subject to setting and thermal expansion. J.Dent.Res. v.57.No.5-6 May 1978 pp.715-723

3. McLean,J.W. - The quiet revolution in the art and science of dentistry. Proc. R.S.A. Journal. May 1989 pp333-348.

4. Black,G.V. - An investigation of the physical characters of the human teeth in relation to their diseases, and to practical dental operations, together with the physical characters of filling materials. Third paper: Filling Materials. Dent.Cosmos 37,553 - 1895

5. Elderton,R.J. - A new look at cavity preparation. Proc.Brit.Orthodontics Soc. v9. pp25-30 1977.

6. Robbins,J. - Dentistry Materials Edge, April 1988.

7. Reisbeck,M.H. - Predicting the clinical success of restorative dental materials. Biomat.Med.Rev.,Art.Organs 7(1) pp.89-98 1979

8. Combe,E.C. & Grant,A.A. - The selection and properties of materials for dental practice. 1.-Priciples of selection Brit.Dent.J.,v134 pp6-20 1973.

9. Wilson,A.D. - Dental silicate cements Fiftieth anniversary symposium on dental research, Programme and abstracts. National Bureau of Standards, Gaithersburg, Maryland. 1969.

10. Cook,W.D., Beech,D.R., - Tyas,M.J. Structure and properties of methacrylate based dental restorative materials. Biomaterials v6 Nov.1985 pp.362-368.

11. Cook,W.D. - Setting of dental polyelectrolyte cements. J.Biomed.Mat.Res. v.17 Pt.2 Mar.1983 pp283-291.

12. Rabchinsky,D.S., - Powers,J.M. Colour stability and stain resistance of direct bonding orthodontic cements. Am.J.Orthod. v.76. Pt.2 Aug.1979 pp170-177

13. Prevost,A.P., Fuller,J.L.,- Peterson,L.C. The use of an intermediate resin in the acid-etch procedure: retentive strength, microleakage, and failure mode analysis. J.Dent.Res. v.61 No.2 Feb.1982 pp.412-417.

14. Wilson,A.D., Prosser,H.J.,- Powis,D.M. Mechanism of adhesion of polelectrolyte cements to hydroxyapatite. J.Dent.Res. v.62 Pt 5 May 1983 pp590-592

15. Strachan,J.F. & Harris,N.L. The attack of unstressed metals by liquid mercury. J.of Ins.Metals 1956-7 v85.

16. Craig,R.G. & Peyton,F.A. - Restorative dental materials pp8-9. Pub. Mosby 5th Edition 1975.

17. Black,G.V. - Operative Dentistry Medico Dental : Chicago 1908.

18. Bates,J.F. & Knapton,A.G. - Metals and alloys in dentistry. International Metals Reviews. No.215. Mar.1977. pp.39-60

19. Report of the - Government Chemist Dental materials. 1978 p.71.

20. Skinner,E. & Phillips,R. - The science of dental materials 5th.edition 1966. Pub.W.B.Saunders Co. Philadelphia

21. Kirk-Othmer(Ed.) - Encyclopedia of chemical technology. Pub. Wiley 3rd.Edition v.7 1977 pp461-521.

22. Elderton,R.J. - Assessment of the quality of restorations. A literature review. J.Oral Rehab. v4 pp217-226 1977.

23. Jendreson,M.D., Charbeneau, G.T., Hamilton,A.I., Phillips,R., Ramfjord,S.P. - Report of the committee on scientific investigation of the American Academy of Restorative Dentistry. The J.Prosth.Dent. v.41 Pt.6 Jun.1979 pp.671-695.

24. Wennberg,A., Mjor,I.A. - Henston-Pettersen,A. Biological evaluation of dental restorative materials - A comparison of different test methods. J.Biomed.Mat.Res. v.17. 1983. pp.23-36.

25. Osborne,J.W.,Schlissel,E.-Gale,E.N. Clinical test for the development of new amalgam alloys. J.Dent.Res. v.60 No.6 1981 p.999

26. Institute of Occupational Health. - Private correspondence. 1982.

27. National Union of Mineworkers. Private correspondence (General Secretary) 1982.

28. Allan,D.N. - Longitudinal study of dental restorations Br.Dent.J. v.143 1977 pp87-89.

29. Robinson,A.D. - Life of a filling Br.Dent.J. v.143 1977 pp.87-89.

30. Elderton,R.J. - The prevalence of failure of restorations - A literature review J.of Dentistry, v4 No.5 1976 pp.207-210.

31. Elderton,R.J. - The relationship between objective measurements at the marginal regions of amalgam restorations and subjective judgements of their quality. Monographs London Hospital Medical College 1977 Pt.II(4) Ed. Allred,H.

32. Braly,B., Maxwell,E.H. - Potential for tooth fracture in restorative dentistry. J.Prosth.Dent. v.45 Pt.4 April 1981 pp.411-414

33. British Standards - Dental amalgam alloy BS 2938:1985.

34. Cruickshanks-Boyd,D. - The structural and physical properties of silver-tin amalgams containing copper. PhD thesis Univ.of London 1981

35. Fairhurst,C.W. & Cohen,J.B. - The crystal structures of two compounds found in dental amalgam. Adv.X-Ray J.. 1972. B28 pp.371-7.

36. Fairhurst,C.W. & Ryge,G. - X-ray diffraction investigation of the Sn-Hg phase in dental amalgam. Adv.X-Ray Analysis. v.5. No.64 1962

37. Espevik,S. - Dental amalgam. Ann.Rev.Mater.Sc. 1977. v.7. pp.55-72.

38. Hero,H. - On creep mechanisms in amalgams. J.Dent.Res. 62(1). Jan.1983 pp.44-50

39. Abbott,J.R. & Makinson,O.F. - Removal of γ_2 phase in amalgam. J.Biomed.Mat.Res. v.13. 1979. pp.857-863

40. Paffenbarger,G.C., Rupp,N.W., Waterstrat,R.M. - Metals in solution expressed from copper rich dental amalgams. J.Dent.Res. 61(1). Jan.1982. pp.30-32.

41. Crawford,W.H. & Larson,J.H. - Residual mercury determination process. J.Dent.Res. 3(34). Jun.1955. pp.313-317

42. Wing,G. - Phase identification in dental amalgam. Aus.Dent.J. v.11. Apr.1966. pp.105-113

43. Gayler,M.L.V. - The constitution of the alloys of silver,tin and mercury. J.Inst.Metals. v.60. 1937 p.379.

44. Craig,R.G.(Ed.) - Dental materials review. 1979 Mosby Jan.1989

45. Mueheler,J.C. - US Patent 3 676 112 July 11th 1972 Assigned to Indiana Univ.Foundation.

46. Saffir,J. - US Patent 3 513 123 May 19th.1970. Assigned to Dentsply Int.Inc.

47. Sarkar,N.K. - US Patent 3 997 329 Dec.14th.1976 Assigned to Engelhard Minerals and Chemicals Corp.

48. Tobler,R.L., Rostoker,W.,- Massler,M. Development of a ductile amalgam. J.Dent.Res. 53(4). 1974. pp.907-911.

49. Kropp,R. - US Patent 4 008 073 Feb.15th 1973 Assigned to Deutsche Gold Und Silber Scheideanstat vormals Roessler Germany

50. Baum,L. - US Patent 3 495 972 Feb.17th.1970 Assigned to Loma Linda Univ.

51. Beldham,V.E. - US Patent 3 554 738 Jan.12th.1971. Assigned to Metaltronics Inc.

52. Johnson,L.B. - US Patent 3 762 917. Oct.2nd.1973

53. Waterstrat,R.M. - US Patent 4 078 921 Mar.14th.1978. Assigned to Am.Dent.Ass.Health Found.

54. Simpson,H.M. - US Patent 3 985 558 Oct.12th.1976. Assigned to Sybron Corp.

55. Okabe,T et al. - Changes in microstructure of silver-tin and admixed high copper amalgams during creep. J.Dent.Res. 62(1). Jan.1983. pp.37-50.

56. Darvell,B.W. - Some studies on dental amalgam - Metallography of amalgam and alloys. Surface Technology. v6. 1978. pp.211-228

57. Innes,D. & Youdelis,W. - Dispersion strengthened amalgams. J.Can.Dent.Ass. v29. No.9. 1963. pp.587-593

58. Boswell,P.G. - The suppression of γ_2 precipitation and the kinetics of the gettering of Sn in a dispersed phase dental amalgam. J.Mater.Sci. v.15. 1980 pp.1311-1314.

59. Young,F. & Wilsdorf,H. - Influence of acid-treated Ag_3Sn on the tensile strength and fracture of dental amalgam. J.Biomed.Mat.Res. v.2. 1968 pp.401-403.

60. Abbott,J.R., Miller,D.R., Netherway,D.J. - Reaction of mercury with silver-tin dental amalgam alloy. J.Biomed.Mat.Sc. v.16. 1982. pp.535-547

61. Wood,J.V. & Jacombs,V. - Rapid quenching of a commercial dental alloy. J.Mat.Sc. v.11. 1976. pp.865-871.

62. Grenoble,D.E. - The pressure induced disappearance of the γ_2 phase in dental amalgam. J.Dent.Res. v.50. Pt1. Jan.1971 pp.109-115

63. Vrijhoef,M.M.A., Vermeersch,A.G., Spanauf,A.J. - Dental amalgams Quintessence Pub.Co. 1980

64. Stecher,P.(Ed) - New dental materials. Pub.Noyes Data Corp. USA.1980

65. LeMaitre,L, - A method for the measurement of dimensional change in dental amalgam. J.Biomed.Mat.Res., V.13 1979 p.887-992.

66. Wood,J.V. & King,S.C. - Production of dental alloy by the melt extraction technique. J.Mat.Sc.v.13.1978.pp.1119-1124.

67. Darvell,B.W. - Some studies of dental amalgam -Preparation of uniform samples. Surface Technology. v.4. 1976. pp.195-200

68. Wing,G. - The microstructure of dental amalgam. Aus.Dent.J. v.10. Pt.2. 1965. pp.113-120

69. Johnson,L. & Wilsdorf,H. - Basic metallurgy of dental amalgam. National Bureau of Standards Pub.354 Dent.Mat.Res. Proc.50th Ann.Symposium. Oct.6-8,1969. Gaithersburg. (Issued 1972)

70. Okabe,T. - IADR Prog.& Abstracts 58 No.26. 1979.

71. Okabe,T. - Structure,fracture mode and properties of high copper amalgams. IADR Prog. & Abstracts 57 No.498. 1978.

72. Jorgensen,K. & Saito,T - Structure and corrosion of dental amalgam. Acta. Odontol. Scan. v.28. 1970 p.129

73. Makinson,O.F. & Abbott,J.R. - Etchants for the tin-mercury phase of dental amalgam. J.Biomed.Mat.Res. v.12. Pt.4. 1978. pp.579-584.

74. Allan,F.C.,Asgar,K., Penton,F.A. Microstructure of dental amalgam. J.Dent.Res. Sep.1965 pp.1002-3.

75. Sweeney,W. & Burns,C. - Application of the diametral-compression test to dental materials. IADR Abstracts 43 1965 p.122.

76. Young,F.A. & Wilsdorf,H. - The tensile failure of dental amalgam. Research in Dental and Medical Materials. New York: Plenum Press. 1969 p.69.

77. Nagai,K., Ohashi,M., Habu,H., Makino,K. Usui,T., Matsuo,M., Matsuo,M.,Hama,M., Kawamoto,M. - Studies on the tensile strength of dental amalgams by the application of diametral compression test Part 2 Effect of manipulative variables. J.Nippon Sch of Dent. v.13. 1971 pp.21-32.

78. London,D.- Ibid Bates & Knapton.

79. Rodriguez,M. & Dickson,G. - Some tensile properties of amalgam. J.Dent.Res. v.41 1962 pp.840-852.

80. Young,F.,Wilsdorf,H. & Paffenbarger,G. - Some relationships between microstructure and strength of Ag_3Sn and dental amalgam. J.Dent.Res. v.52(2) Mar. 1973 pp.281-290

81. Mahler,D.& Mitchem,J. - Transverse strength of amalgam. J.Dent.Res. 43. 1964 pp.121-130.

82. Kusy,R. & Greenberg,A. - Dynamic properties of amalgams. J.Biomed.Mat.Res. v.15. 1981 pp.47-59.

83. Gardner,J. & Dickson,G. - Application of diffraction gratings to measurement of strain of dental materials. J.Dent.Res.v.47. Nov.1968. pp.1104-1110.

84. Dickson,Oglesby.- Elastic constants of dental amalgam. J.Dent.Res. v.28 No.3 1949 pp.228-241.

85. Katz,J. & Grenoble,D. - Composite model of the elastic behaviour of dental amalgam. J.Biomed.Mat.Res. v.5 pt.5 1971 pp.515-527.

86. Bray,D.E. & Stanley,R.E. - Non-destructive evaluation - a tool for design, manufacturing & service. Ch.9 Ultrasonics techniques for stress measurement and material studies. p.162. McGraw Hill 1989.

87. Grenoble,D. & Katz,L. - The elastic contants of the constituents of dental amalgam. J.Biomed.Mat. Res. v.5. 1971 pp.503-513.

88. Taylor,N.O.,Sweeney,W.T. Mahler,D.B., Dinger,E.J. - The effect of variables on the crushing strengths of dental amalgams. J.Dent.Res. v.46 1967 pp.147

89. Caputo,A. & Reisbick,M. - Loading rate and temperature as variables in amalgam bending. J.Dent.Res. v.56 No.8 Aug.1977 pp.933-936.

90. Grenoble,D.& Katz,L. - The pressure dependence of the elastic constants of dental amalgam. J.Biomed.Mat. Res. v.5 1971 pp.489-502.

91. Outhwaite,W.,Twiggs,S.W.,- Fairhurst,C.W.,King,G.E. Slots v pins: A comparison of retention under simulated chewing stresses. J.Dent.Res. v.61 No.2 Feb.1982.pp400-402

92. Craig,R. & Farah,J. - Stress analysis and design of single restorations and fixed bridges. Oral Sc.Rev. v.10 1977 pp.45-74.

93. DeLong,R. & Douglas,W. - Development of an artificial environment for the testing of dental restoratives: Biaxial force and movement control. J.Dent.Res. v.62 Pt.1 Jan.1983 pp.32-36.

94. Watkins,E.C. - Static stress measurements in amalgam. J.Dent.Res. v.50.No.3. May 1971 pp.577-585

95. Vrijhoef,N., Gubbels,G., - Driessens,F.C.M. Creep of dental amalgam versus composition and prolonged homogenisation of amalgam alloy. Scripta Metallurgica. v.9. 1975. pp.85-90.

96. Mahler,D.B., Adey,J.D., - Marek,M. Creep and corrosion of amalgam. J.Dent.Res. v.61. Pt.1. 1982.pp.33-35

97. Patel,S. & - Cruickshanks-Boyd,D. The effect of ageing on the creep and compressive strength of high copper content amalgam. British Dent.J. v.147. 1979. pp.42-44.

98. Cruickshanks-Boyd,D. - & Roswati, The tensile creep characteristics of dental amalgam. Stress dependence. J.Biomed.Mat Res. v.15. 1981 pp.769-780.

99. Mahler,D.B. - Marginal fracture vs mechanical properties of amalgam. J.Dent.Res. v.49. 1970 pp.1452-1457.

100. Mahler,D.B. - Marginal fracture of amalgam restorations. J.Dent.Res. v.52. 1973 pp.823-827.

101. Rehberg,H. & Gramberg,U.- Trituration and Creep
J.Biomed.Mat.Res. 13(8)
Nov.1979 pp.833-842

102. Rheberg,H. - Creep of amalgams dependent upon different storage conditions.
J.Dent.Res.
v.59. Special issue p.1850.

103. Mahler,D. & Nelson,L. - Effect of age on the creep of high copper amalgam. J.Biomed.Mat.Res.
v.15. 1981. pp.829-833.

104. Greener,K.,Szurgot,K., - Lautenschlager,E.P. The creep compliance of dental amalgam in the stress range 20-80MPa. J.Biomed.Mat.Res.
v.16. 1982. pp.599-608.

105. Vrijhoef,M.,Lourens,F.L. - Leijdekkers-Govers,A.F.M. Simultaneous description of transient and steady-state creep of dental amalgam.
J.Bioeng. v.2 Pt.5 1978 pp447-455.

106. Katan,T. & Ryge,G. - Corrosion penetration in crevices of dental amalgam.
J.Dent.Res. 53(4).
1974. pp.907-911.

107. Guthrow,C.,Johnson,L.B., - Lawless,K.R. Corrosion of dental amalgam and its component phases.
J.Dent.Res.
v.46 Nov.1967 pp.1372-1381.

108. Johnson,L. & Lawless,K. - Corrosion under stress of materials composing dental amalgam. J.Biomed.Mat.Res.
v.3 Pt.4 1969 pp.569-576.

109 Marshall,S., Lin,J.H.C., - Marshall,G.W. Cu_2O and $CuCl_2.3Cu(OH)_2$ corrosion products on copper-rich dental amalgams. J.Biomed.Mat.Res.
v.16 1982 pp.81-85.

110. Gettelman,D - The problems of corrosion and tarnish of dental restorative and implant metals.
Biomed.Med.Dev.Art.Org.
v.7 Pt.2 1979 pp.191-198.

111. Hearn,E.J. - Mechanics of materials - Pergamon Press.

112. Knott,J.F. - Theoretical background to LEFM - The Welder J. No.198 Pt.II.

113. Griffith,A.A. - The theory of rupture. - Proc. 1st.Int.Con.App.Mech. Delft,1924.

114. Warnock,F.V. - Strength of materials. - 7th Ed. Pub. Sir Isaac Pitman & Sons Ltd.

115. Bueckner,H.F. - Propagation of cracks and the energy of elastic deformation. Trans.Am.Soc.Mech.Engrs. 1958,80E,1225.

116. Irwin,G.R. & Kies,J.A. - Fracturing and fracturing dynamics. - The Welder J. Res.Sup. 1952,17,95S.

117. Irwin,G.R. - Relation of stresses and strains near the end of a crack traversing a plate. - J.App.Mech. 1957,24,361.

118 Irwin,G.R. - Relation of stresses near a crack to the crack extension. - 9th Int.Cong. App.Mech. Brussels,1957.

119. Knott,J.F. - The fracture toughness of metals. Ch.3 General Introduction to Fracture Mechanics. J.Strain Monograph.

120. British Standard - Methods of test for plane strain fracture toughness (K_{1c}) of metallic materials. - BS 5447:1977.

121. Rice,J.R. - Third Int.Con.on Fracture - Munich 1973 Paper 441.

122. Larsson,S.G.,- & Carlsson,A.J. Article - J.Mech.& Phys.Solids 21;263,1973

123. Hayes,D.J. - Origins of the stress intensity approach to fracture. Ch.2 Ibid.

124. Cartwright,D.J.- & Rooke,D.P. Evaluation of stress intensity factors. Ibid.

125. Westegaard,H.M. - Bearing pressures and cracks. - J.App.Mech. 1939,61,A49.

126. Mushkelishvili,N.I.- Some basic problems of the mathematical theory of elasticity. - Source: A general Introduction to fracture mechanics, Ch.5. - J.Strain Monograph 1978.

127. Cartwright,D.J. - Rooke,D.P. Methods of determining stress intensity factors. - Tech. report TR73031 RAE Farnborough 1973.

128. Rooke,D.P., - Cartwright,D.J. Compendium of stress intensity factors HMSO 1975.

129. Knott,J.F. - An Introduction to fracture mechanics Pt.III. - The Welder J. Iss.199, v40.

130. Rice,J.R. - Ibid.

131. Lewis,L.D. - On the a/W ratio in plain strain fracture toughness testing - Int.J.of Fracture, 1975, 11,179-183.

132. Hargreaves,A. - The effect of the environment on the crack initiation toughness of dental poly(methyl-methacrylate). J.Biomed.Mat.Res. v.15 No.5 pp.757-768

133. Causton,B. - Fracture mechanics of dental polymethyl methacrylate. J.Dent.Res. v.54 No.2 1975 pp.339-343.

134. Lloyd,C.H. - The fracture toughness of dental composites. J.Oral Rehab. v.9 1982 pp.133-138.

135. Goldman,M. - Fracture properties of composite and glass ionomer dental restorative materials. J.Biomed.Mat.Res. v.19 1985 pp.771-783.

136. Sutfin,L.V. - Fracture of dental amalgam. J.Dent.Res.v.49 No.5 Sep.1970 pp.1159-1165.

137. Younis,O. et al - Initiation of cracks in dental amalgam. J.Dent.Res. v.54 No.6 1975 pp.1133-1137

138. Koblitz,F.,Luna,V., - Glenn,J.P.,DeVries,K., Draughn,R.A. Fracture toughness of dental biomaterials. Organic Coatings & Plastics Chemistry. v.38 Am.Chem.Soc. Anaheim,Cal. Mar.1978.

139. Morozov,E.M. - Some problems in experimental fracture mechanics. - Eng.Fracture Mech. v13,Pt.3, p.541-561.

140. Timoshenko,S. - Strength of materials. D.Van Nostrand Co.Inc.N.Y.

141. Jayatilaka,A. de S. - Fracture of engineering brittle materials. App.Sc.Pub.Ltd., London.

142. Tattershall,H.G. - The work of fracture and its measurement in metals,ceramics and other materials. J.Mat.Sc. v.1 1966 pp.296-301.

143. Lewis,I.D.,Smith,R.F. - & Knott,J.F. On the a/W ratio in plane strain fracture toughness testing. Int.J.Fracture v.11 1975 pp.179-183.

144. Edwards,B. - The readable maths and statistics book. Pub. George Allen & Unwin 1980.

145. Murdoch,J. &- Barnes,J.A. Statistical tables. Pub. Macmillan Press. 1976

146. Knott,J.F. - Fundamentals of fracture mechanics. Pt.III Iss.200 The Welder v.40

147. Pearson,W.B. - A handbook of lattice spacings and structures of metals and alloys.

148. Butts,A. - Copper, the science and the technology of the metal, its alloys and compounds. Hafner 1970.

149. Taylor,A. - X-ray metallography. Pub. Chapman & Hall Ltd. 1949.

150. Evans,A.G. & Wilshaw,T.R. - Quai-static solid particle damage in brittle solids-I observations, analysis and implications. Acta Metallurgica v.24 pp.939-956 1976

151. Evans,A.G. & Charles,E.A. - Fracture toughness determinations by indentation. J. American Ceramic Society. v.59 No.7-8 pp.371-372. Jul.-Aug.1976.

152. Lawn,B.R. & Wilshaw,R. - Review - Indentation fracture: principles and applications. J.Mat.Sc. 10(1975) pp. 1049-1081

153. Gallagher,D. & Harthill,J.- Finite element modelling of the material response to hardness testing. B.Eng(Hons) Project (Supervisor:D.A.Hayes) Birmingham Polytechnic 1991

154. Murakami,Y.& Yuan Lu Ping.- Analysis of Brinell hardness by the finite element method 1990 (Translated from Chinese by Lucas(Japan)

155. Sih,G.C. - Handbook of stress intensity factors. Institute of fracture and solid mechanics. Lehigh Univ. 1973.

156. Mindlin,R.D. - Physics v.7 p195 1936

157. Hill,R. - The mathematical theory of plasticity. Oxford:Clarendon Press 1950.

158. Marsh,D.M. - Plastic flow in glass - Tube Investment Research Labs. Hinxton Hall, Cambridge, Tech.Report 159 June 1963.

159. Williams,D.P.& Evans,A.G.- Simple method for studying slow crack growth. J.Test.Eval. 1(4) pp.264-270 1973.

160. Tabor,D. - The hardness of metals. Oxford:Clarendon Press 1951.

161. Weiderhorn,S.M.- Mechanical and thermal properties of ceramics. J.Am.Ceramic Society 52,99 (1969).

162. Hassan,R.,Vaidyanathan,T.-
Schulman,A.
Fracture toughness determination of dental amalgams through microindentation.
J.Biomed.Mat.Sc. v.20 1986 pp.135-142

163. Haggag,F.M., Nanstad,R., -
Hutton,J.,Thomas,D.
Swain,R.
Use of automated ballindentation testing to measure flow properties and estimate fracture toughness in metallic materials.
ASTM Special Technical Publication n.1092 Publ.by ASTM Philadelphia, USA pp.188-208.

164. Haggag,F.M.,Nanstad,R.K. -
Estimating fracture toughness using tension or ball indentation tests and a modified critical strain model.
American Society of Mechanical Engineers. Pressure Vessels and Piping Division (Pubn.) PVP. v.170 ASME New York USA pp.41-46 1989.

165. Reuss,S.,Vehoff,H. -
Temperature dependence of the fracture toughness of single phase and two phase intermetallics.
Scripta Metallurgica et Materialia. v.24 n.6 June 1990 pp.1021-1026.

166. Fahmy,Y.,Russ,J.,Koch,C. -
Application of fractal geometry measurements to the evaluation of fracture toughness of brittle intermetallics.
J.Mat.Res. v.6 n.9 Sept.1991 pp.1856-1861.

167. Ochi,Y.,Saski,S,Ishii,A. -
Kawai,M
Effect of Vicker's indented load and microstructure on hardness, bending strength and fracture toughness in sintered silicon carbide ceramics.
Fracture and strength '90.
Key Engineering Materials v.51-52 Pub.by Trans.Tech.Publ. Zuerich, Switz. 1990 pp.155-160.

168. Duncan-Hewitt,W.C., -
Weatherly,G.C.
Evaluating the hardness, Young's modulus and fracture toughness of some pharmaceutical crystals using microindentation techniques.
J.Mat.Sc.Letters. v.8 n.11 Nov.1989 pp.1350-1352.

169. Ashizuka, M.,Murakami,A. - Elastic modulus, Vicker's hardness and fracture toughness of borate glasses.
Nipon Kinzoku Gakkaishi/
Journal of the Japan Institute of Metals. v.53 n.1 Jan.1989
pp.88-92.

170. Byakova,A.V.,Gorback,V.G., Vlasov,A.A. - Determination of the fracture toughness of structurally heterogeneous silicide layers.
Soviet Powder Metallurgy and Metal Ceramics. v.28 Pt.4
pp.294-298. 1992.

171 Laugier,M.T. - New formula for indentation toughness in ceramics.
J.Mat.Sc.Letters. v.6
1987 pp.355-356

172. British Standard - Vickers hardness testing
BS. 427:Part 1:1961

173. British Standard - Specimen design for tensile testing. BS 18 : 1971.

174. Mahler,D.B. - An analysis of stress in amalgam restorations.
J.Dent.Res. 37 p.518.